Mio-Pleistocene sedimentation and structure of the Romanian shelf, northwestern Black Sea

Dissertation
zur Erlangung des Doktorgrades
der Naturwissenschaften im Fachbereich
Geowissenschaften
der Universität Hamburg

vorgelegt von

Cătălina Konerding

aus Gura-Rîului, Rumänien

Hamburg, November 2005

Als Dissertation angenommen vom Fachbereich Geowissenschaften der Universität Hamburg

auf Grund der Gutachten von Prof. Dr. H. K. Wong (Universität Hamburg)
und Prof. Dr. C. Dinu (Universität Bukarest, Rumänien)

Hamburg, den 1. Februar 2006

Professor Dr. H. Schleicher

Dekan des Fachbereichs Geowissenschaften

TABLE OF CONTENTS

ZUSAMMENFASSUNG

Die Zielsetzung dieser Dissertation ist die Kartierung der bis heute unbekannten Verteilung und des strukturellen Aufbaus der Mio-Pleistozänen Sedimente auf dem rumänischen Schelf des Schwarzen Meeres. Desweiteren sollen sowohl die Prozesse rekonstruiert werden, die die Sedimentation steuerten als auch die strukturelle Entwicklung des untersuchten Schelfbereichs. Diese sind für die Zeit vor Beginn des Miozäns bereits untersucht, im Rahmen der Vorliegenden Dissertation sollen die Kenntnisse über die folgende Zeit bis zum Pleistozän erweitert werden. Ein besonderes Augenmerk wurde dabei auf das Verhältnis zu der Entwicklung der Übergangszone von den Karpaten zum Schwarzen Meer gelegt. Zu diesem Zweck wurden 70 gleichförmig über das Arbeitsgebiet verteilte seismische Profile mit einer Gesamtlänge von 5300 km aus den Jahren 1980 bis 1994 ausgewertet, darüber hinaus standen Informationen aus 60 Bohrungen der Rumänischen Ölindustrie auf dem inneren Schelf zur Verfügung. Die seismischen Daten wurden in Hinblick auf die sedimentologische und strukturelle Entwicklung der Ablagerungen untersucht, die Bohrungsdaten lieferten sowohl Tiefenangaben und lithostratigraphische Informationen zu spezifischen Sedimentpaketen als auch die benötigte Tiefenkalibrierung der seismische Interpretation.

In der vorliegenden Dissertation kommen die folgenden Untersuchungsmethoden zur Anwendung: (1) Seismische Stratigraphie, (2) Rekonstruktion der Subsidenzgeschichte (in zwei Richtungen entlang des Schelfs: WNW-ESE und NE-SW) und (3) stratigraphische Modellierung der Mio-Pleistozänen Sedimentation.

Basierend auf der strukturellen Analyse der seismischen Daten wurden Sequenzgrenzen und die wichtigsten Erosionsflächen identifiziert. Von der Basis des Miozäns bis heute sind dies in erster Linie: Die BBU (*unconformity* an der Basis des *Pontian*), die innerhalb des *Pontian* gelegenen *unconformities* IPU 1, IPU 2 und IPU 3 sowie die PDU, eine *unconformity* an der Basis des *Dacian*. Die genannten *unconformities* unterteilen die Mio-Pleistozäne Abfolge in die folgenden Einheiten: *Badenian-Sarmatian*, *Pontian* (weiterhin unterteilt in P1, P2, P3 und P4), *Dacian* und das kombinierte *Romanian*-Quartär; die Grenze zwischen *Romanian* und Quartär ist dabei *conformal* ausgebildet. Seismische Daten und Bohrungsdaten zeigen dabei nur lokale, geringmächtige Vorkommen (selten mehr als 250 m) von Sedimenten des *Badenian-Sarmatian* auf dem inneren und mittleren Schelf, während das *Pontian* über den gesamten Schelf verbreitet auftritt und bei zunehmender Mächtigkeit in Richtung des tieferen Beckens ein auf dem äußeren Schelf bis zu 4000 m mächtiges Sedimentpaket bildet. Ebenso sind die Abfolgen des *Dacian* bis zum Quartär auf dem gesamten Schelf ausgebildet, allerdings weisen sie mit bis zu 1200 m (*Dacian*) bzw. 600 m (Quartär) eine geringere Mächtigkeit als das *Pontian* auf. Die Änderungen in der Entwicklung der Mio-Pleistozänen Sedimentation sind die Konsequenz eines wechselnden Sedimenteintrags (seinerseits direkt von der Hebung der Karpaten abhängig) und der tektonischen Aktivität. Die Abhängigkeit des Sedimenteintrags von Prozessen auf dem Rumänischen Festland lässt sich im Vergleich zur Entwicklung des Vorlandbeckens der Karpaten (Focşani

Depression**)** ablesen. Während des *Badenian-Sarmatian* (als die Hebungsprozesse in den Karpaten begannen) wurden bedeutende Mengen Sedimente geliefert und im Vorland abgelagert (>5000 m), auf dem Schelf treten sie jedoch nur lokal und geringmächtig auf (<250 m). Sedimente des *Meotian* sind auf das Vorlandbecken beschränkt und bilden dort bis zu 1600 m mächtige Abfolgen, während sie auf dem Schelf fehlen. Das *Pontian* wiederum ist im Bereich der Focşani Depression 1500-1600 m mächtig, tritt auf dem Schelf, wohin ein Grossteil der Sedimente geliefert wurde, jedoch mit bis zu 4000 m Mächtigkeit auf. Die Serien des *Dacian* bis zum Quartär sind im Karpatenvorland bis zu 4500 m mächtig, auf dem Schelf werden nur 1500 m erreicht. Nachdem eine Meeresspiegelschwankungskurve für das Mio-Pleistozän abgeschätzt wurde und eine sequenz-stratigraphische Einordnung der entsprechenden Einheiten vorgenommen wurde, konnte die tektonische Entwicklung des Arbeitsgebiets seit dem Miozän rekonstruiert werden. So ergeben sich tektonisch ruhige Verhältnisse während des *Badenian-Sarmatian*; im Gegensatz dazu weist das nachfolgende *Pontian* die tektonisch stärkste Aktivität auf. Während des Dacian bis zum Quartär verlangsamten sich die tektonischen Prozesse oder kamen sogar zum Erliegen. Die tektonischen Ereignisse während des Pontian wurden nach ihrer zeitlichen und räumlichen Abfolge klassifiziert. In zeitlicher Hinsicht wurden drei Typen von Störungen unterschieden: Störungen, die bereits vor dem Oligozän aktiv waren und deren Aktivität bis ins *Pontian* anhielt; Störungen, deren Aktivität während des Oligozäns oder *Pontian* einsetzte; sowie Störungen, die nur während des *Pontian* aktiv waren. Die räumliche Klassifikation ordnet Störungen einer NE-SW orientierten Senkungszone zu (in dieser Dissertation *„Pontian Depression“* genannt), deren Ablagerungszentrum im Bereich der Bohrungen 1 *Ovidiu* und 75 *Cobălcescu* lag. Andere Störungen wurden mit der Entwicklung der Schelfkante in Verbindung gebracht. Die Subsidenzgeschichte des Arbeitsgebietes wurde mit Hilfe der lithostratigraphischen Informationen aus Bohrungsdaten sowie der erstellten Meeresspiegelschwankungskurve rekonstruiert. Erwartungsgemäß sind die Abfolgen des *Badenian-Sarmatian* und des *Dacian*-Quartär weniger von Subsidenz beeinflusst, während im Verlauf des *Pontian* eine starke Subsidenz auftrat. Dies ist die Konsequenz der Änderungen des Sedimenteintrags, der tektonischen Aktivität und der Meeresspiegelschwankungen nach Ende des Oligozäns.

Ein stratigraphisches Modell wurde mit Hilfe iterativer Techniken erstellt, um unter Verwendung aller oben dargestellten Ergebnisse die Verhältnisse, wie sie auf den seismischen Profilen abgebildet sind, zu simulieren. Diese Modellierung belegt nochmals die Abhängigkeit der Sedimentation auf dem rumänischen Schelf während des Mio-Pleistozäns von den drei Faktoren veränderlicher terrigener Sedimenteintrag (in Verbindung mit der Entwicklung auf dem Festland), veränderliche Subsidenz (kontrolliert durch die tektonische Aktivität) und Meeresspiegelschwankungen.

ABSTRACT

The purpose of this dissertation is to map the hitherto unknown distribution and structure of the Mio-Pleistocene succession on the Romanian Black Sea shelf in time slices, as well as to reconstruct (1) the processes controlling sedimentation, and (2) the structural evolution of the shelf, known for pre-Miocene times, for the Miocene and the post-Miocene in relation to that of the transition zone from the Carpathians to the Black Sea basin. For this purpose, about 70 seismic lines distributed uniformly in the study area with a total length of 5300 line-km and recorded between 1980 and 1994, as well as information from 60 boreholes drilled by the Romanian oil industry largely on the inner shelf were used. The seismic data give information on the structural and sedimentological evolution of the deposits, while the boreholes provide the depth and lithostratigraphy of specific sediment packages as well as ground-truth for the seismic interpretation.

The following methods were used in the present study: (1) seismic stratigraphy, (2) reconstruction of the subsidence history (in two directions along the shelf, *viz*. WNW-ESE and NE-SW respectively), and (3) stratigraphic modelling (of the Mio-Pleistocene success-sion).

On the basis of our structural analysis of the seismic data, the sequence boundaries and the major erosional unconformities were identified. From the base of the Miocene to the present, the main erosional unconformities are: the BBU (the unconformity at the base of the Badenian), the BPU (the unconformity at the base of the Pontian), the IPU 1, IPU 2 and IPU 3 (the intra-Pontian unconformities), and the PDU (the unconformity at the base of the Dacian). They separate the Mio-Pleistocene section into the following units: Badenian-Sarmatian, Pontian (subdivided into P1, P2, P3, and P4), Dacian, and Romanian-Quaternary. The boundary between the Romanian and Quaternary formations is conformal. Seismic and borehole data show that while the Badenian-Sarmatian section occurs only locally on the inner and middle shelves and is very thin (rarely reaching 250 m in thickness), the Pontian is widespread over the shelf and increases in thickness from the coast basinward, reaching thicknesses of about 4000 m on the outer shelf. The Dacian and Quaternary successions are also widespread over the shelf, but are thinner than the Pontian, with a maximum of 1200 m and 600 m respectively on the continental slope. This change in the evolution of the Mio-Pleistocene section with time is the consequence of a varying sediment input and tectonic activity. The varying sediment input from the Romanian onshore is directly connected to the evolution of the foreland basin (the Focşani Depression) of the Romanian Carpathians. Thus, during the Badenian-Sarmatian period (when uplift of the Carpathians started), a large amount of sediment was delivered to and deposited in the foreland (> 5000 m), while on the Black Sea shelf, the Badenian-Sarmatian sediments are present only locally and are very thin (< 250 m). The Meotian deposits are present only in the foreland basin and reach up to 1600 m, while on the shelf they are absent. In the Pontian, the Focşani Depression received only a sediment layer of up to 1500-1600 m; most of the sediment was transported to the shelf, where the

Pontian reached a thickness of up to 4 km. During the Dacian-to-Quaternary, sediment up to 4500 m was deposited in the foreland basin, while on the shelf thicknesses of only about 1500 m were reached. After a sea level curve for the Mio-Pleistocene was estimated and a sequence-stratigraphic characterization of the Mio-Pleistocene units was completed, the tectonic evolution of the study area starting with the Miocene was reconstructed. It shows that the Badenian-Sarmatian was tectonically quiescent. In contrast, tectonic activity was the most active in the Pontian, slowing down or coming to a halt from the Dacian to the Quaternary. We classified Pontian tectonics both temporally and spatially. Temporally, 3 types of faults were separated: those that were active from the pre-Oligocene to the Pontian, those that developed during Oligocene-Pontian times, and those that were active only in the Pontian. Spatially, we recognized faults that developed along a NE-SW oriented depression (which we call the "Pontian Depression") having its depocenter crossing the wells *1 Ovidiu* and *75 Cobălcescu*, and faults that developed along the shelf-break. A subsidence history was reconstructed using lithostratigraphic information from boreholes and the estimated sea level curve. As expected, the Badenian-Sarmatian and the Dacian-to-Quaternary sections were less affected by subsidence, while strong subsidence occurred during the Pontian. This is the consequence of changes in sediment input, tectonic activity and sea level fluctuations during the post-Oligocene.

A stratigraphic model was constructed iteratively by integrating all previous results to simulate the seismic data. This model shows that sedimentation on the Romanian shelf during the Mio-Pleistocene was strongly affected by a variable terrestrial sediment input (which is connected to the evolution of the Romanian onshore), changing subsidence (controlled mostly by tectonic activity) and sea level fluctuations.

REZUMAT

Această teză de doctorat îşi propune analiza distribuției şi structurii succesiunilor Mio-Pleistocene de pe platoul continental românesc al Mării Negre şi reconstituirea (1) proceselor care controlează sedimentarea şi (2) a evoluției structurale a şelfului - deja analizată pentru perioada pre-Miocenă - pentru intervalul Miocen şi post-Miocen, în directă legatură cu zona de tranziție dintre Carpați şi bazinul Mării Negre. În acest scop au fost folosite 70 de profile seismice înregistrate între anii 1980 si 1994, acoperind relativ uniform zona analizată şi însumând aproximativ 5300 km, şi informații litologice şi de adâncime din 60 de sonde, situate în mare parte în zona şelfului intern.

În actualul studiu au fost utilizate următoarele metode: (1) principii ale stratigrafiei seismice, (2) reconstituirea istoriei subsidenței (în direcție VNV-ESE şi respectiv NE-SV de-a lungul şelfului) şi (3) modelarea stratigrafică a formațiunilor Mio-Pleistocene.

Pe baza analizei structurale a datelor seismice, au fost identificate principalele limite de secvență şi discordanțe Mio-Pleistocene. Astfel, de la baza Miocenului până în prezent acestea sunt: BBU (discordanța de la baza Badenianului), BPU (discordanța de la baza Ponțianului), IPU 1, IPU 2 şi IPU 3 (discordanțele intra-Ponțiene) şi PDU (discordanța de la baza Dacianului). Aceste discordanțe separă perioada Mio-Pleistocenă în următoarele unități: Badenian-Sarmațian, Ponțian (subdivizat, la rândul său, în P1, P2, P3 şi P4), Dacian şi Romanian-Cuaternar. Limita dintre secvența Romaniană şi cea Cuaternară are un caracter concordant. Analiza datelor seismice şi de sondă arată că, în timp ce secvența Badenian-Sarmațiană este distribuită local de-a lungul şelfului intern şi mediu şi atinge doar grosimi reduse (de până la 250 m), cea Ponțiană este răspândită de-a lungul întregului şelf şi creşte în grosime dinspre zona proximală spre cea distală, atingând grosimi de 4000 m în zona şelfului extern. Dacianul şi Cuaternarul sunt de asemenea răspândite de-a lungul întregului şelf, dar prezintă grosimi mai reduse decât Ponțianul, ajungând la doar 1200 m, respectiv 600 m în zona pantei continentale.

Această evoluție variabilă a formațiunilor Mio-Pleistocene în timp se datorează aportului variabil de material sedimentar dinspre uscat (direct legat de formarea Carpaților) şi a activității tectonice a acestor formațiuni. Aportul variabil de material sedimentar dinspre uscat este direct legat de evoluția „foreland”-ului Carpaților (Depresiunea Focşani). Astfel, în timpul perioadei Badenian-Sarmațiene (când a început ridicarea Carpaților), o mare cantitate de material sedimentar a fost transportată şi depusă în „foreland” (> 5000 m), în timp ce pe şelful Mării Negre secvența Badenian-Sarmațiană este prezentă doar local şi atinge grosimi reduse (< 250 m). Depozitele Meoțiene sunt prezente doar în „foreland”-ul carpatic şi ating grosimi de până la 1600 m, în timp ce în zona şelfului acestea lipsesc. În timpul Ponțianului, Depresiunea Focşani a acumulat sedimente de până la 1500-1600 m, mare parte din aportul de material sedimentar fiind transportat înspre şelf, unde Ponțianul atinge grosimi de 4000 m în zona proximală. Secvența Dacian-Cuaternară atinge valori de grosime de până la 4500 m în Depresiunea Focşani, în timp ce pe şelf aceste depozite ajung doar până la 1500 m.

După estimarea unei curbe de variație a nivelului mării şi caracterizarea unităților Mio-Pleistocene d.p.d.v. al stratigrafiei secvențiale, s-a urmărit o reconstituire a evoluției tectonice a zonei studiate începând cu Miocenul. Spre deosebire de perioada Badenian-Sarmațiană, care este calmă d.p.d.v. tectonic, în timpul Ponțianului activitatea tectonică devine puternică, atenuându-se sau dispărând complet în intervalul Dacian-Cuaternar. Activitatea tectonică ponțiană a fost clasificată atât d.p.d.v. temporal, cât şi spațial. Astfel, temporal au fost separate 3 tipuri de falii: cele care au fost active începând cu perioada pre-Oligocenă şi au continuat să fie active până în Ponțian, falii active în timpul Oligocenului şi al Ponțianului şi falii active doar în Ponțian. D.p.d.v. spațial, au fost evidentiate două tipuri de falii: cele formate de-a lungul unei depresiuni orientate NE-SV (numită de noi „Depresiunea Ponțiană"), cu depocentrul traversând sondele 1 Ovidiu şi 75 Cobălcescu, şi falii formate de-a lungul „shelf-break"-ului. De asemenea, s-a realizat o reconstituire a istoriei subsidenței de-a lungul şelfului, utilizând informații din sonde şi curba de variație a nivelului mării estimată în actualul studiu. Asa cum era de aşteptat, secvențele Badenian-Sarmațiană şi Dacian-Cuaternară au fost mai puțin afectate de subsidență, în timp ce o subsidență accentuată a fost înregistrată în timpul Ponțianului. Această subsidență variabilă de-a lungul perioadei analizate este consecinta mai multor factori, şi anume: a aportului variabil de material sedimentar, a activității tectonice variabile şi a fluctuațiilor nivelului mării în perioada post-Oligocenă.

Pe baza rezultatelor anterioare, s-a realizat un model stratigrafic în vederea simulării datelor seismice reale. Acest model arată că procesele sedimentare de-a lungul şelfului în timpul Mio-Pleistocenului au fost puternic afectate de aportul variabil de material sedimentar dinspre uscat (care este direct legat de evolutia „onshore"ului românesc), subsidența variabilă (controlată, la rândul ei, de activitatea tectonică) şi variațiile nivelului mării.

1. Introduction

The Black Sea is located between Romania, the Ukraine, Russia, Georgia, Turkey and Bulgaria. It is one of the largest enclosed marine seas with an area of 423,000 km^2, a volume of 534,000 km^3 and water depths up to a maximum of 2206 m (Ross et al., 1978). The Black Sea basin exists since about 200 million years ago and sediments of more than 15 km thickness have accumulated in some parts (Neprochnov et al., 1978).

At present, the Black Sea has only a single connection to the global oceans through the Sea of Marmara and the Mediterranean Sea. The connection to the Sea of Marmara, namely the Bosporus, is especially shallow (the present-day sill depth is around 50 m) so that the Black Sea was repeatedly disconnected from the ocean at times of low sea level. During the Pleistocene, for example, when the sea level dropped, the Black Sea was isolated from the Mediterranean and its conditions changed from marine to lacustrine. Connections to the global oceans through other basins might have existed in the past as well: a link through the Caspian Sea is well established and connections via the Carpathian basin might have existed (Neprochnov et al., 1978). The opening and closure of these links have an important influence on the water chemistry, fauna, and the sediment composition in the Black Sea (Neprochnov et al., 1978). Today, the Black Sea is the largest body of anoxic water in the world. From about 100 m depth to the bottom, the water contains hydrogen sulfide, which is deadly to all form of life except anaerobic bacteria (Neprochnov et al., 1978).

The Black Sea has been explored scientifically for more than a century. In 1890, Andrusov started to examine its bathymetry and took the first sediment sample from the basin (Andrusov, 1890). In 1967 and 1969, two modern oceanographic cruises took place to explore its recent geological and geochemical evolution. In 1976, in the framework of the Deep Sea Drilling Project, three deep-water boreholes (sites 379, 380, and 381) were drilled and cored with the Glomar Challenger during Leg 42B (Leg 42B; Ross, Neprochnov et al., 1978).

The first seismic data were acquired on the Romanian shelf and the first wells drilled in the late 1960's. Up to now about 75,000 km of reflection seismic profiles covering an area of 33,160 km^2 have been recorded and 120 boreholes were drilled (Ionescu, 2000). Since 1995, parts of these industrial data became available for scientific research.

The purpose of this study is to describe the sediment distribution, its structures and controlling processes, as well as the structural evolution of the Mio-Pleistocene formations on the Romanian Black Sea shelf and to relate them to the evolution of the transition zone from the Carpathians to the Black Sea basin. In addition, the evolution of the Black Sea basin known for Pre-Miocene times (Ionescu, 2000) will be deduced for the Miocene and post-Miocene. For this purpose, about 70 industrial reflection seismic profiles recorded between 1980 and 1994 with a total length of 5300 line-km, and data from 60 boreholes drilled by the Romanian oil industry were used.

This thesis starts with a synthesis of the Black Sea basin and its surrounding regions (Chapter 2). The structural and sedimentological evolution of the basin, especially of the northwestern Black Sea, will be briefly described, and the evolution of its pre-Miocene geology in relation to characteristics on land reviewed. Then, in Chapter 3, a general description of the available seismic and borehole data and a description of the main methods used in this study (including seismic stratigraphy, the calculation of subsidence, and the procedures for stratigraphic modeling) will be presented. In Chapter 4, the Mio-Pleistocene structural evolution of the Romanian shelf will be reconstructed. This includes a detailed description of the sequence boundaries and the major unconformities, a sequence-stratigraphic characterization as well as a structural description of the Mio-Pleistocene subunits, and a subsidence analysis along two profiles (in WNW-ESE and NE-SW directions respectively) based on borehole information. Chapter 5 begins with a general presentation of the borehole data used in this thesis and a lithological description of the Mio-Pleistocene period from borehole information. The results obtained in the previous chapters will be integrated and a stratigraphic model developed to match the seismic data. The last chapter gives some general conclusions of the present study.

2. Geological Framework of the Black Sea

2.1. Introduction

The Black Sea is an extensional back-arc basin developed along the northern active margin of the Tethys Ocean which was subducted northward from the Triassic to the Miocene. It consists of two parts: the western Black Sea which is underlain by oceanic to suboceanic crust, and the eastern Black Sea underlain by continental crust. The western Black Sea basin has a sedimentary cover that reaches 19 km in thickness, while the eastern Black Sea basin contains 10-12 km of sediments. The two basins are separated by a strike-slip fault system along the Mid-Black Sea/Andrusov Ridge, which comprises continental crust including a sedimentary cover 5-6 km in thickness.

The Black Sea basin is surrounded by the following tectonic units (Fig. 2.1):

- the *East European Platform* to the north, which extends from the Ukraine onto the northwestern shelf. It has a pre-Riphean (Late Proterozoic) basement of gneiss, granite-gneiss and granitoids with some basic and ultrabasic rocks (Dinu et al., 2002). The Riphean-Palaeozoic, Mesozoic and Cenozoic sedimentary cover, 8-10 km in thickness, accumulated during three major sedimentation cycles separated by gaps corresponding to periods of uplift and erosion (Seghedi et al., 2004; Barbu et al., 1969; Macarovici, 1971; Pătruliuş and Iordan, 1974; Iliescu, 1974; Paraschiv, 1985). The first cycle developed during the Late Vendian to the Devonian and includes Late Vendian-Ordovician coarse detrital siliciclastics, Silurian calcareous and shaly graptolitic facies and Early Devonian black limestones passing to quartz sandstones. The second cycle corresponds to the Cretaceous-Middle Eocene and includes Lower Cretaceous shallow marine clastics, evaporites and limestones, and Upper Cretaceous terrigenous clastics and chalky limestones. It is characterised by frequent but short breaks in sedimentation. The last cycle developed during the Late Badenian to Meotian and includes gaps that indicate long periods of uplift. It starts with the Kossovian marine transgression over the entire platform and includes clastics and carbonates which interfinger with air-fall tuffs and evaporites (Seghedi et al., 2004);

- the *Scythian Platform* to the northeast consisting of a Riphean, Vendian and Palaeozoic basement which was deformed around the Triassic-Jurassic boundary (Muratov, 1969; Milanovsky, 1991; Nikishin et al., 2001, 2003; Dinu et al., 2002). Its sedimentary cover extends over several cycles (Lower and Middle Jurassic, Lower and Upper Cretaceous, Palaeocene-Eocene, Oligocene-Lower Miocene and Neogene) and has a thickness ranging from several hundreds meters to 5 km. It is made up of sandstones and limestones with associated intrusive and effusive basic and acidic rocks (Dinu et al., 2002);

- the *Moesian Platform* to the west of the Romanian and Bulgarian shelves, consisting of Neoproterozoic metamorphic rocks and Vendian turbidites in the uplifted block of Central Dobrogea, and Cretaceous to Miocene sediments in Southern Dobrogea, overlain by a discontinuous blanket of Quaternary loess (Seghedi et al., 2004). The basement includes Archaean and Palaeoproterozoic metamorphic complexes and a Late Proterozoic volcano-sedimentary suite in Southern Dobrogea (Seghedi et al., 2004). It was affected by Late Variscan deformations (Okay et al., 1994; Banks, 1997; Nikishin et al., 2003). The sedimentary cover is made up of Paleaozoic, Mesozoic and Cainozoic successions separated by frequent gaps. The Palaeozoic includes: Upper Cambrian-Middle Devonian marine clastics, Middle Devonian-Lower Carboniferous carbonates and a Carboniferous paralic series of coal-bearing clastics. The Permian-Triassic time span is represented by a Germanic facies, with lower and upper detrital sequences separated by carbonates (Seghedi et al., 2004). The Jurassic-Cretaceous is detrital during the Middle Jurassic, calcareous during the Upper Jurassic-Barremian, and calcareous-marly in the Late Cretaceous. The Eocene is made up of limestones, while the Badenian-Pleistocene sediments include detrital deposits reflecting basin evolution from shallow marine to continental (Seghedi et al., 2004);

  The Bulgarian part of the Moesian Platform comprises up to 5 km of relatively undeformed, dominantly shallow marine Mesozoic formations overlying a folded Palaeozoic basement. These formations are overlain by Palaeogene, Neogene and Quaternary deposits (Dabovski et al., 2004). The oldest sediments encountered in boreholes are Late Ordovician shales and Silurian shales and carbonates (Dabovski et al., 2004; Haydoutov and Yanev, 1997). They are followed by Devonian shales and carbonates, locally covered by Carboniferous coal-bearing formations and Permian red beds. The Mesozoic begins with Lower and Middle Triassic carbonates. They are overlain by terrigenous and calcareous Jurassic and Cretaceous formations, followed by continental or marine Palaeogene and locally Badenian to Pontian marine sediments belonging to a transitional zone between the Central and Eastern Para-thethys (Dabovski et al., 2004);

- the *North Dobrogea Orogen,* which developed between the Scythian and Moesian platforms and consists of a former Permo-Triassic rift basin that underwent thrusting and folding from the Jurassic-Cretaceous boundary to the Neocomian (Banks, 1997; Seghedi, 2001; Nikishin et al., 2001, 2003). Syn-rift sedimentation began during the Late Permian and Early Triassic and recorded during the Lower Scythian the transition from a continental siliciclastic to a carbonate-dominated environment (Seghedi et al., 2004). Late Triassic to Middle Jurassic syn-inversion deposits are represented by terrigenous turbidites derived from the Hercynian basement that was uplifted in the western part of the belt, whereby compressional reactivation of syn-rift extensional faults was involved (Seghedi et al., 2004). During the Jurassic, inversion movements ceased but were reactivated from the Early Cretaceous to the Albian. Late Cretaceous shallow marine sediments overlap the deeply truncated Cimmerian structures (Seghedi et al., 2004);

- the *Balkanides*, representing an Alpine fold-and-thrust belt developed between the Moesian Platform to the north and the Rhodope Massif to the south. They are formed by three north-vergent units: Fore-Balkan, Stara Planina and Srednogorie (Banks, 1997; Dinu et al., 2002).

- the *Rhodope Massif* between the Balkanides to the north and the Western Pontides to the east, consisting of a Palaeozoic and Precambrian basement which was affected by Variscan and Mesozoic (pre-Maastrichtian) deformations (Burg et al., 1996; Banks, 1997; Nikishin et al., 2003);

- the *Western Pontides* (or Istanbul Zone) characterized by a Late Proterozoic Pan-African crystalline basement (Stephenson et al., 2004; Ustaömer and Rodgers, 1999), with granitoids of 590 to 560 Ma age (Stephenson et al., 2004; Chen et al., 2002). The basement is overlain by a semi-continuous Palaeozoic succession, which ranges from the Early Ordovician to Late Carboniferous (Stephenson et al., 2004; Görür et al., 1997; Dean et al., 2000). The Carboniferous succession comprises coal measures of economic importance in the eastern part of the Western Pontides (Stephenson et al., 2004). The Palaeozoic deposits are overlain by thick Triassic red terrigenous sandstones and conglomerates. Jurassic sandstones and limestones lie unconformably over the Triassic deposits and are in turn overlain by thick Lower Cretaceous turbidites possibly related to the initial opening of the western Black Sea (Stephenson et al., 2004; Görür, 1988; Tüysüz, 1999; Sunal and Tüysüz, 2002). The Maastrichtian-Palaeocene time span is represented by chalk and the Eocene by thick turbidites (Stephenson et al., 2004). The region has been above sea level since the Miocene;

- the *Central and Eastern Pontides* (or Sakarya Zone) having a stratigraphy and tectonic development different from that of the Western Pontides. The basement comprises Triassic accretion-subduction units called the Karakaya Complex (Stephenson et al., 2004; Tekeli, 1981; Okay and Tüysüz, 1999). In the Central Pontides, this complex includes a metabasic phyllite-carbonate association and voluminous highly deformed clastic rocks (probably representing accreted seamounts), deepsea cherts and trench turbidites (Stephenson et al., 2004; Ustaömer and Robertson, 1994, 1997). The Jurassic-Lower Cretaceous time span is represented by sandstones and limestones (Stephenson et al., 2004; Yigitbas et al., 1999). The juxtaposition of the Sakarya Zone and the Istanbul Zone occurred in the Cretaceous during the closing of the Intra-Pontide Ocean and the opening of the western Black Sea basin (Stephenson et al., 2004; Okay et al., 1994);

- the *Achara-Trialet Zone* northeast of the Eastern Pontides, characterised by a Cretaceous magmatic arc lying on a Palaeozoic basement affected by Eocene rifting (Lordkipanidze, 1980; Karyakin, 1989; Nikishin et al., 2001, 2003);

- the *Great Caucasus Alpine Orogen,* which results from the closure of a former Jurassic-Eocene back-arc basin during Late Eocene to Recent times (Milanovsky, 1991; Ershov et al., 1998, 1999, 2003; Nikishin et al., 1998, 2001, 2003); and

- the *Southern Crimea Orogen*, to the north of the Black Sea. It is about 50 km wide and 150 km long and is arcuate in shape, with an E-W structural trend in the east and a NE-SW trend in the west (Stephenson et al., 2004). It has experienced pre-Bajocian, pre-Callovian and intra-Berriasian orogenic phases (Nikishin et al., 2001, 2003).

  The Southern Crimea Orogen consists of three main structural complexes (Stephenson et al., 2004; Mileyev et al., 1996). The Lower complex is made up of a Triassic-Bathonian flysch series, including olistostromes, calc-alcaline volcanics and molasse units. The Middle complex comprises Late Jurassic to Berriasian terranes. Both the lower and middle complexes are deformed, with south and southeast vergent fold and thrusts that culminate in the Berriasian (Stephenson et al., 2004; Koronovsky and Mileyev, 1974; Khain, 1984; Mileyev et al., 1996, 1997). The Upper complex includes Early Cretaceous to Eocene platform cover formations.

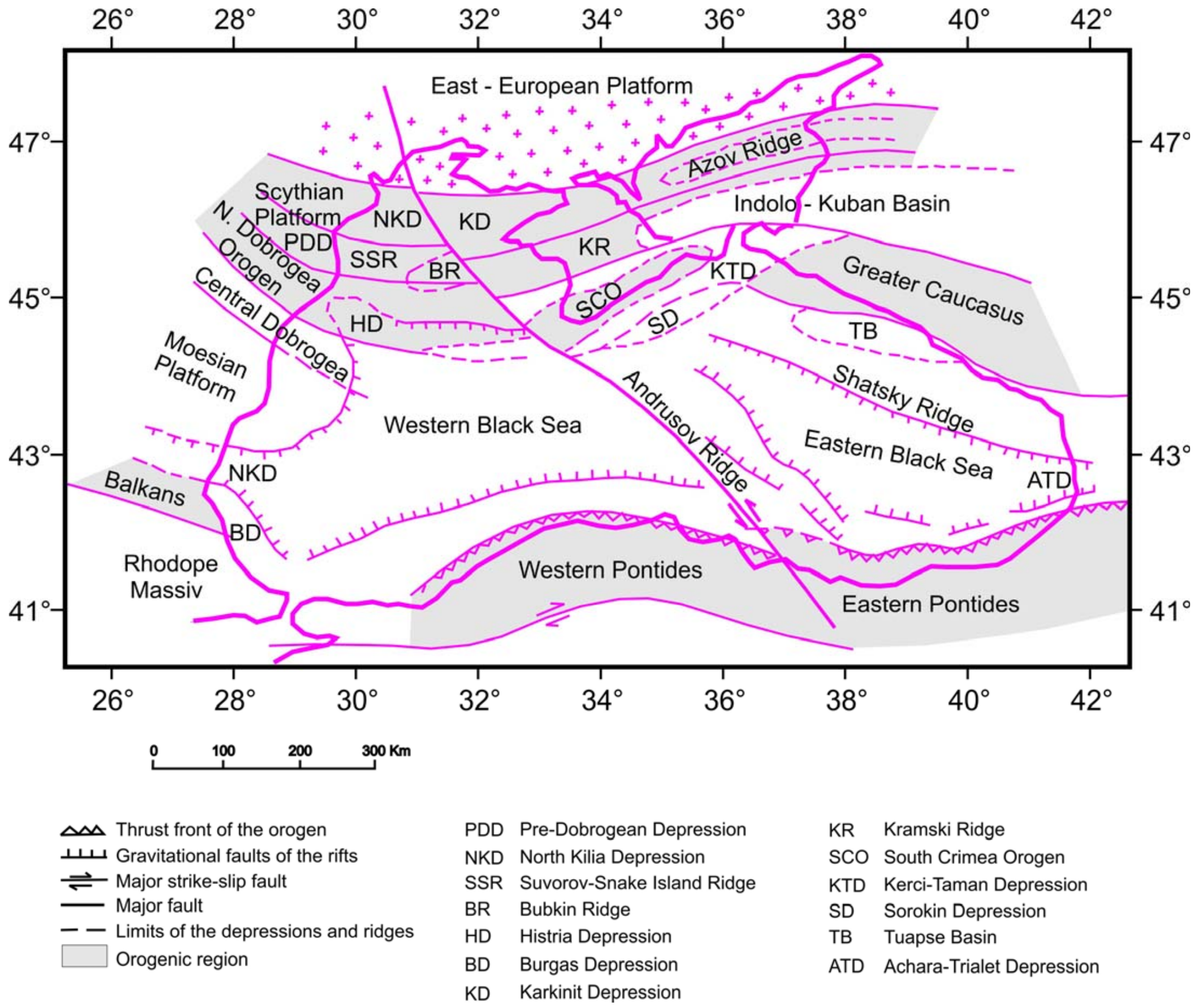

Figure 2.1 Tectonic map of the Black Sea region (from Dinu et al., 2002).

2.2. Physiography of the Black Sea

The Black Sea can be subdivided into four physiographic provinces (Fig. 2.2):

- *Shelf*: delineated by the 100-m isobath except offshore of the Crimean Peninsula and in the Sea of Azov where it extends to 130 m.
- *Basin slope*: it has two subtypes: steep gradients (1:40) highly dissected by canyons, and relatively smooth slopes.
- *Basin apron*: smooth and gently sloping area (1:40 to 1:1000) at the base of the basin slope that is the analogy of a continental rise.
- *Abyssal plain*: very flat area (<1:1000) similar to a deep-sea abyssal plain.

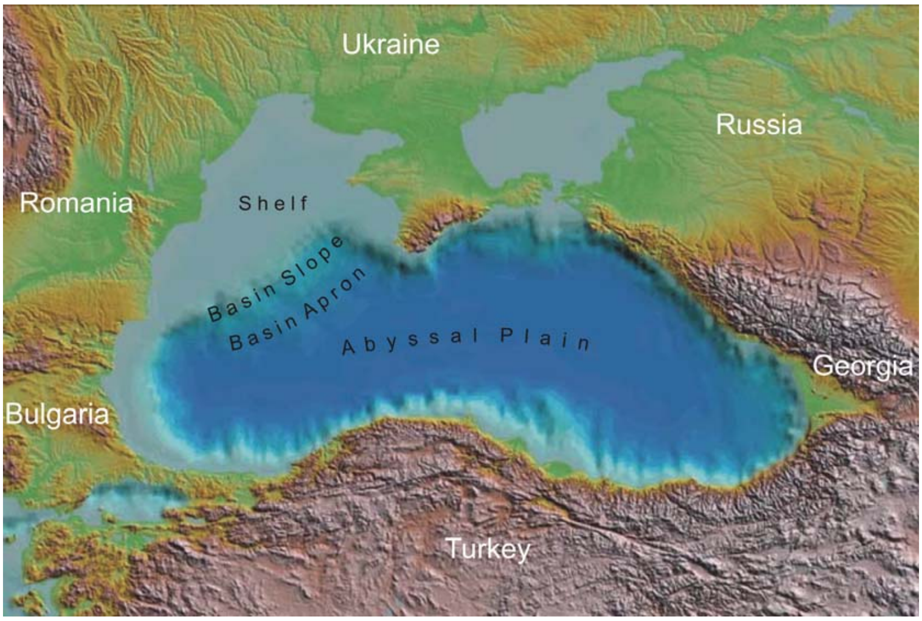

Figure 2.2 Physiographic map of the Black Sea region.

2.3. Structural and sedimentological development of the Black Sea basin

The development of the present-day Black Sea is controlled by Cretaceous and Tertiary events, the Triassic and Jurassic extension and compression have lesser direct relevance (Fig. 2.3).

During the Permo-Triassic to the Middle Jurassic, the Paleotethys Ocean subducted to the south. The Pre-Triassic stratigraphy of the Black Sea consists of Palaeozoic sediments: Silurian to Lower Devonian shales, Devonian to Carboniferous carbonates and Upper Carboniferous clastics and coals. These overlie metamorphic rocks (Proterozoic or Early Palaeozoic sediments) or granitic metamorphic rocks (Robinson et al., 1996). Permian deposits are found on the Moesian Platform and contain red bed clastics, limestones, evaporates and volcanics (Robinson et al., 1996). The Permian is represented by a regional unconformity. The Triassic consists of red beds deposited on this Permian unconformity and contains Middle Triassic limestones and aeolian sandstones on the northern Turkish coast. The Late Triassic is represented by flysch and volcanics with ophiolites, indicating the opening of a short-lived Triassic-Early Jurassic oceanic back-arc basin as a result of the northward subduction of the Neotethys during this time span. Flysch deposition continued through the Early Jurassic in the Pontides, Crimea, Romania and Bulgaria. Above these is another unconformity of Middle to Late Jurassic age which resulted from the Cimmeride Orogeny, when rifting of the Neotethys led to the split-up of the Cimmeride continent from Gondwana (Robinson et al., 1996). A compressive, magmatic event took place as a possible result of microplate collision and closure of the Triassic-Early Cretaceous back-arc basin (Ustaömer and Robertson, 1994; Robinson et al., 1996). This compression is more evident in the Strandzha Range in Bulgaria (Chatalov, 1990), in North Dobrogea (Visarion et al., 1990) and in the Crimea (Karantsev, 1982). During the Late Jurassic and Neocomian, the entire

Black Sea region was covered by carbonate deposits. Evaporites were deposited locally off the coast of Romania and Bulgaria (Robinson et al., 1996).

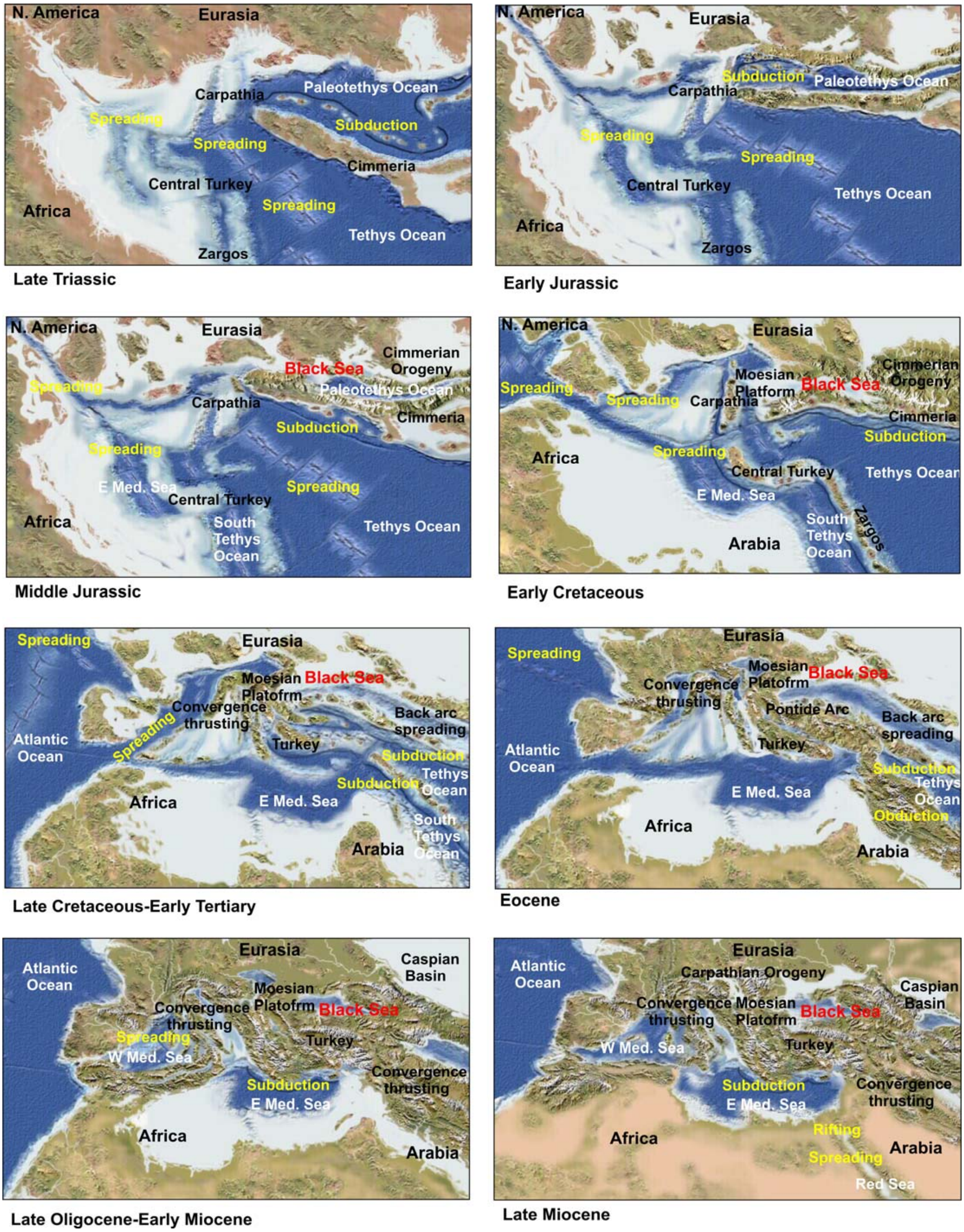

Figure 2.3 Plate tectonic development of the Black Sea area from the Late Triassic to the Late Miocene (http://jan.ucc.nau.edu/~rcb7/paleogeographic_alps.html).

After this period the Black Sea basin started to open on the northern side of an island arc as a result of the northward subduction of the Neotethys.

The time of opening of the Black Sea basin is still a subject of debate. According to Görür (1988) and Banks and Robinson (1997), rifting of the western Black Sea basin began in the Late Barremian, and continued to Albian or Cenomanian time. The time of opening of the eastern basin is less certain, but it may have started to rift in the mid-Palaeocene. The two basins coalesced into a single basin in their post-rift phase in the Pliocene (Banks and Robinson, 1997).

Banks and Robinson (1997) and Okay et al. (1994) suggested that the Western-Central Pontides were a fragment of the Moesian and Scythian platforms that rifted from the Romanian-Ukrainian Black Sea shelf, leaving the Black Sea basin behind. This is based on the similarity between the stratigraphy of the Western Pontides and the Moesian Platform (Săndulescu, 1978; Banks and Robinson, 1997). The Western Pontides became involved in compressional deformation in the Late Eocene-Oligocene (Görür, 1988; Okay et al., 1994; Banks and Robinson, 1997). This required the presence of two strike-slip transfer margins on the eastern and western sides of the western Black Sea. Banks and Robinson (1997) placed the western transfer margin across Thrace between Strandzha and the Western Pontides, but its exact position is obscured by Eocene sediments. Its offshore extension into the Black Sea is also obscured by the Tertiary compressive deformation fronts of Strandzha and the Balkanides (Dachev et al., 1988, Banks and Robinson, 1997). The original Cretaceous position of the western transfer margin also cannot be accurately determined. Banks and Robinson (1997) disagreed with the offshore location proposed by Okay et al. (1994) because the fault (mapped by Okay et al., 1994) is not visible in the seismic data; they suggested a more westerly position.

Okay et al. (1994) and Banks and Robinson (1997) differ in opinion on the proposed location of the eastern transfer margin of the western Black Sea basin as well. Okay et al. (1994) suggested that it stretched from the North Kilia Depression to the present-day depocenter of the western Black Sea basin. Banks and Robinson (1997) could not map any fault seismically in the North Kilia Depression, nor on the Turkish Shelf, nor in the deep basin. They therefore proposed that this margin lay further to the east along the southwestern edge of the Andrusov Ridge (Fig. 2.1).

Nikishin et al. (2003) proposed that the Black Sea basin opened from the Cenomanian to the Coniacian in about 10 million years, and that both the western and the eastern Black Sea basins originated during this period. During the Senonian, a compressional phase took place in the Black Sea, reaching its maximum in Maastrichtian to pre-Eocene times.

Robinson et al. (1996) affirmed that rifting in the Western and Central Pontides started in the mid-Cretaceous based on facies and thickness variations in the Aptian-Albian stratigraphy (Görür, 1988). The age of rifting in the eastern Black Sea basin is more difficult to determine, but Golmshtok et al. (1992) suggested that it may be Jurassic from seafloor heat flow measurements.

Subduction of the Neotethys ceased in the Eocene. The Late Palaeocene to Middle Eocene was a time of passive infill of both basins, with limestones on the shelves and clastic turbidites in the deep basin. Extensional tectonics dominated in the Pontides and in the Trans-caucasus during parts of the Eocene (Yilmaz et al., 1997; Nikishin et al., 2001, 2003). Compression started in the Late Cretaceous in the southern Pontides, and in the Greater Caucasus in the Palaeocene, becoming widespread in the Late Eocene (Robinson et al., 1996). Half-grabens in the Pontides became inverted, minor inversion structures on the Romanian shelf and Gulf of Odessa formed and the Balkanides developed during this period. During the Eocene, the deep basin was affected by a subsidence phase that was accompanied by large-scale basaltic, alkali-basaltic and andesitic volcanism and the accumulation of volcaniclastic flysch (Nikishin et al., 2003). Anoxic conditions developed in all basin deeps, and muds and basin floor clastics were deposited until the Late Miocene. The Oligocene to Quaternary was characterized by multiple phases of compression associated with collision between Eurasia and the Arabian continent that affected the Caucasus-Pontides-Black Sea region (Dercourt et al., 1993; Nikishin et al., 2003). In the Late Miocene, uplift of the Carpathians led to shoaling in the basin (Ross, 1978; Robinson et al., 1996). The water depth at the center of the basin was reduced to a few hundred meters. The sea level rose through the Late Miocene and Pliocene. During the Pleistocene, the Black Sea was disconnected from the Mediterranean Sea and became a lake, changing from marine to lacustrine conditions.

2.4. Pre-Miocene geology of the northwestern Black Sea

2.4.1. Pre-Miocene stratigraphy of the Romanian shelf

2.4.1.1. Introduction

Two megasequences have been identified across the Romanian shelf. The boundary between these two megasequences is the Post-Eocene - Pre-Oligocene unconformity. Within each of these megasequences several seismic sequences can be recognised (Moroşanu, 2002).

- *The lower megasequence* consists of pre-Oligocene formations and can be subdivided into two sequences:
  a) a *pre-Albian sequence*, less known because the seismic resolution decreases with depth and wells reached only its upper part. However, a few wells penetrated the Proterozoic, Ordovician, Silurian, Triassic, Jurassic and Neocomian formations;
  b) an *Albian-Oligocene* sequence, well-known and mapped over the entire Romanian shelf. In this interval oil and gas pools have been discovered.

- *The upper megasequence* is made up of Oligocene to Quaternary formations and covers the entire Romanian shelf. The unconformity that separates the Sarmatian-

Badenian formations from the Oligocene succession divides this megasequence into two sequences: one *Oligocene* in age and the other *Miocene-Quaternary*.

These two megasequences can be recognised only offshore, because the formations onshore are of Jurassic age or older except in the Babadag Basin where the Cretaceous is present, and in Southern Dobrogea where the Cretaceous and the Palaeocene are present locally.

Information on the lithology and age of the main tectonic units in Dobrogea, *viz*. the Pre-Dobrogea Depression, the North Dobrogea Orogen and the Moesian Platform (which is subdivided into Central and Southern Dobrogea), was obtained from wells drilled on the shelf and from geophysical data. The wells drilled in this area reached the Infracambrian, Palaeozoic, Triassic, Jurassic, Cretaceous, Palaeogene and Neogene formations.

2.4.1.2. Stratigraphy of the structural units on land

Pre-Dobrogea Depression

Offshore wells do not exist in the Pre-Dobrogea Depression. To reconstruct its stratigraphy (Fig. 2.4), information from wells drilled onshore and in the Danube Delta was used. The oldest succession in this area is of Vendian-Lower Cambrian age and consists of sandstones, tuffs and argillaceous tuffs. The Ordovician comprises argillaceous sequences, while the Silurian is made up of argillites interbedded with limestones and marls (Dinu et al., 2002). This is followed by a calcareous sequence of the Middle Devonian-Lower Carboniferous *Rosetti Formation* and by silts and sandstones of the Carboniferous-Permian *Sulina Formation*. The Triassic is very well developed and is represented by (1) the Lower Triassic *Lacul Roşu Formation* that contains argillites, sandstones and micro-conglomerates interbedded with effusive rocks, (2) the Middle Triassic *Obretin Formation* consisting of shallow carbonate platform deposits developed only in the southern Danube Delta, and (3) the Upper Triassic *Caraorman Formation* made up of calcareous sandstones interbedded with siltstones and marls (Dinu et al., 2002). The Jurassic is represented by Upper Bajocian-Lower Oxfordian argillaceous sediments and Oxfordian-Tithonian calcareous rocks. These deposits have a thickness of 800-2000 m. The Lower Cretaceous is developed only in several areas and contains a red continental facies of sandstones, siltstones, shales and marls (Dinu et al., 2002).

North Dobrogea Orogen

The North Dobrogea Orogen (Fig. 2.4) is a zone of transpressive deformations of Hercynian and Alpine age, delimited by the Sf. Gheorghe Fault to the north and the Peceneaga-Camena Fault to the south. Onshore, it comprises three tectonic units: the *Măcin unit*, the *Consul-Niculițel unit* and the *Tulcea unit* (Fig. 2.5).

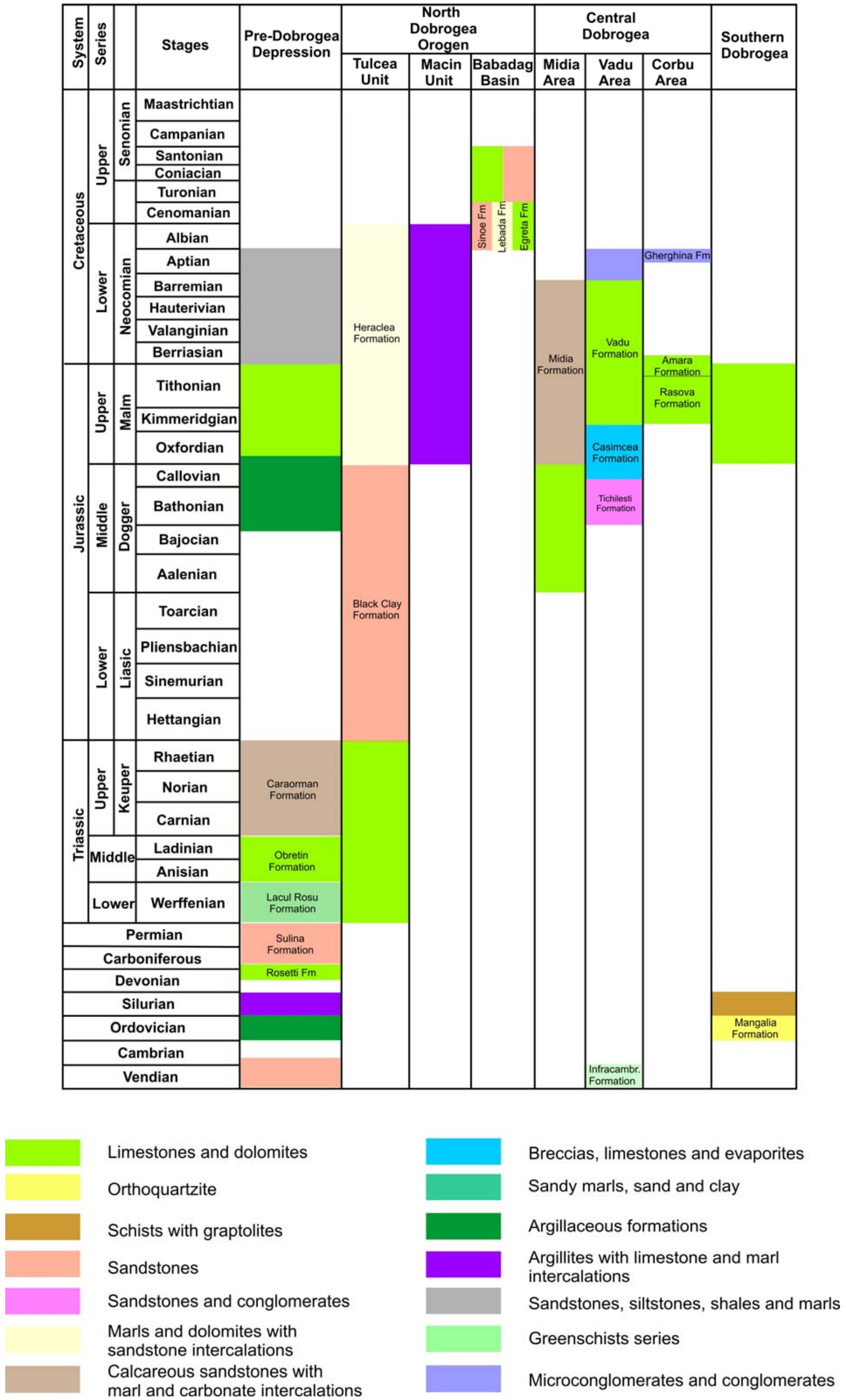

Figure 2.4. Stratigraphic column for the Pre-Dobrogea Depression, North Dobrogea Orogen, and Central and South Dobrogea in Romania on land (from Ionescu, 2000).

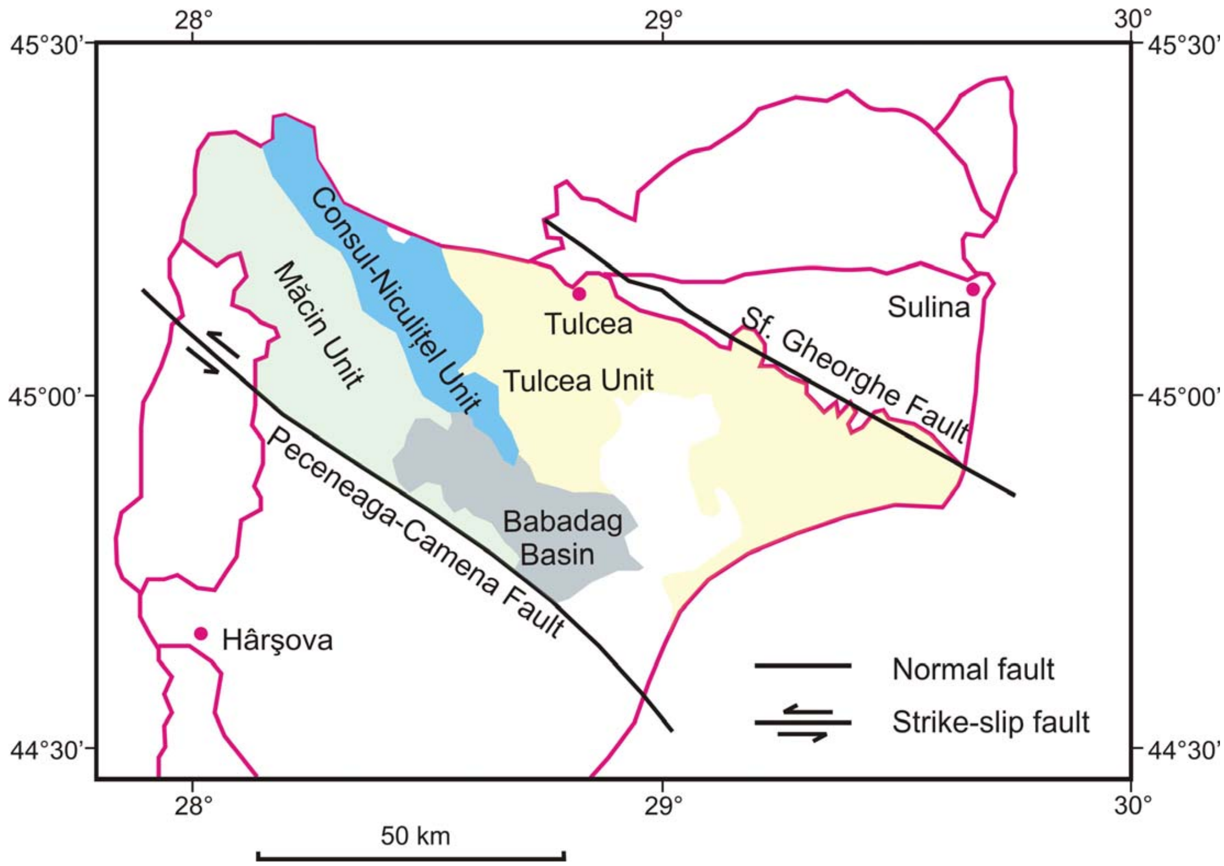

Figure 2.5 Tectonic map of the North Dobrogea Orogen, showing the four main tectonic units: Măcin, Consul-Niculițel and Tulcea units, and the Babadag Basin.

These three units are separated by the following tectonic lines (Mureşan, 1974; Săndulescu, 1984; Ionescu, 2000): the *Luncavița-Consul line* which separates the Măcin and Consul-Niculițel units, and the *West Isaccea-Telița-Posta-Trestenic-Izvoarele-Mihai Bravu-Babadag-Enisala line* that separates the Consul-Niculițel and Tulcea units. The southern part of these units is overthrusted by a post-tectonic cover, the *Babadag Basin*. Geological formations of the Măcin unit, the Tulcea unit and the Babadag Basin have been identified offshore.

An overview of the main tectonic units of the North Dobrogea Orogen from borehole data is given below:

- *The Tulcea unit*. This unit contains formations of Triassic, Jurassic and Lower Cretaceous age. The Triassic succession is made up of microcrystalline limestones and white and yellow dolomites. Its thickness is over 1200 m at the coast (wells *2* and *3 Razelm* in Fig. 2.6), thinning to several tens of meters farther offshore (wells *30 Sinoe*, *814* and *816 Lebăda* in Fig. 2.6). The Jurassic *Black Clay Formation* consists of black and silty argillites with intercalations of siltstones and quartzitic sandstones and is about 1190 m thick (well *13 Heracleea* in Fig. 2.6). The Upper Jurassic-Neocomian *Heracleea Formation* is a marly sequence with intercalations of arenite and siltstones and is about 600 m in thickness (wells *13* and *15 Heracleea* in Fig. 2.6).

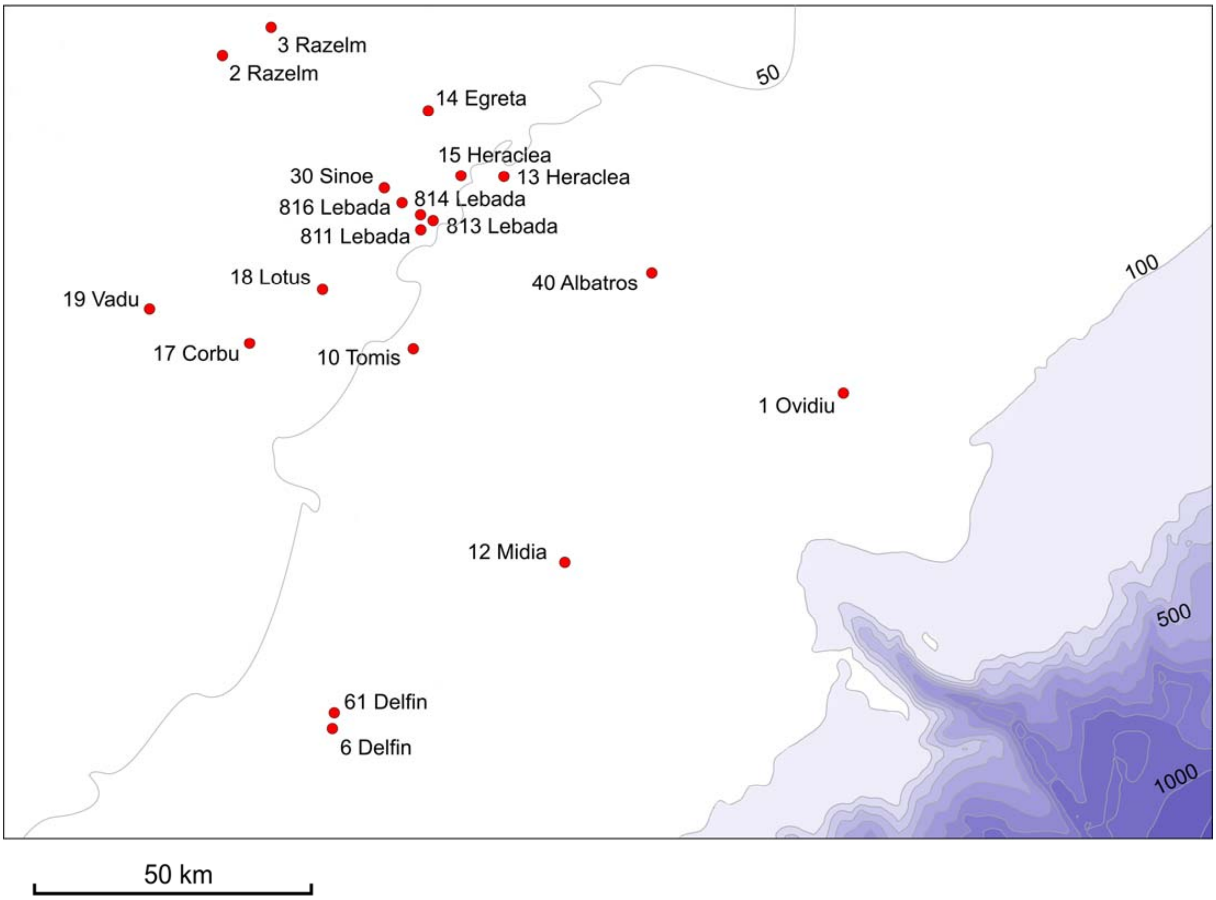

Figure 2.6 Position of the wells on the Romanian shelf used for the stratigraphic description presented here.

- *The Măcin unit*. This unit occurs south of the Lebăda area (wells *18 Lotus* and *10 Tomis* in Fig. 2.6) and consists of Upper Jurassic-Neocomian volcanogenic sedimentary formations. It is made up of black and grey shales and silty argillites. The two wells penetrated a basaltic-andesitic volcanic body with a thickness of 84 m at *18 Lotus* and 441 m at *10 Tomis.* The Lotus formation is 500 m in thickness.

- *Babadag Basin*. It consists of a post-tectonic cover superposed on the Tulcea and Măcin units and is deposited during two different sedimentary cycles:
  <u>*Albian-Cenomanian*</u>. During this time interval sediments of different facies were deposited.
  a) *the Sinoe Formation*: consists of fine to coarse quartzitic sandstones developed in the Sinoe and West Lebăda areas;
  b) *the Lebăda Formation*: marls, marly limestones and argillaceous siltstones developed in the *East Lebăda*, *18 Lotus* and *13 Heracleea* areas (Fig. 2.6);
  c) *the Egreta Formation*: made up of carbonate deposits in the*14 Egreta* and *40 Albatros* areas (Fig. 2.6).
  <u>*Turonian-Senonian*</u>. Two facies have been identified:

c) a *calcareous formation* in the Lebăda, Sinoe, Heracleea, Lotus and Tomis areas. It is represented by micritic limestones, chalky limestones, siliceous limestones, marly limestones and marls;
d) a *shaly sandstone formation* which occurs only in the *811* and *813 West Lebăda* and *40 Albatros* areas (Fig. 2.6), and consists of fine-to-medium sandstones and siltstones with shale intercalations.

Central Dobrogea

Central Dobrogea is bounded by the Peceneaga-Camena Fault to the north and by the Capidava-Ovidiu Fault to the south. Its basement consists of Upper Proterozioc greenschists overlain by Jurassic and Lower Cretaceous rocks of different facies deposited in the areas of the wells *12 Midia*, *17 Corbu* and *19 Vadu* (Fig. 2.6). The major lithostratigraphic units recognised in this area are: the Tichileşti Formation, the Casimcea Formation, the Midia Formation, the Vadu Formation and the Cernavodă Formation (Fig. 2.4).

- *The Midia area*. It lies 60-80 km from the shoreline. The Middle Jurassic here is represented by a calcareous series of grey to yellowish bioclastic limestones. The Upper Jurassic-Neocomian *Midia Formation* contains a calcareous sandstone sequence with limestone and marl intercalations. This sequence is >1 km in thickness.

- *The Vadu area*. It is situated 20-30 km from the shoreline and the oldest deposits drilled here are of Infracambrian age (Dinu et al., 2002). It is made up of the following formations:
  a) the *Infracambrian Formation* containing a greenschists series made up of green greywacke, micro-conglomerates and argillites (Dinu et al., 2002);
  b) the Bathonian-Lower Callovian *Tichileşti Formation* made up of sandstones and conglomerates (Dragastan, 1993; Georgescu, 1994; Băncilă et al., 1997; Dinu et al., 2002);
  c) the Upper Callovian-Lower Kimmeridgian *Casimcea Formation* which contains limestones overlain by an evaporitic to calcareous sequence. It has a thickness of 270 m;
  d) the Upper Jurassic-Lower Cretaceous *Vadu Formation* made up of limestones, salt, gypsum, anhydrite and dolomites. It has a total thickness of 1250 m; and
  e) the Aptian formation comprising micro-conglomerates and conglomerates with intercalations of siltstones and marls. The total thickness is 250 m.

- *The Corbu area*. The oldest formation drilled in this area is Kimmeridgian-Tithonian deposits of a dolomitic to calcareous sabkha series attributed to the *Rasova Formation* (Dragastan, 1993; Dinu et al., 2002). Overlying this formation is another sabkha series made up of micritic limestones and dolomites of Tithonian-Lower Berriasian age, *viz.* the *Amara Formation* (Dragastan, 1993; Dinu et al., 2002). The succeeding section consists of calcareous deposits of foraminiferal limestones attributed to the *Cernavodă*

Formation (Grădinaru et al., 1989; Dragastan, 1993; Dinu et al., 2002). The Barremian-Lower Aptian deposits are made up of calcareous breccia and micritic limestones. The Middle Aptian-Upper Aptian *Gherghina Formation* consists of micro-conglomerates and reddish shales (Dinu et al., 2002).

South Dobrogea

The wells *6* and *61 Delfin* (Fig. 2.6) drilled in this area penetrated the following formations (Fig. 2.4):

- an *Ordovician* formation comprising orthoquartzites and quartzwackes with a thickness between 200 and 520 m; it is equivalent to the *Mangalia Formation* of South Dobrogea;
- a *Silurian* sequence of graptolitic schists about 400 m in thickness; and
- an *Upper Jurassic* calcareous formation made up of limestones and marly limestones.

2.4.1.3. Stratigraphy of the structural units on the Romanian shelf

The wells drilled on the Romanian shelf were concentrated in the offshore continuation of the North Dobrogea Orogen because of its importance for hydrocarbon exploration in this area. Very few wells were drilled in the offshore continuation of the Central and Southern Dobrogea, namely in the Corbu, Delfin and Vadu areas. Most of the wells – *Ovidiu*, *Cobălcescu*, *Midia*, *Histria*, *Pescăruş*, *Poseidon*, *Sinoe*, *Iris*, *Tomis*, *Lotus*, *Unirea*, *West Lebăda*, *East Lebăda*, *Portița* and *Minerva* – penetrated only the Mesozoic and Cenozoic deposits. Only the wells drilled in the Delfin area penetrated Palaeozoic rocks.

Offshore North Dobrogea Orogen

The oldest deposits drilled in the offshore prolongation of the North Dobrogea Orogen are Triassic in age and are represented by a detrital and a calcareous facies (Fig. 2.7). Well *50 Venus* reached the Lower Triassic Veruccano conglomerates with a thickness of about 400 m (Luțac, 2000). These deposits are made up of polymicritic conglomerates and greyish-red and brownish-red argillaceous sandstones. The onshore wells *2* and *3 Razelm* penetrated the Middle Triassic succession with 1211 m of microcrystalline carbonates (*2 Razelm*) and 1390 m of white-yellowish and yellow dolomites (*3 Razelm*). The well *30 Sinoe* reached carbonates including greyish dolomites and brownish limestones. The wells *814*, *816* and *817 Lebăda West* penetrated the Upper Triassic, which contains grey, compacted limestones. These are correlated with the Middle Triassic rocks from the North Dobrogea Orogen and the Pre-Dobrogea Depression and have some similarities with the stratigraphic equivalents on the Moesian Platform.

The Middle Jurassic is represented by the *Black Clay Formation* (Fig. 2.7) which reaches a thickness of 100-300 m in the West Lebăda area, becoming thicker northward (up to about 1200 m in the Heracleea area). It is made up of black to reddish shales intercalated with polygenic conglomerates and greyish sandstones. These deposits are similar to the Middle Jurassic formations of the Pre-Dobrogea Depression, but they are more affected by faulting. The Upper Jurassic was drilled on the southern margin of the Histria Depression – the offshore continuation of the North Dobrogea Orogen – in the Vadu, Corbu and Heracleea areas. The Upper Jurassic-Neocomian interval is represented by the *Lotus Formation* (Fig. 2.7; Grădinaru et al., 1989) made up of calcareous sandstones, micro-conglomerates, marls and carbonates with a thickness of about 1000 m (Luțac, 2000). The Lotus Formation was also found in the 10 Tomis, 18 Lotus and 16 Iris wells. Rocks of the *Heracleea Formation* (Fig. 2.7) were also found in Upper Jurassic-Neocomian formations of the Heracleea and Egreta areas. The lower part of this formation is made up of greyish-green and greyish-brown, compacted marls and marly-limestones intercalated with white-greyish, compacted limestones. The middle part has predominantly fine-to-coarse grained, brown-greyish, compacted, quartzitic sandstones intercalated with compacted quartzitic micro-conglomerates and greyish to grey-brownish, compacted clays and silty-clays. The fossil-rich upper part is represented by greyish, compacted marls and carbonates. Microscopically, fragments of ostracodes, foraminifers and gastropods were identified. In the well *15 Heracleea*, two sequences of this formation could be separated: a lower sequence made up of green-greyish, compacted dolomites intercalated with green-greyish, compacted marls and quartzitic sandstones, and an upper sequence which contains grey to brown-greyish, compacted marls intercalated with clays and limestones. In the well *14 Egreta*, this succession is represented by greyish marls and marly carbonates. The depositional environment for the Heracleea Formation is supposedly shelfal to lagoonal.

The Lebăda area comprises Barremian-Albian detrital deposits (Fig. 2.8) made up of compacted, grey to greyish-green quartzitic sandstones with a shaley-calcareous cement alternating with weakly cemented porous-permeable quartzitic sandstones. The Barremian has a thickness ranging from 40 to 150 m here, while it is missing in the western and northern part of the study area. These deposits are similar to the Southern Dobrogea marine facies.

The Cenomanian section (Fig. 2.8) represents the continuation of the sedimentation that started in the Albian and has a thickness of 13 to 84 m in the Lebăda area and up to 200 m in the western part of the Histria Depression. Lithologically, it is made up of greyish, quartzitic marls, quartzitic sandstones with a carbonate cement, and greyish, coarse-grained carbonates. In the upper part, it is intercalated with white, shaley carbonates that announce the succeeding epicontinental, calcareous sedimentation.

Turonian deposits (Fig. 2.8) occur only in the Lebăda area and are up to 50 m in thickness. In the lower part, they comprise greyish to green-greyish, quartzitic sandstones with argillaceous-carbonate cement, fine- to coarse-grained carbonates intercalated with polygenic breccio-conglomerates. In the upper part, they are made up of white, argillaceous carbonates. The change from a quartzitic to a carbonate facies is the result of a sea-level rise accompanied by an increase in the accommodation space and a decrease in the source area. The detrital facies is similar to the Turonian deposits in Southern Dobrogea.

The Senonian (Fig. 2.8), represented by the Coniacian, Santonian, Campanian, and the Maastrichtian, occurs in the Lebăda and Midia areas and has a thickness ranging from 150 to 400 m in the Lebăda area and 57 m in the Midia area. Calcareous sedimentation of the Turonian continued during this time interval and is represented by white to white-yellowish, argillaceous carbonates succeeded by fine-grained, calcareous sandstones. In the Midia area, the Senonian overlies the Aptian deposits and is overlain by Eocene deposits. It is made up of white-greyish argillaceous, silty carbonates and argillaceous carbonates with foraminifera. It is similar to the same formations in the Babadag Basin, and in Central and Southern Dobrogea.

Offshore Central Dobrogea

Middle Jurassic deposits (Fig. 2.7) were the oldest drilled on the offshore continuation of Central Dobrogea. The well *12 Midia* penetrated Bathonian-Callovian deposits made up of 43 m of yellow-greyish limestones (Ionescu, 2000). The well *19 Vadu* penetrated a detrital sequence of sandstones and conglomerates having a thickness of 14 m. Dragastan et al. (1993), Georgescu (1994) and Băncilă et al. (1997) attributed this sequence to the *Tichileşti Formation*.

The Upper Jurassic-Neocomian *Midia Formation* was reached in the well *12 Midia* (Fig. 2.7). It comprises calcareous sandstones, locally micro-conglomerates, intercalated with marls, breccia and limestones. In the well *19 Vadu*, a 200 m thick sequence made up of limestones and calcareous breccias was recognized. It can be correlated to the *Casimcea Formation* (Grădinaru et al., 1989; Dragastan et al., 1993; Băncilă et al., 1997). Breccio-calcareous evaporitic deposits of the *Vadu Formation* overlie the Casimcea Formation. These are in turn overlain by a sequence of limestones with foraminifera, attributed by Grădinaru et al. (1989), Dragastan et al. (1993) and Băncilă et al. (1997) to the *Cernavoda Formation*.

Starting with the Barremian (Fig. 2.8), a transgressive sedimentary regime began on the Romanian shelf that was interrupted in the Aptian and resumed in the Albian until the end of the Cretaceous. The Barremian-Lower Aptian deposits were recognized by Băncilă et al. (1987) in the well *17 Corbu*. They are represented by calcareous breccias intercalated with Valanginian limestones (Ionescu, 2000). The Middle and Upper Aptian deposits were drilled in the well *19 Vadu*. They are lithologically similar to the *Gherghina Formation* and are represented by micro-conglomerates with effusive rocks, Triassic and Jurassic limestones, sandstones and red to yellow, kaolinitic clays.

Offshore Southern Dobrogea

Offshore Southern Dobrogea, about 40 km from Mangalia, two wells in the Delfin area (*6* and *61 Delfin*) have been drilled (Fig. 2.6). The oldest deposits penetrated by the well *6 Delfin* are Ordovician in age and comprise 350 m of white-greyish orthoquartzites (Fig. 2.7). These deposits are overlain by Silurian schists with graptolites, which have a thickness

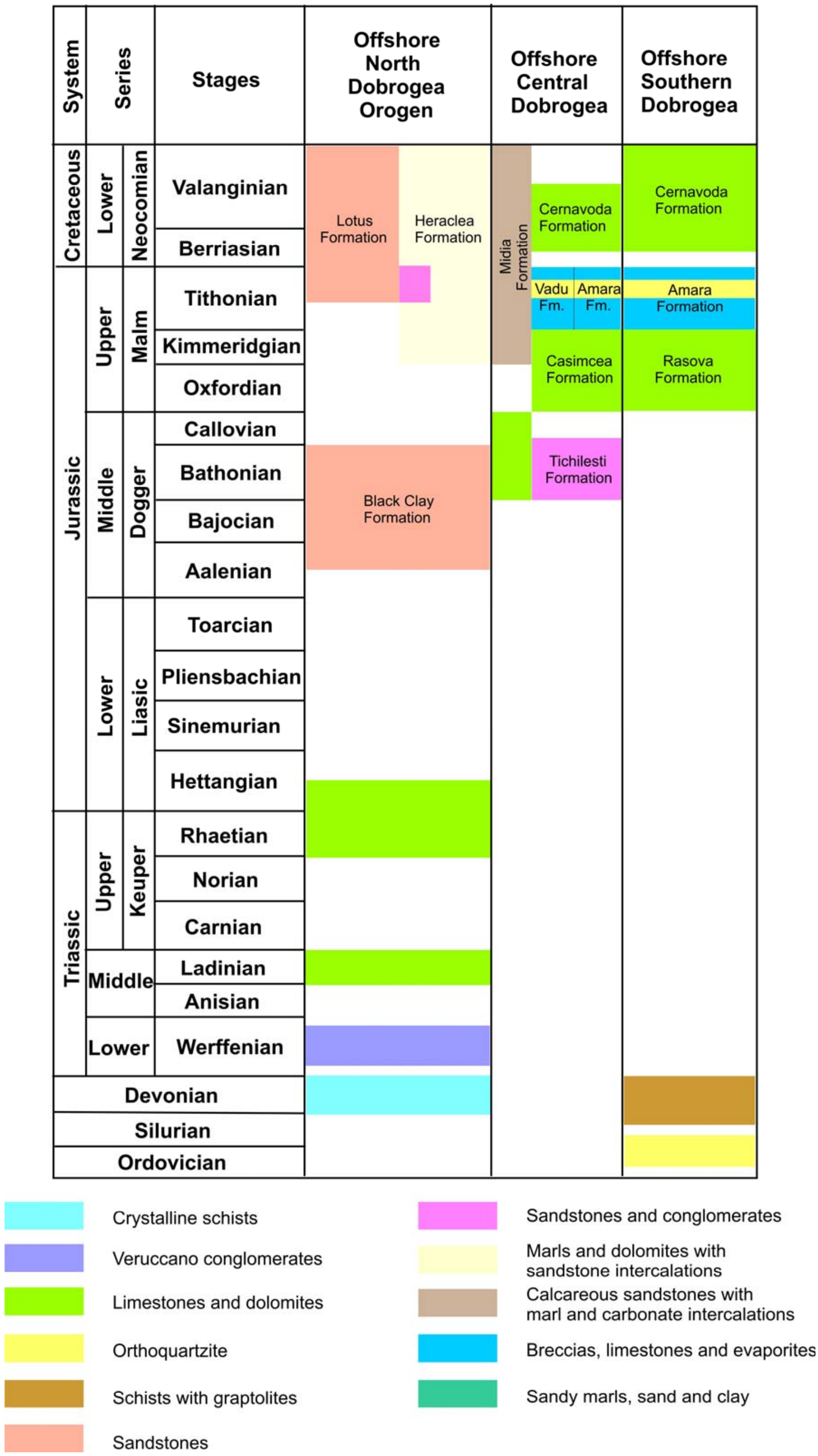

Figure 2.7 Stratigraphic column of the Romanian shelf from the Ordovician to the Lower Cretaceous (from Ionescu, 2000).

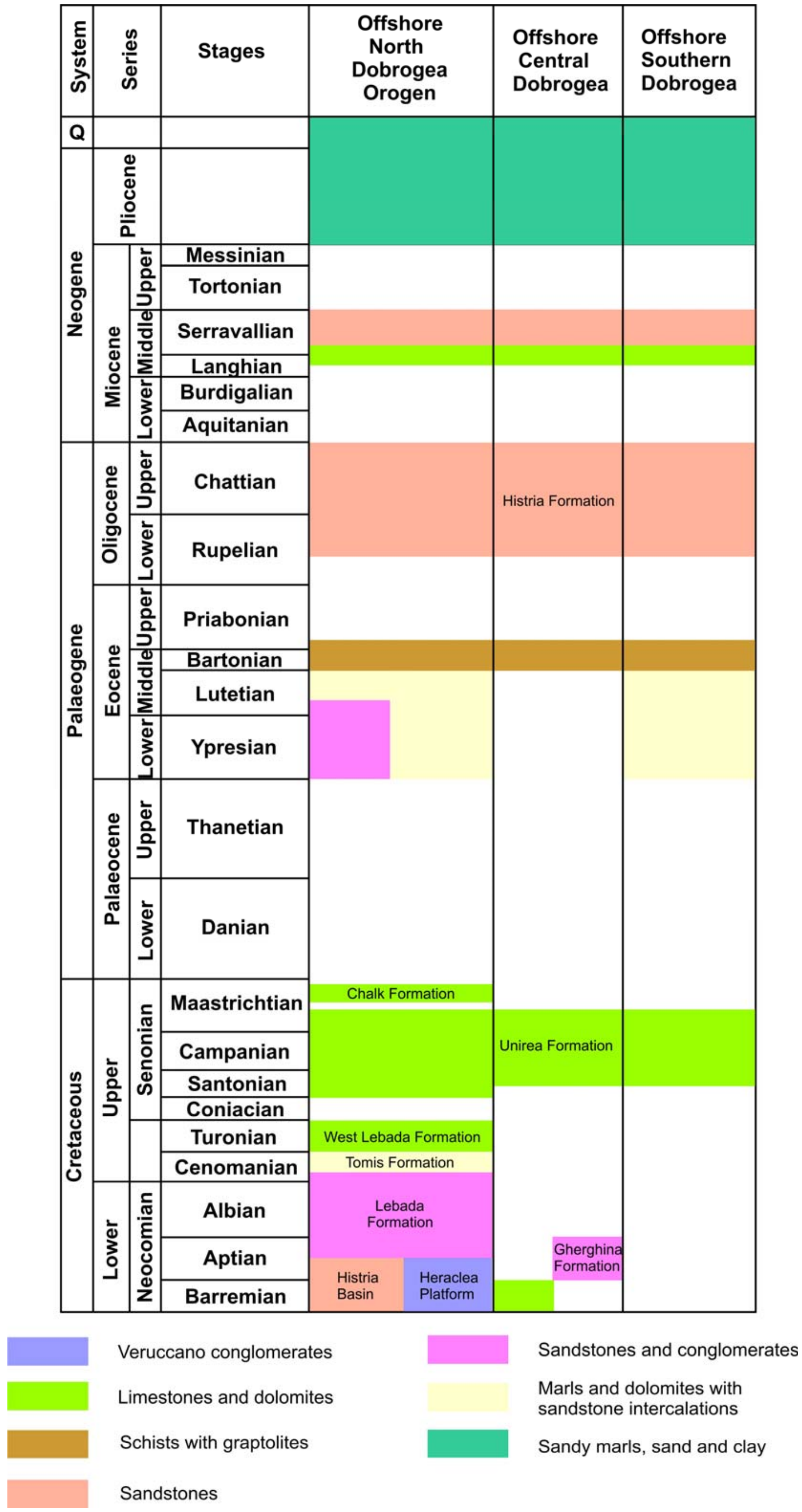

Figure 2.8 Stratigraphic column of the Romanian shelf from the Lower Cretaceous to the present (from Ionescu, 2000).

of about 400 m. Above these deposits is a carbonate sequence, the *Rasova Formation*. It is Upper Jurassic (Oxfordian-Tithonian) in age and is made up of micritic limestones intercalated with rhombohedral dolomite crystals.

Palaeogene formations

The Palaeogene and Neogene deposits are not related to onshore sections of the same age but are uniformly distributed over the entire shelf (Fig. 2.8). The depositional area was affected by the Cretaceous-Lower Palaeocene *Laramian movements*, the Eocene seccession being deposited directly over the Cretaceous. In the Lower Eocene, turbidite sedimentation predominated, especially in the West Lebăda area (Dinu et al., 2002). The depo-area expanded in the Middle Eocene and the shale fraction increased during this time (Dinu et al., 2002). The Eocene section varies in thickness, depending on the tectonic units of the Dobrogea. Offshore of the North Dobrogea Orogen, where the basement was more mobile, the Eocene sediments are over 1500 m thick. In tectonically less active Central Dobrogea, the Eocene reaches a thickness of only about 200 m, while in Southern Dobrogea, the deposits are about 600 m thick. The Middle-Upper Eocene is represented by two facies, a *marly-calcareous* (deep-sea) facies and a *calcareous-argillaceous* facies (Dinu et al., 2002). The former occurs in the East Lebăda, Venus, Albatros and Lotus areas and has a thickness up to 2000 m. Lithologically it is made up of greyish, compacted shaley limestones and greyish to white-greyish marls. The calcareous-argillaceous facies is present everywhere on the Romanian shelf but is thinner. It is made up of greyish, black-greyish to green-greyish, compacted calcareous shales.

At the end of the Upper Eocene and the beginning of the Oligocene, the Pyrenean orogenesis dominated. The sea level dropped, leading to widespread erosion. Eocene sediments from the shelf were removed and transported into the basin (Dinu et al., 2002). During the Oligocene, the sea-level rise associated with rapid subsidence led to pelagic sedimentation. The Oligocene basin filled during this time. The onlap terminations of the strata suggest that sedimentation kept pace with subsidence (Dinu et al., 2002). Except *13 Heracleea*, all wells drilled on the Romanian shelf penetrated the Oligocene section. They are represented by a bituminous shale facies which is the main source rock for hydrocarbons. At the base of the Oligocene, there is an increase in carbonate sedimentation interspersed with deposition of greyish quartzitic sandstones and brown-yellowish dolomites. The Oligocene deposits have a thickness of up to 2500 m on the outer shelf and thin to the northwest until they wedge out, being absent in the Vadu area. To the north, its thickness is below seismic resolution.

2.4.2. Pre-Miocene structure of the Romanian shelf

2.4.2.1. Introduction

The Romanian sector of the Black Sea lies to the east and southeast of the Danube Delta and has an area of over 35,000 km^2. The Romanian shelf with an area of 20,000 km^2 is very wide. It has a water depth of less than 100 m (Robinson et al., 1996) and is dominated by Mid-Cretaceous extensional structures and their sedimentary cover (Robinson, 1996). Subsequently, the area was affected by Tertiary compression (Robinson, 1996).

Seismic data show a continuation of the main faults in the Dobrogea region onto the Romanian Black Sea shelf. These faults include the *Sf. Gheorghe Fault* which separates the Pre-Dobrogea Depression from the North Dobrogea Orogen, the *Peceneaga-Camena Fault* which separates the North Dobrogea Orogen from the Moesian Platform (identified on the shelf for over 60 km) and the *Capidava-Ovidiu Fault* separating Central and South Dobrogea from the Moesian Platform (Fig. 2.9).

The seaward extension of the land structures dips to the east and is covered by Eocene, Oligocene and Neogene deposits. Beginning with the Oligocene, the geological evolution of the Romanian shelf was decoupled from that of the land.

According to Moroşanu (2002), three main tectonic phases can be distinguished on the Romanian shelf:

- *The first stage* begins in the Jurassic and continues until the Albian. During this period, extensional tectonics took place with the opening of a NW-SE oriented rift. This rift developed in direct connection with opening of the western Black Sea basin. In the Albian, the Histria Depression and its landward continuation, the Babadag Syncline to the north of the Peceneaga-Camena Fault, were created (Dinu et al., 2002). Extension was very active in the Albian and continued until the Upper Cretaceous with reduced activity.

- *The second stage* took place from the Upper Cretaceous to the Eocene. During this time, rifting ceased and the depositional rate increased. The entire depression was filled with Upper Cretaceous deposits, with Eocene carbonates covering only the highest areas. On the margins of these areas, the Eocene is a sandy-calcareous prograding facies.

- *The third stage* developed during the post-Eocene to Lower Oligocene. It is characterised by inversion tectonics, going from an extensional to a compressional regime. In the Moesian Platform, reverse faulting occurred; in the central unit, former listric faults became inverted as a result of compression.

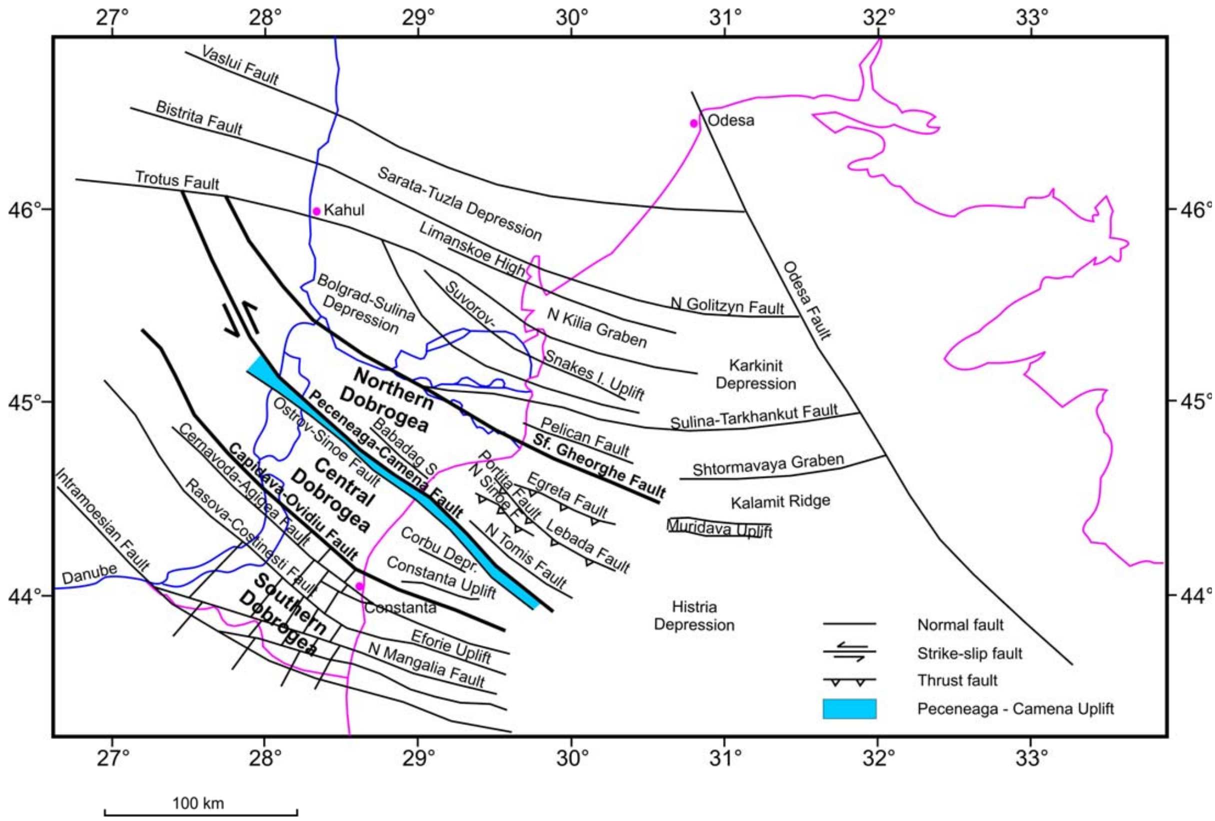

Figure 2.9 Structural map of the major Romanian onshore tectonic structures and their offshore prolongations (from Dinu et al., 2002).

The Oligocene succession was deposited in a deep subsiding basin and Mio-Pliocene sediments filled the entire depositional area. The subsidence decreased in the Miocene and the Pliocene and very thick detrital deposits accumulated on the eastern part of the Romanian shelf.

2.4.2.2. Pre-Albian structures

These structures are the offshore continuations of the tectonic units that existed in the Dobrogea region before the opening of the western Black Sea basin. They include major strike-slip faults, normal faults and reverse faults which divide the area into a series of horsts and grabens. Deposits up to the Albian were affected. Reactivation of some of these faults has led to deformations up to the Upper Cretaceous and in places the Eocene strata.

From the north to the south, the following faults on the Romanian shelf were seismically identified (Fig. 2.9):

- the *Sulina-Tarkhankut Fault*, a reverse fault which probably represents the contact between the North Dobrogea Orogen and the Pre-Dobrogea Depression;
- the *Sf. Gheorghe Fault*, representing a strike-slip system that developed as a continuation of the Sf. Gheorghe branch of the Danube Delta;

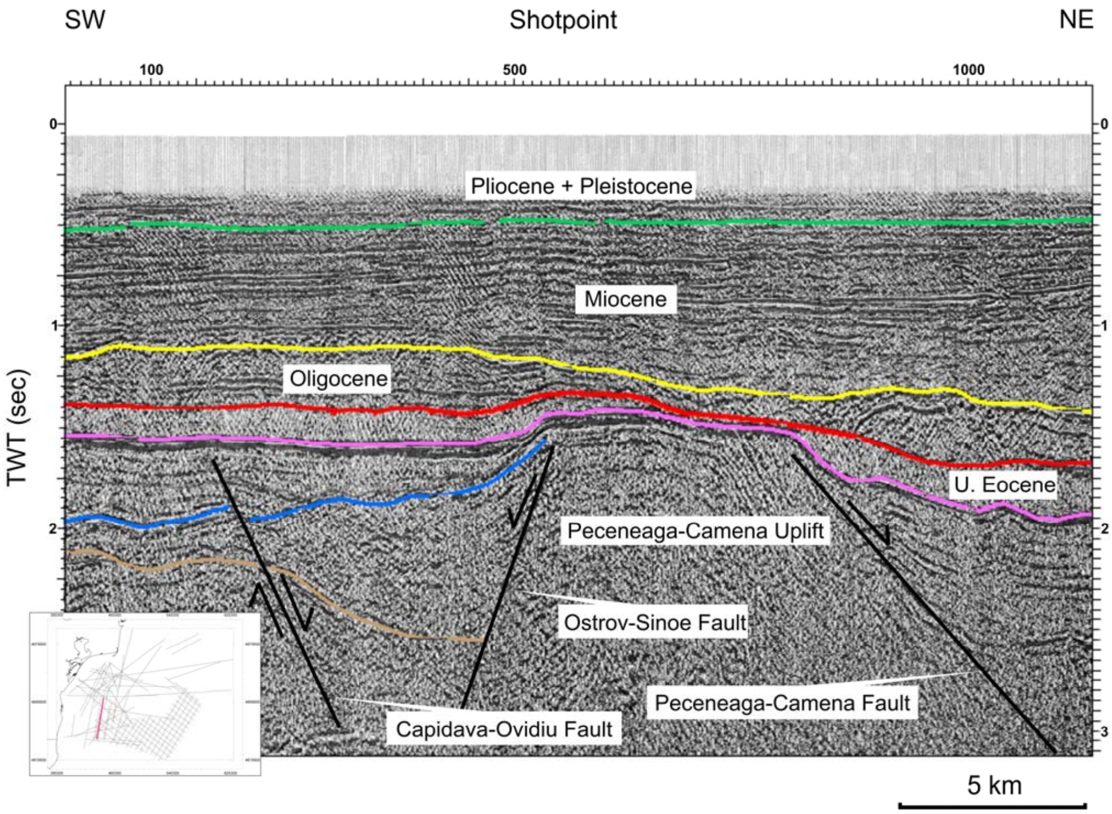

Figure 2.10 Seismic profile illustrating the position of the Peceneaga-Camena, Ostrov-Sinoe and Capidava-Ovidiu faults and the Peceneaga-Camena Uplift.

- the *Peceneaga-Camena Fault* (Fig. 2.10), which is a sinistral strike-slip fault that separates the North Dobrogea Orogen in the north from the Moesian Platform in the south. This fault can be followed very well offshore up to and including the Midia area. To the southeast is the Peceneaga-Camena Uplift, an uplifted block 5-7 km in width and bounded to the south by the *Ostrov-Sinoe Fault* (Fig. 2.10). The Peceneaga-Camena Uplift bends in the vicinity of the wells *18 Lotus* and *10 Tomis* to the north and *17 Vadu* to the south. Why this occurs is unknown from the available seismic data. The Peceneaga-Camena Uplift controlled sedimentation during the Upper Cretaceous because it separated the uplifted Central Dobrogea from the subsiding Histria Basin. During the Palaeogene, although sedimentation took place in a single basin, this uplift still separated two areas of different mobility: While in the Histria Basin the Eocene sediment reaches 1500 m, offshore Central Dobrogea only a few hundred meters were deposited;

- the *Capidava-Ovidiu Fault* (Fig. 2.10), which is a deep-reaching fault that separates Central Dobrogea from Southern Dobrogea. It is well-identified on the seismic sections near the coast and poorly-defined eastward; and
- a series of subvertical faults south of the Capidava-Ovidiu Fault that produced many uplifted and subsided blocks (Fig. 2.11).

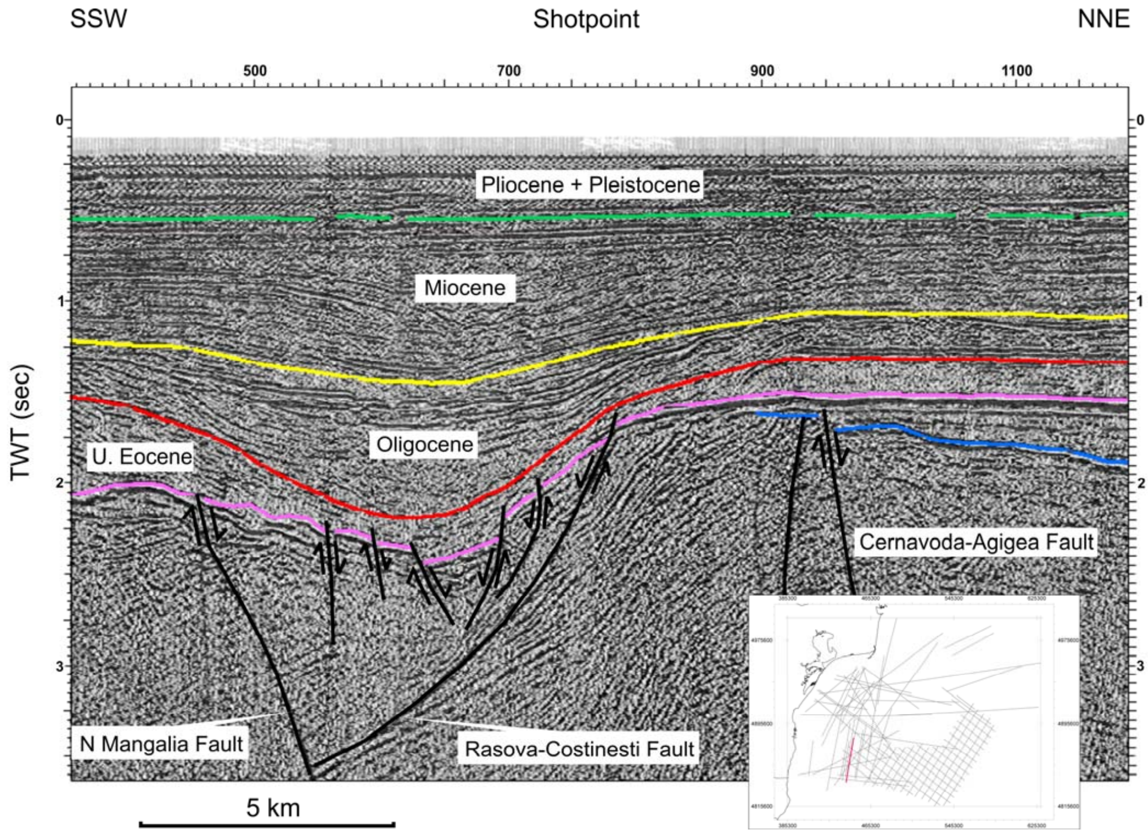

Figure 2.11 Seismic profile illustrating the position of the North Mangalia, Rasova-Costineşti and Cernavodă-Agigea faults.

2.4.2.3. Extensional structures

Extensional tectonics on the Romanian shelf is directly related to opening of the western Black Sea basin. North of the Peceneaga-Camena Fault, a half-graben was created during the Albian, namely the Histria Depression and its landward continuation, the Babadag Basin. The northern flank of this half-graben is marked by several faults affected by inversion tectonics (Egreta, Portița, Lebăda and Sinoe).

- The *Egreta Fault* is a reverse fault and is the northernmost fault that can be mapped on our seismic profiles (Fig. 2.12). The total thickness of sediments affected by this fault is more than 4000 m, while the displacement of the fault at the basement is about 600 m (Ionescu, 2000).

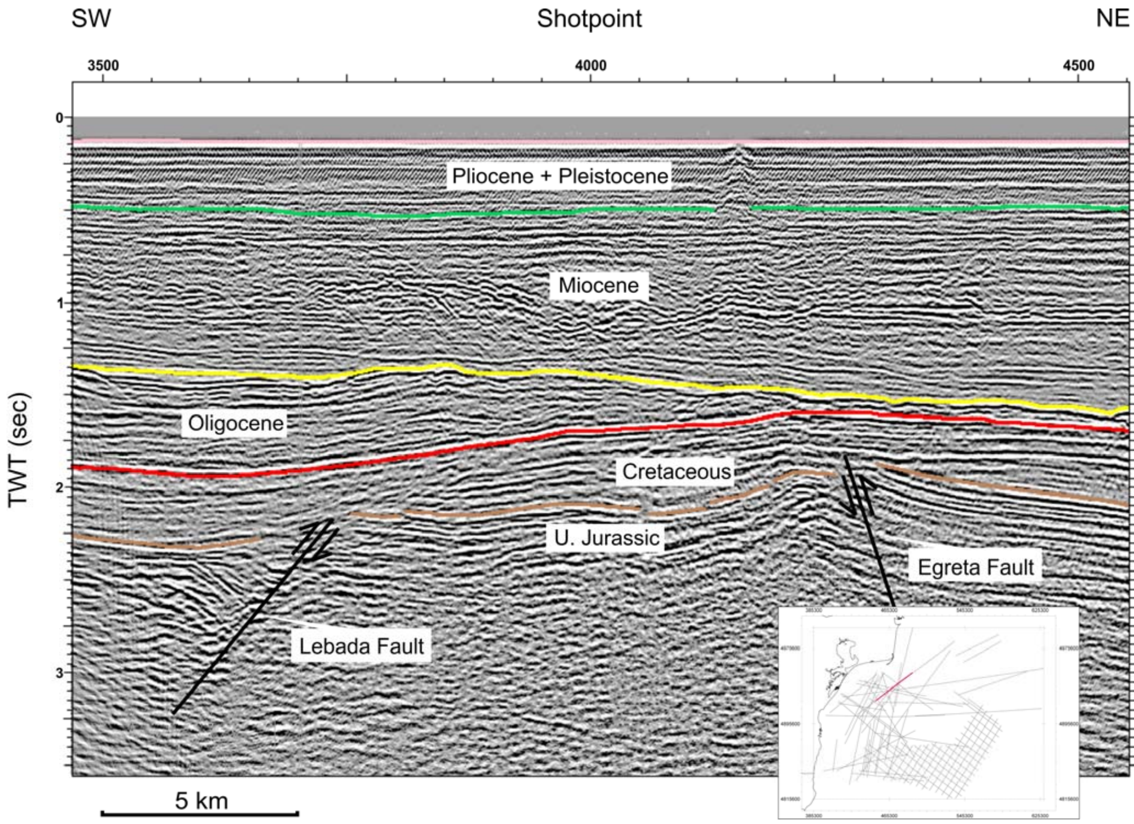

Figure 2.12 Seismic profile illustrating the Egreta and Lebăda faults.

- The *Portița Fault* (Fig. 2.13) played an important role in the evolution of the northwestern Histria Basin because it exercised an active control on the sedimentary processes (Ionescu, 2000). This fault can be followed only over a small distance. To the west it cannot be mapped because of the lack of seismic data and east of the mapped segment it is not recognisable on our seismic profiles. The depth and displacement of the Portița Fault are difficult to estimate because of the low seismic resolution, but are supposed to be similar to those of the Egreta Fault (Ionescu, 2000).
- The *Sinoe Fault* (Fig. 2.13) is situated south of Portița Fault and has a similar extent. Seismic data suggest a reactivation of this fault up the Eocene. The displacement of the fault varies from 300-400 m at its base to about 100 m at the top of the Eocene (Ionescu, 2000).

Eocene and Oligocene sedimentation in the Histria Depression was controlled by the Laramian and Pyrenean orogenic phases when inverted structures were produced. The reverse faults on the northern flank of the Histria Depression were presumably also formed during this period (Dinu et al., 2002).

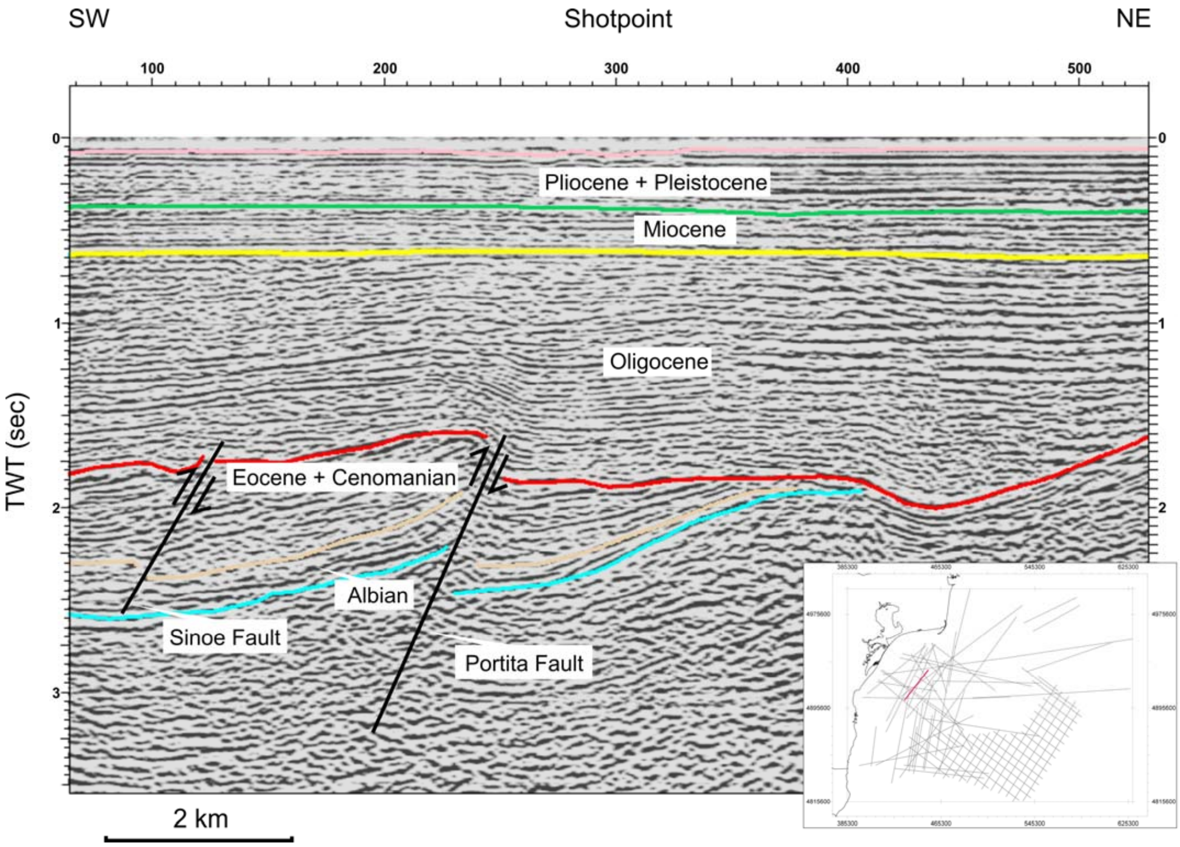

Figure 2.13 Seismic profile illustrating the Portița and Sinoe faults.

3. Data and Methods

3.1. Data

The present study is based on reflection seismic profiles and borehole data that were made available by the Romanian oil industry.

The seismic profiles were recorded and processed by the Romanian company Prospecțiuni S.A. between 1980 and 1994. For this study about 70 profiles situated on the Romanian shelf and on the continental slope with a total length of 5300 line-km are used for interpretation of the Mio-Pleistocene sequences. Velocity information from processing was used for depth conversion.

Apart from seismic data, depth and lithological information from 60 boreholes drilled on the Romanian shelf were available. Most of them are located on the inner shelf, particularly on the offshore prolongation of the North Dobrogea Orogen because of extensive hydrocarbon exploration in this area.

Locations of the seismic and borehole data are shown in Fig. 3.1.

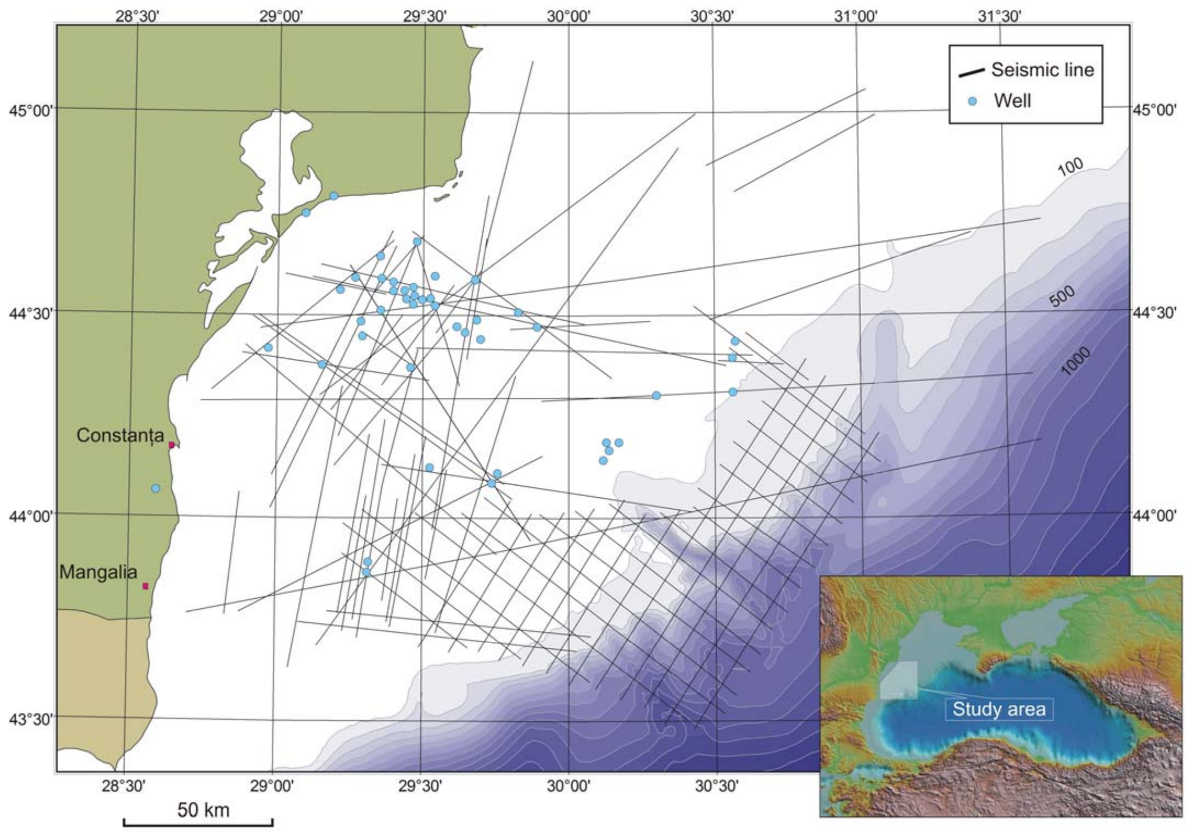

Figure 3.1 Location of the seismic lines and boreholes used in the present study.

3.2. Methods

3.2.1. Seismic stratigraphy

For an analysis of the sediment architecture, seismo-stratigraphic techniques were used. The seismo-stratigraphic method is based on the principle of seismic sequence and seismic facies analyses. Sequence stratigraphy is the study of genetically related facies within a framework of chronostratigraphically significant surfaces (Van Wagoner et al., 1990). A sequence is defined as a relatively conformable succession of genetically related strata bounded by unconformities or their correlative conformities (Mitchum, 1977). An unconformity is a surface separating younger from older strata, along which there is evidence of subaerial exposure and erosion that lead to a significant hiatus (Van Wagoner, 1988). A conformity is a surface separating younger from older strata, along which there is no evidence of erosion or non-deposition. In seismic stratigraphy, reflection terminations give information on the type of an unconformity: a non-depositional hiatus is represented by onlap, downlap, or toplap, while erosion is characterized by an erosional truncation.

Depositional sequences consist of major stratal surfaces and systems tracts, which are defined as a linkage of contemporaneous depositional systems (Brown and Fisher, 1977; Van Wagoner et al., 1990). Sequences are controlled by changes in relative sea level and are composed of the following elements: sequence boundary, lowstand systems tract, transgressive surface, transgressive systems tract, maximum flooding surface, highstand systems tract and the subsequent sequence boundary.

The *lowstand systems tract* (LST) follows the formation of the sequence boundary and forms during the time of relatively low sea level. If a distinct shelf-break exists and the relative sea level falls sufficiently, the LST may include two distinct parts: the *lowstand fan*, which consists of slope and basin-floor submarine fans and the *lowstand wedge*, built up by a progradational set of parasequences. In case of a system with no distinct shelf-break or if the relative sea level does not fall sufficiently, only a lowstand wedge may form. Following the relative fall, sea level reaches a stillstand and eventually begins to rise at a very slow rate. The slow rate of increase in accommodation coupled with a relatively high sediment input produces a progradational pattern corresponding to the lowstand wedge.

The lower boundary of the *transgressive systems tract* (TST) is formed by the transgressive surface, the TST itself consists of a retrogradational set of parasequences. The TST forms as the relative sea level continues to rise, producing additional accommodation space at a rate faster than it can fill with sediments. The upper boundary of the TST is marked by the maximum flooding surface.

The *highstand systems tract* (HST) overlies the maximum flooding surface. It consists of aggradational to progradational set of parasequences formed as the rate of relative sea level rise begins to slow, reaches a stillstand and eventually begins to fall. During the HST, accommodation space is created or destroyed at a relatively slow rate. As relative sea level begins to fall, the next sequence boundary forms, marking the end of the HST and completing the sea level cycle.

3.2.2. Depth-conversion of seismic data

The sequence boundaries and unconformities mapped on the seismic profiles, available in two-way travel time (TWT), have to be converted into depth for geological interpretation. This conversion was performed using the software package KingdomSuite.

For depth conversion, two types of data are required: a *TWT map*, available from the interpreted seismic data, and an *average velocity map*, computed from borehole information and velocities from processing. The average velocity describes the velocity between the seismic datum and a time surface (grid or horizon) or a specific formation top.

A *depth map* is generated by multiplying the average velocity values by the corresponding time surface values. The resulting depth map has the seismic datum as reference.

3.2.3. Subsidence analysis

3.2.3.1. Introduction

To reconstruct the subsidence history of the Romanian shelf starting with the Miocene, a subsidence analysis was carried out using the software package BasinWorks (a geohistory analysis program for Apple Macintosh computers).

The aim of a geohistory analysis is to produce a subsidence curve and the sediment accumulation rate through time. In order to do this, three corrections to the present-day stratigraphic thicknesses need to be done:

- *Decompaction*: present-day compacted thicknesses have to be corrected to account for the loss in porosity with depth of burial.
- *Paleobathymetry*: for correction of the effect of the water depth at the time of deposition.
- *Absolute sea level fluctuations*: to correct the paleosea level relative to the present-day sea level.

The addition of a sediment load to a sedimentary basin causes an additional subsidence. The total subsidence is therefore represented by the tectonic subsidence and subsidence due to the sediment load. The technique used to remove the effect of sediment load from the total subsidence to obtain the tectonic subsidence is called *backstripping*, which was also carried out using BasinWorks.

3.2.3.2. Data Input

The program requires an input of two files, one describing the stratigraphy, and a second containing compaction parameters.

- *The stratigraphic data file* contains a description of rock intervals and unconformities, which are defined by nine attributes:
  - *Top Depth* (*in feet*): represents the top of the interval, which is described in a data row. The top depth is referenced from the top of the lithologic column.
  - *Interval Name*.
  - *Surface Type*: this could have the following abbreviations: SB (sequence boundary), MFS (maximum flooding surface), CS (condensed section), TS (top of the lowstand prograding wedge or shelf margin wedge), TSFS (top of the slope fan), TBFS (top of the basin floor fan), or TOP (formation top).
  - *Age*: in million years before present.
  - *Paleobathymetry*: water depths in meters determined either from paleontology, paleoenvironmental data from lithofacies, measured from seismic data or approximated by compensating for sea-level fluctuations and a smooth tectonic subsidence history.
  - *Eustatic sea level*: altitude in meters of eustatic sea level for that time period.
  - *Top Depth* (*in meters*)*:* same as column 1.
  - *Thickness of each layer*
  - *Lithologic description*: up to 4 lithologies per interval are allowed; the total percentage must add up to 100%.

- *The compaction parameter file* permits a flexible definition of lithologies and their porosities as a function of depth and/or time. It contains the lithologic names, litho-logic ID number, rock density, maximum depth for which equation or constants are applied, equation number, initial porosity, and constants.

3.2.3.3. Main calculation

The main calculation in BasinWorks comprises five steps:

- Computation of the maximum burial depth for each unit.
- Estimation the present-day porosity using the maximum burial depth.
- Calculation of the initial thickness of each unit.
- Determination of the geological history of the stratigraphic column by calculating the compaction after the addition of each layer.
- Adjustment of the depth of the interval boundaries for changes in sea level and paleo-bathymetry.

The first step is the determination of the present-day porosity. This is done by calculating the maximum burial depth for each interval while accounting for erosion and compaction. The present porosity state is determined from the maximum burial depth since the time of deposition. The compaction functions are then used to calculate the typical porosity for that depth. Assuming that porosity did not change from that condition by time-variant processes, the resulting porosity is considered the present state. This computation is based on the following equation:

$$\phi = \phi_0 * e^{-cy} \tag{3.1}$$

where ϕ represents the porosity at the depth y, ϕ_0 is the present-day porosity, and c is a coefficient that shows the variation of porosity with depth (Athy, 1930; Hedberg, 1936; Rubey and Hubbert, 1960; Allen and Allen, 1990). The initial thickness of each interval is calculated by decompacting the present interval thickness and porosity to the porosity typical for each lithology at the average initial depth of the interval. The following equation was used for this computation (Allen and Allen, 1990):

$$y_2' - y_1' = y_2 - y_1 - \frac{\phi_0}{c} * \left[e^{-cy_1} - e^{-cy_2} \right] + \frac{\phi_0}{c} * \left[e^{-cy_1'} - e^{-cy_2'} \right] \tag{3.2}$$

where y_1 and y_2 are the present depth of the sedimentary section, y_2' and y_2' are the decompacted depths, and ϕ_0 and c are the same as in Eq. 3.1.

After the decompaction, a correction for sediment load follows. The density of the new layer (ρ_s) is a function of porosity and density of the sediment grain (ρ_{sg}):

$$\rho_s = \phi \rho_w + (1 - \phi) \rho_{sg} \tag{3.3}$$

where ρ_w is the density of water. Having calculated ρ_s for an individual layer, the mean sediment density for the total column $\overline{\rho_s}$ is given by:

$$\overline{\rho_s} = \sum_i \left[\frac{\overline{\phi_i} \rho_w + \left(1 - \overline{\phi_i}\right) \rho_{sgi}}{S} \right] * y_i' \tag{3.4}$$

where $\overline{\rho_i}$ is the mean density of the *i*th layer, ρ_{sgi} the sediment grain density of the same layer, y_i' the individual layer thickness, and *S* the total thickness of the column corrected for compaction (Allen and Allen, 1990).
The sediment load is then calculated using the following equation:

$$Y = S \left(\frac{\rho_m - \overline{\rho_s}}{\rho_m - \rho_w} \right) \tag{3.5}$$

where Y is the actual depth of the basement, S the observed thickness of sediment, $\overline{\rho_s}$ the mean sediment density, ρ_m the density of the mantle, and ρ_w the density of water (Allen and Allen, 1990).

The final corrections are adjustments for changes in sea level and paleobathymetry. Information on paleobathymetry comes from sources such as benthic microfossils, less importantly, sedimentary facies, and distinctive geochemical signatures. The true tectonic subsidence is calculated by accounting for all these corrections (Bond and Kominz, 1984; Allen and Allen, 1990):

$$Y = \Phi\left[S\left(\frac{\rho_m - \overline{\rho_s}}{\rho_m - \rho_w}\right) - \Delta_{SL}\left(\frac{\rho_w}{\rho_m - \rho_w}\right)\right] + \left(W_d - \Delta_{SL}\right) \tag{3.6}$$

where Φ is a basement function equal to unity for Airy isostasy, Δ_{SL} the paleosea level relative to the present, and W_d the paleowater depth.

3.2.3.4. Calculation of other parameters

BasinWorks also calculates some other parameters from the stratigraphic data, including:

- Interval thickness: the thickness of each interval through time corrected for compaction due to burial.
- Burial history: burial depth versus time for each interval corrected for sediment compaction.
- Geohistory: depth versus time for each interval corrected for sediment compaction, changes in sea level, and paleobathymetry.
- Interval density: average density of each interval calculated from theoretical compaction functions and maximum burial depth.
- Average density: average density for the entire sedimentary column through time corrected for sediment compaction and water loading.
- Total and tectonic subsidence history.
- Total and tectonic subsidence rates during the deposition of the section.

3.2.4. Stratigraphic modeling

3.2.4.1. Introduction

Stratigraphic modeling is an excellent tool for the reconstitution of depositional processes in a sedimentary basin. It estimates at the same time the influence of sedimentation rate, subsidence rate, and sea level changes during these processes.

In the present study, stratigraphic modeling of the Mio-Pleistocene deposits was carried out using the software package STRATA, a Unix program developed in the framework of the "Basin Research" program at the Pennsylvania State University, U.S.A.

STRATA consists of four separate programs:

- *Setbasin*, a pre-processor that allows the user to set the model parameters.
- *Simbasin,* which runs the simulated basin model with the user-defined parameters.
- *Plotbasin*, a post-processor that displays the model results.
- *Filmbasin*, which combines processing and post-processing to make a movie.

The simulation is based on the assumption that sediment transport behaves diffusively (volumetric flux is proportional to local gradient). For carbonate simulations, the sediment source is proportional to water depth, while for clastic simulation, the sediment source is a user-specified function.

3.2.4.2. Discussion of the controlling variables

In the following, the parameters defined in *Setbasin* and the way they influence the simulation will be discussed.

- Measures Group Parameters:
  - *Total width cover* specifies the horizontal span of the simulation.
  - *Spatial division* determines how many intervals the total width is divided into.
  - *Total time covered* specifies the duration of the simulation.
    - *Temporal divisions* determine how many intervals the duration will be divided into in calculating the time evolution of the basin.
    - *Timelines* determines how many recordings the simulator makes of the state of the simulation.

- Ages Group Parameters:
  - *Use even increments* specifies whether the ages of the time slices should be even divisions of the total duration.
  - *Age of nth time slice* specifies the ages of the individual time slices if they are not being automatically set to even increments.

- Clastic Group Parameters:

Both marine and non-marine transport rates are controlled by the topographic gradient:

$$q = -k \frac{\partial h}{\partial x} \tag{3.7}$$

where q is the volumetric sediment flux (L^2T^1) h is the elevation (L), x is the horizontal position (L), and k is the diffusion constant (L^2T^1). To generate a realistic shelf-break, the non-marine diffusion constant is set to a high value, while the marine diffusion constant is set to a much lower value.

Non-marine diffusion constant sets k in Eq. 3.7 in at least the non-marine zone (water depth less than zero).

Simulate marine sedimentation allows for k to vary between marine and non-marine zones.

Marine diffusion constant sets k in the marine zone if marine sedimentation is being simulated.

Decay coefficient for marine diffusion constant controls the rate of decay for marine diffusion from non-marine to marine values.

Left, right clastic fluxes define the flux entering the basin from each side.

- Carbonates Group Parameters:

This group of parameters deals with calcium carbonate sedimentation. The difference between $CaCO_3$ sedimentation and clastic sedimentation is that $CaCO_3$ sedimentation depends on water depth and can occur anywhere along the cross-section, while clastic sedimentation is defined by an input flux on the left- or right-side of the model, this flux being then redistributed by slope-dependent diffusion.

Carbonate file. Two carbonate deposition algorithms can be mixed together in a single profile, epeiric and carbonatic sedimentation. The carbonate file specifies what carbonate deposition operates at each point.

Epeiric sedimentation is given by the following equation (Gildner and Cisne, 1990):

$$\frac{d}{dt} sed = c_1 * \frac{w}{w_0} * e^{1-\frac{w}{w_0}}, w > 0 , \tag{3.8}$$

Epeiric $CaCO_3$ – maximum rate specifies c_1 in Eq. 3.8.

Epeiric $CaCO_3$ – depth of maximum rate specifies w_0 in Eq. 3.8.

Oceanic sedimentation is given by the equation (Gildner and Cisne, 1990):

$$\frac{d}{dt} sed = c_1 * e^{-c_2(w-w_0)}, w > w_0 , \tag{3.9}$$

Oceanic $CaCO_3$ sedimentation – maximum rate specifies c_1 in Eq. 3.9.

Oceanic $CaCO_3$ sedimentation – exp decay constant specifies c_2 in Eq. 3.9.

Oceanic $CaCO_3$ sedimentation – depth of maximum rate specifies w_0 in Eq. 3.9.

Lag on zero water depth controls carbonate lags when the system shoals to sea level.

- Sea-level Group Parameters:

  Sealevel file may be omitted completely or used to specify the eustatic curve in great detail.

  Time offset. At time T, eustatic calculations will use (T-offset) as the time.

  Datum for sealevel oscillations; sealevel oscillation amplitude, period define the eustatic curve in the absence of a sea-level file.

- Subsidence Group Parameters:

  Subsidence rate determines the driving subsidence rate, either as a number (a constant subsidence) or as a file.

  Profile is cratonic, foreland, or passive.

  Flexural isostatic compensation determines whether or not the surface of the earth behaves as an elastic plate.

  Flexural rigidity controls the elastic flexural response of the earth to loads.

  Densities of air, crust, mantle, water; gravitational constant have obvious impact upon the loads flexing the surface.

- Compaction Group Parameters:

Compact sediments determines whether compaction occurs at all. STRATA accounts for the approach of Sclater and Christie (1980) and assumes that porosity is an exponential function of depth:

$$\phi = f * \phi_{0,sand} * e^{-\lambda_{sand} z} + (1-f) * \phi_{0,shale} * e^{-\lambda_{shale} z}, \tag{3.10}$$

where f is the sand fraction. The constant parameters are defined below:

  Let erosion affect compaction determines whether the effects of erosion is considered when compaction is calculated.

  Decay constant for sand, shale compaction specifies λ_{sand} and λ_{shale} in Eq. 3.10.

  Initial porosities for sand, shale specifies $\phi_{0,sand}$ and $\phi_{0.shale}$ in Eq. 3.10.

  Cut off for sand composition, decay constant for composition. STRATA may calculate in two different ways the sand-shale percentages: from diffusion constants or as a function of water depth. If c*ut off for sand composition* is set to a negative number, *decay constant for composition* becomes irrelevant and the composition is determined by linear interpolation of the diffusion constants. If c*ut off for sand composition* is zero or positive, then the composition is considered to be pure sand between the surface and this depth and decays exponentially with the specified constant below the cut off depth.

- Heat Flow Group Parameters:

STRATA calculates temperature distributions and thermal evolution of the basin by accounting only for vertical heat transport and assuming that the only heat source is flux supplied at the base of the basin. The temperature distribution is calculated from the following equation:

$$q = -k\frac{dT}{dz} \ , \tag{3.11}$$

where k is the thermal conductivity (W/mºC), T is the temperature (ºC), and q is the heat flux (W/m^2). The temperature is set at the sediment surface by specifying the temperature at the air interface and using

$$T = T_{air} - \alpha z \tag{3.12}$$

to determine the temperature at the sediment-water interface for underwater areas. Then the temperature at any location can be calculated.

The thermal conductivity is assumed to vary as a function of lithology and porosity:

$$k = \phi * k_{fluid} + (1-\phi) * [f * k_{sand} + (1-f) * k_{shale}], \tag{3.13}$$

where f is the sand fraction in the sand and shale, and ϕ the porosity.

Thermal flux specifies q in Eq. 3.11. It may be a number (constant flux) or a file, giving the thermal flux as a function of time.

Thermal conductivities of sand, shale, fluid specifies $k_{sand}, k_{shale}, k_{fluid}$ in Eq. 3.13.

Surface temperature specifies T_{air} in Eq. 3.12.

Surface temperature fall off specifies α in Eq. 3.12.

4. Geological Structure of the Mio-Pleistocene Formations on the Romanian Shelf

4.1. Introduction

An important tectonic element on the Romanian Black Sea shelf is the Histria Depression, the offshore prolongation of the Babadag Syncline, which represents the southern part of the North Dobrogea Orogen. This depression is bounded by a major structural feature, the "Euxinian Threshold", a zone in which the Palaeogene deposits are strongly subsiding (Ionescu, 2000; Pătruț, 1975). The Euxinian Threshold has three components:

- a NNE-SSW-oriented southern component,
- a NW-SE-oriented central component developed along the Peceneaga-Camena fault, and
- an ENE-oriented northern component, which is tectonically controlled by uplifted and subsided pre-Oligocene blocks.

The Euxinian Threshold represents a continental palaeo-slope developed during the Upper Eocene, but may also represent the limit of the shelf deposits during the Upper Cretaceous (Ionescu, 2000). The Histria Depression is the subsided block that developed between the central and the northern components of the Euxinian Threshold. Mio-Pleistocene sedimentation and tectonic processes in the study area are closely related to the development of this depression.

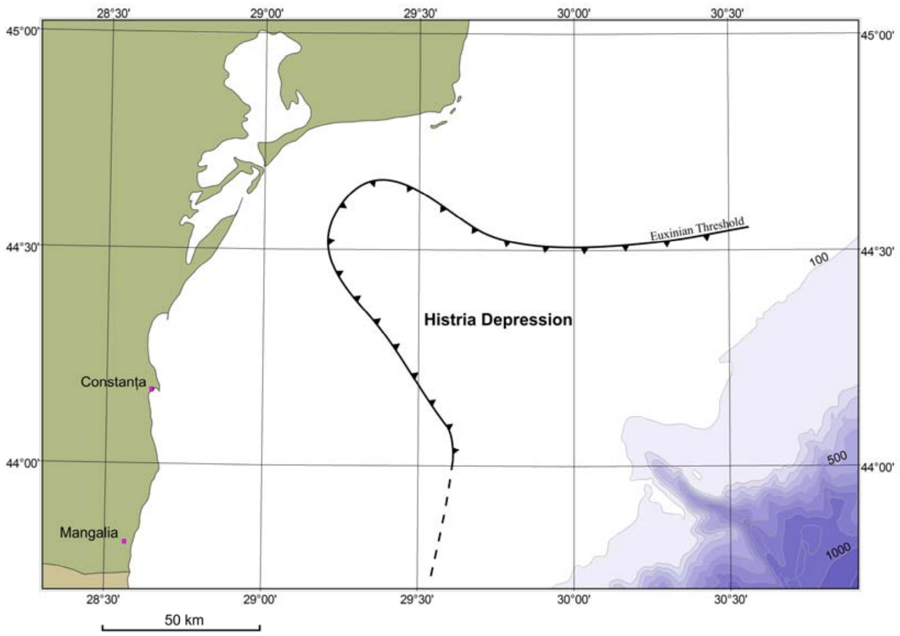

Figure 4.1 Position of the Histria Depression on the Romanian shelf. The thick black line gives the approximate position of the "Euxinian Threshold".

This chapter consists of a detailed characterization of the Mio-Pleistocene unconformities, a sequence stratigraphic description of the seismic facies, a tectonic characterization and a subsidence analysis of the Mio-Pleistocene sequences.

4.2. Mio-Pleistocene sequence boundaries and unconformities

4.2.1. Base of Badenian and Sarmatian (Middle Miocene)

The Neogene deposits on the Romanian shelf begin with an erosional hiatus that developed for about 8 myr and marks the boundary between the Oligocene and the Badenian-Sarmatian sequences. The erosional unconformity at the base of the Badenian formed about 15.8 myr ago as a result of a relative fall in sea level. This unconformity occurs only on the inner shelf. In the south, it is restricted to the area surrounding the Delfin wells and in the north it is developed around the northern component of the Euxinian Threshold where Badenian-Sarmatian deposits are present. Outside this area, the Neogene begins with an unconformity that marks the base of the Pontian. The erosional unconformity at the base of the Badenian (BBU in Fig. 4.2) is characterized by a reflector with high amplitude and good lateral continuity.

A depth distribution map of the BBU (in ms TWT) is shown in Figure 4.3. The depth of this unconformity increases from 720 ms in the vicinity of the coastline to 2400 ms basinward. In the southern area, the corresponding depth in ms TWT is more-or-less constant.

In order to transform the TWT times to depth, a RMS velocity map for the section from the sea level to the BBU was constructed from depth information from boreholes and RMS velocities from processing (Fig. 4.4). The RMS velocity increases from 1800 m/s in the coastal areas to 2400 m/s in deeper waters to the east.

A depth distribution map of the BBU (in meters) is given in Figure 4.5. The general trend is an increase in depth eastwards, both in the northern and in the southern areas. In the northern area, there is an abrupt increase in depth from 655 m in the vicinity of the coast to about 2750 m to the east. In the southern area, the depth increases up to 1400 m.

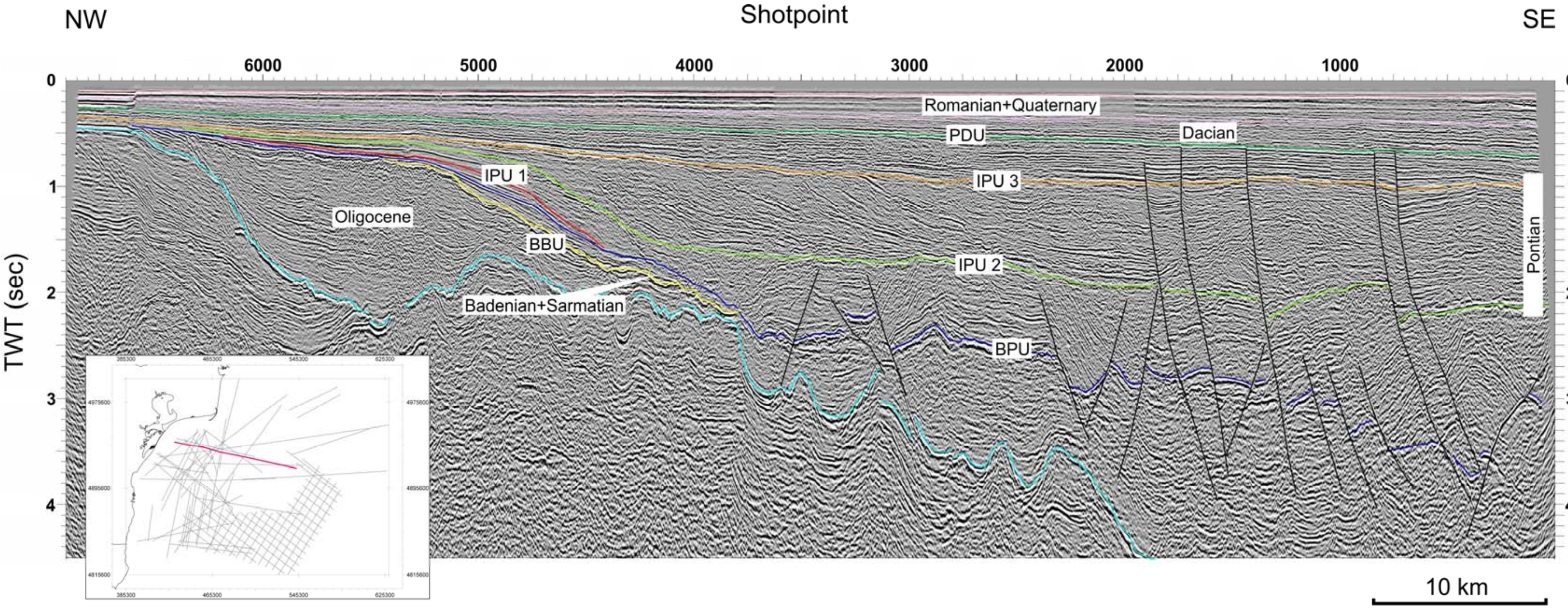

Figure 4.2 Seismic line illustrating the main erosional unconformities: the BBU (the unconformity at the base of the Badenian), the BPU (the unconformity at the base of the Pontian), the IPU 1, IPU 2, IPU 3 (intra-Pontian unconformities), and the PDU (Pontian-Dacian unconformity).

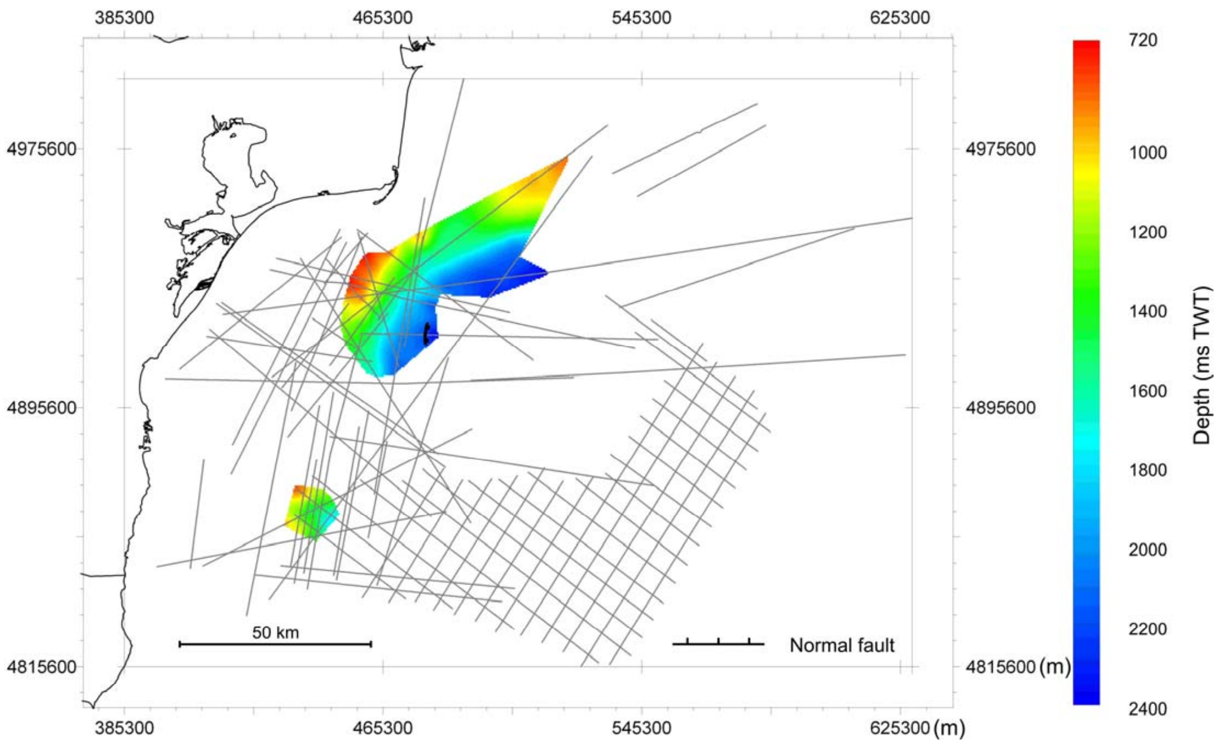

Figure 4.3 Depth distribution of the base of the Badenian and Sarmatian formations (in ms TWT below sea level).

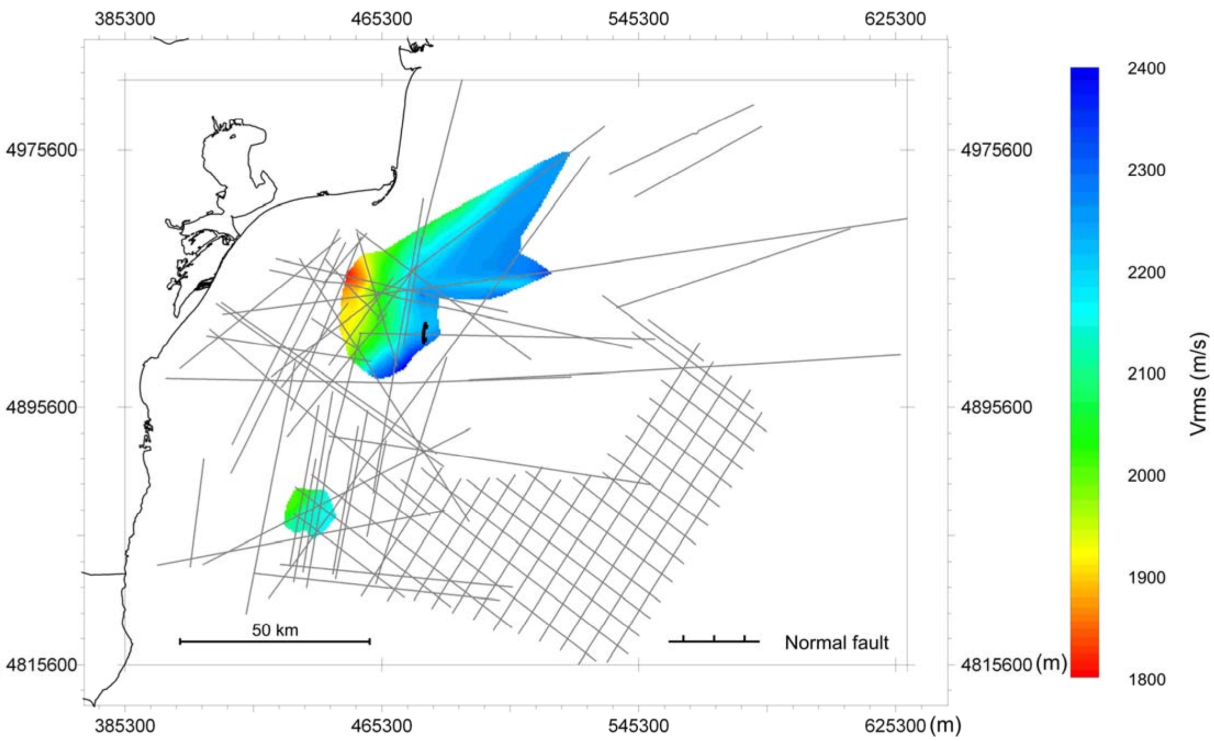

Figure 4.4 RMS velocity model from the sea level to the base of the Badenian and Sarmatian successions (in m/s) used for converting the seismic data from TWT to depth.

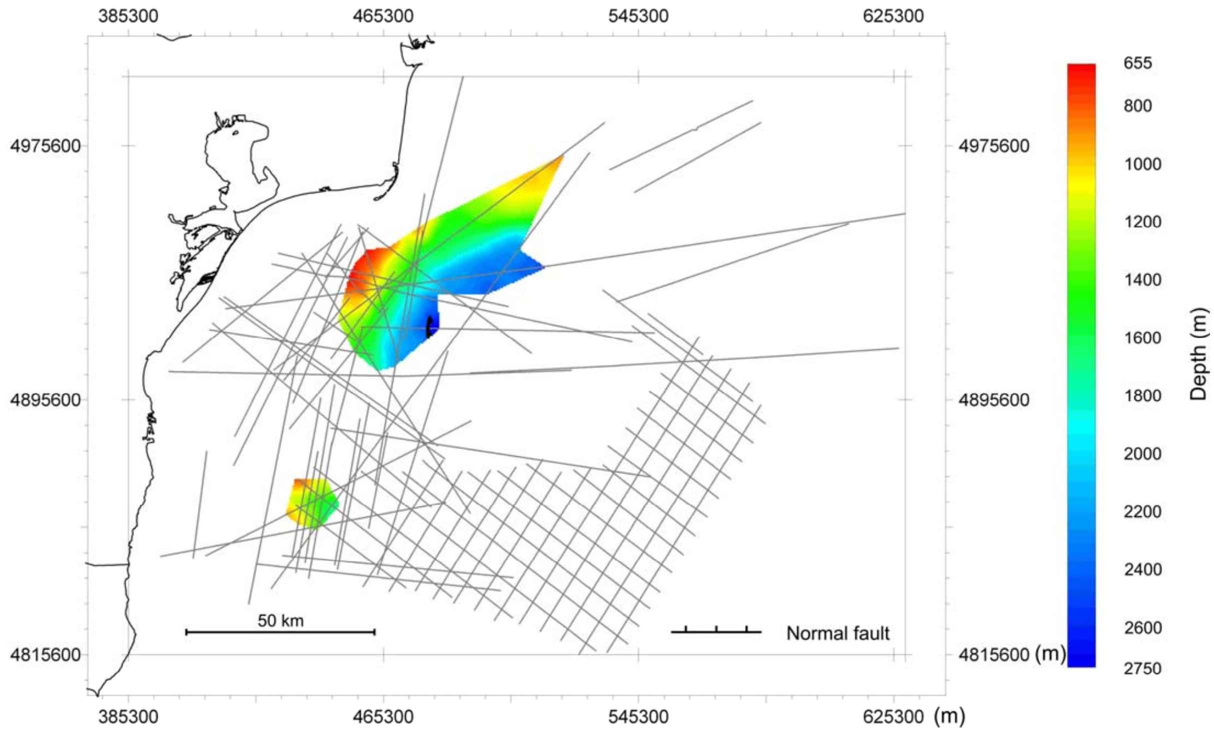

Figure 4.5 Depth distribution of the base of the Badenian and Sarmatian successions (in meters below sea level).

4.2.2. Base of Pontian (Upper Miocene)

The second major erosional surface that could be mapped on the seismic lines is the base of the Pontian (BPU in Fig. 4.2). In the area where the Badenian-Sarmatian sequence is present, it marks the unconformable contact between the Sarmatian and the Pontian. Outside this area, it represents the contact between the Oligocene and the Pontian. The unconformity is very well developed along the entire Romanian shelf and is represented by a high-amplitude reflector with good lateral continuity.

On the seismic line of Figure 4.2, the gradient of the BPU increases considerably from the inner to the outer shelf. The line shown in Figure 4.6 crosses the entire Romanian shelf from SW to NE. On this line, the BPU marks the bottom of the graben that corresponds to the Histria Basin.

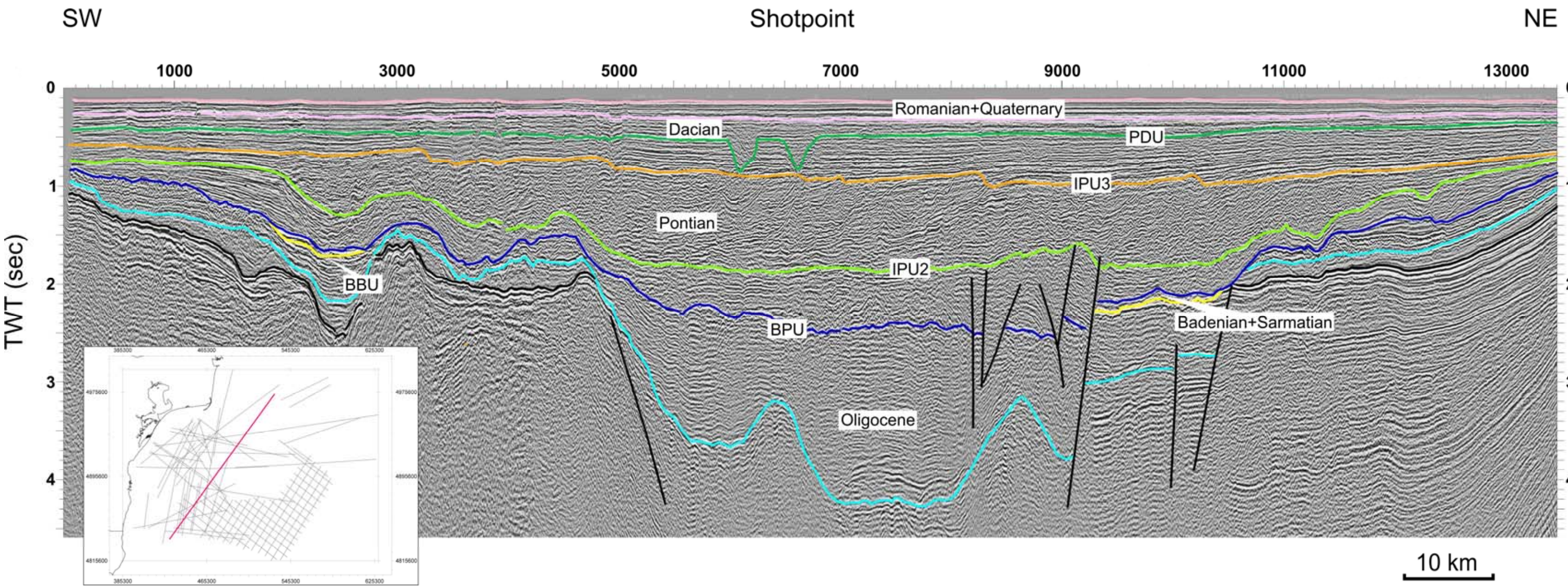

Figure 4.6 Interpreted NE-SW seismic line across the Romanian shelf.

Figure 4.7 shows a depth distribution map of the BPU (in ms TWT), with values varying from 230 ms to 4550 ms. The RMS velocity distribution for the same sediment section used to transform the data from TWT times to depth suggests an increase from 1600 m/s in the coastal areas to 2600 m/s eastward (Fig. 4.8). Low RMS velocities are observed in the southeastern part of the study area.

A depth distribution map of the BPU (in meters below sea level; Fig. 4.9) shows a very sharp southeasterly increase in depth, starting from 200 m along the coast to 4940 m on the outer shelf.

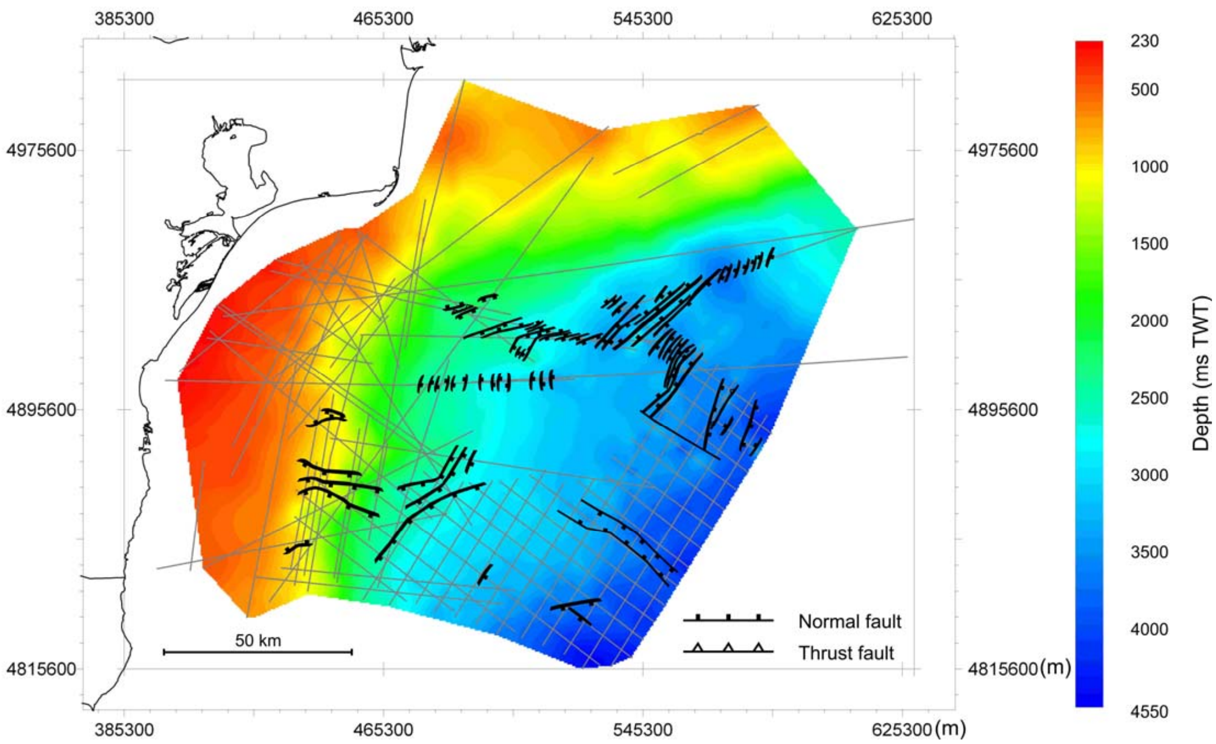

Figure 4.7 Depth distribution of the base of the Pontian formations (in ms TWT below sea level).

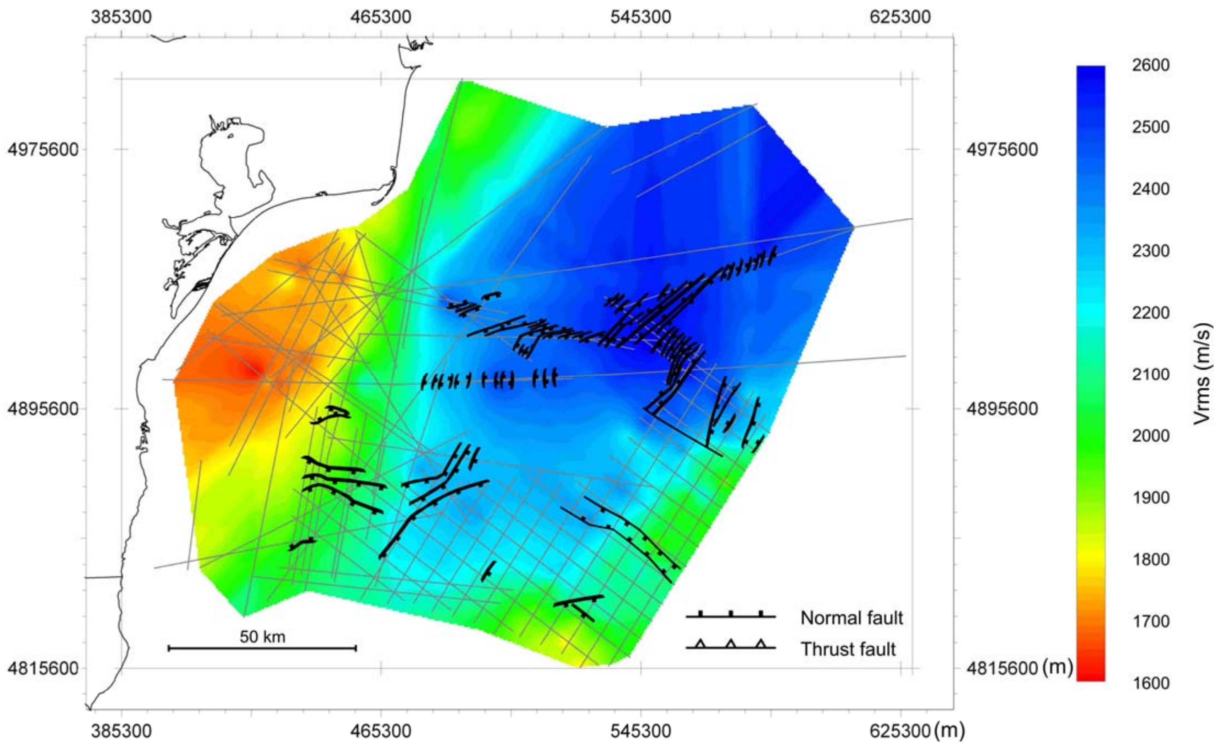

Figure 4.8 RMS velocity model for the sediments from the sea level to the base of the Pontian (in m/s).

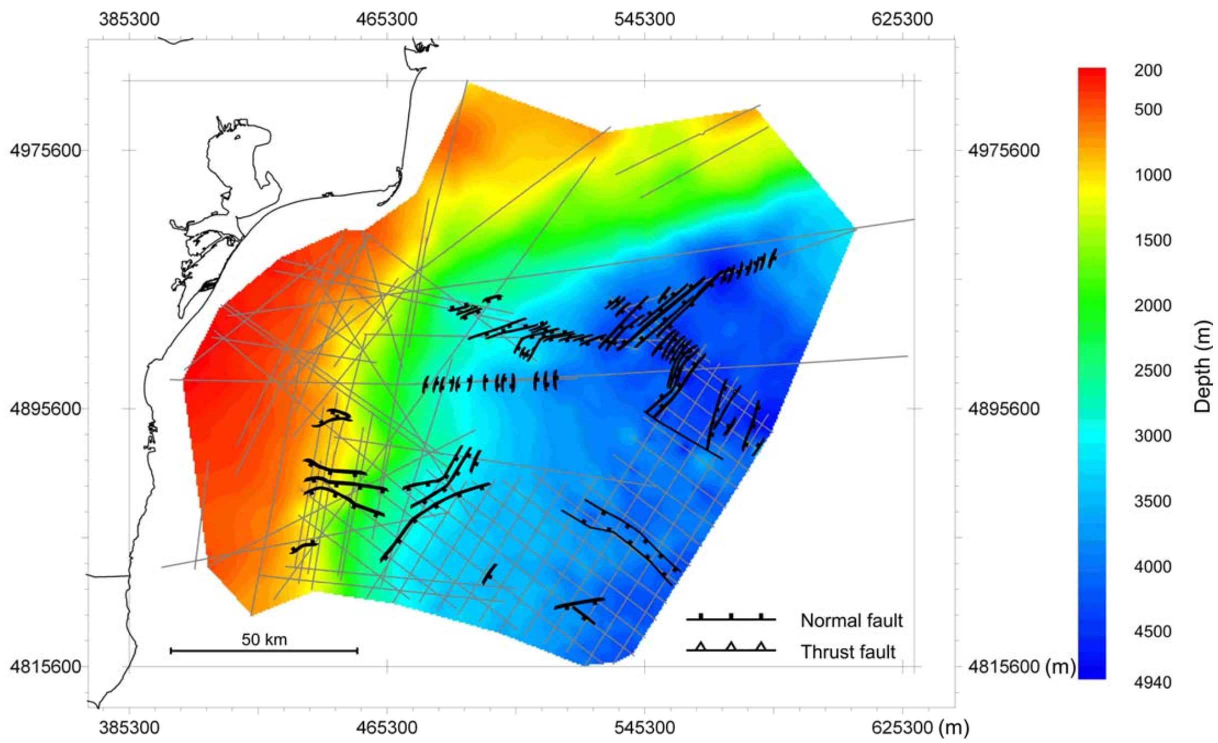

Figure 4.9 Depth distribution map of the base of the Pontian formations (in meters below sea level).

4.2.3. Intra-Pontian unconformities

Three Intra-Pontian erosional unconformities (IPU1, IPU2 and IPU3 in Fig. 4.2) have been mapped using the available seismic data. A description of these unconformities follows.

4.2.3.1. IPU1

The first Intra-Pontian unconformity (IPU1; Figures 4.2 and 4.13) is developed only in a limited area of the western and northwestern part of the study area. The unconformity is characterized by a reflector with high amplitudes and good lateral continuity. IPU1 begins in the vicinity of the coast and increases abruptly in depth basinward, downlapping the base of the Pontian.

Figure 4.10 is a depth distribution map (in ms TWT) of this unconformity. The depth increases from 500 ms along the coast to 1900 ms in the direction of the Histria Depression. The RMS velocity of the successions between the sea level and IPU1 varies from 1650 m/s to 2200 m/s (Fig. 4.11). The depth distribution (in meters) of IPU1 shows an increase in depth from 425 m in the west to 1900 m in the Histria Depression (Fig. 4.12).

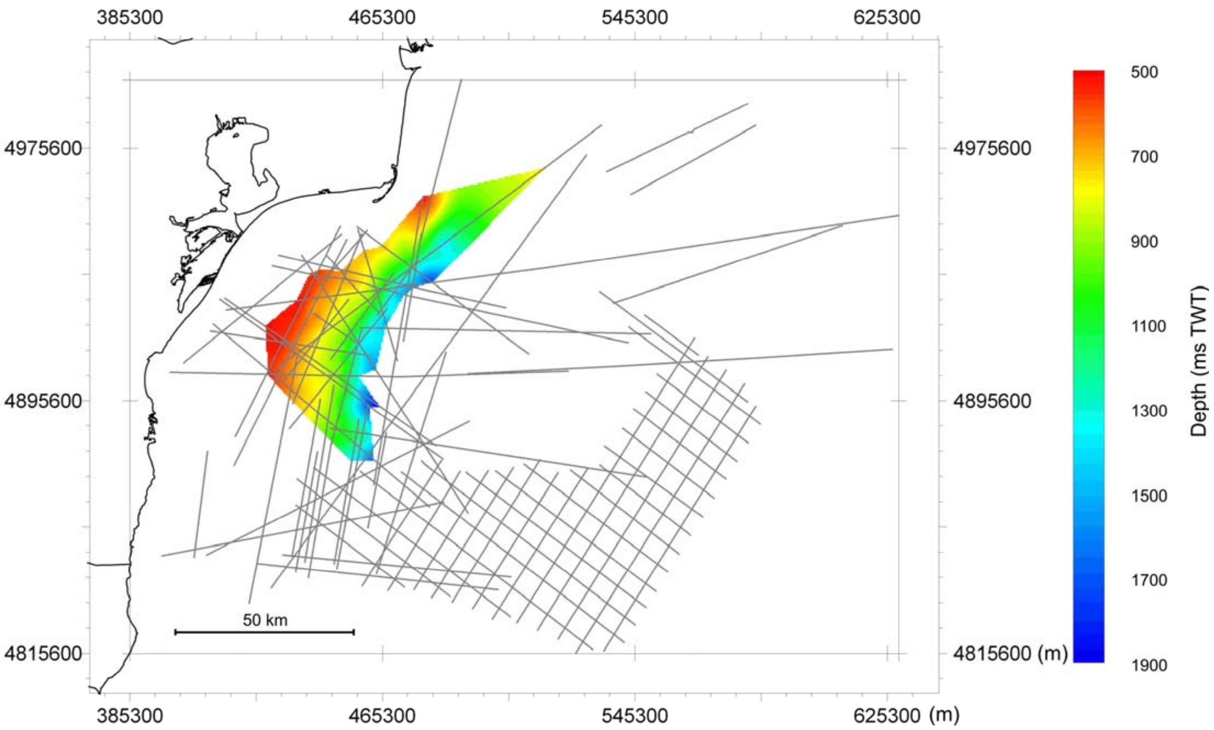

Figure 4.10 Depth distribution of IPU 1 (in ms TWT below sea level).

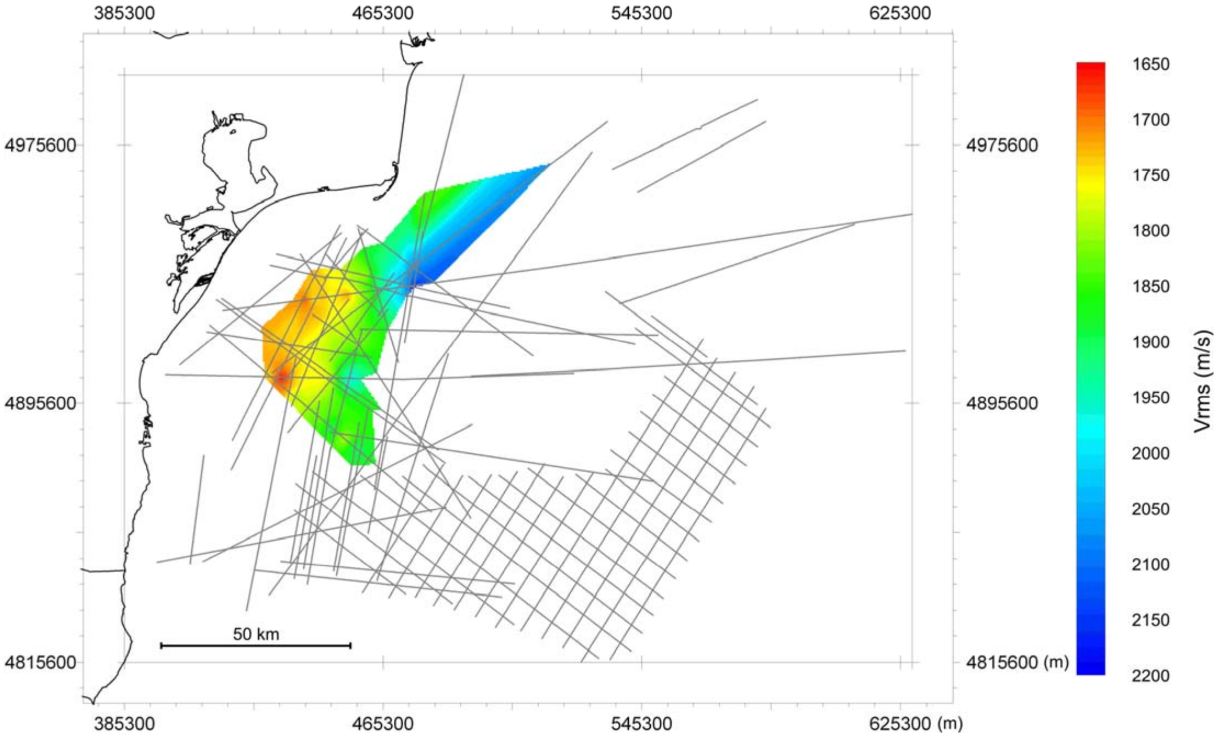

Figure 4.11 RMS velocity model from the sea level to IPU1 (in m/s).

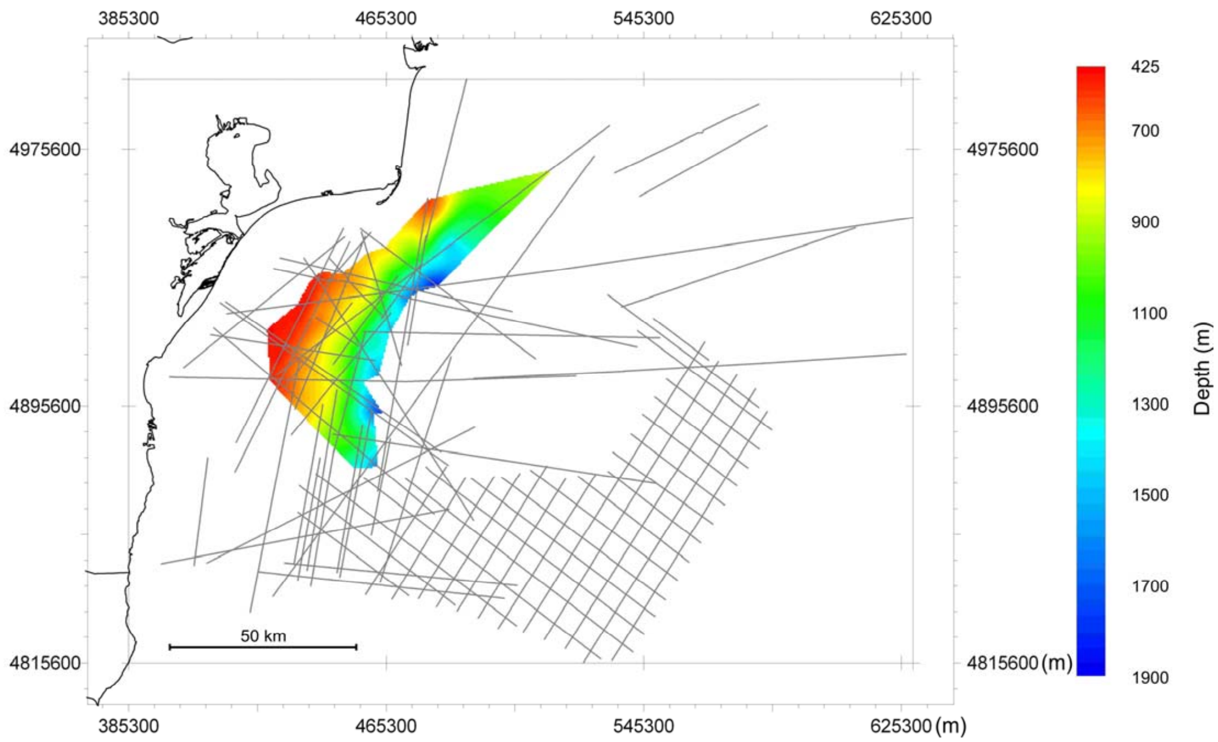

Figure 4.12 Depth distribution of IPU1 (in meters below sea level).

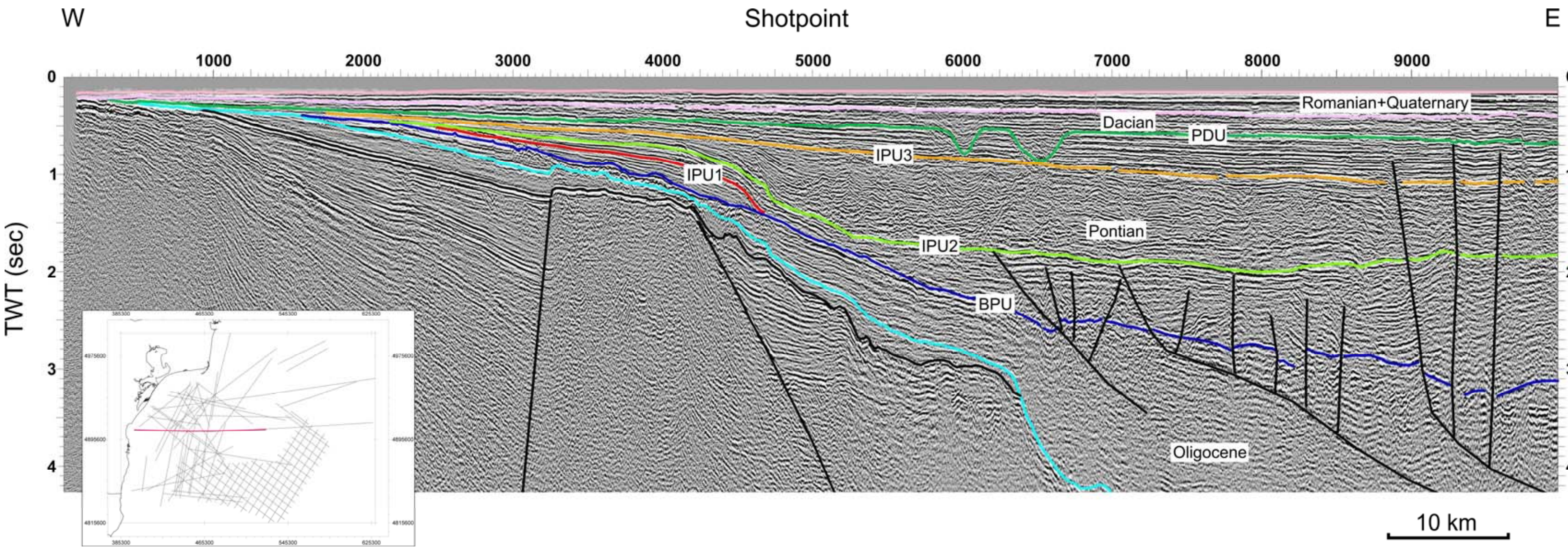

Figure 4.13 Interpreted seismic profile showing the Mio-Pleistocene unconformities in the northwestern Black Sea.

4.2.3.2. IPU2

The second Intra-Pontian unconformity (IPU2 in Figures 4.2, 4.6 and 4.13) has an erosional character and is widespread over the study area, extending from the coast to the outer shelf. It represents the unconformity between two different facies: an aggradational facies deposited when sediment supply and subsidence were in balance, overlying a progradational facies developed when sediment supply exceeded the rate of subsidence.

The depth distribution of IPU2 (in ms TWT) is shown in Figure 4.14. The depth of IPU2 varies from 390 ms TWT near the coast to 3700 ms on the southern outer shelf.

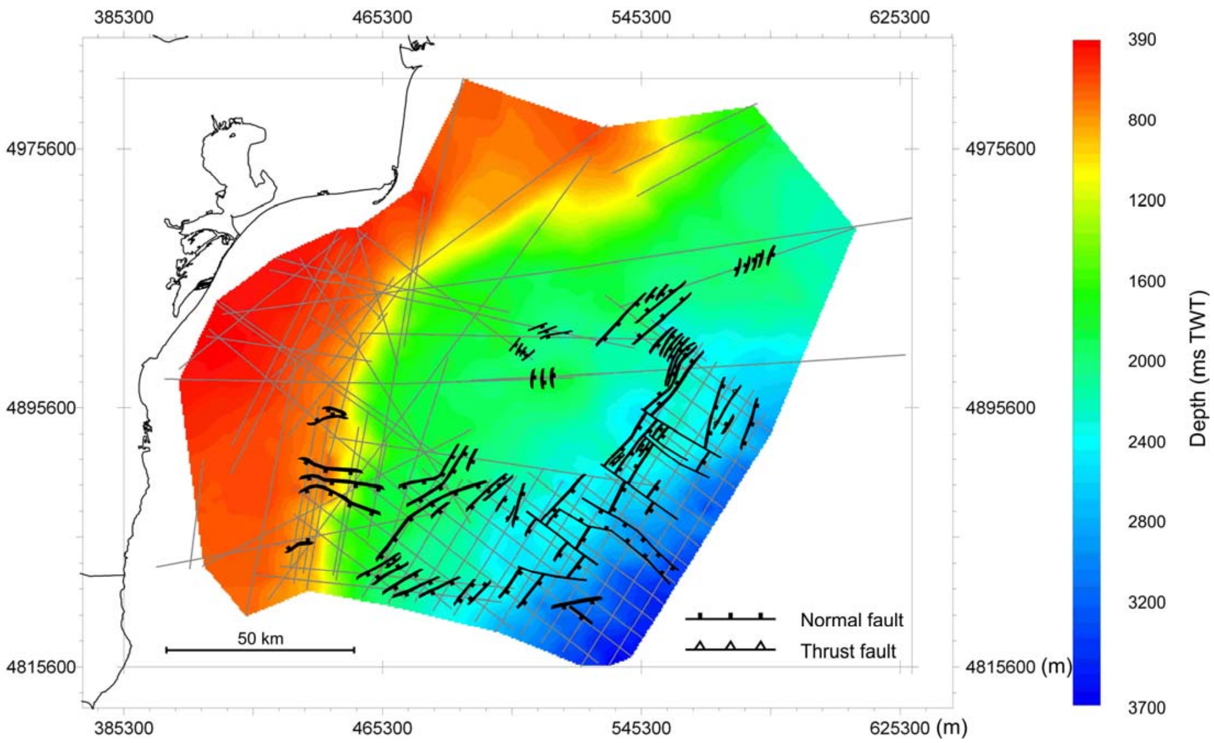

Figure 4.14 Depth distribution of IPU2 (in ms TWT below sea level).

Figure 4.15 is a map of the RMS velocity from the sea level to unconformity IPU2. The values increase from 1600 m/s in the west to almost 2400 m/s in the distal area. The depth distribution of IPU2 (in meters; Fig. 4.16) shows a sudden increase from the coast to the middle shelf, followed by a relatively slow increase basinward. The depth values increase from 340 m near the coast to 4090 m on the outer shelf.

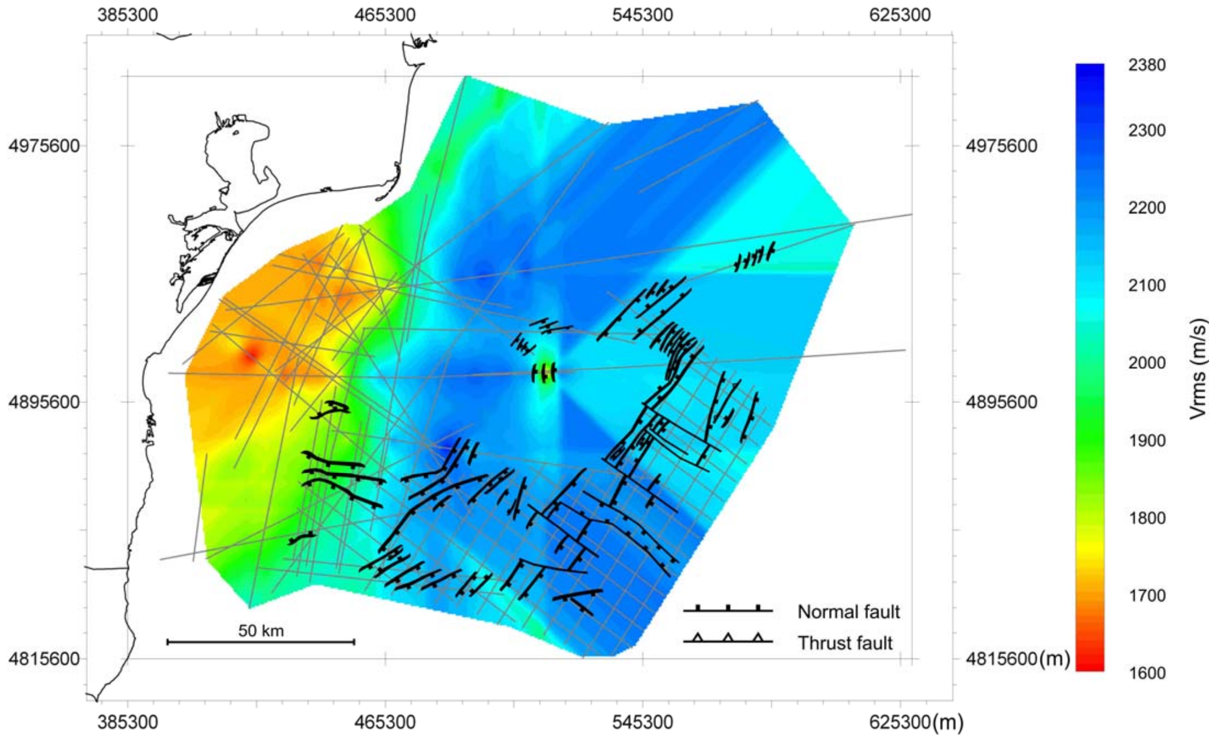

Figure 4.15 Distribution of the RMS velocity from the sea level to IPU2 (in m/s).

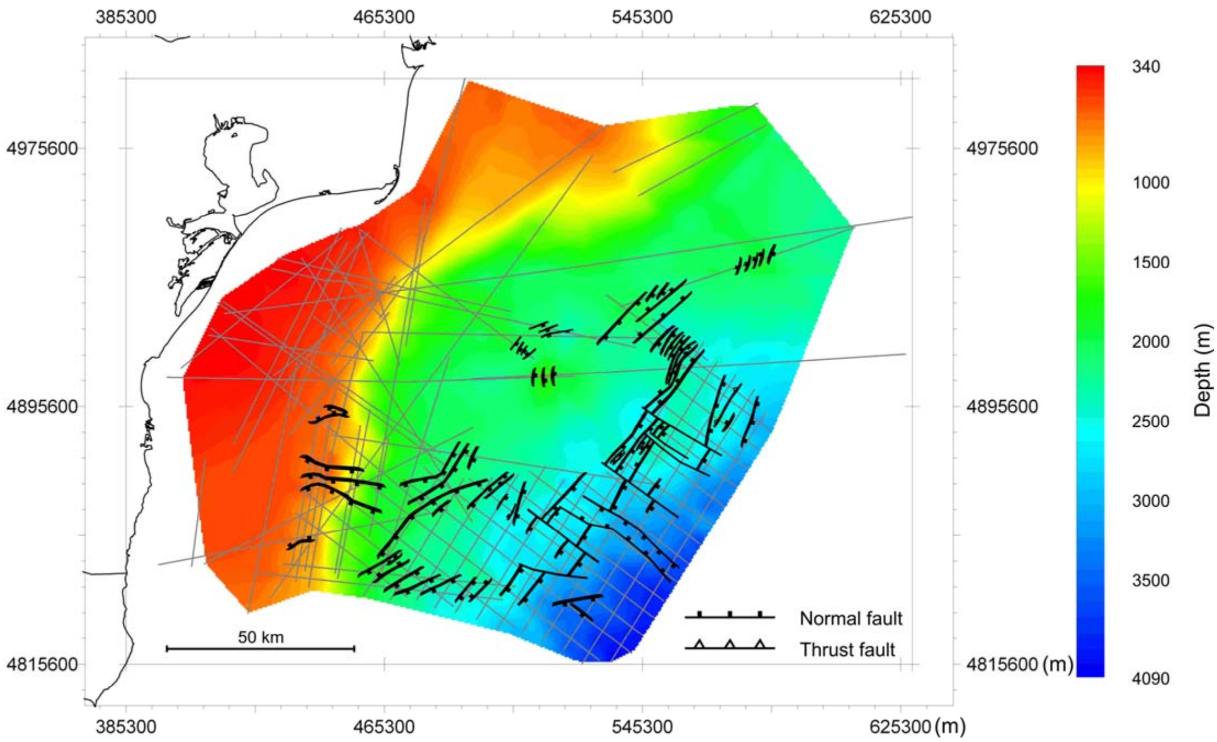

Figure 4.16 Depth distribution of IPU2 (in meters below sea level).

4.2.3.3. IPU3

The base of the Uppermost Miocene is marked by the youngest Intra-Pontian unconformity (IPU3 in Figures 4.2, 4.6 and 4.13) developed when the progradational sediments deposited during the Upper Pontian were eroded. This unconformity is characterized by very high amplitudes and good lateral continuity over the entire shelf. It could be related to the Messinian salinity crisis in the Mediterranean Sea as proposed by Hsü (Hsü et al., 1979) and Gillet (Gillet, 2004).

In contrast to IPU1 and IPU2 which show abrupt increases in depth from the inner to the middle shelf, the depth of the IPU3 suggests a gradual increase from 260 ms TWT in the coastal areas to about 3400 ms TWT on the outer shelf (Fig. 4.17). The RMS velocity from the sea level to IPU3 varies only between 1500 and about 2050 m/s over the shelf (Fig. 4.18), yielding a depth of IPU3 that lies between 210 m along the coast to 2860 m in the east (Fig. 4.19).

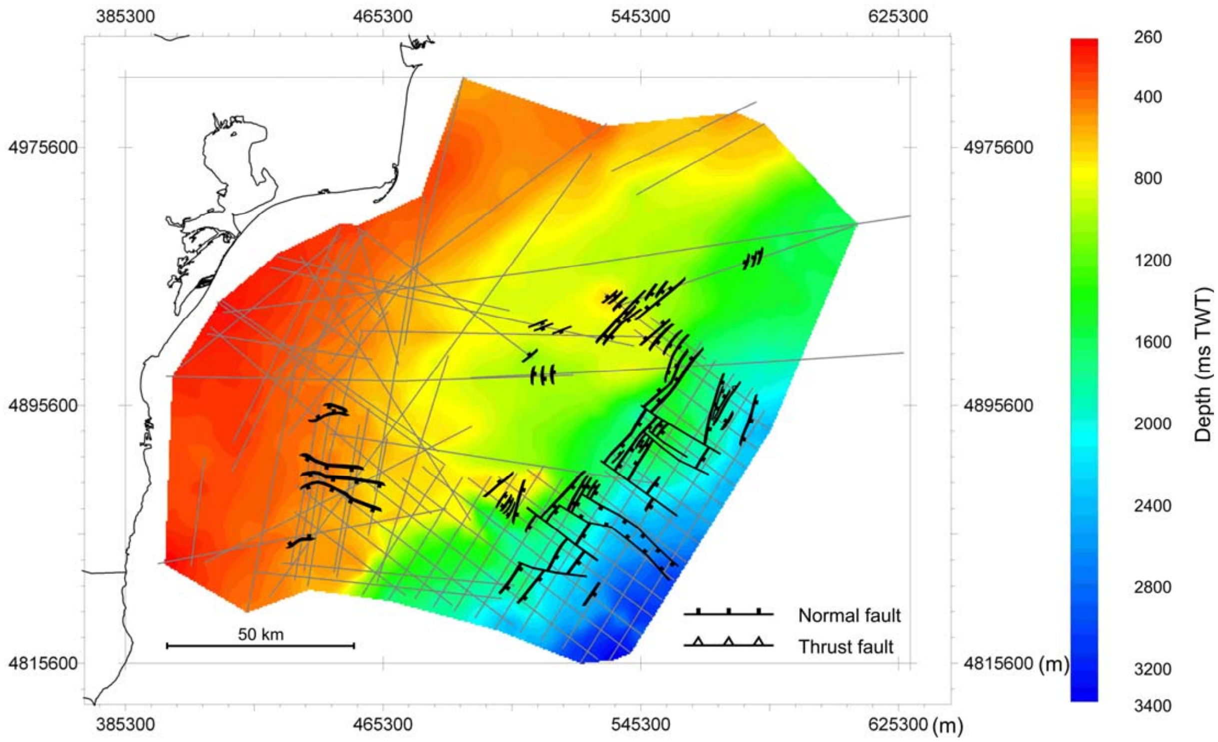

Figure 4.17 Depth distribution of IPU3 (in ms TWT below sea level).

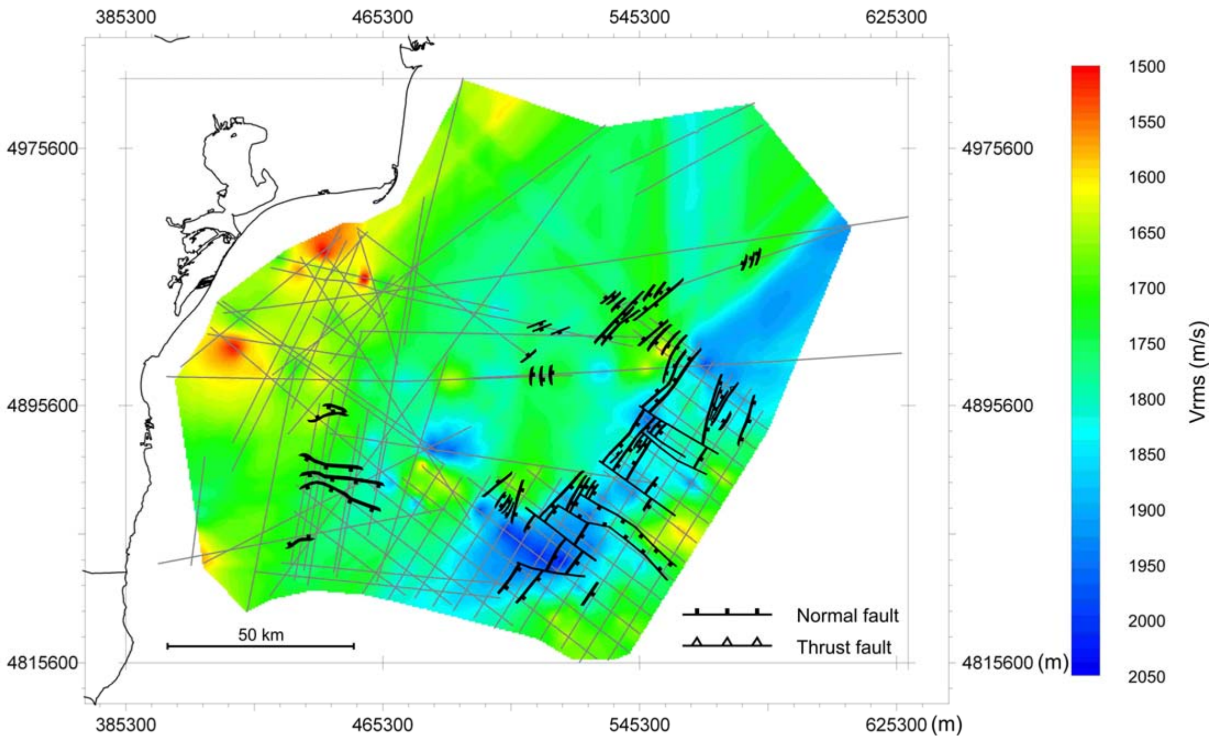

Figure 4.18 Model of RMS velocities from the sea level to IPU3 (in m/s).

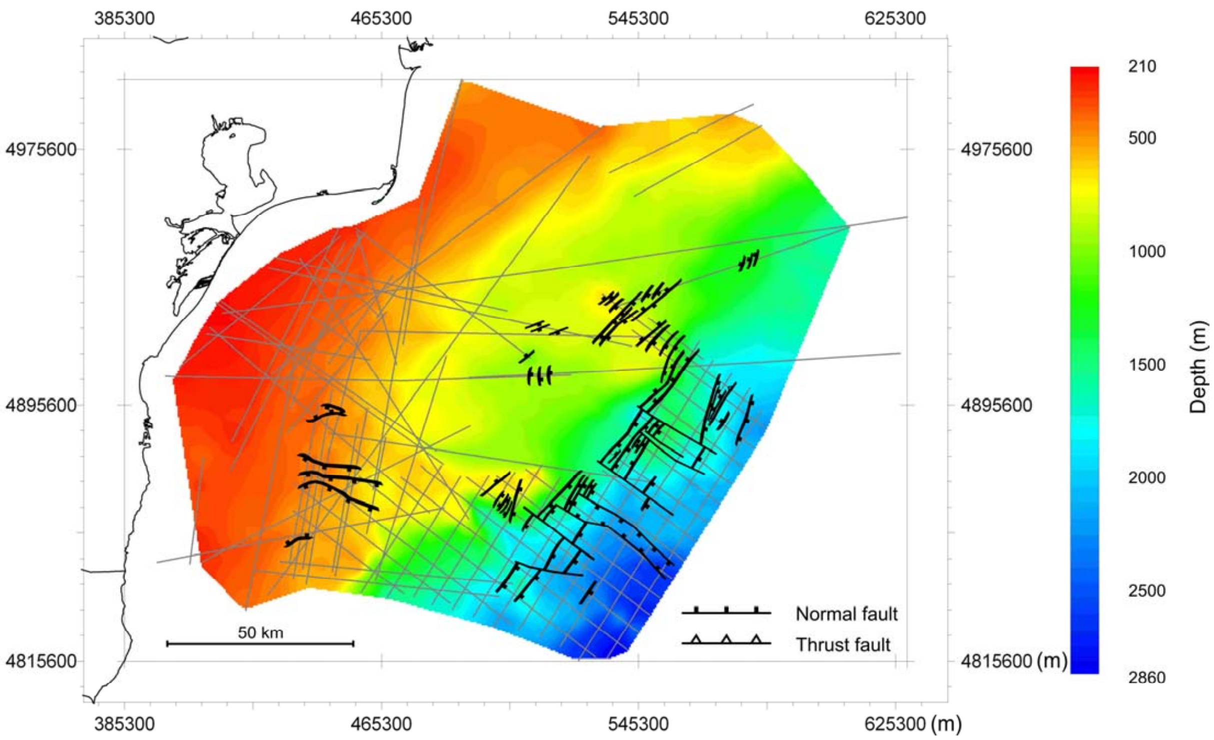

Figure 4.19 Depth distribution of IPU3 (in meters below sea level).

4.2.4. Base of Dacian (Pliocene)

The transition from the Pontian to the Dacian is marked by a conformity (PDU in Fig. 4.2) that changes into an erosional unconformity (Figures 4.6 and 4.13). This unconformity is characterized by local valleys incised up to 500 m into the seafloor on the middle shelf (Figures 4.6 and 4.13). It might have formed about 5.3 myr ago when the relative sea level was at its lowest. The PDU is characterized by a reflector with medium amplitude and a good lateral continuity.

Figure 4.20 is a depth distribution map of the base of the Dacian (in ms TWT). The depth of this unconformity varies from 160 ms near the coast to 2960 ms on the upper slope. RMS velocities for the succession above the PDU change from 1500 m/s in the west to 1950 m/s on the upper slope (Fig. 4.21). The corresponding depth distribution in meters (Fig. 4.22) is uniform on the inner shelf, but increases rapidly on the outer shelf and upper slope.

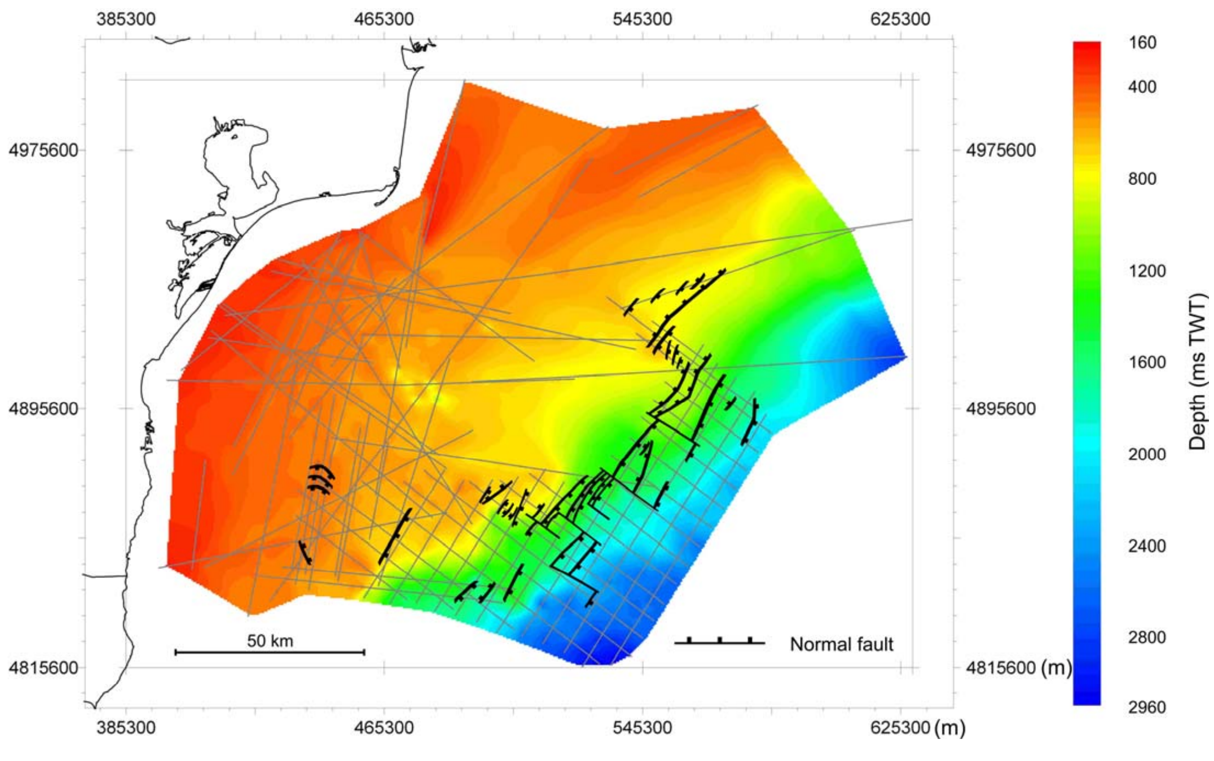

Figure 4.20 Depth distribution of the base of the Dacian (in ms TWT below sea level).

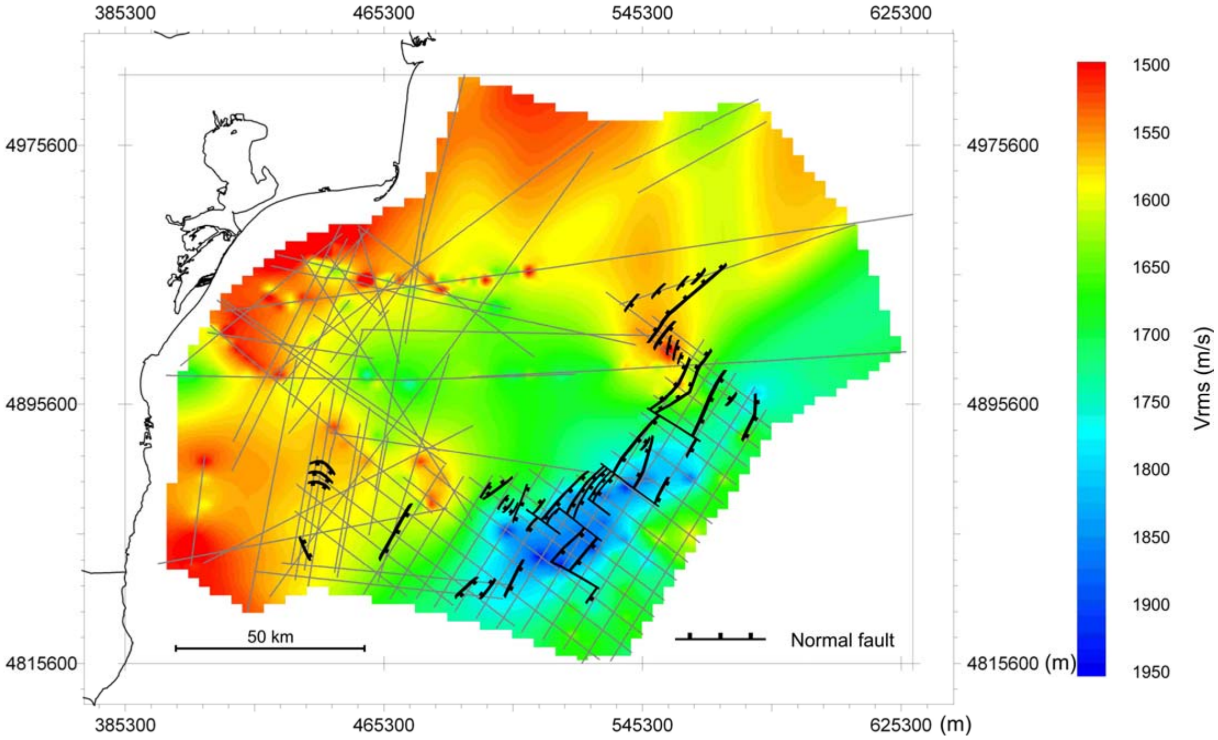

Figure 4.21 Model of the RMS velocity from the sea level to the base of the Dacian (in m/s).

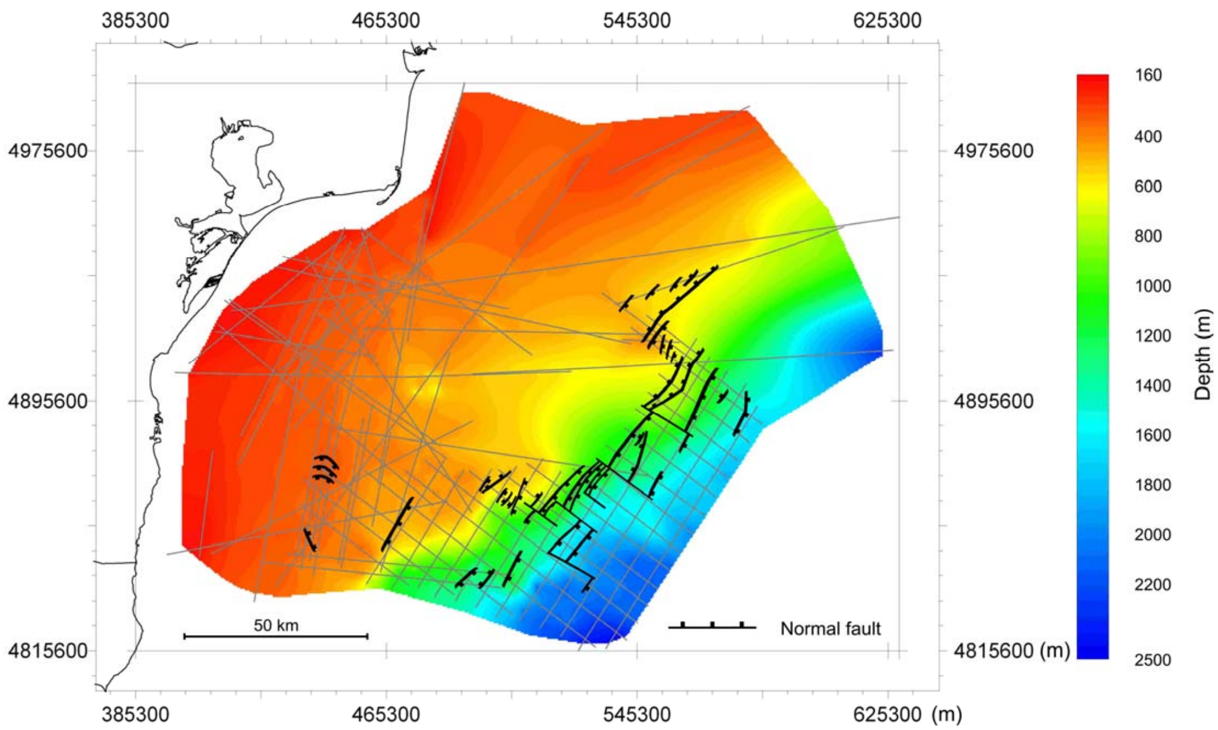

Figure 4.22 Depth distribution of the base of the Dacian (in meters below sea level).

4.2.5. Base of Romanian and Quaternary (Pleistocene)

The base of the Romanian is a conformity marked by a reflector with medium to low amplitudes and medium lateral continuity (Figures 4.2, 4.6 and 4.13).

The depth from the seafloor to the base of the Romanian and Quaternary (in ms TWT) is shown in Figure 4.23. It varies from 50 ms TWT on the inner shelf to 2200 ms on the southern outer shelf. With the RMS velocity distribution of the Romanian-Quaternary deposits shown in Figure 4.24 (1400 m/s to 1600 m/s), the depth converted to meters ranges from 100 m on the shelf to about 1615 m on the upper slope (Fig. 4.25).

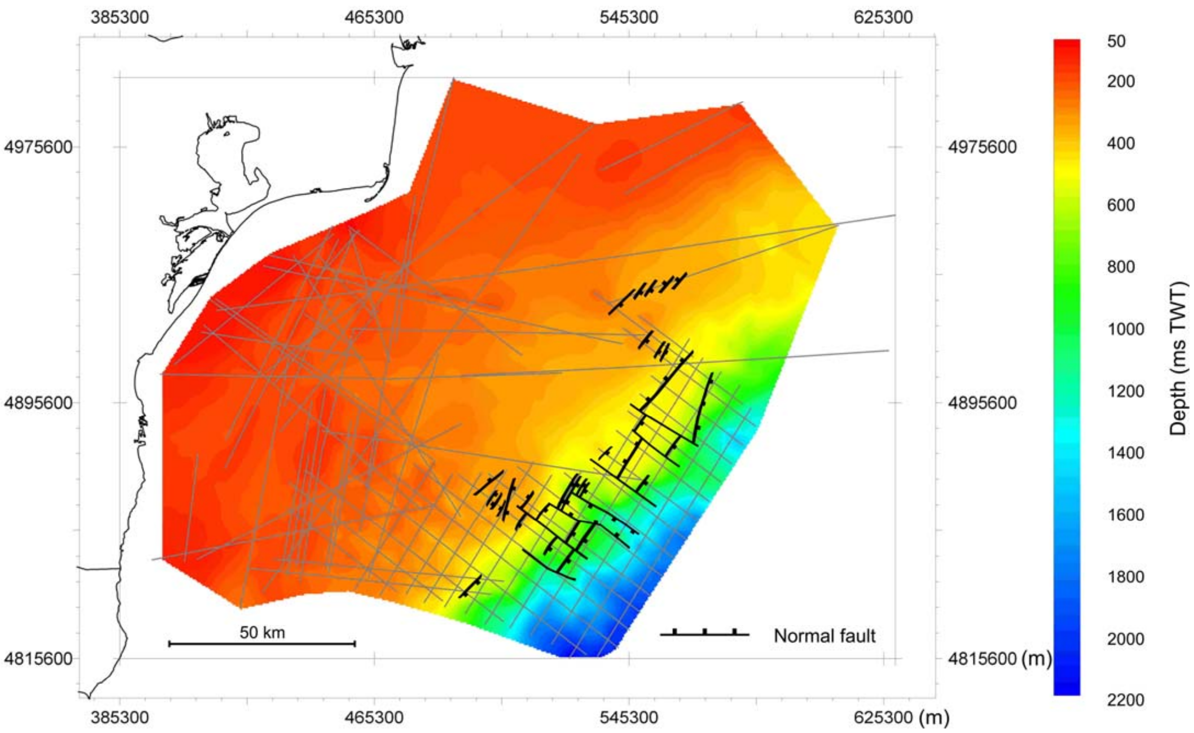

Figure 4.23 Depth distribution of the base of the Romanian and Quaternary (in ms TWT below sea level).

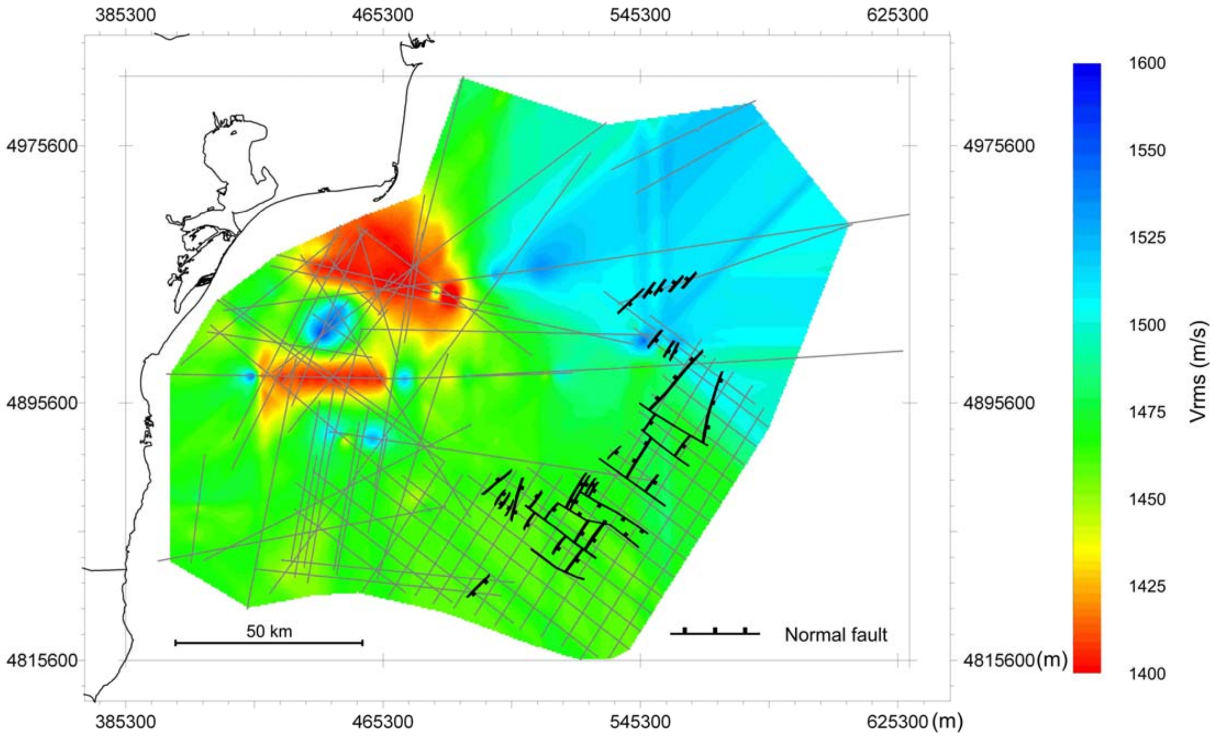

Figure 4.24 Model of RMS velocities from the sea level to the base of the Romanian and Quaternary (in m/s).

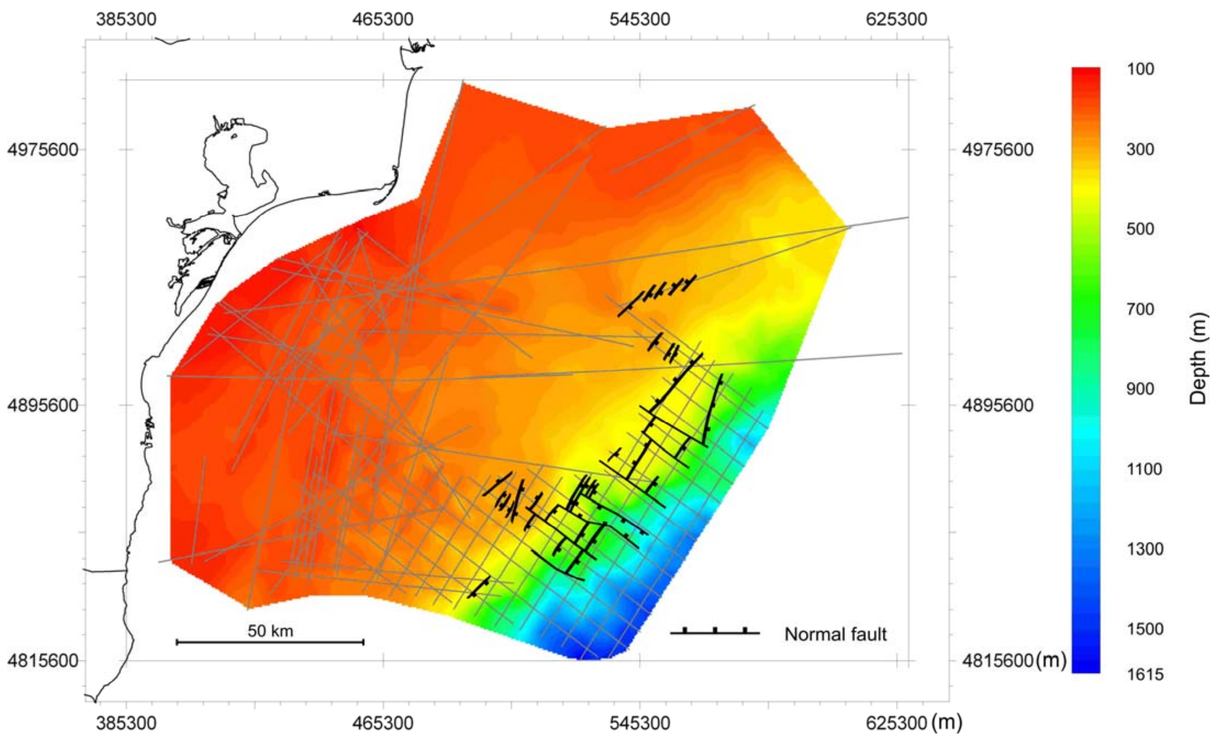

Figure 4.25 Depth distribution of the base of the Romanian and Quaternary (in meters below sea level).

4.3. Sequence stratigraphic characteristics of the Mio-Pleistocene section

Based on an interpretation of the seismic lines and their correlation with borehole data from the Romanian shelf, seven seismic units (Fig. 4.27) bounded by unconformities and their correlative conformities were recognized. They are described in detail in this section and their characteristics are summarized in Table 4.1.

The Mio-Pleistocene units on the Romanian shelf were chronostratigraphically calibrated using seismic and borehole data. Their occurrence divides the shelf into three distinct provinces (Fig. 4.26): a province on the inner shelf where the Badenian-Sarmatian section is present (Table 4.2), a second province on the inner shelf where the Badenian-Sarmatian section is absent (Table 4.3), and the middle and outer shelf province (Table 4.4).

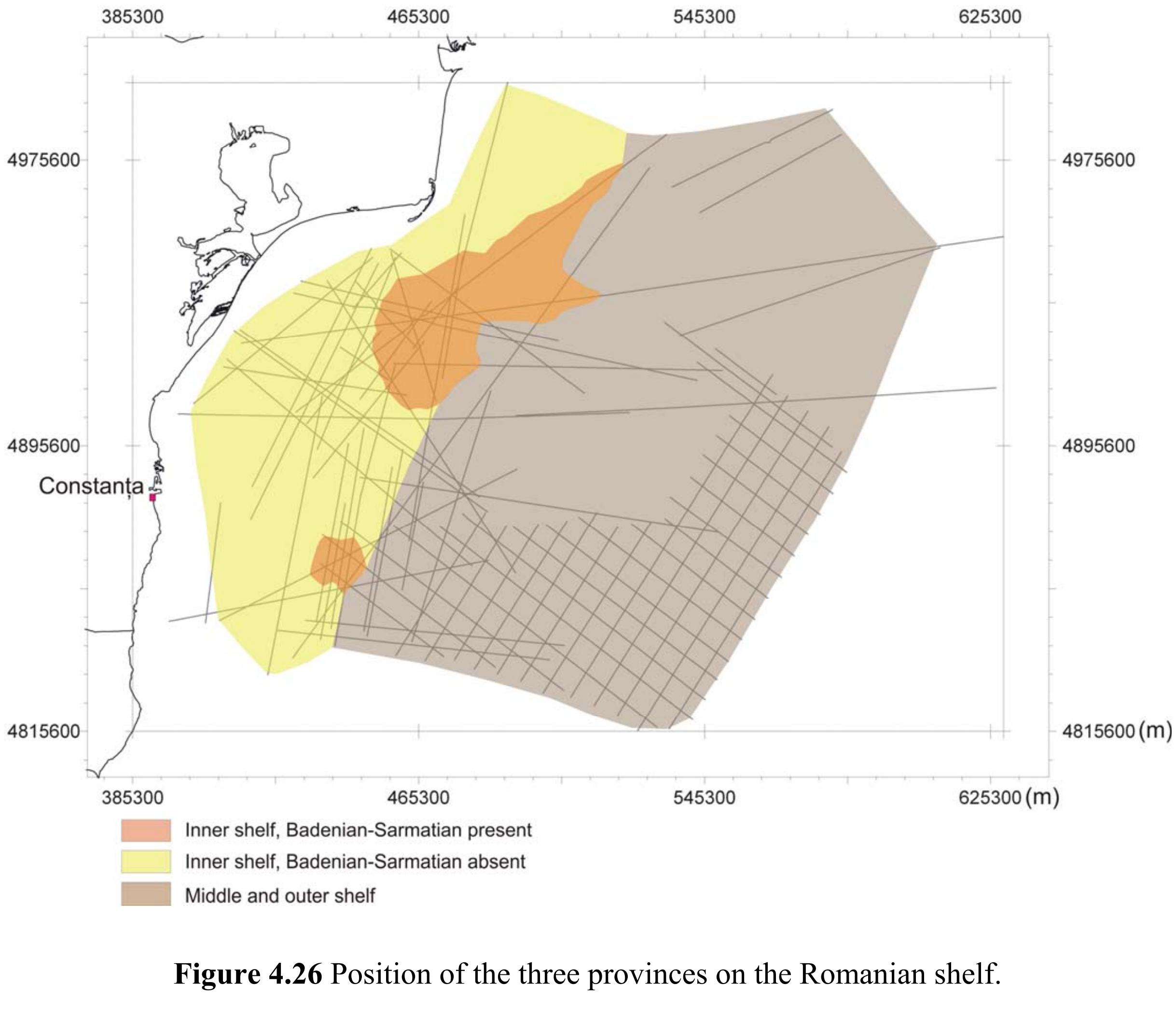

Figure 4.26 Position of the three provinces on the Romanian shelf.

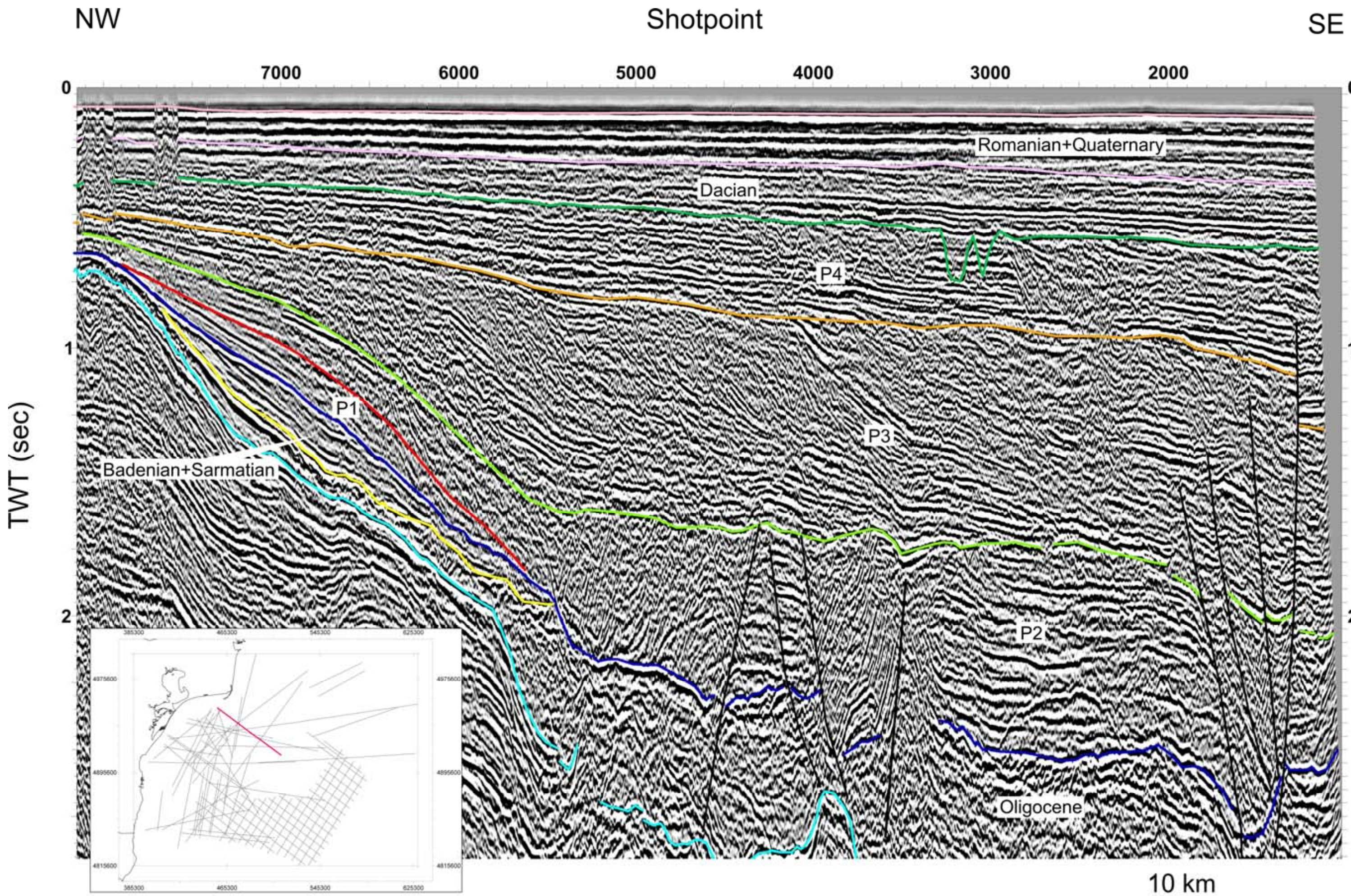

Figure 4.27 Seismic line showing the characteristics of the Mio-Pleistocene seismo-stratigraphic units: Badenian-Sarmatian, P1 (Pontian 1), P2 (Pontian 2), P3 (Pontian 3), P4 (Pontian 4), Dacian, and Romanian-Quaternary.

Formation	LB - Termination	UB - Termination	Internal configuration	External geometry	Occurrence	Lithology from boreholes	Systems Tract	Facies exemple
Romanian + Quaternary	conformity	conformity	parallel reflection; low amplitude	thin drape sheet	in the entire study area	sands and argillaceous sands	HST	
Dacian	erosional truncation	conformity	parallel reflection; low to medium amplitude; incised valley fill	channel fill; drape sheet	in the entire study area	sands and argillaceous sands on the inner and middle shelf, and sandy shales on the outer shelf	TST	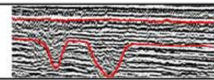
Pontian 4	onlap	erosional truncation	parallel reflection; medium amplitude	drape sheet	over the entire shelf	sands and argillaceous sands	TST + HST	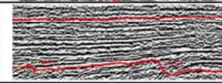
Pontian 3	downlap	erosional truncation	steep to medium gradient; high amplitude; prograding deltaic wedges	wedge	in the entire study area	shales, marls, sands and argillaceous sands	LST	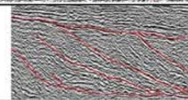
Pontian 2 (E)	erosional truncation	erosional truncation	low gradient; parallel and chaotic reflection; medium amplitude	thick drape sheet	on the middle and outer shelves	shales, marls, sands and argillaceous sands	LST	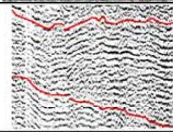
Pontian 2 (W)	onlap	erosional truncation	medium to steep gradient; divergent, discontinuous reflection; low amplitude	lenticular	on the inner shelf	sandy shales, shales and marls	LST	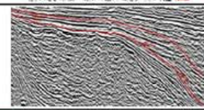
Pontian 1	onlap	erosional truncation	steep gradient; parallel reflection; medium amplitude	lenticular	on the inner shelf	sandy shales, shales and marls	LST	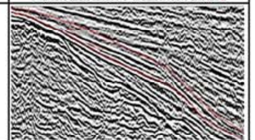
Sm + Bd (Lebada area)	downlap	toplap	steep gradient; parallel reflection; low to medium amplitude	lenticular	in the northwestern part of the inner and middle shelves	shales, marls and sandy shales	HST	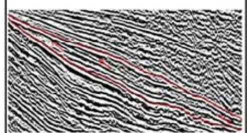
Sm + Bd (Delfin area)	downlap	erosional truncation	steep gradient; parallel reflection; low to medium amplitude	lenticular	in the southern part of the middle shelf	shales, marls and argillites	HST	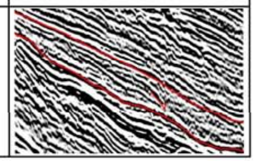

Table 4.1 Sequence-stratigraphic characteristics of the seismic units from the Romanian shelf (LB - lower boundary, UB - upper boundary, HST - highstand systems tract, TST - transgressive systems tract, LST - lowstand systems tract).

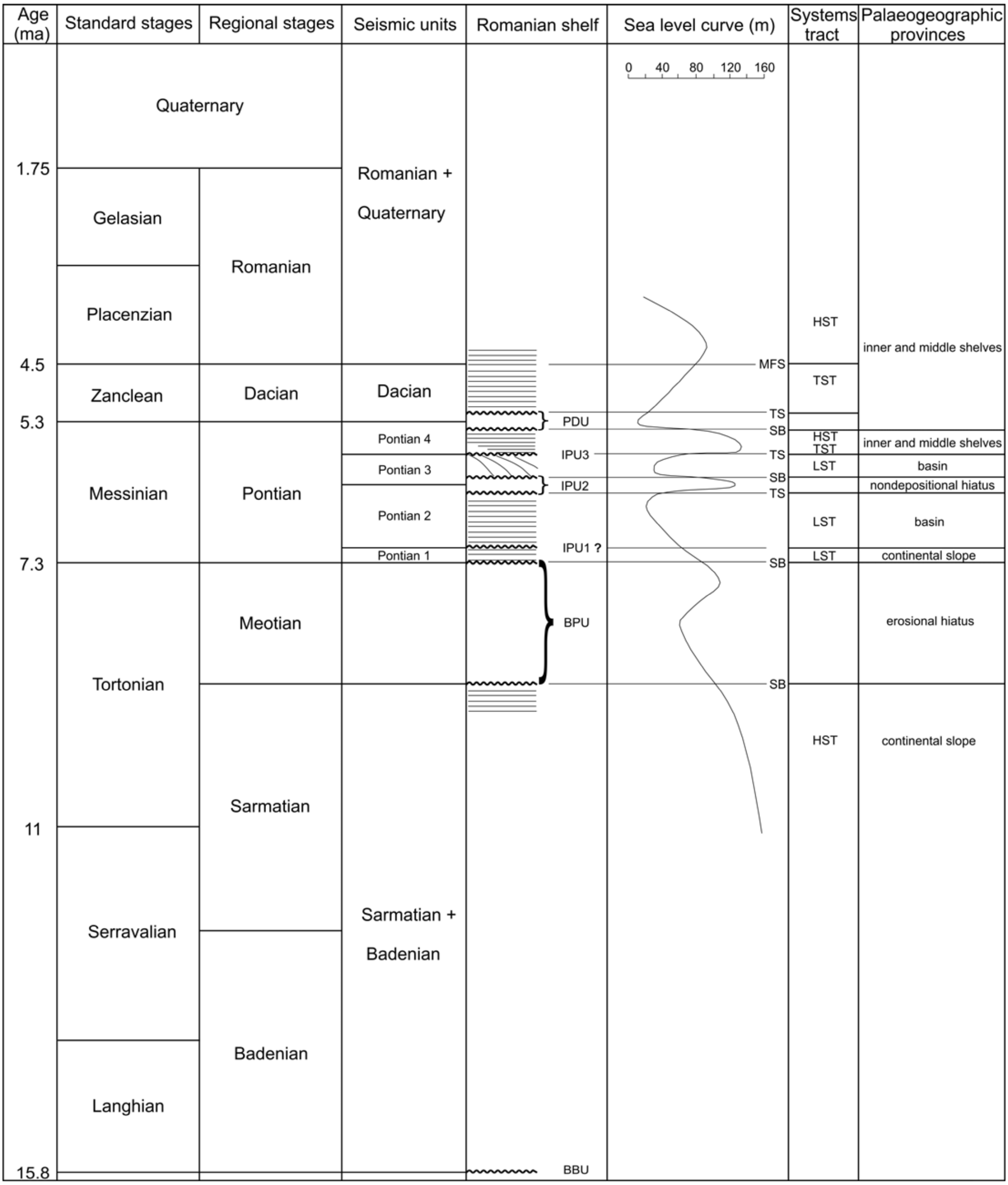

Table 4.2 Chronostratigraphic calibration of the Mio-Pleistocene seismic units from the Romanian Black Sea shelf (valid for areas where the Badenian-Sarmatian section exists). PDU - Pontian-Dacian unconformity, IPU1, IPU2, IPU3 - intra-Pontian unconformities, BPU - erosional unconformity at the base of the Pontian, BBU - erosional unconformity at the base of the Badenian, ? - IPU1 occurs only locally in a limited area, MFS - maximum flooding surface, TS - transgressive surface, SB - sequence boundary. Sea level curve is relative to the present-day sea level (0 m).

A sea level curve for the Black Sea shelf during the Mio-Pleistocene time span was estimated. This was done using the global sea level curve of Haq et al. (1987), an unpublished sea level curve based on seismic data from the northeastern Black Sea shelf, and salinity information (Jones et al., 1997). Because the unpublished sea level curve for the northeastern Black Sea shelf gives only *relative* sea levels, it was correlated with the sea level curve of Haq et al. (1987) to convert it into a curve with *absolute* values for the present study. This correlation was carried out by choosing two points on the curve of Haq et al. (1987) during a period when the Black Sea was connected to the global oceans. To identify these points, information on the paleo-salinity was used, assuming that salinities of 20-30 ‰ indicate marine conditions. At the two points chosen, the absolute sea levels on the two curves were identical. This provides the necessary calibration of the absolute sea-level scale.

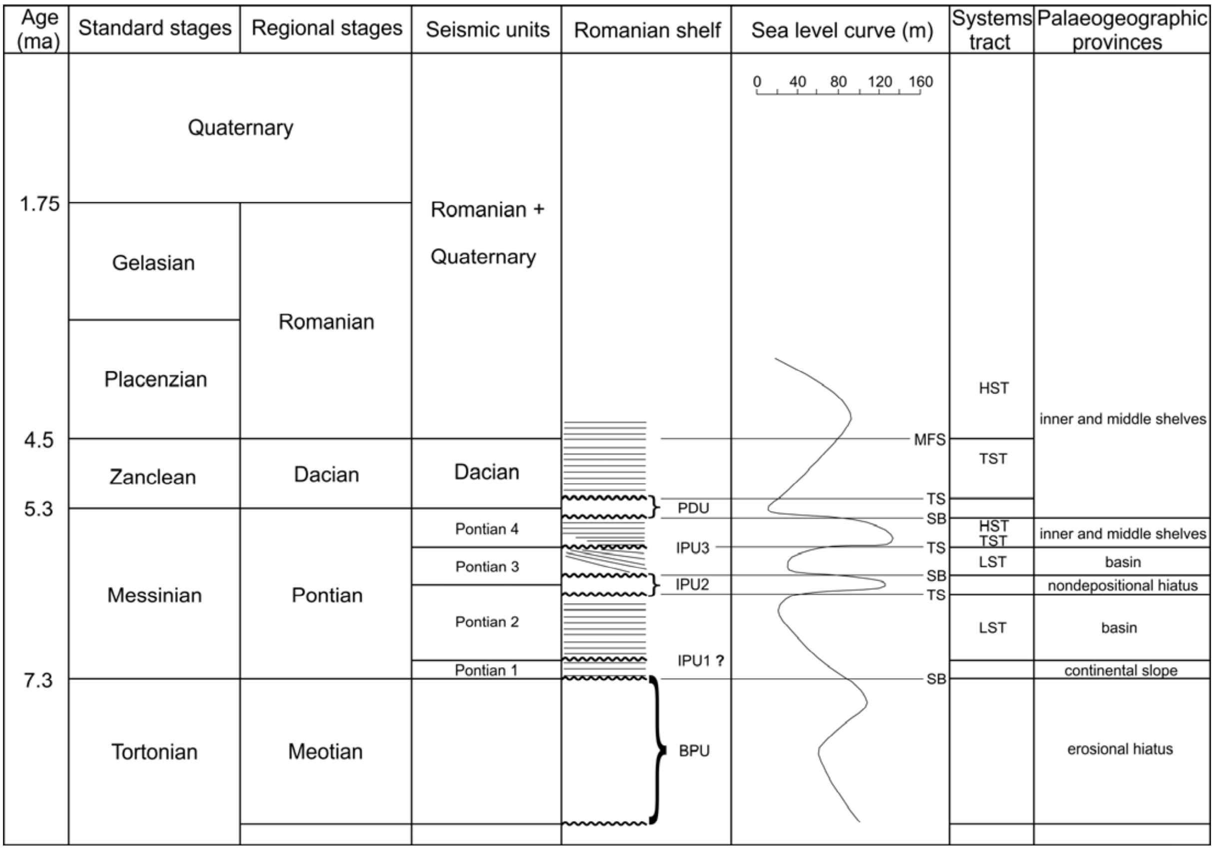

Table 4.3 Chronostratigraphic calibration of the Mio-Pleistocene seismic units from the inner and middle shelves (valid for the area where the Badenian-Sarmatian section is absent). See Table 4.2 for abbreviations.

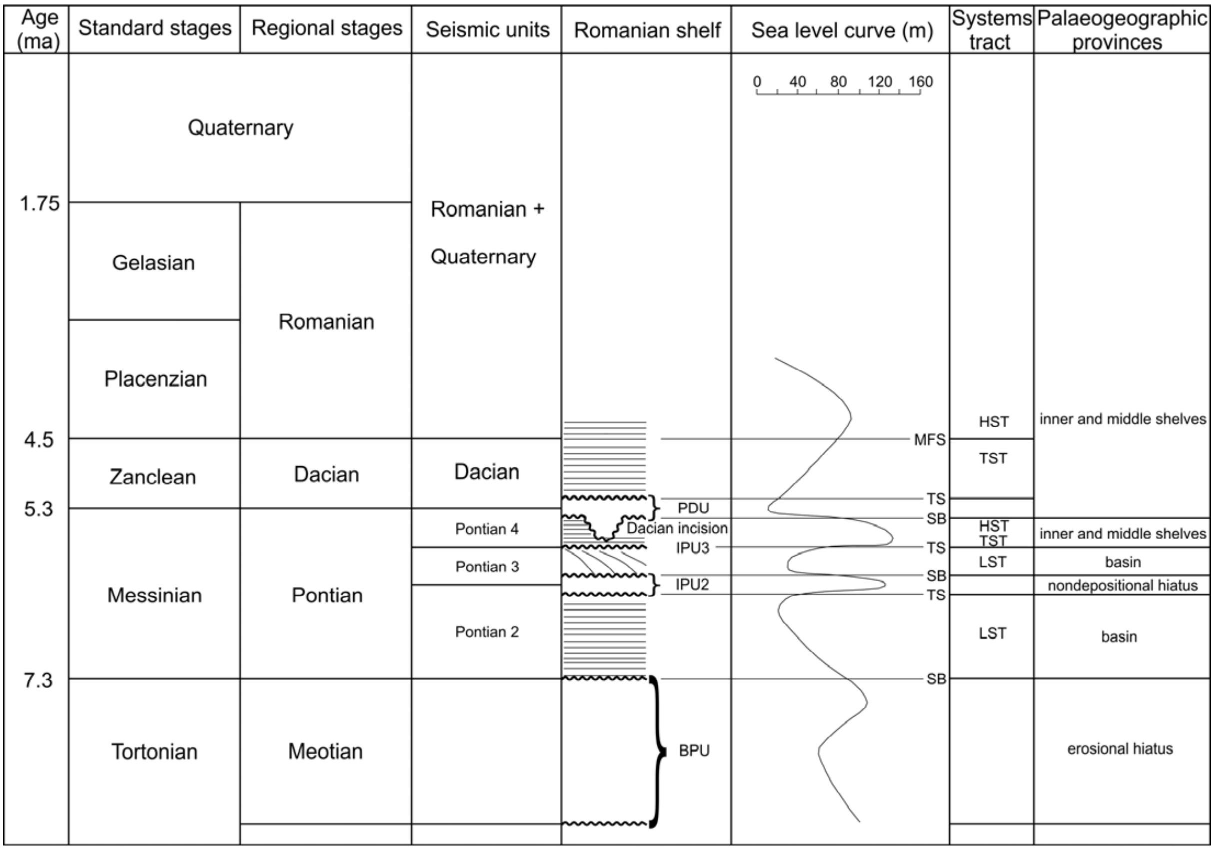

Table 4.4 Chronostratigraphic calibration of the Mio-Pleistocene seismic units for the middle and outer shelves. See Table 4.2 for abbreviations.

4.3.1. Badenian and Sarmatian

The Badenian and Sarmatian are undifferentiated on the Romanian shelf because of their limited thickness. Our seismic data suggest that they are present only in two distinct areas: in the southern part of the middle shelf in the area surrounding the Delfin wells, and in the northwestern inner and middle shelves and on the palaeo-slope around the Histria Depression. Borehole data suggest their presence also at the *1 Ovidiu* and *12 Midia* wells (Fig. 4.1), but the reduced vertical resolution makes their identification on adjacent seismic lines difficult.

Based on the depth distributions (in ms TWT and meters) of the lower (Figures 4.3 and 4.5) and upper boundaries (Figures 4.7 and 4.9) of the Badenian-Sarmatian section, the thickness distribution of these deposits were computed (Figures 4.28 and 4.29). It varies from 0 m at the periphery to 245 m in the internal part of the northwestern area (Fig. 4.29). In the southern area, the distribution pattern is similar but thickness values of only about 100 m are reached.

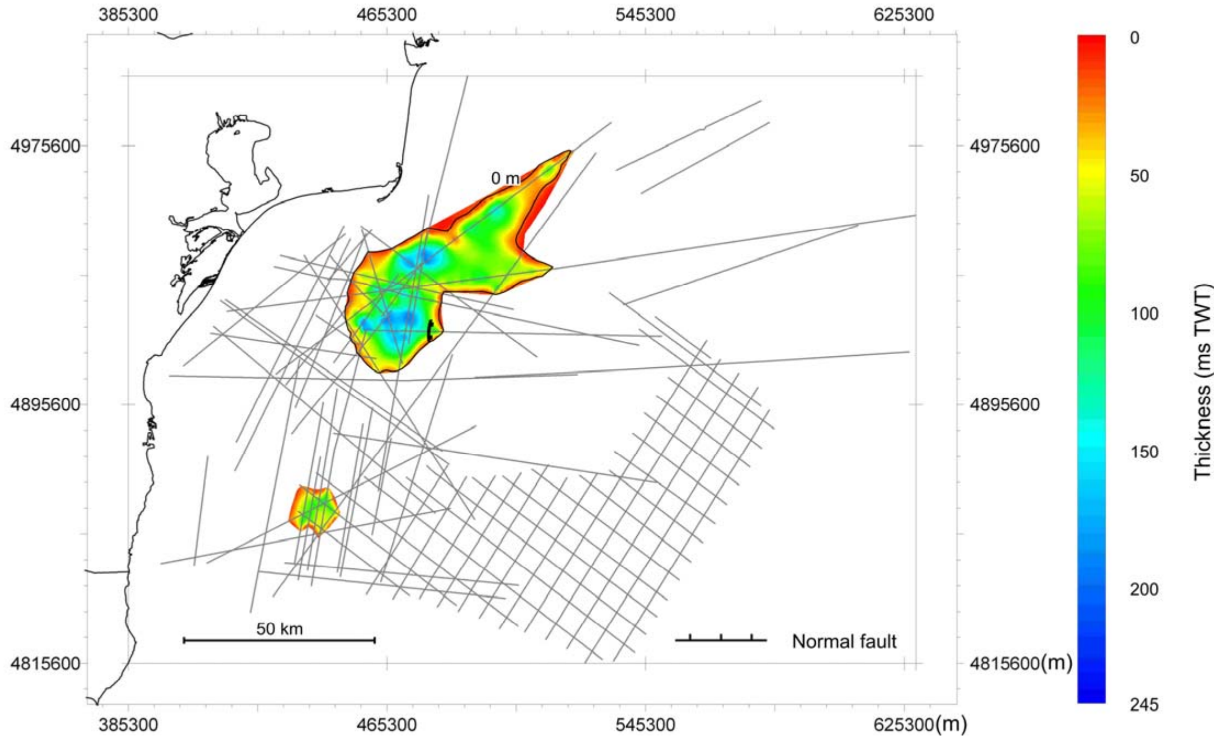

Figure 4.28 Isopach map of the Badenian-Sarmatian section (in ms TWT).

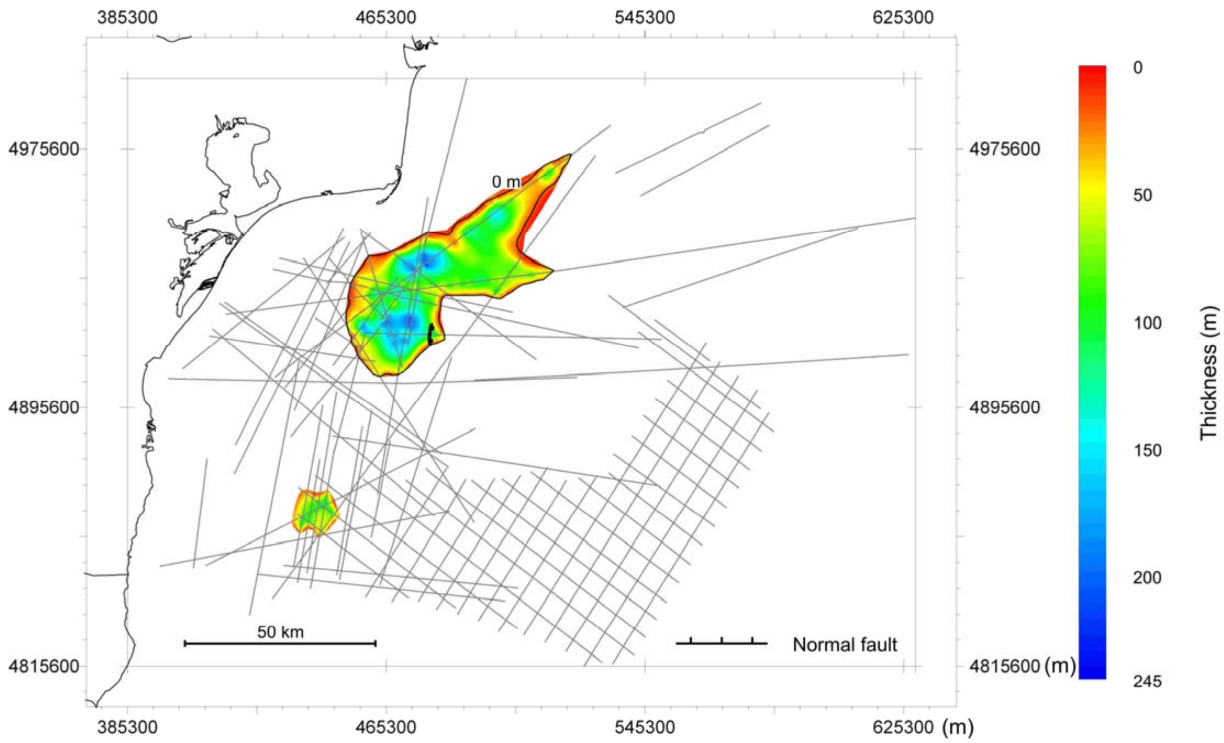

Figure 4.29 Isopach map of the Badenian-Sarmatian section (in meters).

The Badenian-Sarmatian unit is bounded below by the BBU and above by the BPU (Fig. 4.2). It is lenticular in cross-section and dips steeply eastward (Figures 4.30 and 4.31). In the northwestern area, the internal reflection pattern is characterized by parallel to subparallel, low- to medium-amplitude reflectors that downlap against the lower sequence boundary and terminate by toplap at the upper boundary (Fig. 4.30). In the southern area, the terminations are downlap at the base and erosional truncations at the top (Fig. 4.31).

To estimate the depth of the sequence at the time of deposition, the influence of subsidence from the Badenian to the present was taken into account (see Chapter 3.2.3 for details). In the northwestern area, this total subsidence is 38 m, suggesting that the Badenian-Sarmatian section was located 38 m higher that the present-day seafloor at the time of deposition. Borehole information points to a palaeo-water depth of 50 m in this area, implying that the section was located 12 m below the present-day sea level on the inner shelf at the time of deposition. In the south, the total subsidence is 35 m and the palaeo-water depth was about 65 m, yielding a location 30 m below the present-day sea level on the inner shelf at the time of deposition. The internal configuration of the unit and its inner shelf position suggest that it was deposited during a late highstand when the sea level began to fall slowly after reaching a maximum. At that time, the rate of deposition was higher than that of sea level fall; the parasequences prograded basinward and downlapped onto the lower sequence boundary.

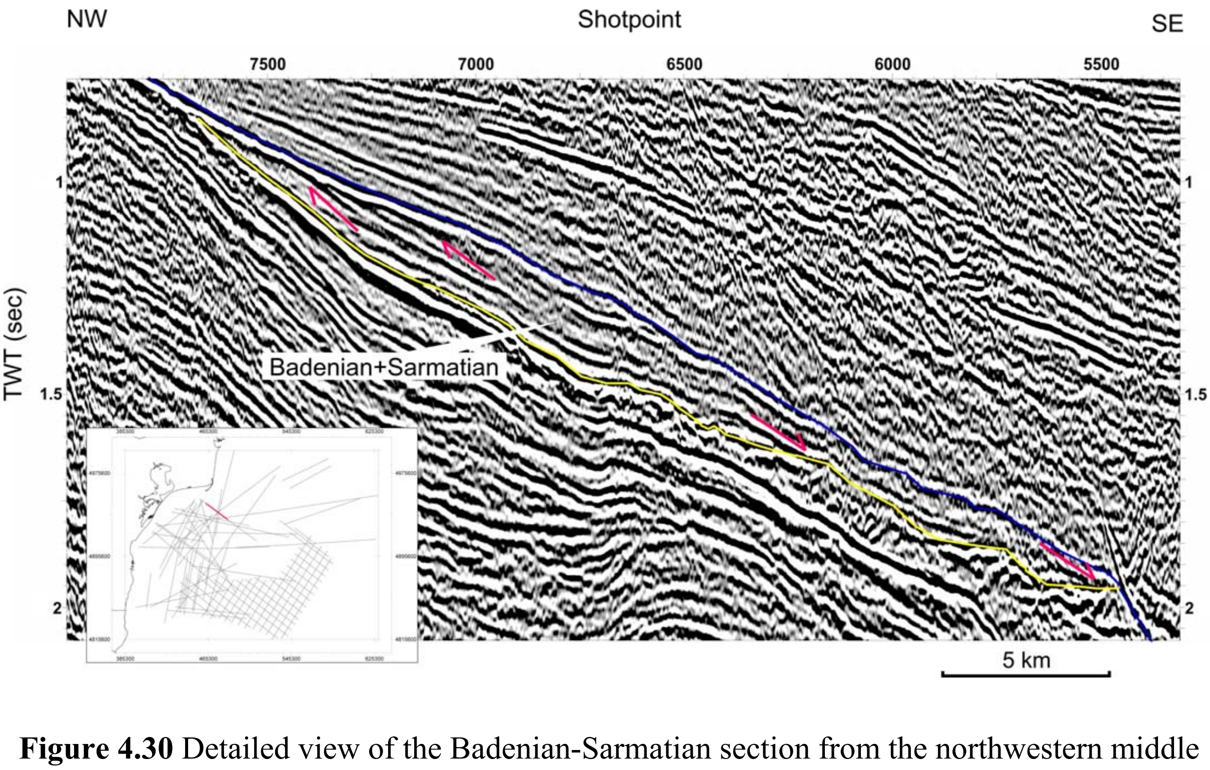

Figure 4.30 Detailed view of the Badenian-Sarmatian section from the northwestern middle shelf; red arrows mark downlap and toplap terminations respectively.

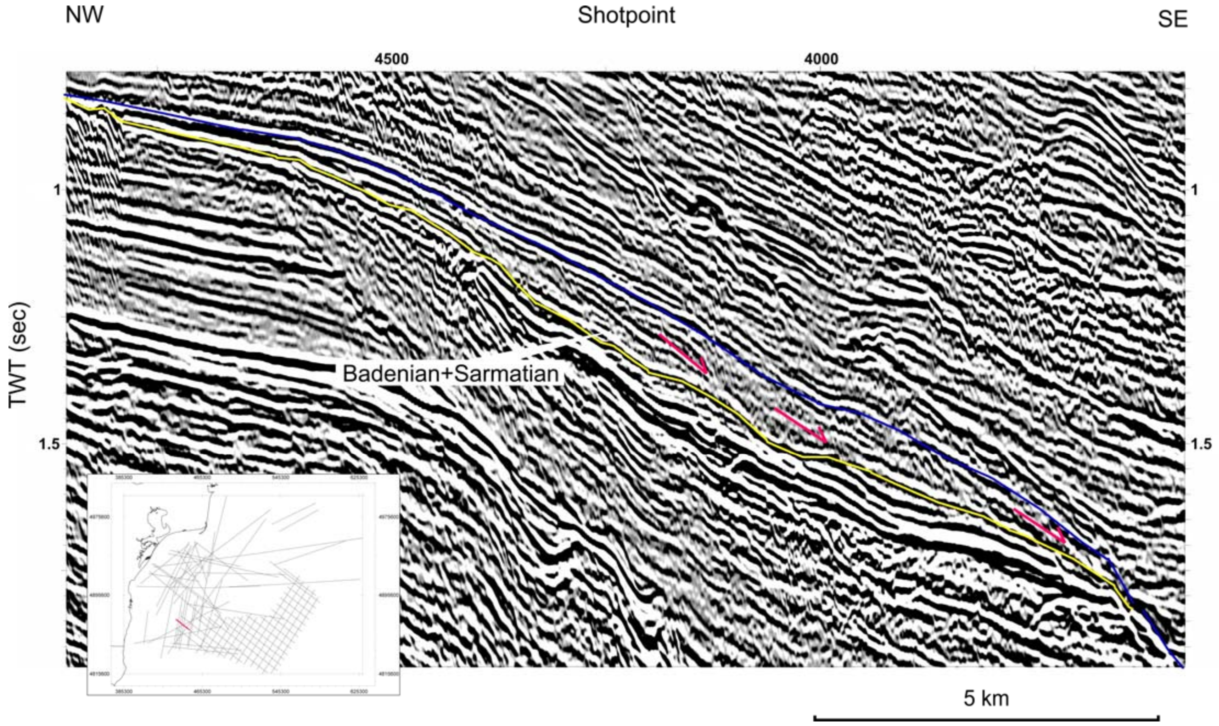

Figure 4.31 Detailed view of the Badenian-Sarmatian section from the southern middle shelf; red arrows mark downlap terminations against the lower sequence boundary.

4.3.2. Pontian

Pontian deposits were encountered in all wells drilled on the Romanian shelf. They have a thickness that varies from 0 m on the inner shelf to 4000 m on the outer shelf in the Cobălcescu area to the east (Fig. 4.1). This notable change in thickness is due primarily to an increase in subsidence of the base of the Pontian to the east, non-uniform sedimentation rates on the shelf and complex tectonics in the Cobălcescu area.

Figures 4.32 and 4.33 show isopach maps of the Pontian section in ms TWT and meters respectively. The observed thickness increases from the inner shelf to the center of the Cobălcescu area, as well as from south to north until the centre of the Histria Depression is reached. In the Histria Depression, the Pontian deposits are strongly tectonically deformed, while farther basinward (beyond the shelf-break) they developed under a quiet depositional regime.

Based on our seismic data, the Pontian was divided into four sequence-stratigraphic units: P1, P2, P3, and P4 in ascending order of age (Fig. 4.27).

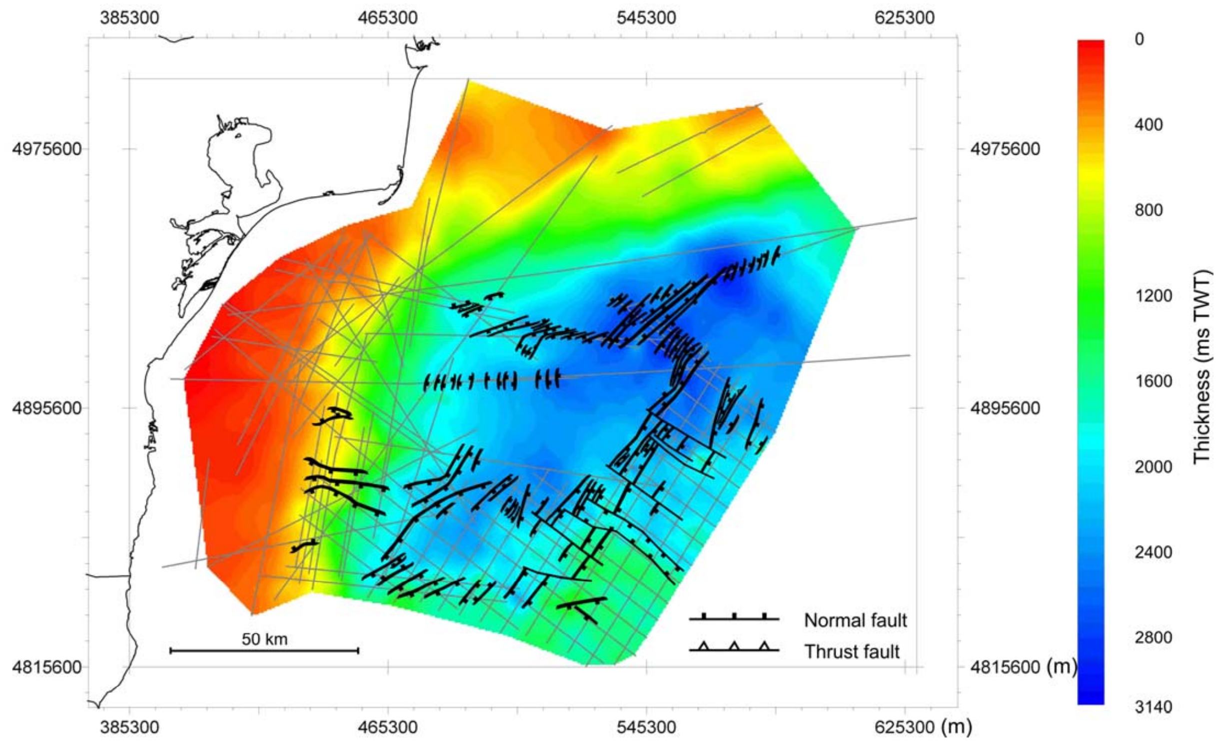

Figure 4.32 Isopach map of the Pontian section (in ms TWT).

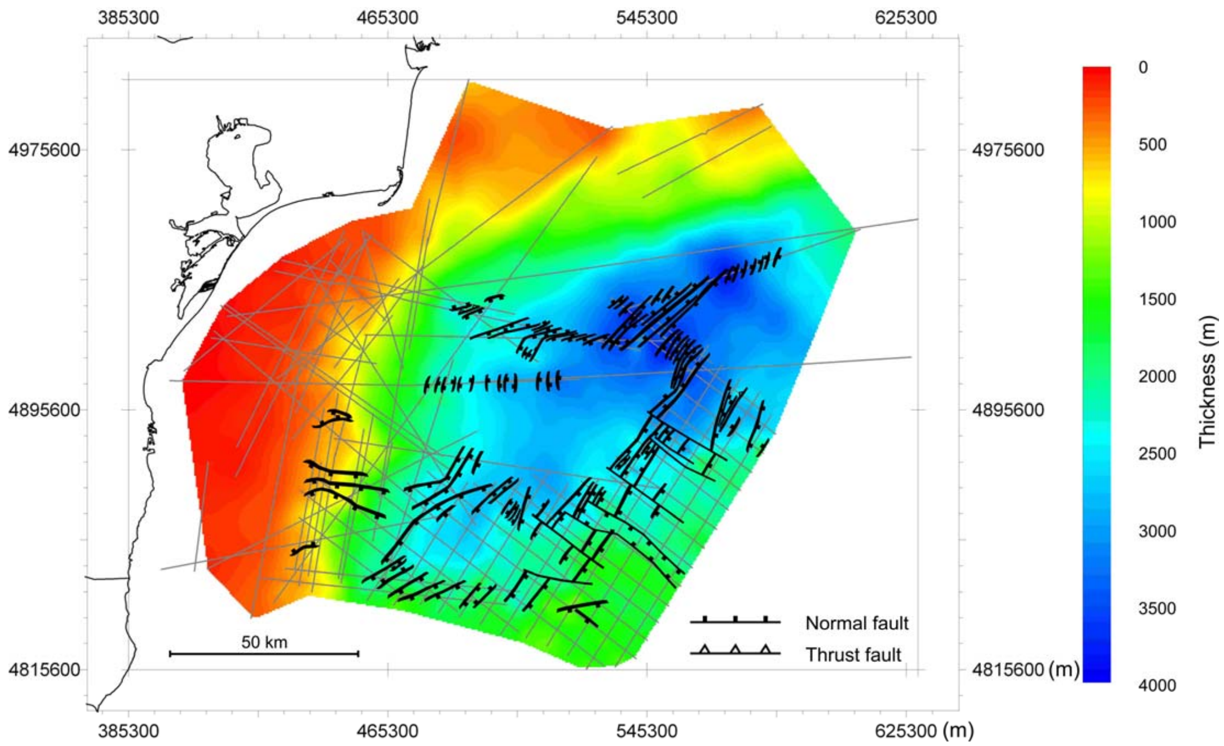

Figure 4.33 Isopach map of the Pontian section (in meters).

4.3.2.1. Pontian 1 (P1)

The occurrence of Pontian 1 is restricted to the western and northwestern inner shelf and part of the middle shelf. It was deposited above the palaeo-slope that marks the base of the Pontian formations, being bounded below by the BPU and above by IPU1 (Fig. 4.13). This subunit was not affected by tectonic processes that dominated during the rest of Pontian time.

In the west, isopach maps (in ms TWT and meters; Figures 4.34 and 4.35) show an increase in thickness of P1 from 0 m at the periphery to about 350 m at the centre of the area of occurrence.

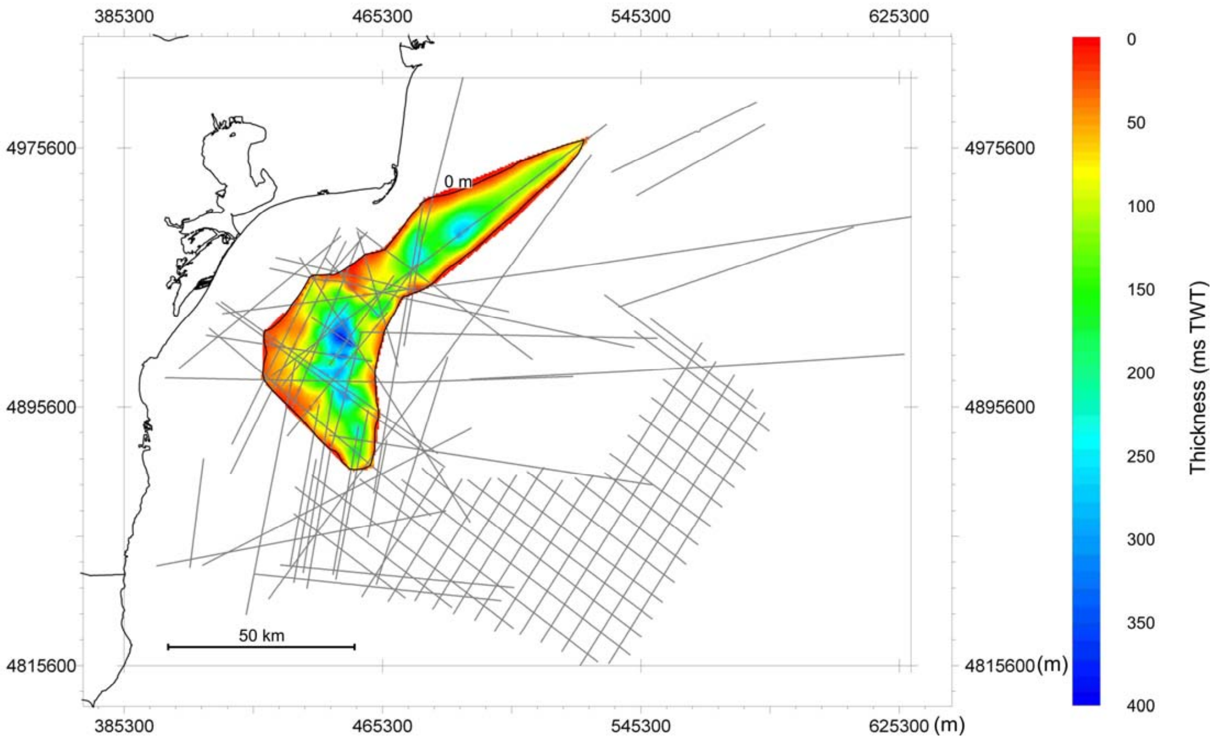

Figure 4.34 Isopach map of Pontian 1 (in ms TWT).

Figure 4.36 is a seismic section showing the characteristics of the subunit Pontian 1. This subunit is lenticular in shape and has a steep dip to the east. It terminates with onlap against the lower sequence boundary and with an erosional truncation at the upper boundary. It consists of medium-amplitude reflectors that are subparallel to the lower boundary.

Where P1 is developed, the total subsidence is 89 m from the beginning of the Pontian to the present. This suggests a position of P1 89 m below the present-day seafloor, which was 50 m below the present-day sea level. This in turn implies a location on the slope at the time of deposition. The onlap terminations against the lower sequence boundary coupled with the progradational nature of the subunit suggests that it was deposited during a late lowstand, when sea level began to rise very slowly. The high sediment supply and slow sea level rise led to a progradational depositional pattern, corresponding to the lowstand wedge of a lowstand systems tract (LST).

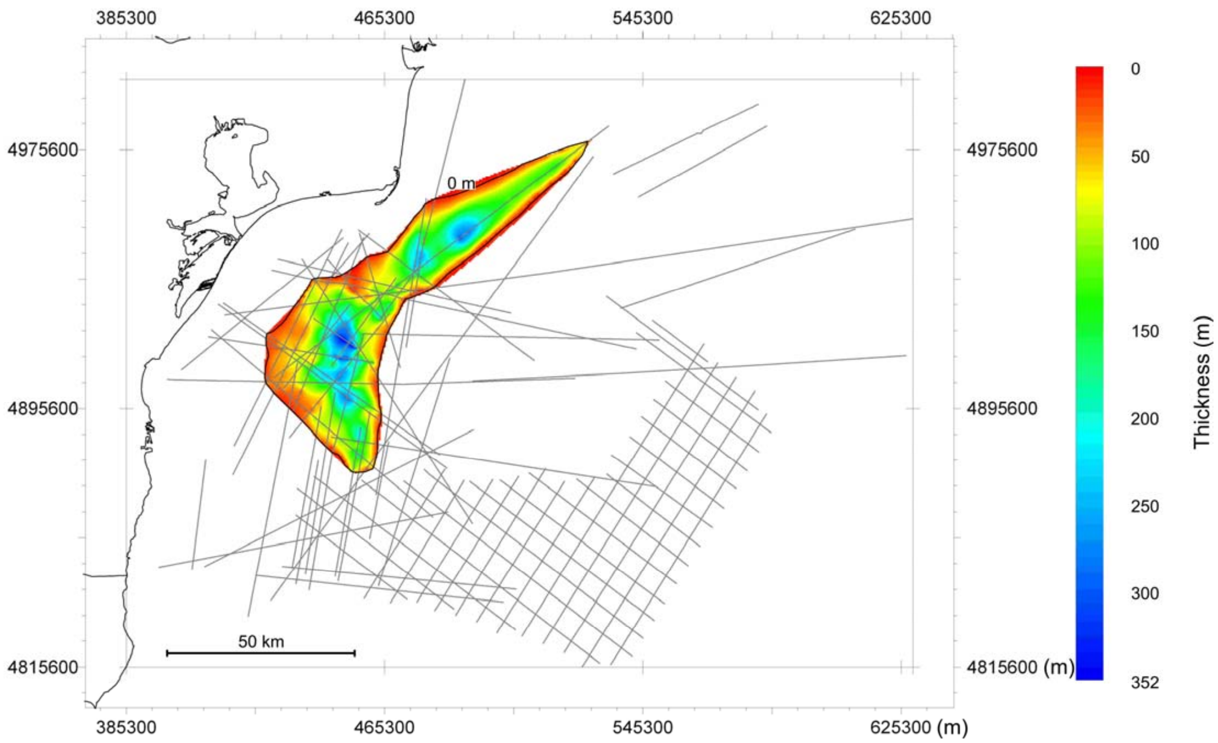

Figure 4.35 Isopach map of Pontian 1 (in meters).

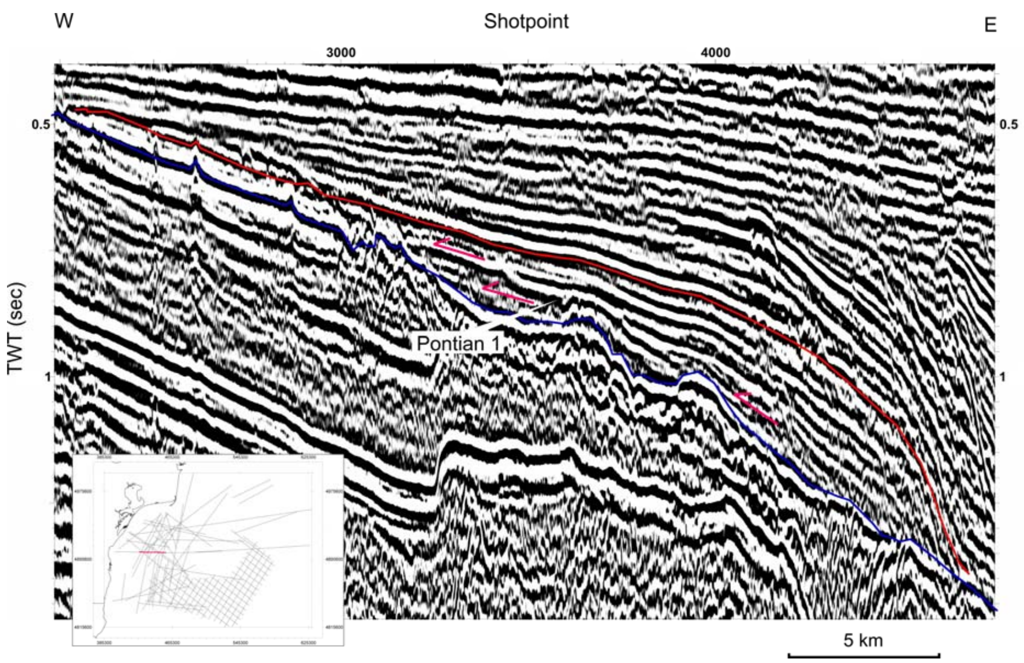

Figure 4.36 Detailed view of the section P1; red arrows indicate onlap terminations against the lower subunit boundary (also a sequence boundary).

4.3.2.2. Pontian 2 (P2)

The Pontian 2 subunit (P2 in Fig. 4.27) is developed over the entire study area. It is bounded below by IPU1 on the inner shelf and by BPU on the middle and outer shelves, as well as by IPU2 above (Figures 4.2 and 4.13). This subunit underwent a complex evolution and was affected by the most tectonically active period of the Pontian. Tectonic activity took place in the entire Histria Depression during this interval, with a widespread reactivation of the tectonic structures that dominated the Oligocene basin. Some of the faults continued to be active during the Upper Pontian and the Dacian-to-Quaternary. Others ceased their activities at the end of P2. The area basinward of the shelf-break was tectonically quiescent during P2 time.

Figures 4.37 and 4.38 are isopach maps (in ms TWT and meters respectively) of subunit P2 showing a large increase in thickness from 0 m near the coast to over 2400 m in the Cobălcescu area. This increase is probably due to a high sediment supply, active tectonics and significant subsidence.

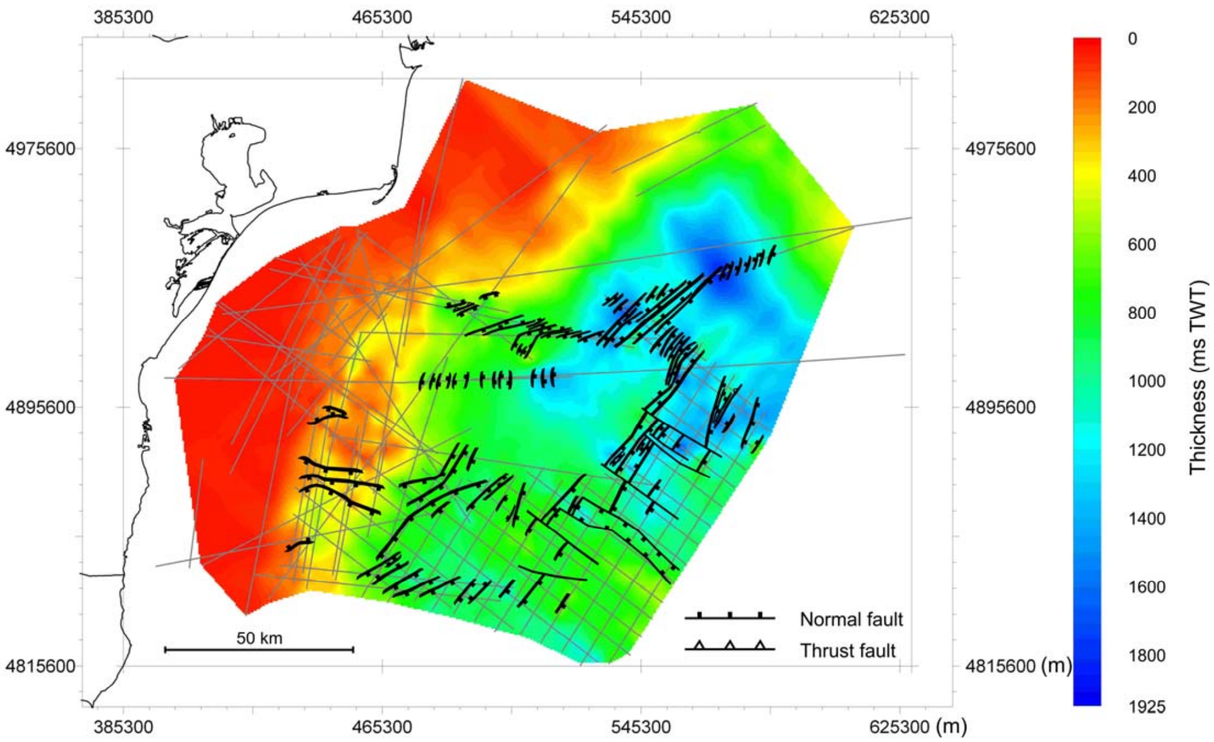

Figure 4.37 Isopach map of the P2 subunit (in ms TWT).

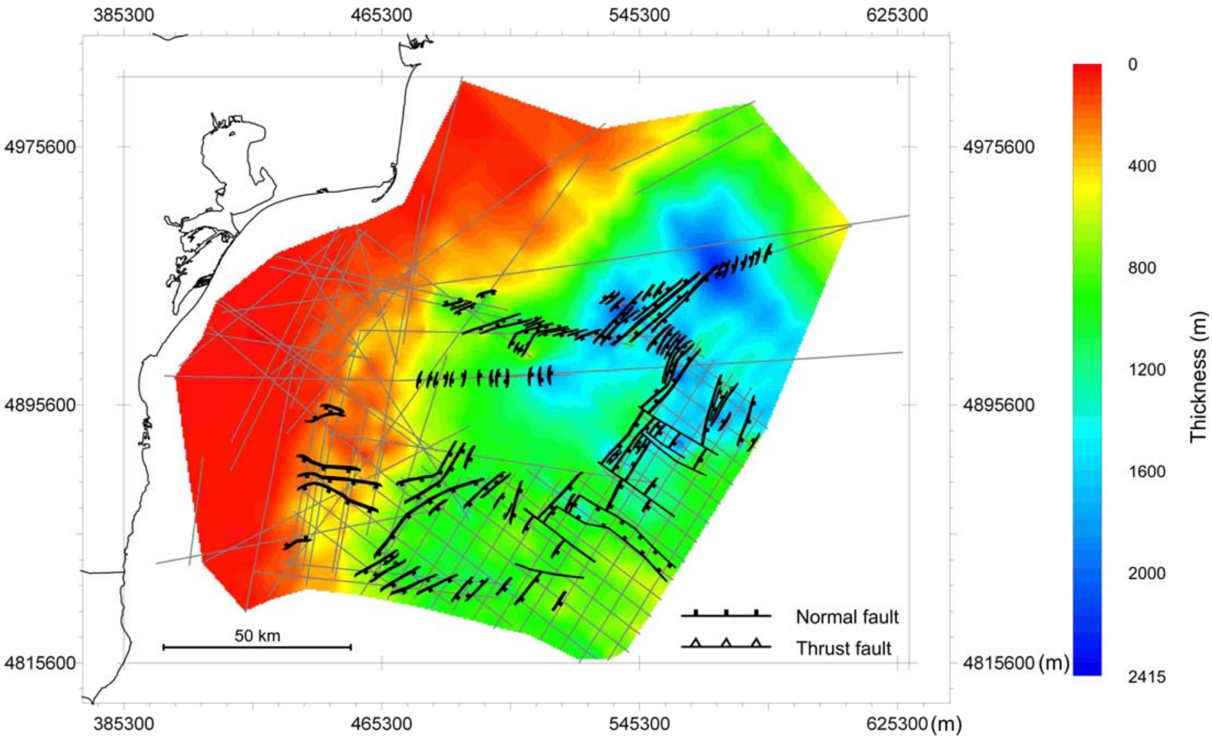

Figure 4.38 Isopach map of the P2 subunit (in meters).

Subunit P2 exhibits two different seismic facies patterns. On the western inner shelf, it is thin, and is characterized by divergent, discontinuous, low-amplitude reflectors that onlap the lower boundary (IPU1), while the upper boundary (IPU2) is represented by an erosional truncation (Fig. 4.39). On the middle and outer shelves, its thickness increases rapidly eastwards and it is characterized either by medium amplitude reflectors that are parallel to the lower boundary (BPU), or occasionally by chaotic reflections (Fig. 4.40). Both the lower and the upper (IPU2) boundaries are erosional.

The internal configuration and external geometry of subunit P2 suggests that at the time of deposition, it straddled the continental slope and the deep basin. Since basinal deposition is possible only during a lowstand when the shelf is exposed and the sediment bypasses the shelf to be laid down on the slope and in the basin, this unit is attributed to a LST.

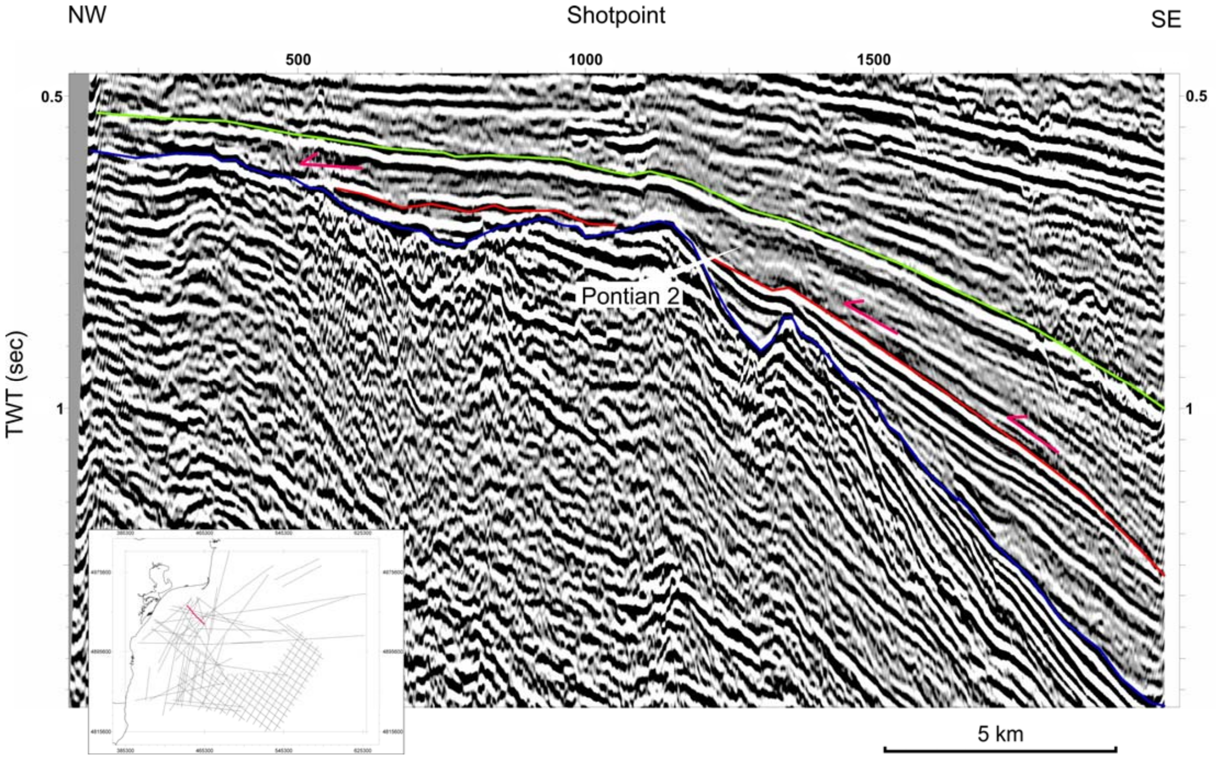

Figure 4.39 Details of subunit P2 showing its characteristics on the inner shelf. Red arrows indicate onlap terminations against the lower subunit boundary.

4.3.2.3. Pontian 3 (P3)

The subunit Pontian 3 covers almost the same area as subunit P2 and has a similar external geometry. It is bounded below by IPU2 and above by IPU3 (Figures 4.2, 4.6 and 4.13). Its thickness varies from 0 m near the coast to a maximum of 1595 m in the Histria Depression (Figures 4.41 and 4.42). On the inner shelf, subunit P3 is very thin, while on the middle and outer shelves, it increases abruptly in thickness.

Progradation of P3 on the middle and outer shelves is due to over-compensation of syn-depositional subsidence by sediment supply. Subunit P3 is characterized by high amplitude reflectors that downlap the lower boundary and by an erosional truncation at the top (Fig. 4.43). It dips steeply in the west but becomes almost horizontal in the east. Compared to the previous subunit, P3 is a period of quiet sedimentation in the central Histria Depression. Only on the outer shelf and on the shelf-break was P3 affected by tectonic processes that started in the Oligocene or in pre-Oligocene time.

For subunit P3, only an approximate subsidence correction is possible because of insufficient borehole information. On the outer shelf, a difference of >200 m between the present-day depth of P3 and the total subsidence was estimated. At the time of deposition, P3 was over 300 m below the present-day sea level. The reflection terminations and the wedge-shape suggest that this subunit was deposited during a sea level lowstand. The sea level fall that produced the lower subunit boundary was beyond the shelf-break; the shelf became subaerial and rivers incised into the exposed shelf. The rate of sea level fall exceeded the rate of subsidence, and a large sediment supply produced basinward progradation of sediments deposited on the slope.

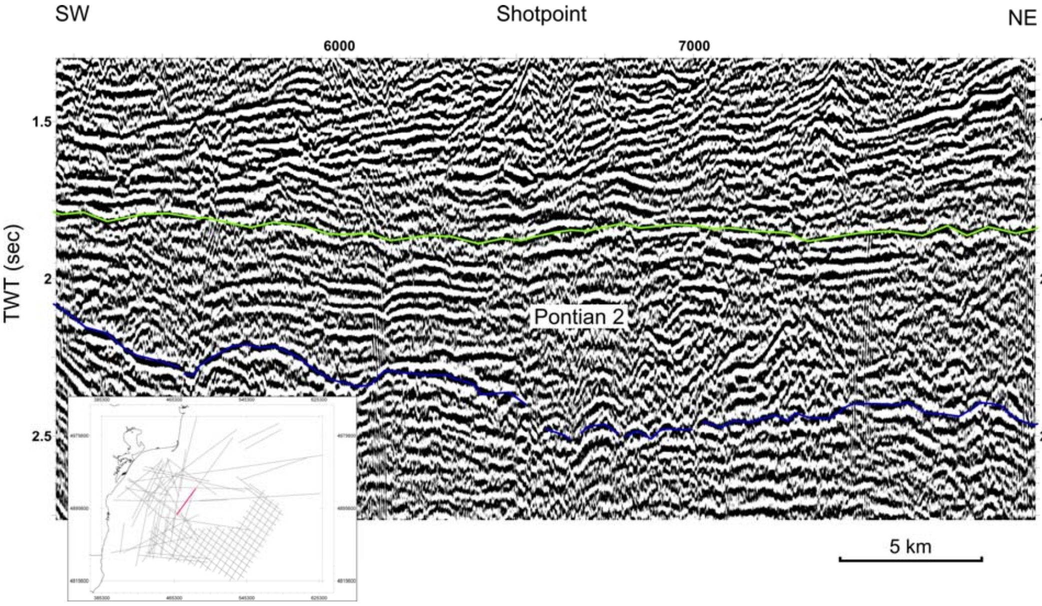

Figure 4.40 Details of subunit P2, showing its characteristics on the middle and outer shelves. Note the erosional truncations at both the upper and lower boundaries.

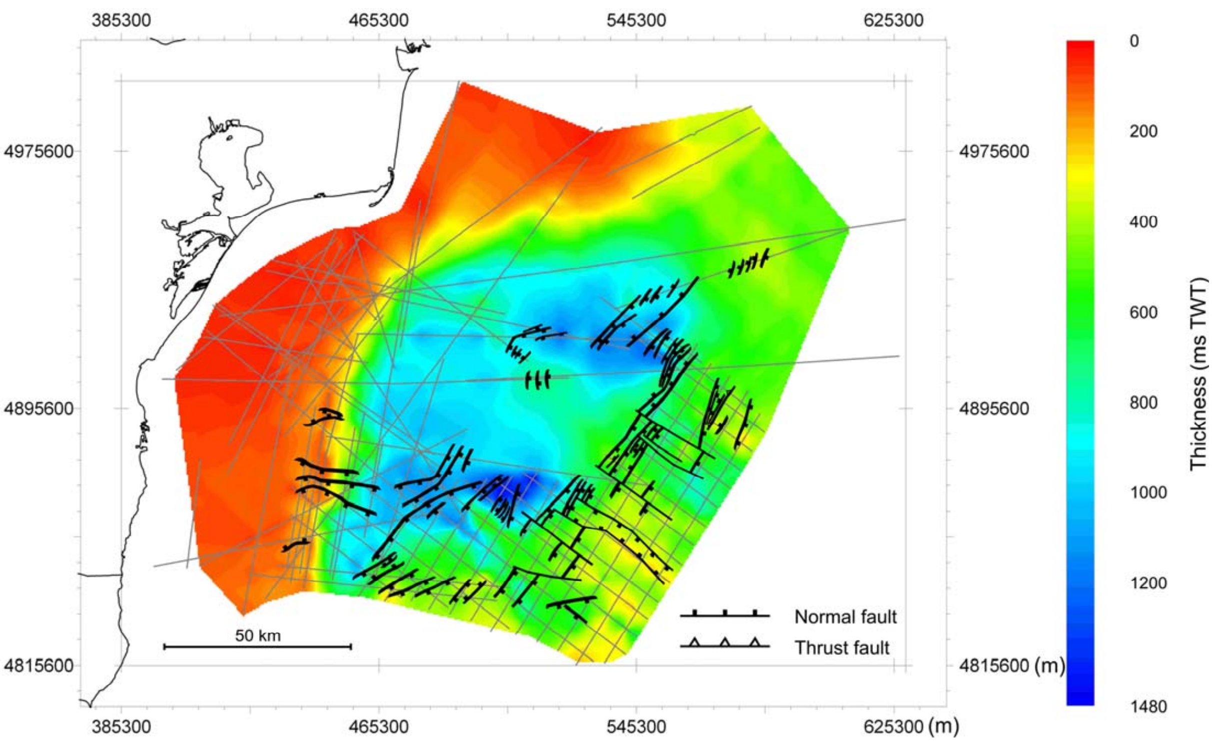

Figure 4.41 Isopach map of the subunit P3 (in ms TWT).

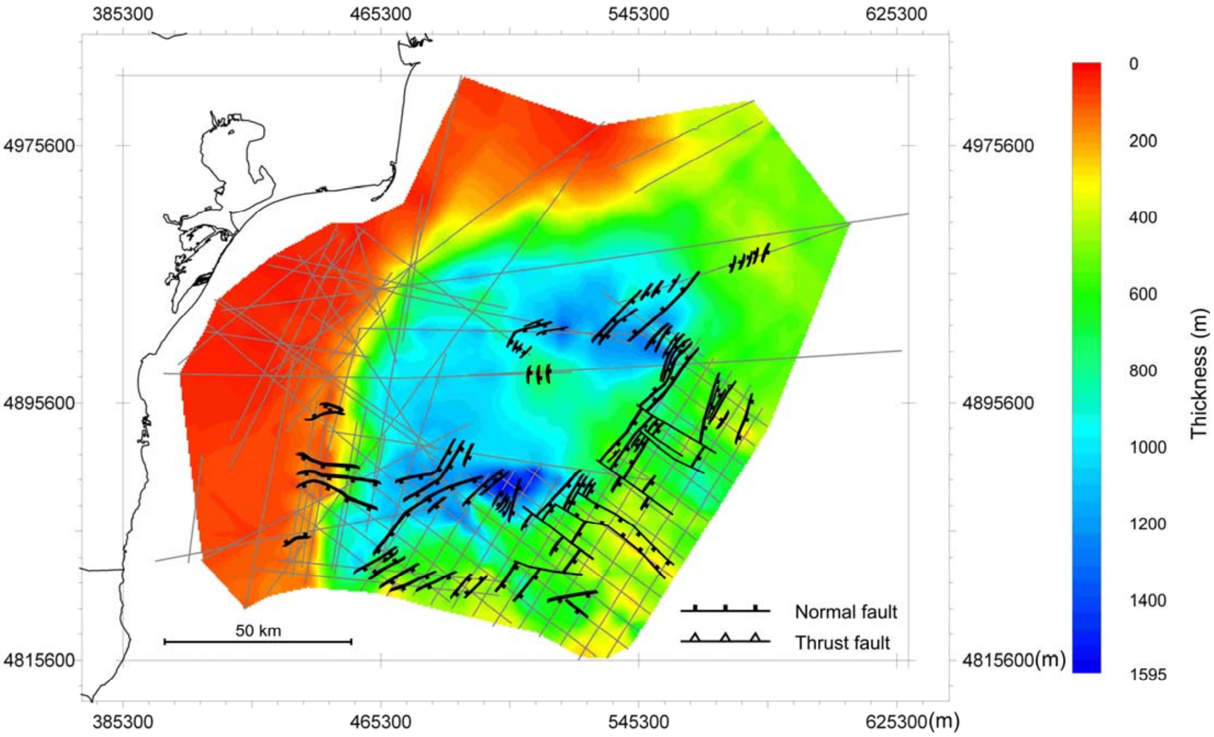

Figure 4.42 Isopach map of the subunit P3 (in meters).

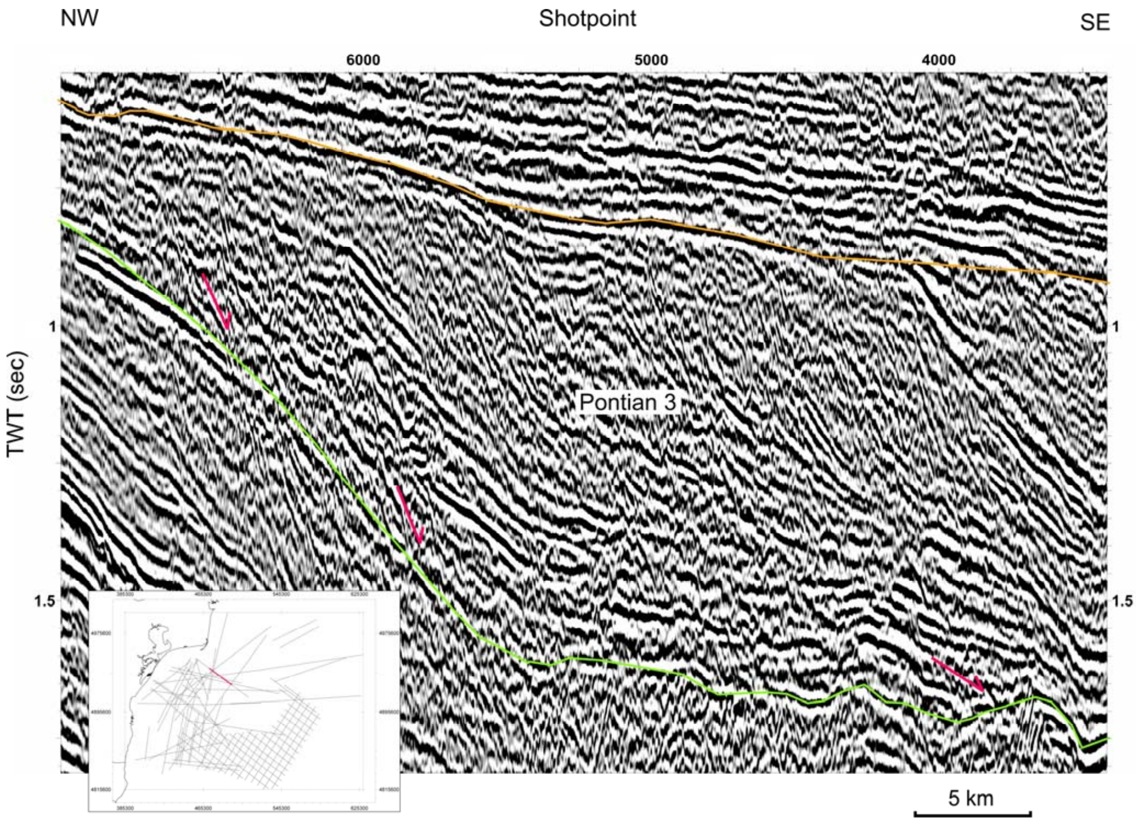

Figure 4.43 Details of the subunit P3. Red arrows indicate downlap terminations against the lower subunit boundary.

4.3.2.4. Pontian 4 (P4)

This uppermost Pontian subunit is present over the entire study area and is bounded below by IPU3 and above by PDU (Figures 4.2, 4.6 and 4.13). The basinward increase in thickness is more moderate compared to the subunits P2 and P3. It ranges between 0 m near the coast to 940 m in the central Histria Depression (Figures 4.44 and 4.45). The section is less affected by tectonics compared to the two older subunits. Tectonic activity occurs only on the outer shelf and on the shelf-break. The faults are continuations of older Pontian faults without significant vertical offsets.

Subunit P4 is represented by parallel, medium amplitude reflectors that onlap against the lower boundary and are conformable or erosional at the upper boundary (Fig. 4.46). On the middle shelf, it is cut by incised valleys of over 300 m depth (Figures 4.6 and 4.13).

For the subunit Pontian 4, a subsidence correction is not possible because of the lack of borehole information for this interval. Based on reflection terminations and the seismic facies characteristics, we speculate that P4 was located on the shelf at the time of deposition. The lower part of the subunit is attributed to a transgressive systems tract (TST), which formed as sea level began to rise and reached the shelf-edge. Thereafter, accommodation space was created at a rate faster than it could be filled with sediment and a retrogradational

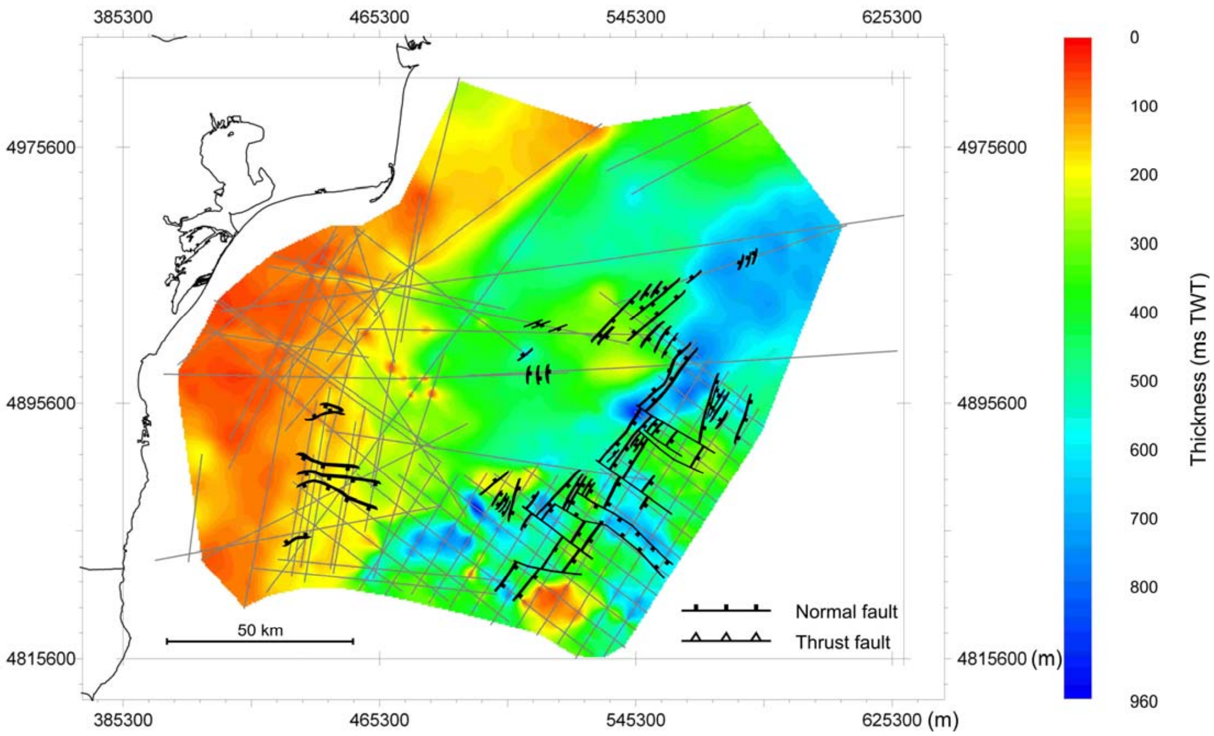

Figure 4.44 Isopach map of subunit P4 (in ms TWT).

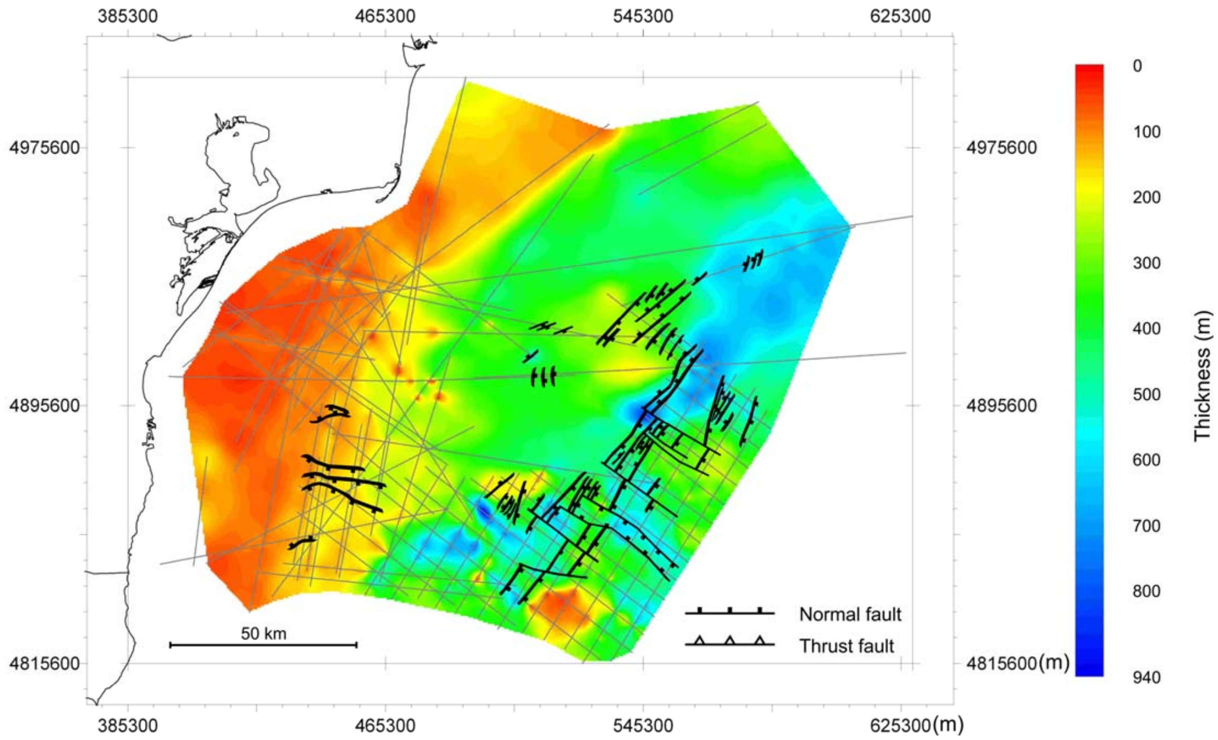

Figure 4.45 Isopach map of subunit P4 (in meters).

pattern marked by onlap terminations developed. At the end of the TST, sea level rose at a rate faster than the rate of sediment supply to the basin and a maximum flooding surface formed. Thereafter, sea level rise slowed down, while the rate of sediment supply increased; an aggradational pattern typical for the HST developed. The subsequent sea level fall led to the formation of a sequence boundary.

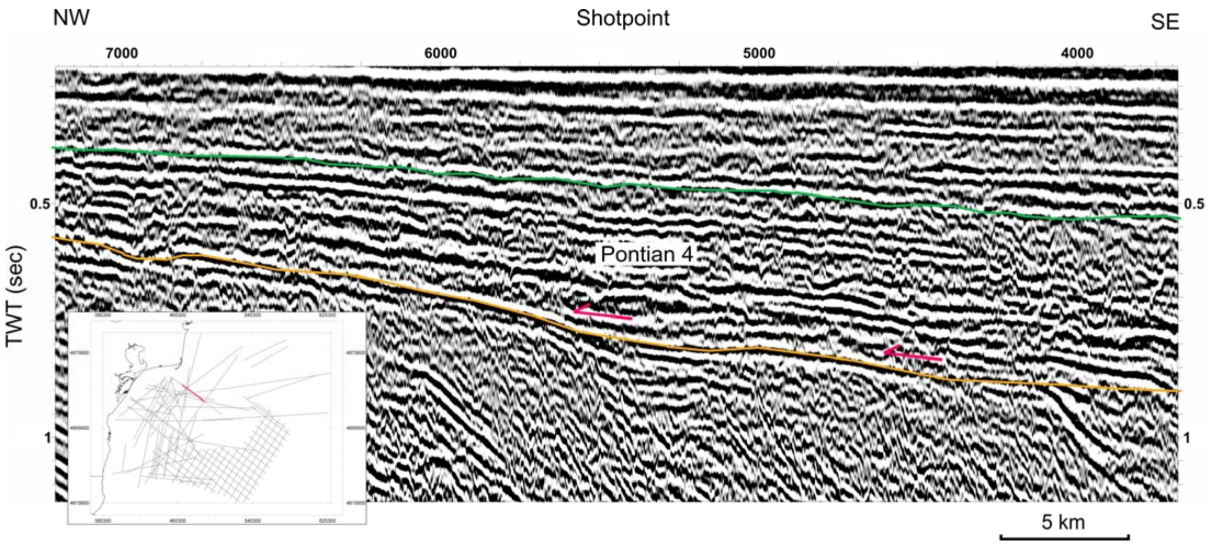

Figure 4.46 Details of subunit P4. Red arrows indicate onlap terminations against the lower subunit boundary.

4.3.3. Dacian

The Dacian unit occurs over the entire study area and increases in thickness from the inner to the outer shelf, from values of 0 m in the vicinity of the coast to 1150 m in the east and southeast (Figures 4.47 and 4.48). It has a drape sheet external form and comprises parallel, low-to-medium amplitude reflectors (Fig. 4.49). Its lower boundary is conformable on the inner shelf, but becomes erosional basinward, where incised valleys of a few hundreds meters in depth are common. During the Dacian, a regime of quiet sedimentation prevailed over wide areas. Only on the outer shelf close to the shelf-break were older faults reactivated.

The external geometry of this unit suggests that it was located on the shelf at the time of deposition. After the formation of the previous sequence boundary, sea level fell below the shelf-break; the continental shelf was exposed and fluvial incision occurred. Subsequent to the lowstand, the incised valleys were filled transgressively during Dacian time.

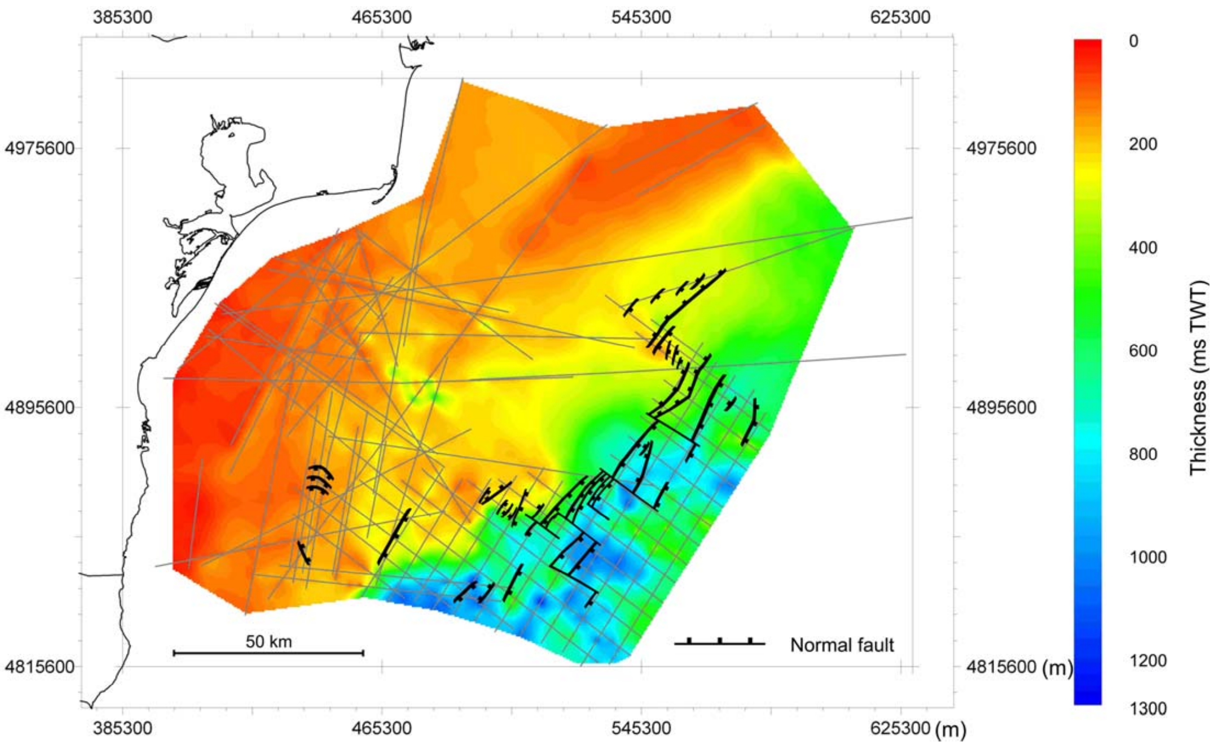

Figure 4.47 Isopach map of the Dacian section (in ms TWT).

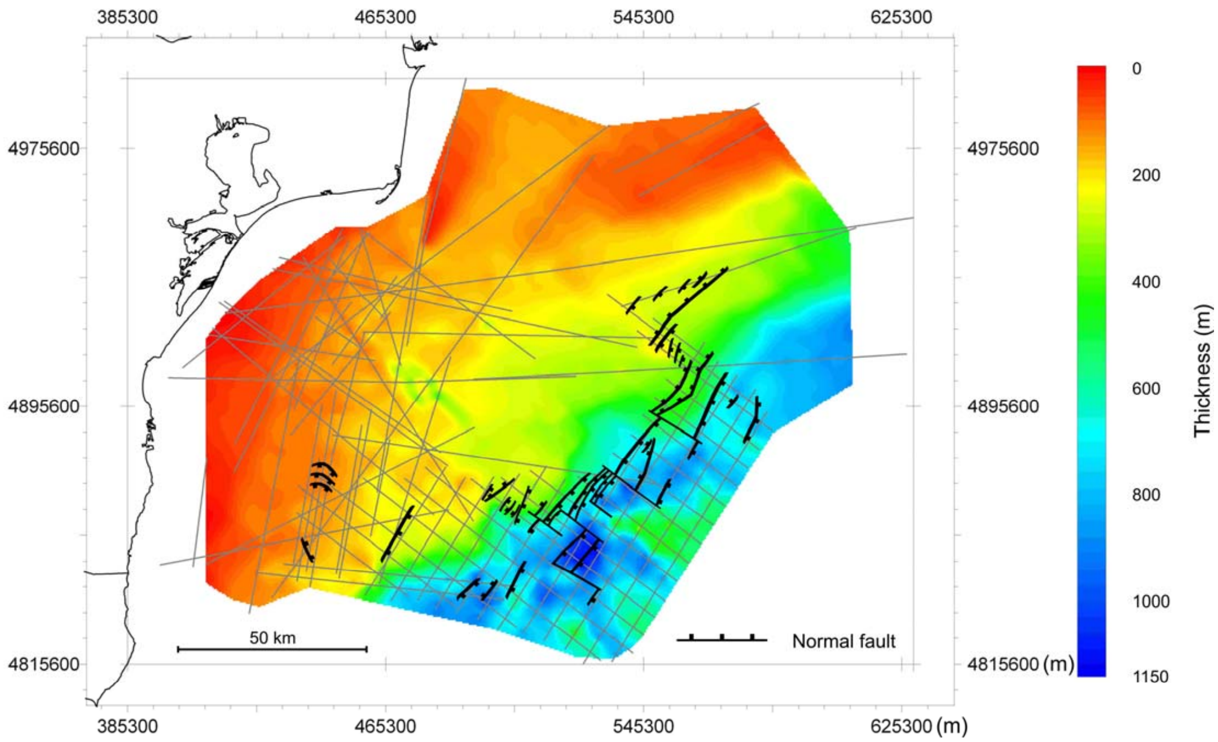

Figure 4.48 Isopach map of the Dacian section (in meters).

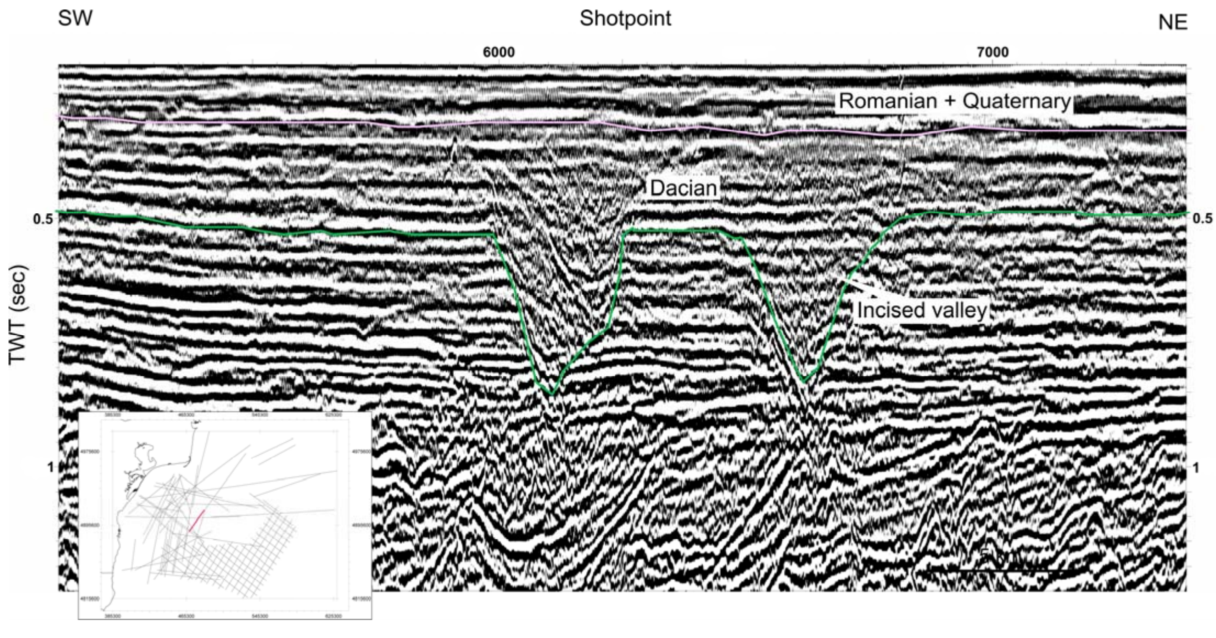

Figure 4.49 Details of the Dacian, Romanian and Quaternary section. Incised valley of about 300 m depth occurs at the base of the Dacian incised into the Pontian.

4.3.4. Romanian and Quaternary

The Romanian-Quaternary section occurs over the entire studied area and shows only small variation in thickness from 0 m in the coastal area to 575 m on the outer shelf and the continental slope (Figures 4.50 and 4.51). The boundary between the Dacian and the Romanian-Quaternary deposits has a conformable character; their separation was possible only based on borehole information. The section has a drape sheet external form, is made up of parallel, low amplitude reflectors (Fig. 4.49), and is characterized by quiet sedimentation.

We presume that this section was deposited after the transgressive phase of the Dacian during a sea level highstand. As the rate of sea level rise slowed down after reaching a maximum, sediment supply increased and a maximum flooding surface formed. Sediment continued to be delivered at a faster rate than that of sea level rise and typical aggradational parasequences developed.

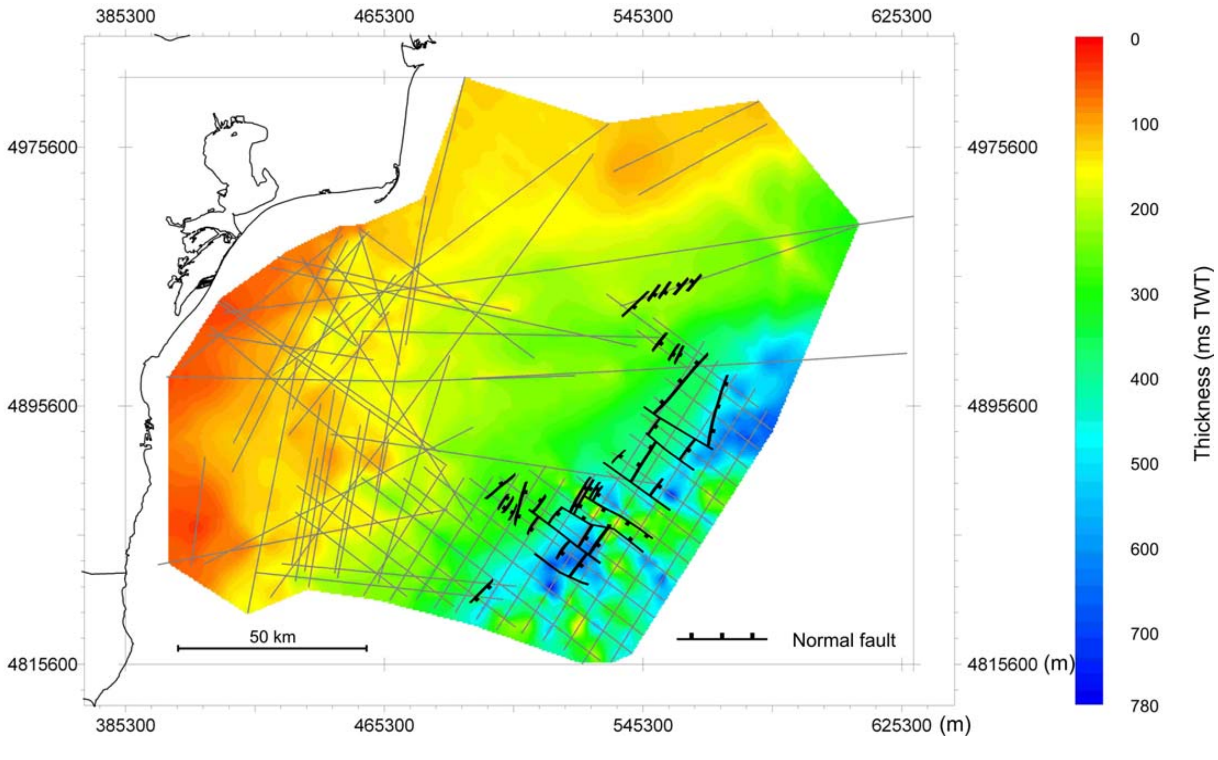

Figure 4.50 Isopach map of the Romanian and Quaternary section (in ms TWT).

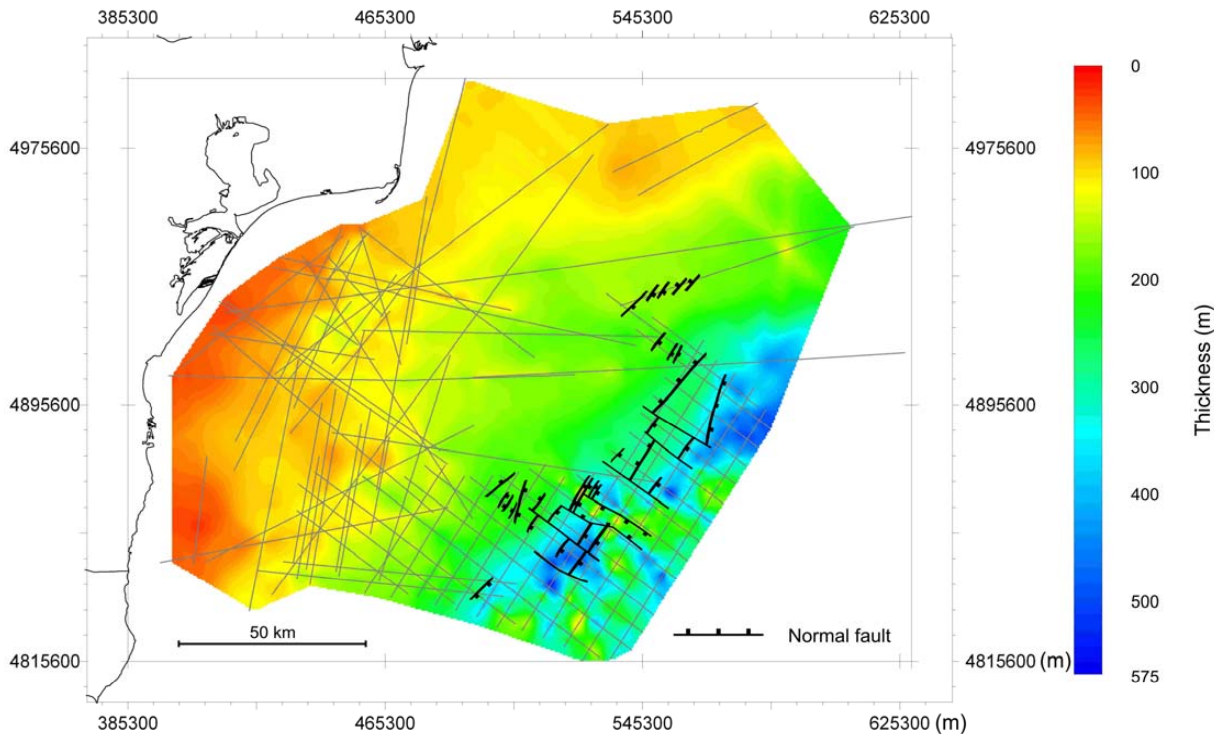

Figure 4.51 Isopach map of the Romanian and Quaternary section (in meters).

4.4. Mio-Pleistocene structural characteristics

4.4.1. Introduction

The Romanian shelf was tectonically most active in the Pontian during the Mio-Pleistocene period. The Badenian-Sarmatian and the Dacian-to-Quaternary deposits are less affected by faulting. The Euxinian Threshold (Fig. 4.1) separates two distinct zones on the shelf: the western and northwestern zone which is practically uninfluenced by tectonic processes, and the eastern and southeastern zone which is tectonically very active in connection with the development of the Histria Depression. A description of the Badenian-Sarmatian, Pontian, and Dacian-to-Quaternary deposits follows.

4.4.2. Badenian and Sarmatian

The Badenian-Sarmatian is a period of tectonic quiescence; extensional structures identifiable on seismic data are developed only locally (Fig. 4.29). The vertical offset of such structures is typically about 350 m (Fig. 4.52).

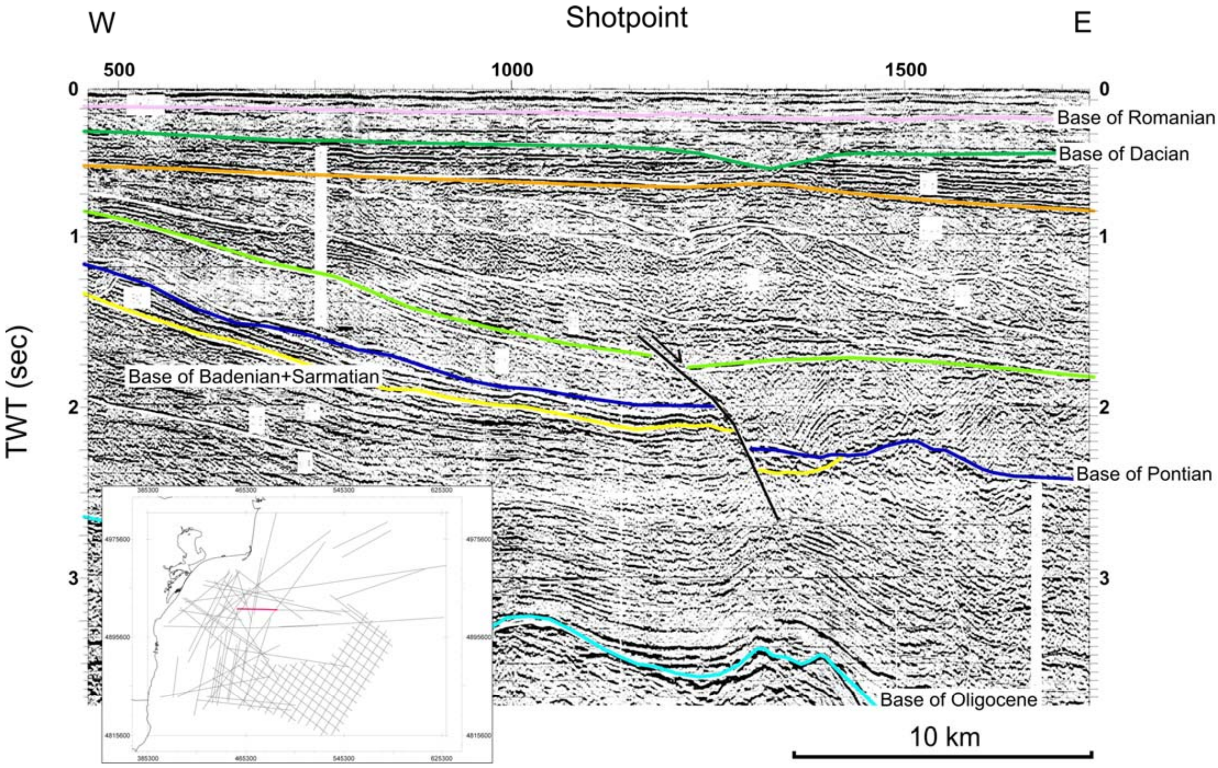

Figure 4.52 Interpreted seismic line illustrating normal faulting within the Badenian-Sarmatian deposits.

4.4.3. Pontian

The Pontian was a time of intense tectonic activity on the Romanian shelf, even though these activities did not affect the entire shelf, but were concentrated in the area basin-ward of the palaeo-slope (the Histria Depression) as well as in a small depression around the Delfin wells (Fig. 4.53). The structures developed are mostly NE-SW trending grabens, horsts and flower structures (Fig. 4.53).

The faulting that affected the Pontian section can be classified in two ways: *temporal* and *spatial*. From the *temporal* point of view, we separate faults that began their activity in the Pre-Oligocene and continued their activities into the Pontian, faults that developed during the Oligocene-Pontian and faults that developed only during the Pontian. *Spatially*, faulting can be related to a NE-SW depression (which we call the “Pontian Depression”) with its depocenter crossing the *1 Ovidiu* and *75 Cobălcescu* wells, and gravitational faulting at the shelf-break.

1. Temporal classification

The faults that began their activities in the pre-Oligocene (Figures 4.56, 4.57 and 4.60) are related to the formation of the Oligocene Histria Depression. It is assumed that the large sediment thicknesses and rapid subsidence led to fault reactivation during the Lower Pontian (Țambrea et al., 2000) in an extensional regime characterized by NE-SW trending normal faults and grabens (Figures 4.54 and 4.56). Vertical offsets are on the order of a few meters to about 800 m (Fig. 4.54). They are mostly present in the central and northern Histria Depression (around and northeast of the well *75 Cobălcescu* in Fig. 4.53), but some of them developed also on the outer shelf (Figures 4.57 and 4.60).

The second category of faults that started their activity in the Oligocene and continued into the Pontian (Figures 4.54 and 4.55) are gravitational faults that developed in sediments of a similar facies existing both during Oligocene and Pontian times. The central and northern Histria Depression is an extensional zone characterized by NE-SW trending normal faults and grabens (Fig. 4.54) that extend northeastward (Fig. 4.56). The vertical offsets vary from a few meters to almost 1000 m. To the south, extensional faulting with offsets of less than 100 m occurred (Fig. 4.55). Because of the lack of seismic data in this area, it is not possible to follow these faults to the northeast. Transfer faulting between these faults and the northern Histria Depression has not been observed. The northeastern part of the outermost shelf is characterized by NE-SW oriented negative flower structures, a horst and normal faults (Fig. 4.56) over a distance of about 20 km (Fig. 4.53). The horst is developed along the shelf-break and has a lateral extent of 13 km in the northeast, increasing to 20 km in the southwest. Vertical offsets are on the order of a few meters to about 700 m. A NW-SE oriented transfer fault separates this complex from the southern fault system. In the southeastern and southern outer shelves, NE-SW striking normal faults, grabens and negative flower structures developed locally (Figures 4.57, 4.58 and 4.59). They are bounded by transfer normal and thrust faults with a NW-SE trend (Fig. 4.60). The Delfin area is less affected by faulting (Fig. 4.53); only normal faults with vertical offsets of a few meters are developed (Fig. 4.61).

The last category contains gravitational faults that developed only during the Pontian. Some of them were active only in the Lower-Pontian and are related to the extensional regime (Figures 4.54 and 4.56), whereas others continued their activity in the Upper Pontian and in the Dacian-to-Quaternary (Figures 4.54 and 4.59). In the Lower Pontian, roll-over structures characteristic of an extensional regime formed (Figures 4.54 and 4.56).

2. Spatial classification

The first category consists of faults related to the development of the Pontian Depression. They strike both NW-SE as the Histria Depression, and SW-NE, crossing the wells *1 Ovidiu* and *75 Cobălcescu* (Fig. 4.53). The SW-NE striking faults were developed during the Pontian extension.

The second group of faults developed along the shelf-break under a gravitational regime (Figures 4.57-4.59). Some of them were formed in the Oligocene (Fig. 4.58), others were developed up to the Pontian (Fig. 4.59). These faults were active till the Quaternary.

Their vertical offsets are on the order of a few meters. Basinward of the shelf-break, the Pontian sediments were deposited in a tectonically quiescent regime.

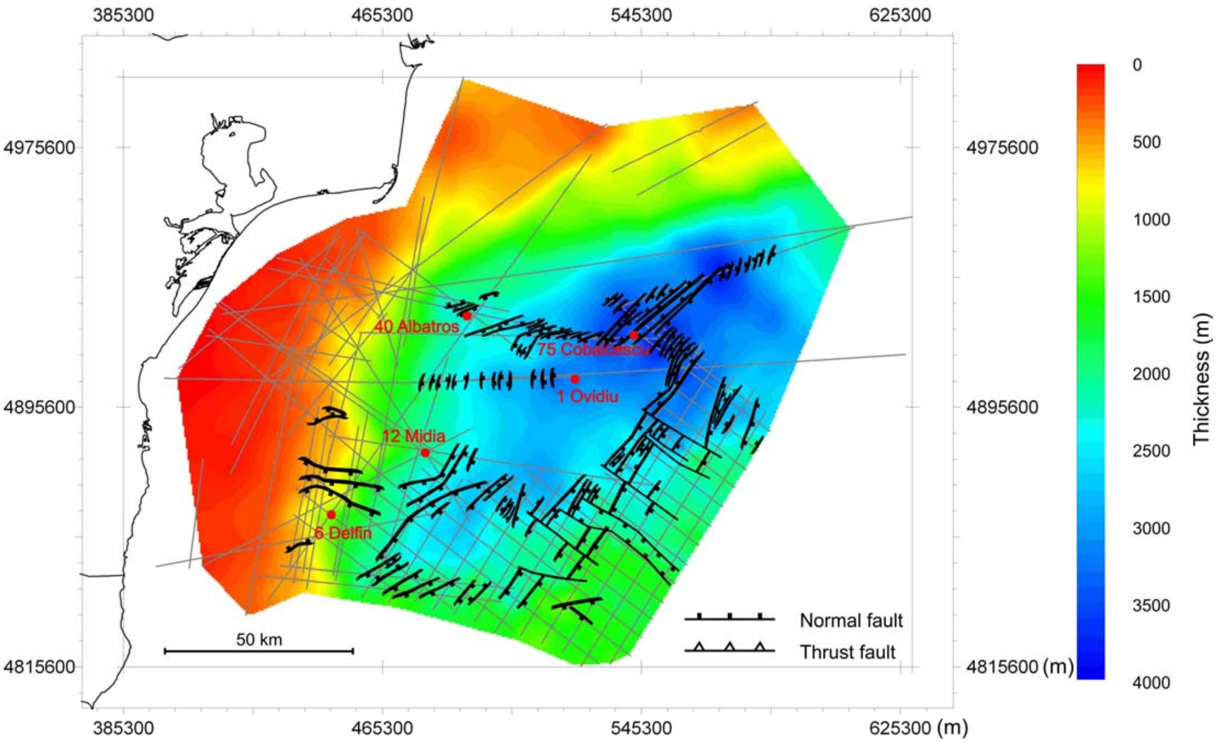

Figure 4.53 The general NE-SW pattern of faulting during the Pontian.

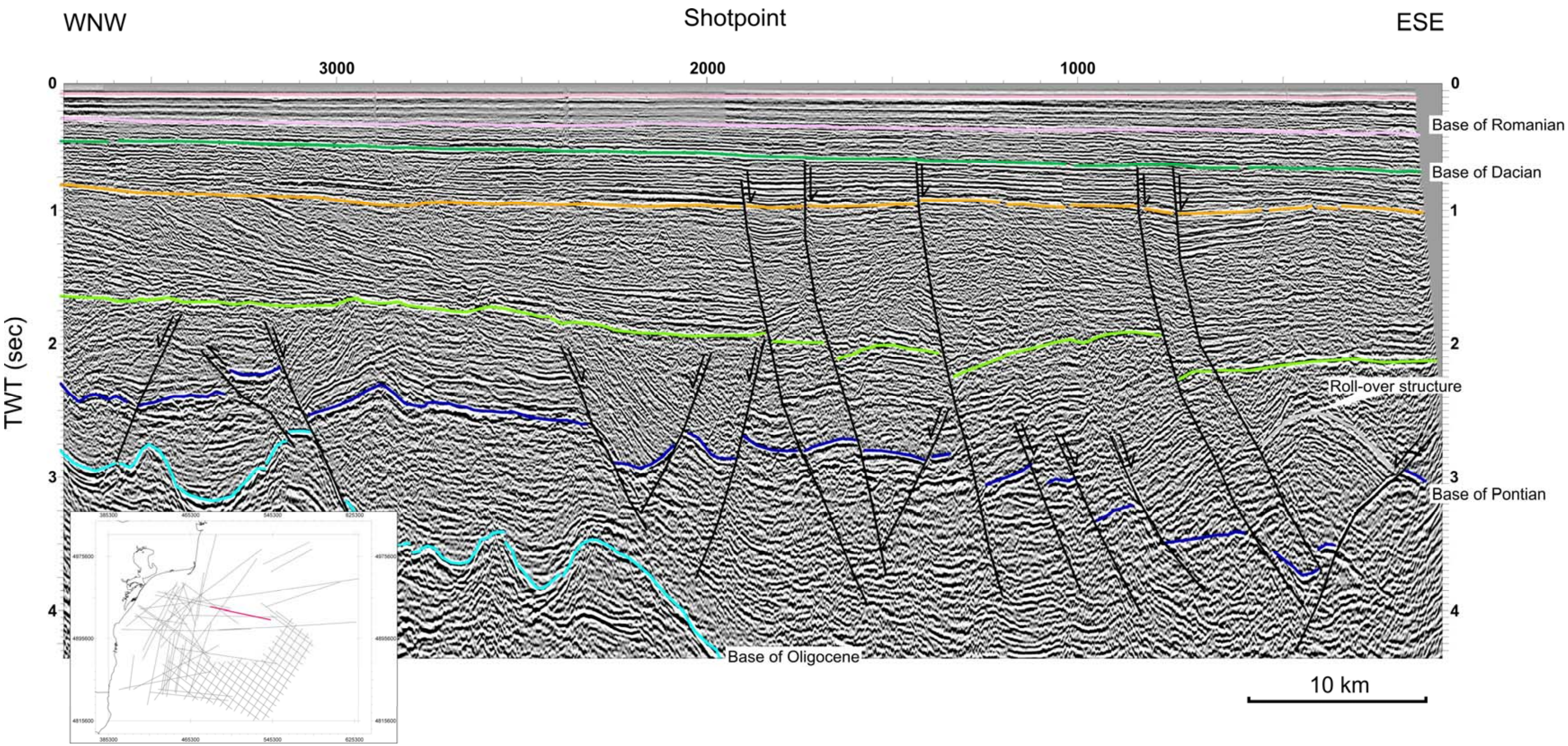

Figure 4.54 Interpreted seismic line from the northern Histria Depression.

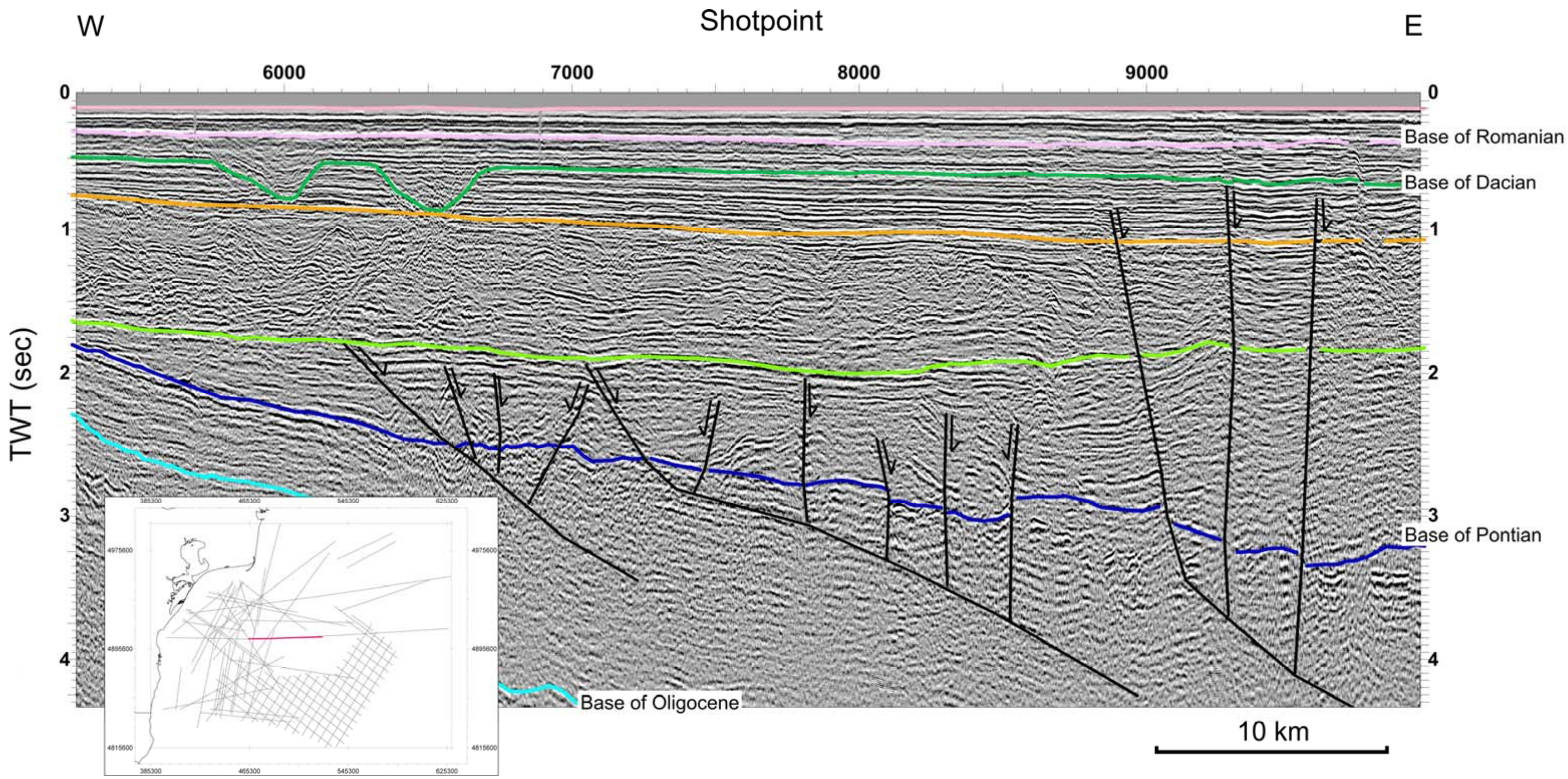

Figure 4.55 Interpreted seismic line from the middle shelf.

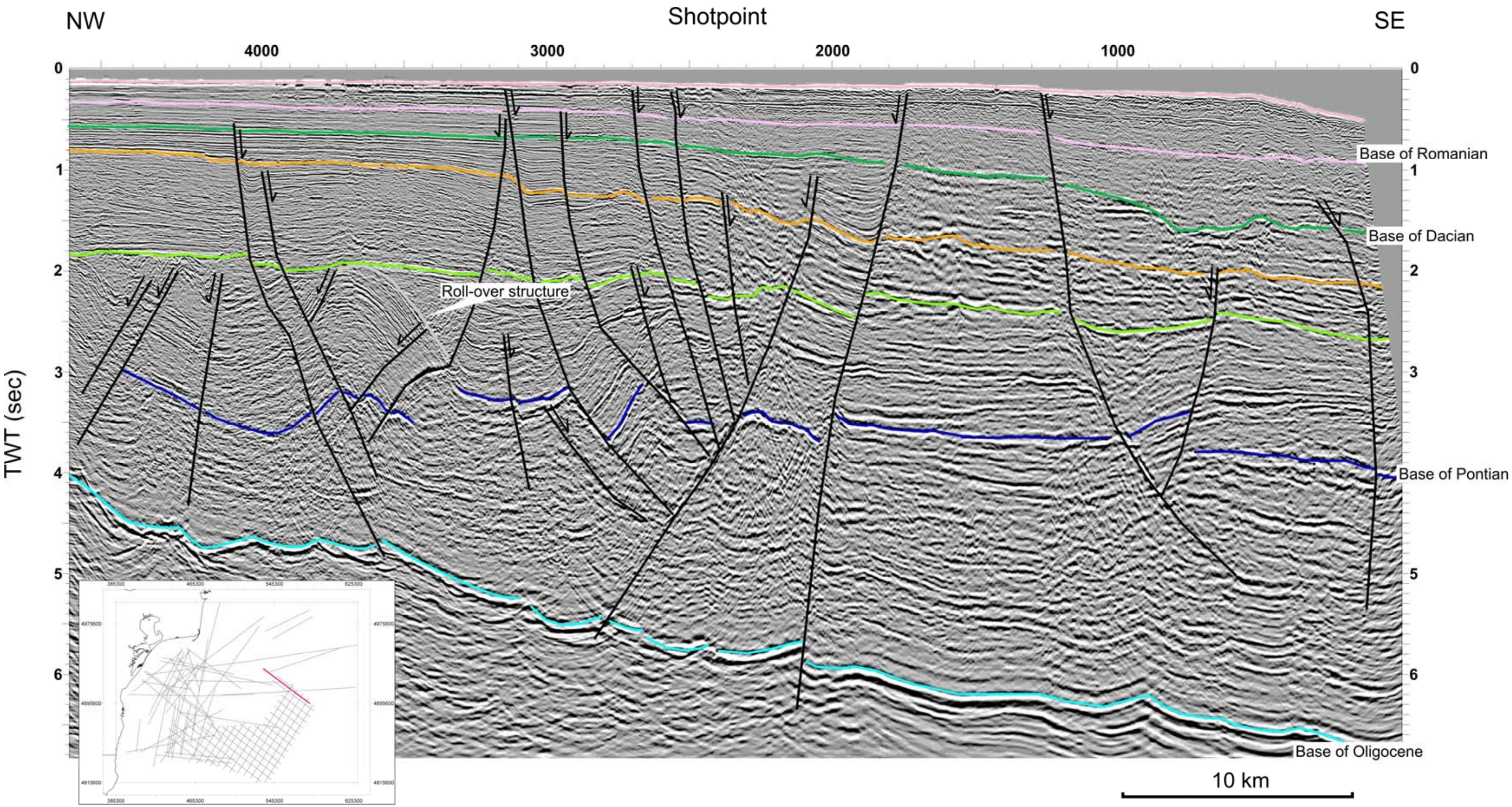

Figure 4.56 Interpreted seismic line illustrating the complex tectonic regime on the northeastern outer shelf. The distal limits of the intra-Pontian unconformities (light green and orange lines) are also shown.

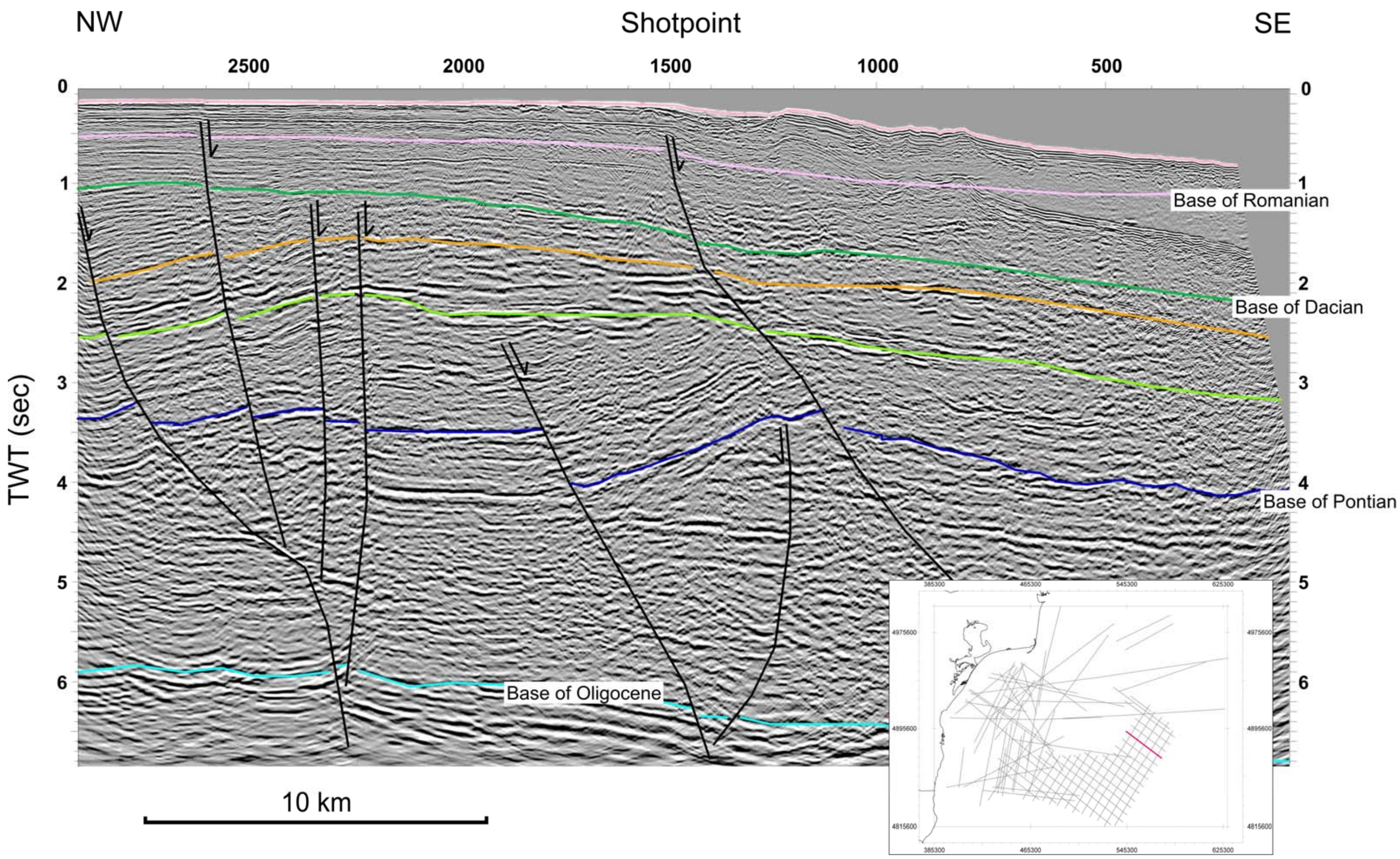

Figure 4.57 Interpreted seismic line from the eastern outer shelf.

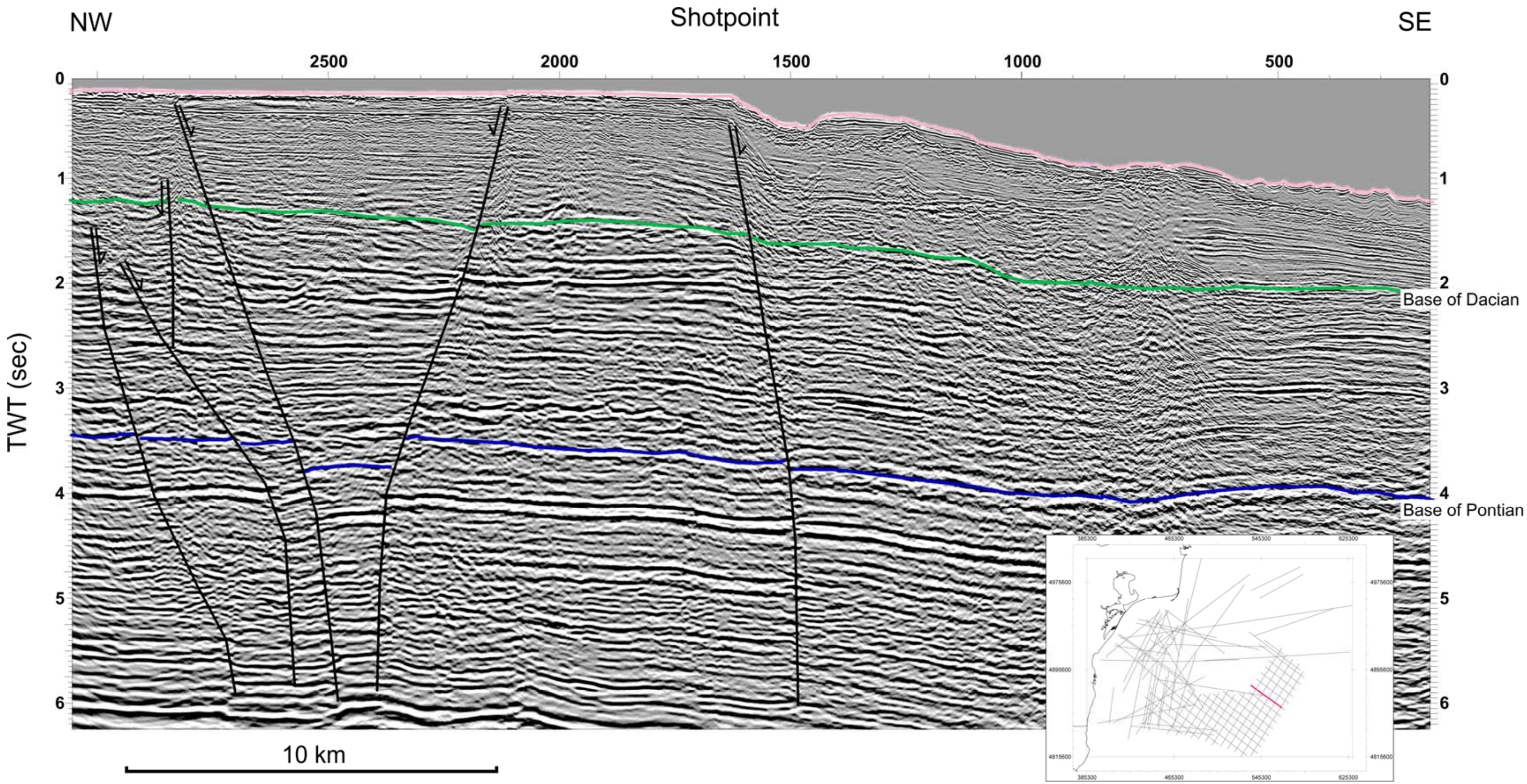

Figure 4.58 Interpreted seismic line from the eastern outer shelf and continental slope.

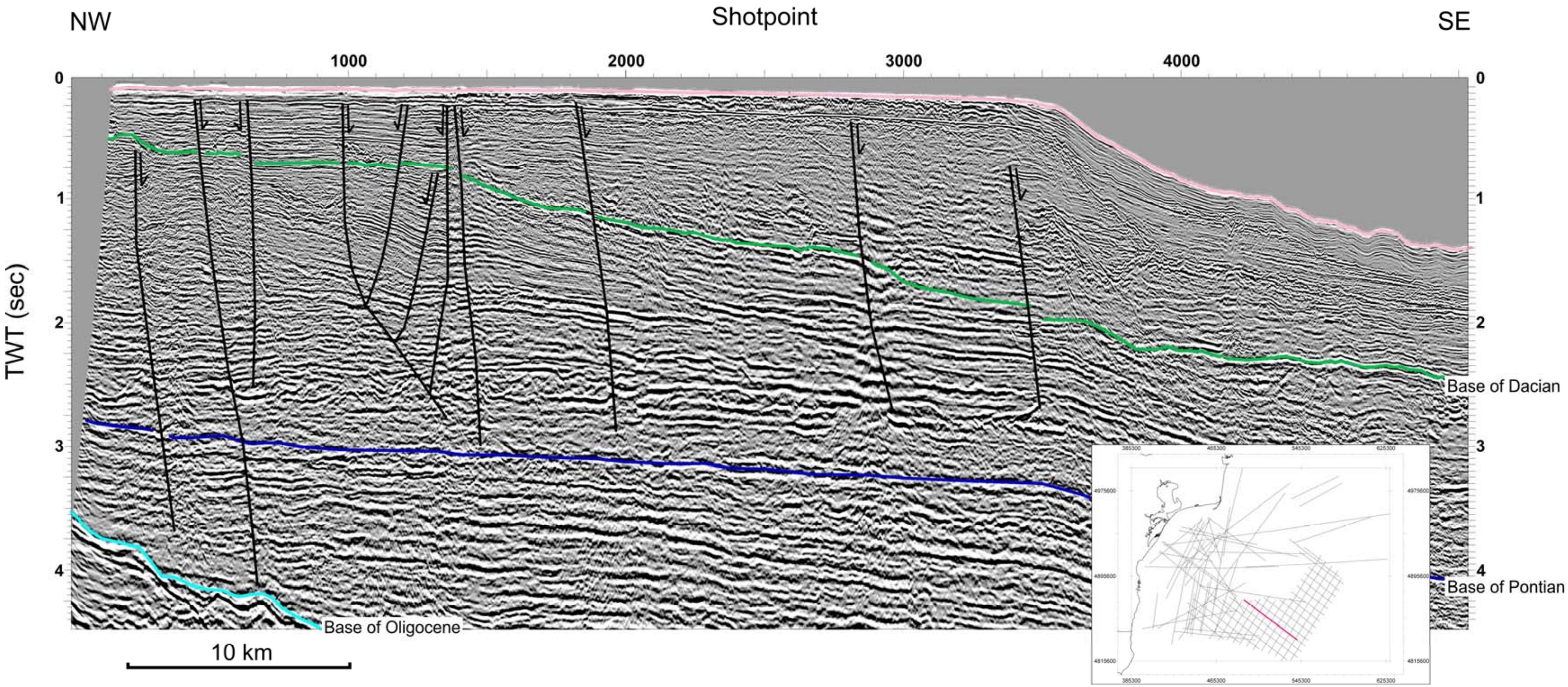

Figure 4.59 Interpreted seismic line from the southeastern outer shelf and continental slope.

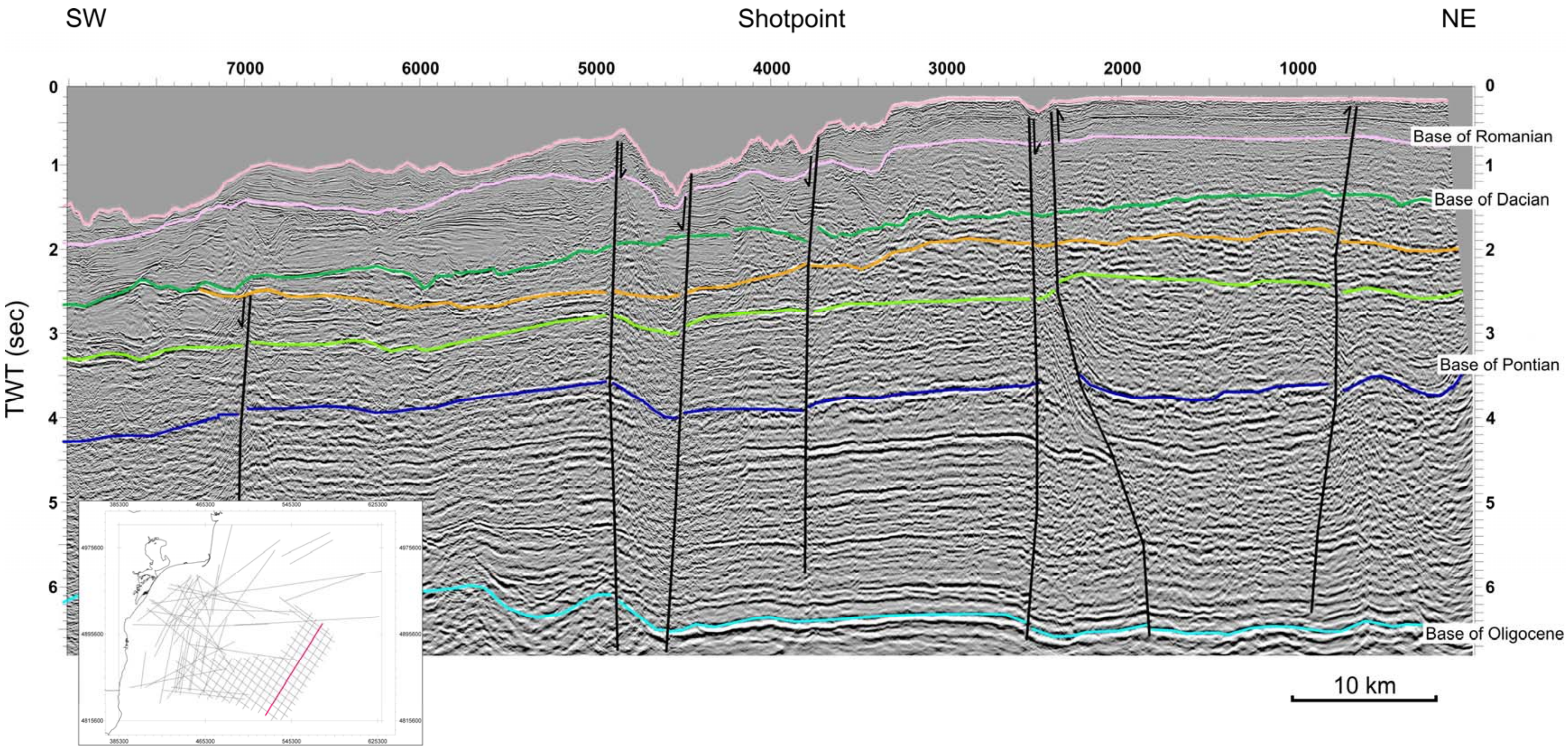

Figure 4.60 Interpreted seismic line from the southeastern study area illustrating the transfer faults that bound the NE-SW trending fault system.

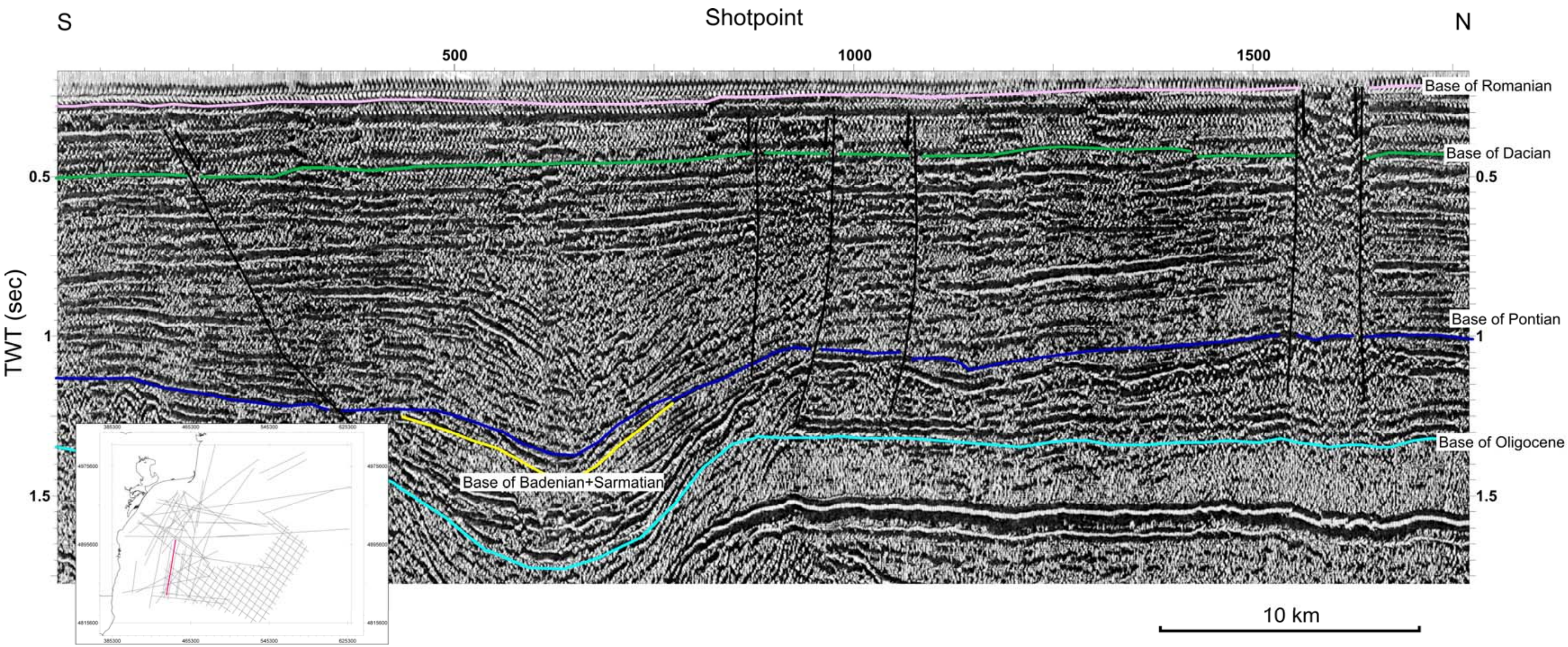

Figure 4.61 Interpreted seismic line showing the fault system in the Delfin area.

4.4.4. Dacian, Romanian and Quaternary

The Dacian-to-Quaternary section is less affected by faulting compared to the Pontian sequences. Most of the faults are Oligocene and older in age, and were reactivated during the Pontian (Figures 4.54 to 4.59). Vertical offsets are on the order of a few meters to tens of meters. The fault systems trend NE-SW and are separated by NW-SE oriented transfer faults. Only in the west does the fault trend change to E-W.

4.5. Mio-Pleistocene subsidence history of the Romanian shelf

4.5.1. Stratigraphic modeling of the subsidence history on the Romanian shelf

The subsidence of a passive continental margin is controlled by a number of factors, of which sediment loading and thermal cooling are the most important. A detailed description of the procedures for subsidence analysis is given in Chapter 3. In the present study, lithological informations from 11 wells situated on the Romanian shelf were used. The wells were projected along two lines across the shelf, one striking WNW-ESE and the other NE-SW. The borehole data are presented in detail in Chapter 5.

The compaction parameters for different lithologies used in this study are shown in Figure 4.62 and in Table 4.5.

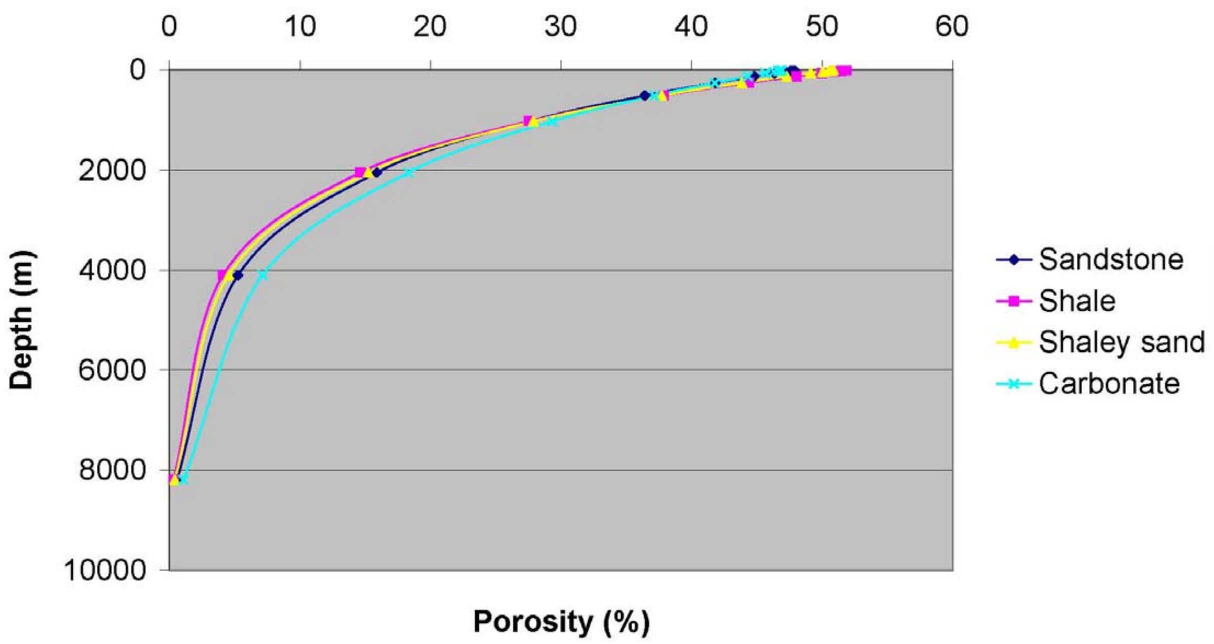

Figure 4.62 Porosity vs. depth for the lithologies used in the present study.

Lithology	Mineral density (kg m^{-3})	Initial porosity (%)	Constant
SANDSTONE	2650	48	0.00054
SHALE	2715	52	0.00062
SHALEY SAND	2700	51	0.00059
CARBONATE	2710	47	0.00046

Table 4.5 Compaction parameters for the lithologies used in the present study.

Tables 4.6 and 4.7 give the input lithological information used for the calculation of the subsidence history along lines 1 and 2. The subsidence was computed over the time interval 16 myr BP (beginning of the Miocene) to the present. The unconformities at the base of the Badenian (15.8 myr BP) and the Pontian (7.3 myr BP) were taken into account. The palaeo-water depth was estimated from palaeontological information (Ţambrea et al., 2000). The occurrence of a relative rich association of ostracodes indicate a brackish-to-fresh water environment with a palaeo-water depth of about 20 m. Information on sea level fluctuations was taken from the sea level curve estimated in the present study (see Table 4.2).

Well	Interval	Age (myr BP)	Palaeowater depth (m)	Eustatic sea level (m)	Top depth (m)	Thickness (m)	Sandstone (%)	Shale (%)	Shaley sand (%)	Carbonate (%)
814 Lebada	Recent	0	0	0	0	0	50	10	40	0
	R - Q	0	0	0	0	183.5	50	10	40	0
	Dacian	4.5	20	80	183.5	111	15	30	55	0
	Pontian	5.3	20	57	294.5	524	5	31	39	25
	Unconformity	7.3	20	87	818.5	0	0	0	0	0
	Bd - Sm	9	20	103	818.5	90	0	100	0	0
	Unconformity	15.8	20	142	908.5	0	0	0	0	0
	Basement	16	20	144	908.5					
94 Lebada	Recent	0	0	0	0	0	92	8	0	0
	R - Q	0	0	0	0	194	92	8	0	0
	Dacian	4.5	20	80	194	132	71	29	0	0
	Pontian	5.3	20	57	326	460	17	83	0	0
	Unconformity	7.3	20	87	786	0	0	0	0	0
	Bd - Sm	9	20	103	786	100	10	90	0	0
	Unconformity	15.8	20	142	886	0	0	0	0	0
	Basement	16	20	144	886					
88 Lebada	Recent	0	0	0	0	0	100	0	0	0
	R - Q	0	0	0	0	194	100	0	0	0
	Dacian	4.5	20	80	194	130	67	33	0	0
	Pontian	5.3	20	57	324	681	22	25	53	0
	Unconformity	7.3	20	87	1005	0	0	0	0	0
	Bd - Sm	9	20	103	1005	100	0	100	0	0
	Unconformity	15.8	20	142	1105	0	0	0	0	0
	Basement	16	20	144	1105					
13 Heraclea	Recent	0	0	0	0	0	88	12	0	0
	R - Q	0	0	0	0	198.23	88	12	0	0
	Dacian	4.5	20	80	198.23	128	70	30	0	0
	Pontian	5.3	20	57	326.23	950	2	74	24	0
	Unconformity	7.3	20	87	1276.23	0	0	0	0	0
	Bd - Sm	9	20	103	1276.23	200	0	68	32	0
	Unconformity	15.8	20	142	1476.23	0	0	0	0	0
	Basement	16	20	144	1476.23					
1 Ovidiu	Recent	0	0	0	0	0	0	16	84	0
	R - Q	0	0	0	0	368	0	16	84	0
	Dacian	4.5	20	80	368	716	9	4	87	0
	Pontian	5.3	20	57	1084	2454	13	32	55	0
	Unconformity	7.3	20	87	3538	0	0	0	0	0
	Bd - Sm	9	20	103	3538	132	28	16	0	56
	Unconformity	15.8	20	142	3670	0	0	0	0	0
	Basement	16	20	144	3670					

Table 4.6 Input data for subsidence analysis of line 1.

Well	Interval	Age (myr BP)	Palaeowater depth (m)	Eustatic sea level (m)	Top depth (m)	Thickness (m)	Sandstone (%)	Shale (%)	Shaley sand (%)	Carbonate (%)
25 Lebada	Recent	0	0	0	0	0	80	20	0	0
	R - Q	0	0	0	0	148.5	80	20	0	0
	Dacian	4.5	20	80	148.5	180	55	45	0	0
	Pontian	5.3	20	57	328.5	380	10	65	25	0
	Unconformity	7.3	20	87	708.5	0	0	0	0	0
	Bd - Sm	9	20	103	708.5	120	33	30	37	0
	Unconformity	15.8	20	142	828.5	0	0	0	0	0
	Basement	16	20	144	828.5					
813 Lebada	Recent	0	0	0	0	0	45	0	55	0
	R - Q	0	0	0	0	168	45	0	55	0
	Dacian	4.5	20	80	168	132	66	34	0	0
	Pontian	5.3	20	57	300	445	16	55	16	13
	Unconformity	7.3	20	87	745	0	0	0	0	0
	Bd - Sm	9	20	103	745	120	0	60	40	0
	Unconformity	15.8	20	142	865	0	0	0	0	0
	Basement	16	20	144	865					
811 Lebada	Recent	0	0	0	0	0	0	100	0	0
	R - Q	0	0	0	0	178	0	100	0	0
	Dacian	4.5	20	80	178	125	0	100	0	0
	Pontian	5.3	20	57	303	355	0	100	0	0
	Unconformity	7.3	20	87	658	0	0	0	0	0
	Bd - Sm	9	20	103	658	140	0	100	0	0
	Unconformity	15.8	20	142	798	0	0	0	0	0
	Basement	16	20	144	798					
18 Lotus	Recent	0	0	0	0	0	0	100	0	0
	R - Q	0	0	0	0	171	0	100	0	0
	Dacian	4.5	20	80	171	105	0	100	0	0
	Pontian	5.3	20	57	276	334	0	85	15	0
	Unconformity	7.3	20	87	610	0	0	0	0	0
	Bd - Sm	9	20	103	610	26	0	0	0	100
	Unconformity	15.8	20	142	636	0	0	0	0	0
	Basement	16	20	144	636					
10 Tomis	Recent	0	0	0	0	0	0	16	84	0
	R - Q	0	0	0	0	212.2	0	16	84	0
	Dacian	4.5	20	80	212.2	125	0	70	30	0
	Pontian	5.3	20	57	337.2	954	0	12	88	0
	Unconformity	7.3	20	87	1291.2	0	0	0	0	0
	Bd - Sm	9	20	103	1291.2	126	0	40	60	0
	Unconformity	15.8	20	142	1417.2	0	0	0	0	0
	Basement	16	20	144	1417.2					
6 Delfin	Recent	0	0	0	0	0	0	100	0	0
	R - Q	0	0	0	0	162.77	0	100	0	0
	Dacian	4.5	20	80	162.77	220	0	100	0	0
	Pontian	5.3	20	57	382.77	840	0	100	0	0
	Unconformity	7.3	20	87	1222.77	0	0	0	0	0
	Bd - Sm	9	20	103	1222.77	130	0	100	0	0
	Unconformity	15.8	20	142	1352.77	0	0	0	0	0
	Basement	16	20	144	1352.77					

Table 4.7 Input data for the Line 2 used for the subsidence analysis.

4.5.2. Results

The subsidence history of lines 1 and 2 are shown in the Figures 4.63 and 4.64 respectively, while the tectonic and the total subsidence rates along these lines are shown in Figures 4.65 and 4.66.

The history of tectonic subsidence and total subsidence are similar along lines 1 and 2 (Figures 4.63 and 4.64). From the beginning of the Miocene to the end of the Sarmatian, subsidence was slow. It increased abruptly during the Pontian, slowed down during the Dacian, and almost came to a halt in the Romanian-Quaternary.

Along line 1 (Fig. 4.63), the rate of total subsidence during the Badenian-Sarmatian was small. Subsidence increased from 27 m in the well *814 Lebăda* (on the inner shelf) to 125

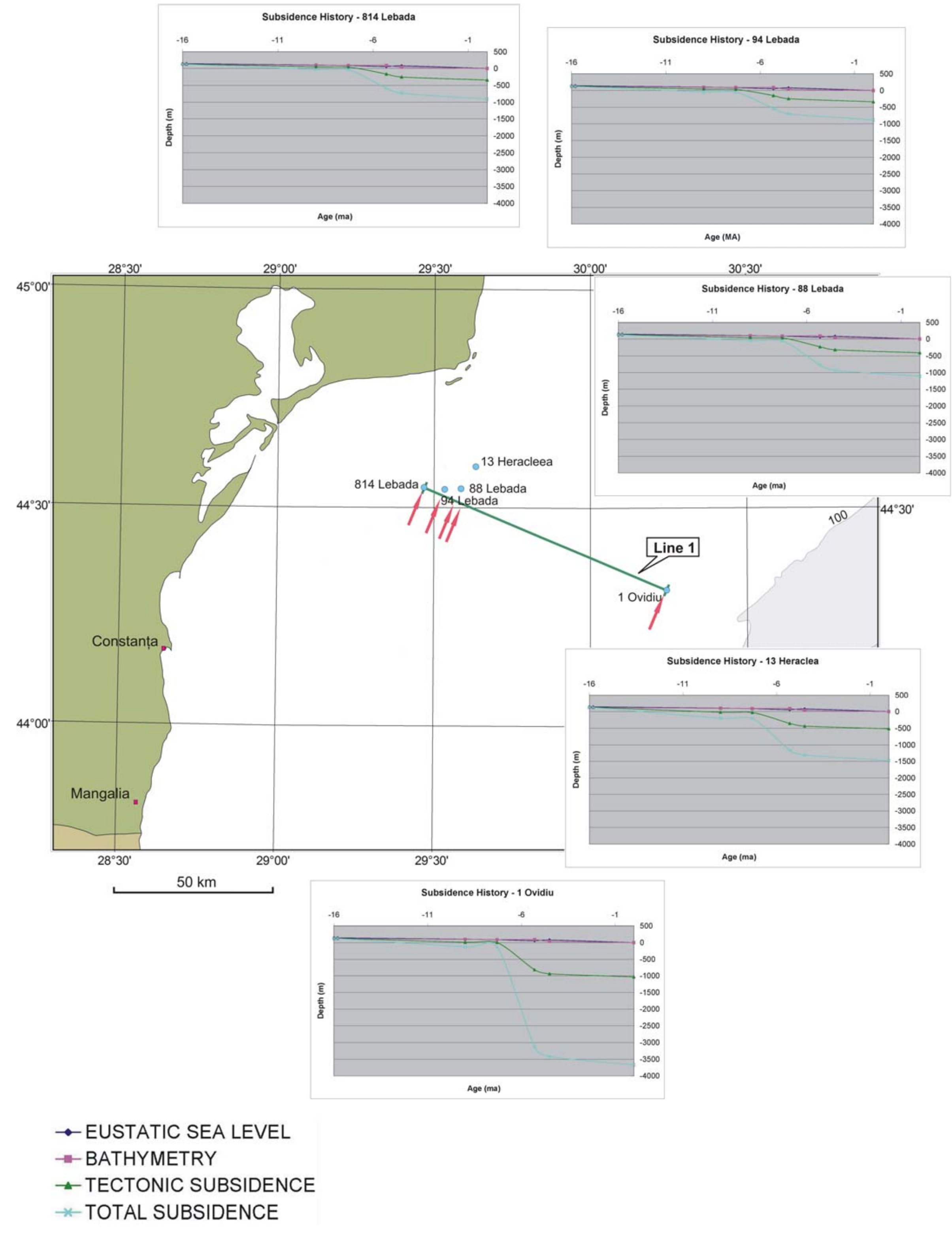

Figure 4.63 Subsidence history along line 1 from the Miocene to the present.

m in the well *1 Ovidiu* (on the outer shelf). By the end of the Pontian, the total subsidence amounted to 584 m on the inner shelf and 2803 m on the outer shelf, implying an increase of 557 m and 2678 m in these two areas respectively. At the end of the Dacian, the total subsidence reached 733 m on the inner shelf and 3428 m on the outer shelf. This suggests a much smaller increase in subsidence during the Dacian, namely 149 m on the inner shelf and 625 m on the outer shelf. The corresponding values for the Romanian-Quaternary are 175 m (inner shelf) and 242 m (outer shelf) respectively. Thus, the Romanian shelf was stable during the Badenian-Sarmatian and the Dacian-to-Quaternary, but was strongly subsiding during the Pontian. This large increase in subsidence, both in the vertical (for each borehole) and horizontal (along the shelf) direction was a result of intense tectonic activities and large sediment supply during this time.

Subsidence changes are smaller along line 2 (NE-SW; Fig. 4.64) than line 1 (WNW-ESE; Fig. 4.63). Line 2 was stable during the Badenian-Sarmatian, with a total subsidence of 9 m except for the well *18 Lotus*, where 11 m of uplift took place. During the Pontian, the total subsidence increased considerably in the south in the area of wells *10 Tomis* and *6 Delfin*. In the first four boreholes, the total subsidence was on the average about 400 m greater than during the Badenian-Sarmatian, while for the last two boreholes it was over 1100 m larger than during the Badenian-Sarmatian. This difference is attributed to the different positions of the boreholes on the shelf. The *Lebăda* wells as well as the well *18 Lotus* are positioned on the inner shelf, whereas *10 Tomis* and *6 Delfin* lie farther basinward where the base of the Pontian began to subside strongly. The Dacian and the Romanian-Quaternary deposits were less affected by subsidence. During the Dacian, the total subsidence decreased from 208 m (compared to the end of the Pontian) in the well *25 Lebăda* to 150 m in the well *18 Lotus* and increased again to 223 m in the well *6 Delfin*. The Romanian-Quaternary is marked by very small changes in subsidence, from 148 m in the north to 142 m in the south.

It can be assumed that the amount of sediment delivered to the Black Sea during Mio-Pleistocene time was directly related to uplift of the Carpathians. The distribution pattern of Mio-Pleistocene sediments in the Romanian foreland basin (the Focşani Depression) is different from that on the Black Sea shelf (Tărăpoancă, 2004). During the Badenian-Sarmatian when uplift of the Carpathians started, a large amount of sediment was delivered to and deposited in the foreland (> 5 km; Tărăpoancă, 2004). In contrast, on the Black Sea shelf, Badenian-Sarmatian sediments are present only locally and are very thin (< 250 m). Upper Miocene (Meotian) deposits are present only in the foreland basin and reach a thickness of up to 1.6 km, while on the Black Sea shelf they are absent. In the Uppermost Miocene (Pontian), the Focşani Depression received only a thin sediment layer of up to 1.5-1.6 km. Most of the sediment supplied from the Carpathians was transported into the Black Sea, where the Pontian reached a thickness of 4 km in the central Histria Depression. During the Dacian-to-Quaternary, sediment up to 4.5 km was deposited in the Focşani Depression, while on the Black Sea shelf thicknesses of only about 1.5 km were reached.

The tectonic subsidence curves, obtained by removing the effect of sediment loading from the total subsidence, show a trend similar to that of the total subsidence curves and suggest that the total subsidence is controlled more by sediment loading than by vertical tectonics. The Badenian-Sarmatian deposits were affected by tectonic subsidence only in the well *13 Heracleea*, at which it was 19 m at the beginning of the Badenian and 28 m at the end of the Sarmatian. In all the other wells, uplift of a few meters took place. During the Pontian, tectonic subsidence along line 1 (WNW-ESE) increased from an average value of 190 m on the inner shelf to 325 m at the well *13 Heracleea* and 751 m on the outer shelf. Thus, tectonics contributed significantly to total subsidence on the outer shelf, where intense tectonic activity took place during the Pontian. In the northeastern segment of Line 2 (NE-SW), the average tectonic subsidence was 130 m except for the well *18 Lotus*, where a value of only 67 m was deduced. In the southwest, it increased to 300 m. During the Dacian, the tectonic subsidence compared to that at the end of the Pontian increased about 90 m along Line 1, except for the well *1 Ovidiu*, where the increase was 205 m. Along Line 2, the corresponding increase was 90 to 100 m. In the Romanian-Quaternary, the tectonic subsidence was between ±80-90 m.

To summarize, vertical tectonics had less influence on the Mio-Pleistocene subsidence than sediment loading. Only on the outer shelf, where intense tectonic activities occurred during the Pontian and in part during the Dacian, did vertical tectonics play an important role.

Figures 4.65 and 4.66 show the total and the tectonic subsidence rates respectively along lines 1 and 2. They show that the rates of subsidence changed little during the Badenian-Sarmatian and the Romanian-Quaternary.

During the Dacian, a relatively uniform total subsidence rate of about 10 cm/kyr occurred on the inner and middle shelves on Line 1 (WNW-ESE), increasing to around 70 cm/kyr on the outer shelf (Fig. 4.65). On Line 2 (NE-SW), the total subsidence rate is more uniform and varies between 12-21 cm/kyr. During the Pontian, the total subsidence rate along Line 1 increased almost linearly from 24 cm/kyr on the inner shelf to 133 cm/kyr at the well *1 Ovidiu*. Along Line 2, the difference in total subsidence rates among the boreholes on the inner and middle shelves is about 30 cm/kyr.

The tectonic subsidence rate curves are shown in Figure 4.66. On Line 1, this rate reached an average of 11 cm/kyr during Dacian times, increasing to 25 cm/kyr on the outer shelf. On Line 2, the tectonic subsidence rate was almost constant (12 cm/kyr). In the Pontian, a linear increase in the tectonic subsidence rate from 11 cm/kyr on the inner shelf to 37 cm/kyr on the outer shelf was deduced. Only at the well *94 Lebăda* is this rate lower (9 cm/kyr). Along Line 2, it varied little, being 7 cm/kyr in the northeast and 15 cm/kyr in the southwest.

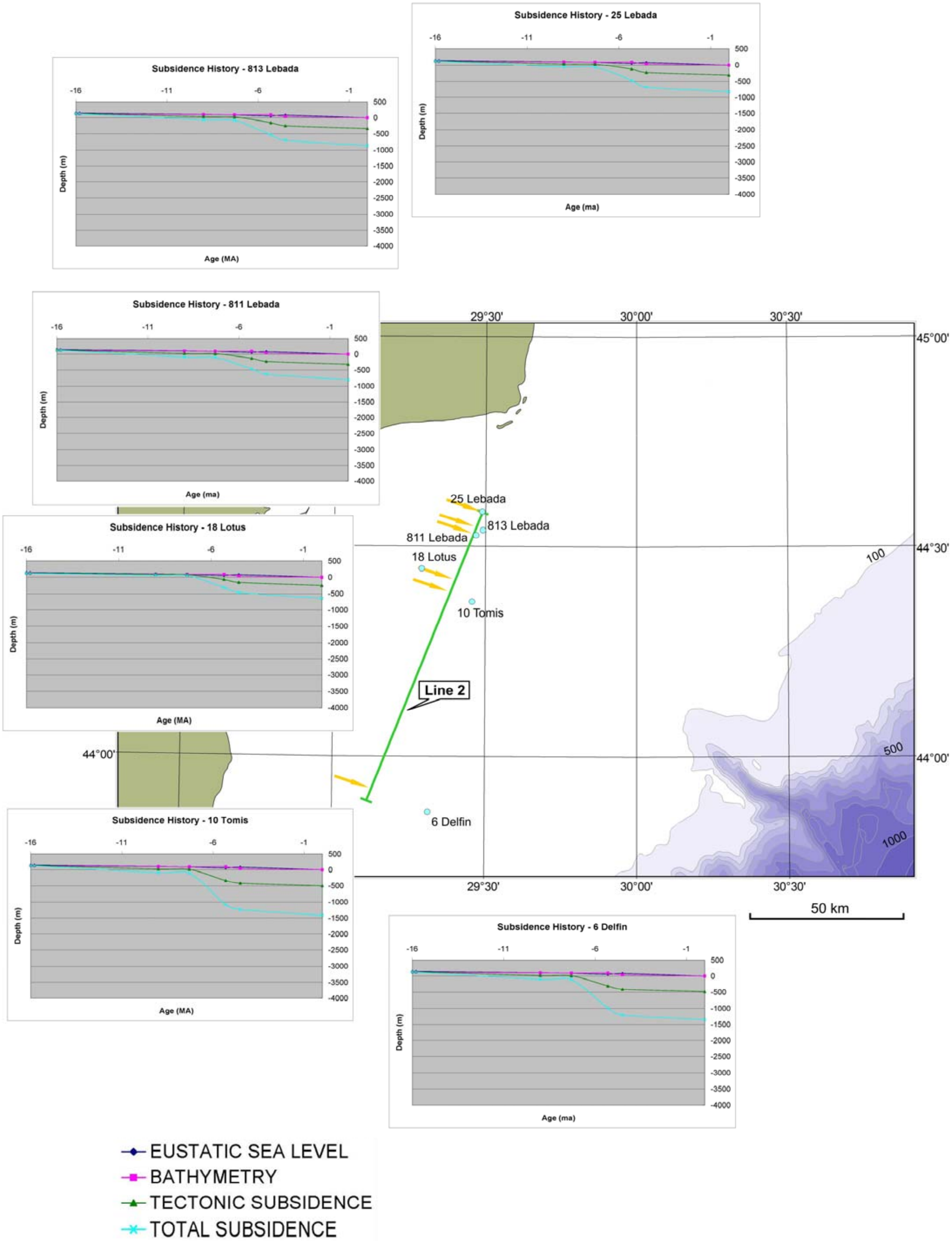

Figure 4.64 Subsidence history along Line 2 from the Miocene to the present.

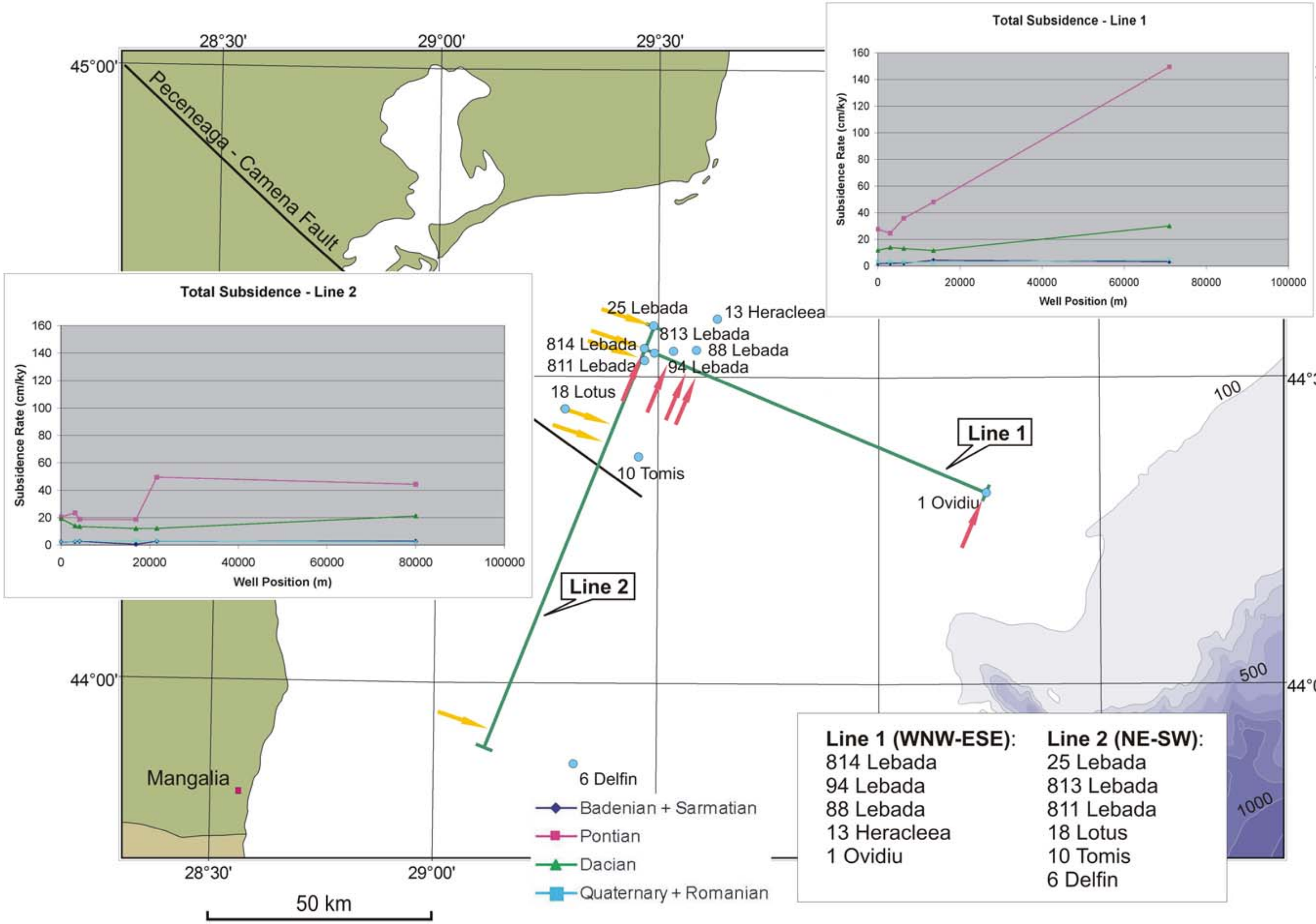

Figure 4.65 Total subsidence rates along lines 1 and 2 for the time intervals: Badenian-Sarmatian, Pontian, Dacian, and Romanian-Quaternary.

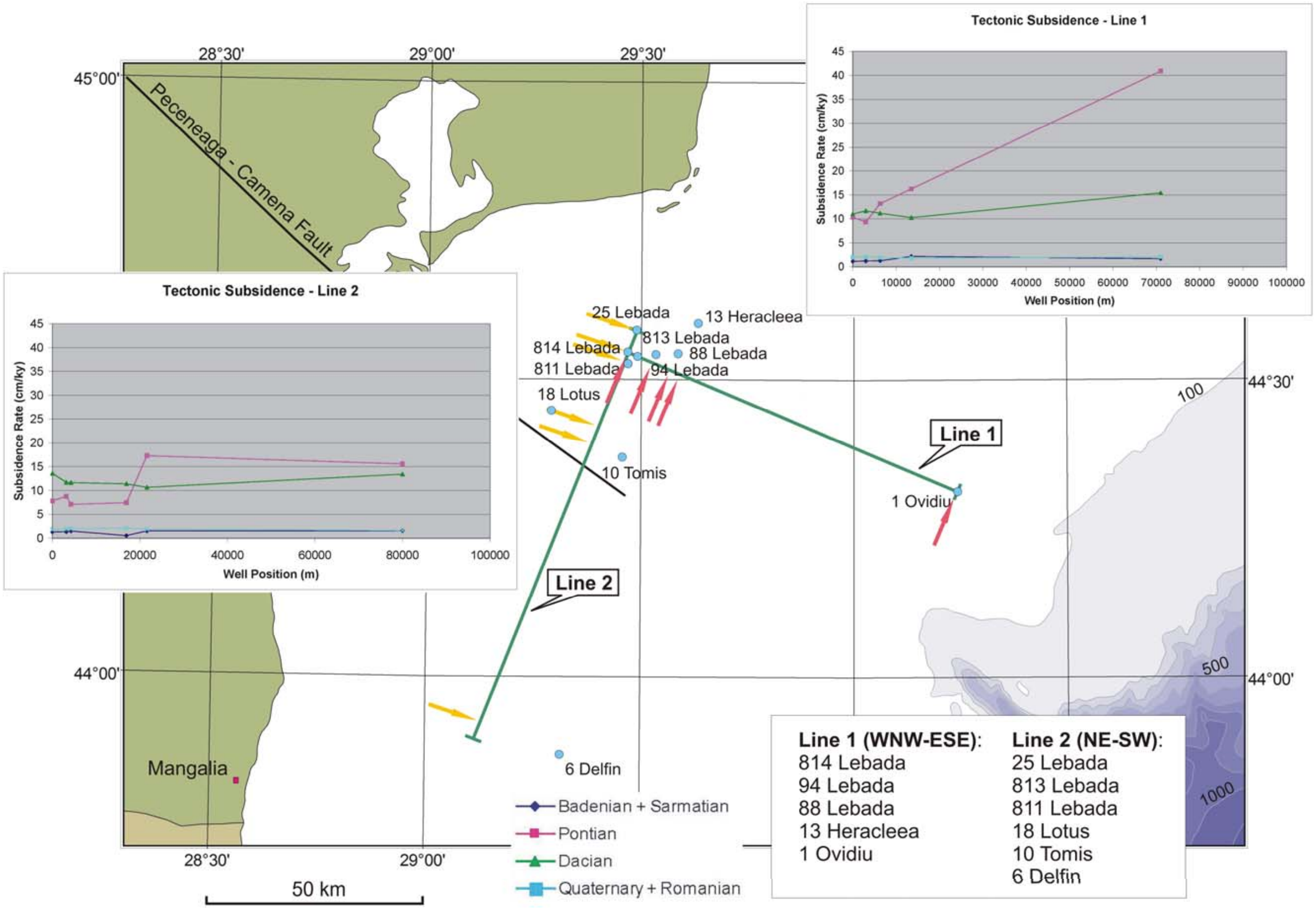

Figure 4.66 Tectonic subsidence rates along lines 1 and 2 for the time intervals: Badenian-Sarmatian, Pontian, Dacian, and Romanian-Quaternary.

5. Mio-Pleistocene sedimentation history of the Romanian shelf

5.1. Borehole Data

5.1.1. Borehole data and their geological implication

The depth and lithological information available from the borehole data was used for a geological interpretation of the Mio-Pleistocene formations.

The regional stratigraphical classification of the Neogene and Quaternary used is shown in Figure 5.1. The Early Miocene is absent in the study area; an erosional unconformity at the base of the Badenian marks the beginning of the Miocene section. The Middle Miocene is represented by Badenian and Sarmatian sequences that are overlain by the Pontian section of the Upper Miocene. The Middle and Upper Miocene are separated by another erosional unconformity, the Meotian being absent on the Romanian shelf. The Pliocene comprises Dacian and Romanian successions; the latter is by-and-large lithologically very similar to that of the Quaternary.

Era	System	Series	Epoch	Stages	Regional Stages	Age (ma)
CENOZOIC	Quaternary					1.75
	Neogene	Pliocene		Gelasian	Romanian	
				Placenzian		4.5
				Zanclean	Dacian	5.3
		Miocene	Late	Messinian	Pontian	7.3
				Tortonian	Meotian	
					Sarmatian	11
			Middle	Serravalian		
					Badenian	
				Langhian		15.8
			Early	Burdigalian	Maykopian	20.3
				Aquitanian		23.5
	Paleogene	Oligocene	Late	Chattian		28
			Early	Rupelian		33.7
		Eocene	Late	Priabonian		37
				Bartonian		40
			Middle	Lutetian		46
			Early	Ypresian		53
		Paleocene	Late	Thanetian		
				Selandian		
			Early	Danian		65

Figure 5.1 Geological time scale comparing regional stages for the Romanian Black Sea shelf with the global stages of the Mio-Pliocene (after Gillet et al., 2003).

Lithological information from 11 wells situated on the shelf was used for a subsidence analysis (Chapter 4). Two profiles across the shelf were constructed (Fig. 5.2): Line 1 oriented WNW-ESE extending from the Lebăda area to the outer shelf, and Line 2 striking NE-SW, crossing the main tectonic units of the inner shelf from the Lebăda to the Delfin area.

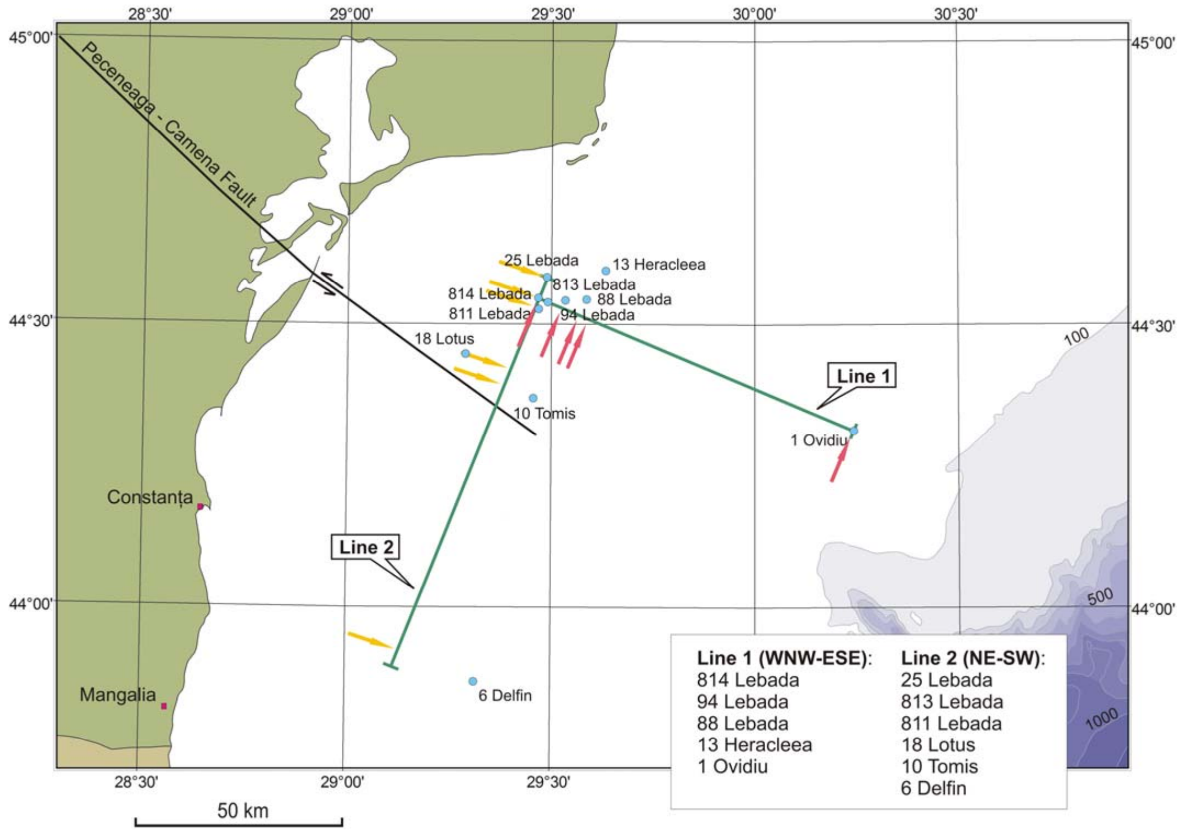

Figure 5.2 Location of the two constructed profiles used for subsidence analysis. Arrows show projections of the 11 wells on these profiles, in red for Line 1 and in yellow for Line 2.

A lithological description of the 11 wells projected onto these two lines is given in Figures 5.3 (Line 1) and 5.4 (Line 2). Along Line 1, there is an eastward thickening of the Upper Miocene to Quaternary section, while the thickness of the Middle Miocene segment remains almost constant over the entire shelf. Along Line 2, there are no significant changes in subsidence along the Middle Miocene to Pleistocene sediments, except from the area between the wells *18 Lotus* and *10 Tomis*, where a sudden increase in subsidence is observed. This change in subsidence comes from the different positions of the two wells relative to the basin. Although the two wells are projected onto the NE-SW trending Line 2, well *10 Tomis* is located further basinward than well *18 Lotus*.

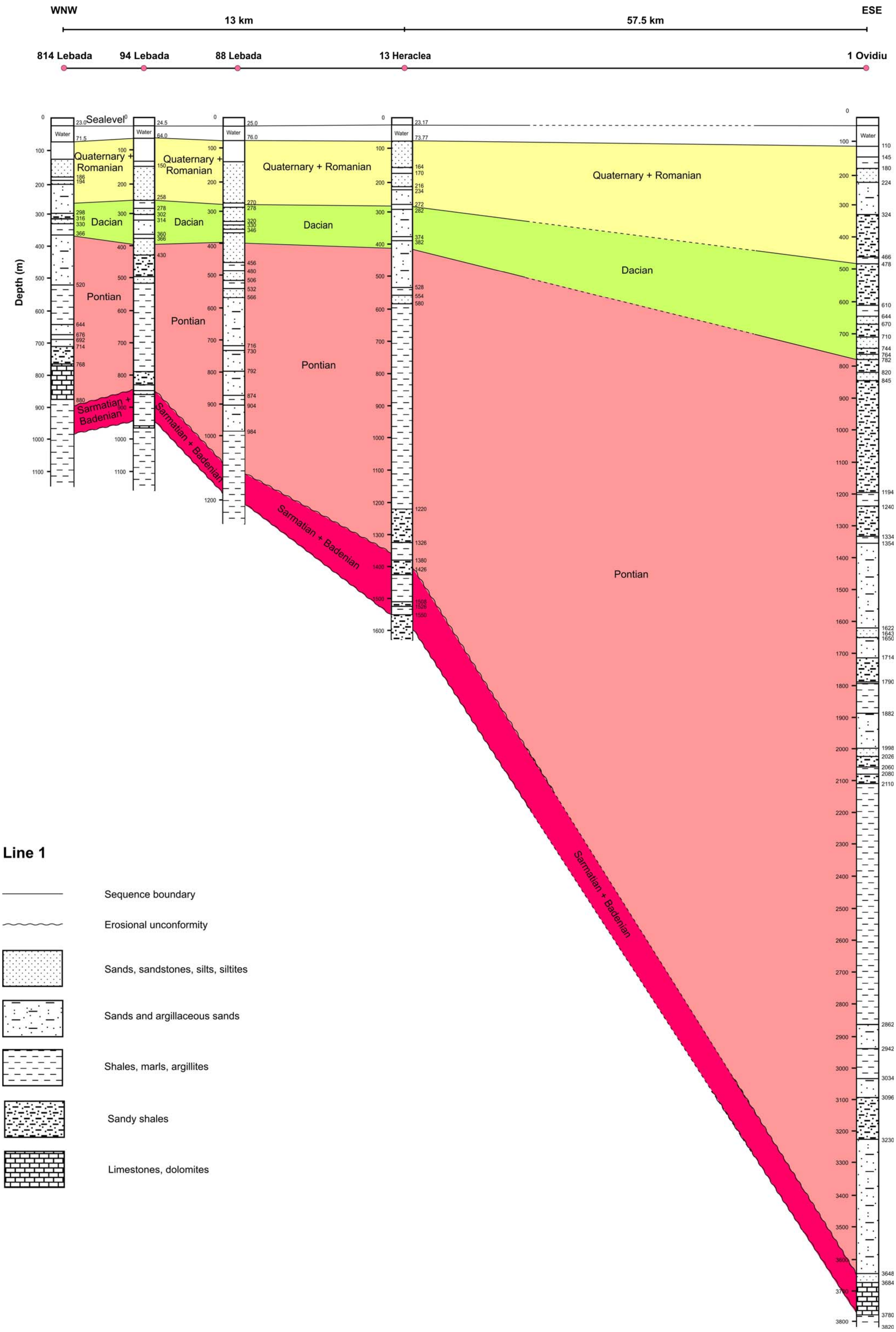

Figure 5.3 Lithological description of the wells projected on Line 1, the WNW-ESE profile.

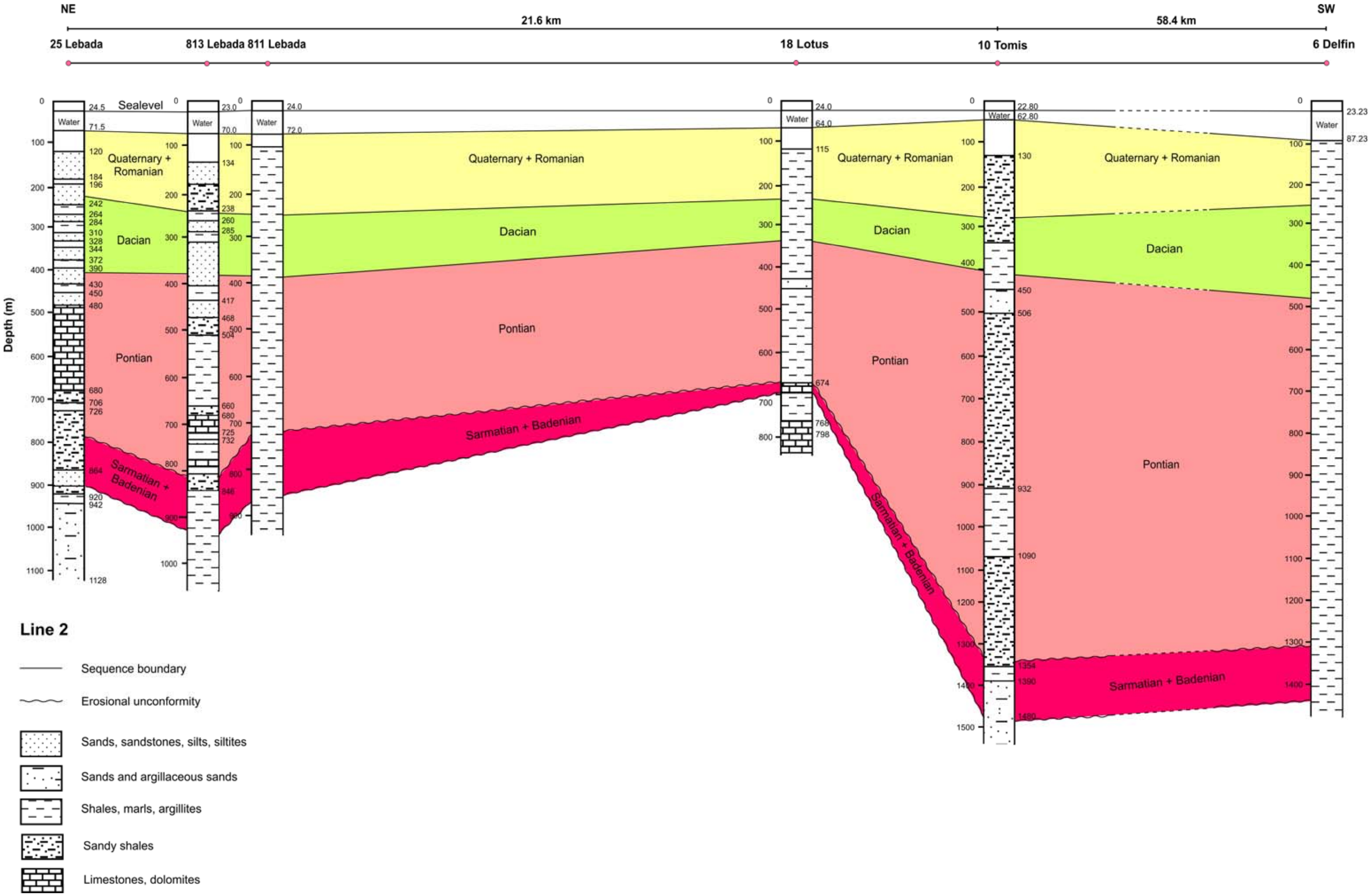

Figure 5.4 Lithological description of the wells projected onto Line 2, the NE-SW profile.

5.1.2. Mio-Pleistocene formations of the Romanian shelf

Sea-level changes during the Neogene led to a complex sedimentary development on the Romanian shelf, with periods of intense sedimentation followed by non-sedimentation and erosion.

The Miocene comprises only the Badenian, Sarmatian and Pontian sections (Fig. 5.1). The Badenian and Sarmatian sections are commonly combined in the literature for the Romanian shelf, because their limited thickness makes a separation difficult. They are bounded by two significant erosional unconformities. The total thickness of these deposits varies from several tens of meters on the inner shelf to about 250 m on the middle shelf. Lithologically, the Badenian is made up of shales, sandy shales and marls, while the Sarmatian is represented by oolitic limestones, fossiliferous limestones, marls, and fine sandstones. A calcareous facies is confined largely to coastal areas, while an argillaceous facies is developed in deeper waters.

Pontian deposits are present in all wells drilled on the Romanian shelf. Their thickness increases from 300 m in the Lebăda area (Fig. 2.6) to about 2500 m in the eastern part of the shelf. This large thickness variation suggests that subsidence was very active during Pontian and post-Pontian times. Lithologically, shales, marls, and sands with interbedded micro-conglomerates, limestones, tuffs, dolomites and coals dominate.

The Plio-Quaternary section is well-developed over the entire area and has thicknesses varying from 100 m on the inner shelf to 700 m in the Ovidiu area (Fig. 2.6). The Dacian is represented by a coarsening-upward sequence of sandy marls and sands with intercalations of shales and coals. The Quaternary overlies conformably the Pliocene; their boundary is often difficult to map because of the reduced seismic resolution. Lithologically, this sequence is made up of sandy marls, shales and sands.

5.2. Sedimentation history from seismic profiles and borehole data

Based on the results described in the previous chapters, the sedimentation history of the Romanian shelf was reconstructed. The seismic and borehole data yielded information on the seismic and litho-stratigraphic characteristics of the strata and their boundaries, so that the evolution of the sedimentary system can now be reconstructed.

The seismic lines and boreholes on the Romanian shelf suggest that the Mio-Pleistocene sedimentary column can be subdivided into five formations, namely the Badenian-Sarmatian, the Pontian, the Dacian, the Romanian and the Quaternary units. The last two are generally undifferentiated because of the conformal character of the boundary that separates them.

The Mio-Pleistocene time begins with an erosional unconformity that separates the Miocene and the Oligocene sediments (BBU in Fig. 4.6). It is well developed over the entire Romanian sector of the Black Sea from both on seismic and borehole data. The Badenian-Sarmatian formation marks the beginning of sedimentation in the Miocene. From borehole data, this formation is widespread over the entire shelf, but shows very small thicknesses on the middle part of the inner and middle shelves and on the outer shelf. Because of the reduced vertical resolution in these areas, the formation could not be mapped using the seismic data available. In the areas where it could be mapped, the Badenian-Sarmatian reaches thicknesses of only 250 m. The upper boundary of the Badenian-Sarmatian section (BPU in Fig. 4.6) is unconformable and separates the Sarmatian from the Pontian. In areas where the Badenian-Sarmatian section could not be followed seismically, the sedimentation in the Miocene was assumed to have started in the Pontian. The Meotian is absent on the borehole data as well as on the seismic data. The Pontian is very well developed over the entire shelf and shows a very complex evolution. Its thickness increases from zero in the coastal area to 4000 m on the outer shelf. It was strongly affected by tectonic activity, especially in the Histria Depression. Significant subsidence occurred in this area, in part also because of the large sediment input. Three intra-Pontian erosional unconformities were mapped using the available seismic data, but these unconformities are not identifiable in the boreholes. They separate the Pontian into four units: P1, P2, P3 and P4 (Fig. 4.27). The upper boundary of the Pontian is unconformable on the inner and middle shelves but becomes conformable basinward. Starting with the Dacian, sedimentation became quiescent over the entire shelf and parallel strata were deposited. The Dacian reaches thicknesses of about 1200 m on the continental slope, while the Romanian-Quaternary is less than 600 m in the same area. Compared to the Pontian, post-Pontian subsidence increased more gradually basinward. The boundary between the Dacian and the Romanian is conformable; therefore the separation of these formations is difficult and was carried out using only borehole data.

The subsidence history along the shelf was reconstructed from borehole data. Based on the seismic lines, the estimated sea level curve and the reconstructed subsidence history, the Mio-Pleistocene was subdivided into 7 seismic units corresponding to 8 systems tracts (Fig. 4.27 and Table 4.2). The Badenian-Sarmatian unit corresponds to a HST (highstand systems tract) deposited during a period of sea level highstand. This period was followed by a transgression and a lowstand, which took place during the Meotian erosional hiatus and are therefore not documented seismically. The Pontian begins with the subsequent LST (lowstand systems tract) which corresponds to the units P1 and P2. The boundary between these units occurs only locally and could not be correlated with sea level fluctuations of the Black Sea. The LST was followed by a TST (transgressive systems tract) and a HST of smaller extent than that of the Meotian hiatus. The LST and the HST took place during the non-depositional hiatus that separates P2 from P3. The third Pontian unit (P3) was deposited during the subsequent LST, which was followed by a transgressive surface (TS) represented seismically by the unconformity that separates P3 from P4. Following the TS, a TST and a HST developed during the deposition of P4. The maximum flooding surface that separates the TST from the HST was not identifiable on the seismic data because of their low vertical resolution.

The following sequence boundary formed at the end of the Pontian. It was succeeded by a LST, which is represented in the seismic data by the erosional hiatus that separates the Pontian and the Dacian formations. The Dacian-to-Quaternary section is interpreted to comprise a TST and a HST, with a MFS (maximum flooding surface) separating the Dacian formation from that of the Romanian-Quaternary.

5.3. Stratigraphic modeling of the Mio-Pleistocene sedimentation history

5.3.1. The modeling procedure

The results obtained in the previous chapter were used here to create a sedimentation model that reproduces the findings described above. This was done in order to determine how different parameters controlled the depositional processes.

In Figure 5.5, the position of the modeled profile is shown. It was constructed on the basis of 6 wells distributed from the inner to the outer shelf. Four of them are situated on the inner shelf where the most borehole information is available; the last two wells are located on the middle and outer shelf respectively. The position of the seismic line for a comparison of the modeling results is also shown in this figure.

The modeled profile has a length of 71 km, and the simulation started at the base of the Badenian (16 ma BP). The non-marine and the marine diffusion constants (see Chapter 3 for details) were set to 75,000 m^2/yr and 300 m^2/yr respectively to simulate the dipping clinoforms of the seismic data. Lithologic information from boreholes suggests that only a marginal amount of carbonates are present within the basin; almost all sediments are clastic. The direction of the simulated deposition is from NW to SE, namely from the left.

Modeling was carried out using two different treatments of isostasy. In the first, isostatic compensation was neglected, while in the second, the effect of isostasy during deposition was taken into account. Table 5.1 contains the input parameters for the two cases. In Table 5.2, the clastic sediment flux file for the case of no isostasy and isostatic compensation at different time intervals are displayed. The sea level file (blacksea.sea) was taken from the sea level curve estimated in the present study (Table 4.2). The subsidence file (blacksea.sub) is displayed in Table 5.3 and contains the results obtained from the subsidence analysis. The compaction parameters for this area were taken from the literature (Ionescu, 2000).

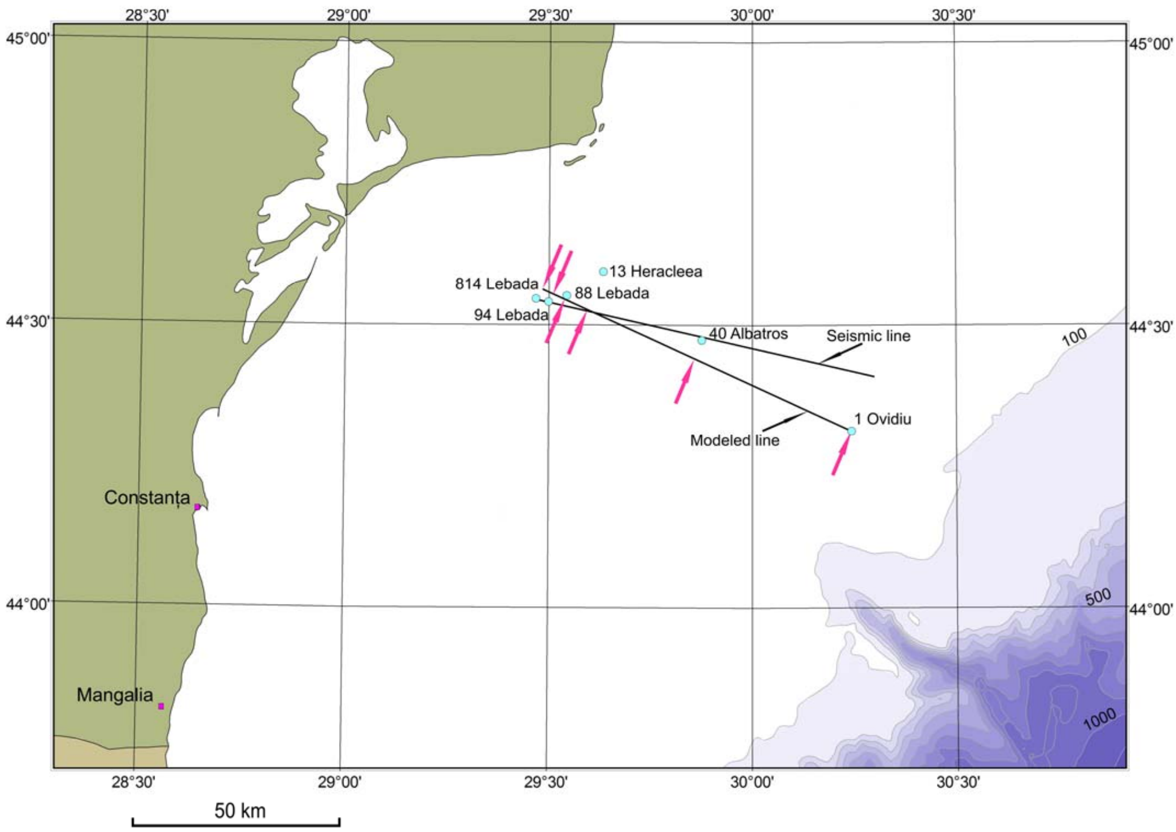

Figure 5.5 Position of the modeled profile on the Romanian shelf; red arrows indicate the position of the projected wells on this line. The position of the seismic profile for a comparison the modeling results with the seismic data is also given.

Measures	No isostatic compensation	Isostatic compensation
total width covered (m)	71000	71000
spatial divisions (m)	100	100
total time covered (myr BP)	16	16
temporal divisions (yrs)	1000	1000
timelines (yrs)	100	100
Ages group parameters (myr BP)		
use even increments	No	No
age of 1th time slice	0.1	0.1
age of 2nd time slice	4.5	4.5
age of 3rd time slice	5.3	5.3
age of 4th time slice	7.3	7.3
age of 5th time slice	9	9
age of 6th time slice	16	16
Clastics group parameters		
nonmarine diffusion constant (m^2/yr)	75000	75000
simulate marine sedimentation	True	True
marine diffusion constant (m^2/yr)	300	300
decay coefficient for marine diffusion constant	0.05	0.05
left clastic flux	blacksea.clas	blacksea_iso.clas
right clastic flux	none	none
pelagic sedimentation rate	0	0
Carbonates group parameters		
carbonate file	none	none
epeiric CaCO3 sedimentation - maximum rate	0.00011	0.00011
epeiric CaCO3 sedimentation - depth of maximum rate	5	5
oceanic CaCO3 sedimentation - maximum rate	0.00001	0.00001
oceanic CaCO3 sedimentation - exp decay constant	1	1
oceanic CaCo3 sedimentation - depth of maximum rate	5	5
lag on zero water depth	True	True
isotope signal file	none	none
isotope offset time	0	0
Sealevel group parameters		
sealevel file	blacksea.sea	blacksea.sea
time offset	0	0
datum for sealevel oscillation	0	0
sealevel oscillation amplitude	0	0
sealevel oscillation period (myr)	1	1
Subsidence group parameters		
subsidence rate	blacksea.sub	blacksea.sub
profile	passive	passive
flexural isostatic compensation	False	True
flexural rigidity		1E+23
density of air		0.001
density of crust		2300
density of mantle		3300
density of water		1000
gravitational constant		9.81
Compaction group parameters		
compact sediments	False	False
let erosion affect compaction	True	True
decay constant for sand compaction	0.00054	0.00054
decay constant for shale compaction	0.0007	0.0007
initial porosity for sand	0.48	0.48
initial porosity for shale	0.55	0.55
cutoff for sand composition	-1	-1
decay constant for composition	0.1	0.1
Heat flow group parameters		
thermal flux	none	none
thermal conductivity of sand	3	3
thermal conductivity of shale	3.01	3.01
thermal conductivity of fluid	0.5	0.5
surface temperature	10	10
surface temperature falloff	0	0

Table 5.1 Input parameters used for stratigraphic modeling of the Mio-Pleistocene sedimentation history; blacksea.clas, blacksea.sea and blacksea.sub represent the clastic-, sea level- and subsidence files respectively.

Age (myr BP)	Sediment input (m^3/yr) (case of no isostatic compensation)	Sediment input (m^3/yr) (case of isostatic compensation)
0.1	0.05	0.05
3	0.75	0.75
5	0.95	0.95
8	0.05	0.05
9	31	65.5
10	30.15	49.15
11	28.25	45
13	25.5	40
14	15.75	17

Table 5.2 The *blacksea.clas* file which gives the amount of clastic sediments entering the basin. The first column is age in myr BP, with zero marking the beginning of the simulation (16 myr BP).

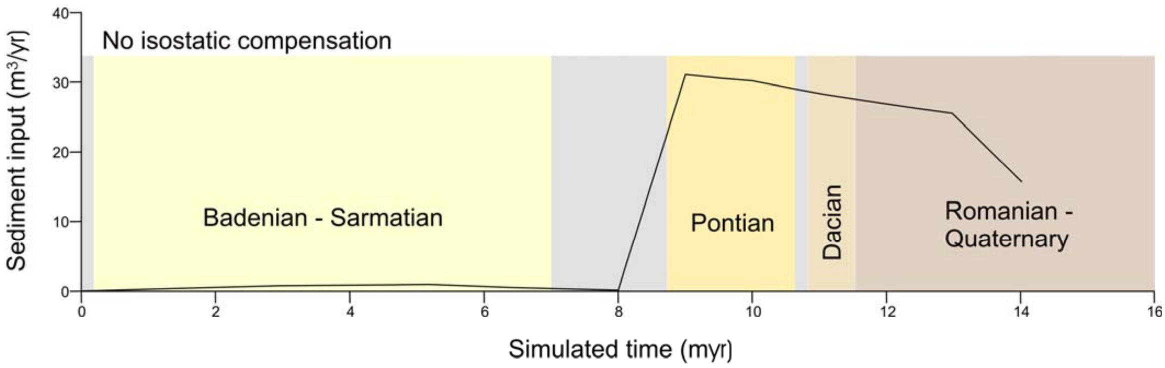

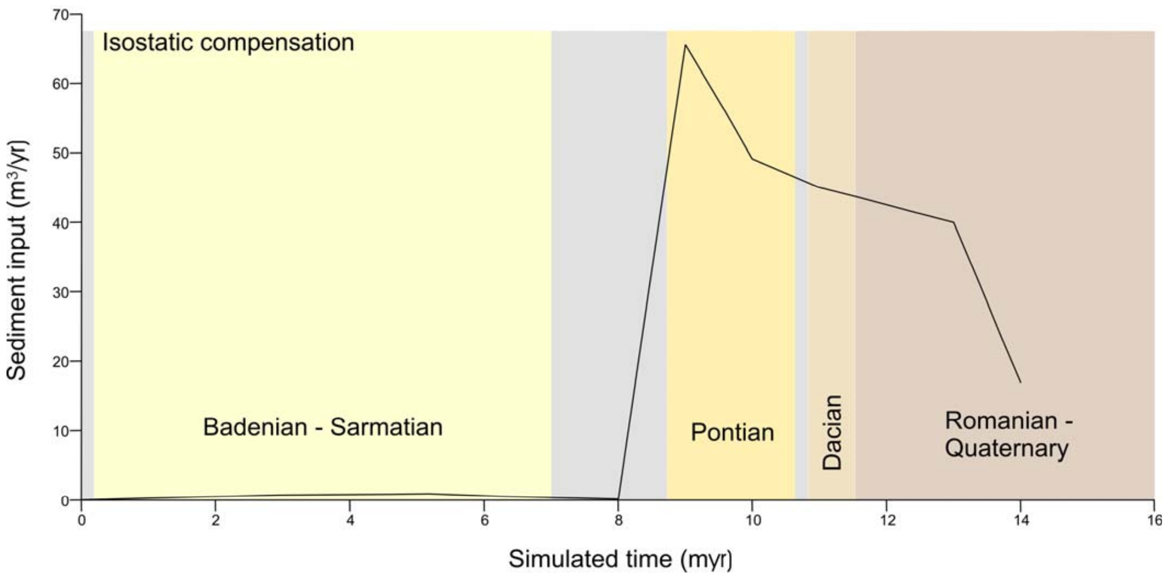

Figure 5.6 Amount of sediment supplied to the basin in the past 16 myr reconstructed from the model. Simulation begins at the base of the Miocene (0 myr BP along the *x*-axis) and ends at the present (16 myr).

814 Lebada	
0	
-16	0
-15.8	0
-9	125.3
-7.3	125.3
-6.5	300
-5.8	400
0	908.5
94 Lebada	
3000	
-16	0
-15.8	0
-9	136.8
-7.3	136.8
-6.5	300
-5.8	375
0	886
88 Lebada	
6300	
-16	0
-15.8	0
-9	145.1
-7.3	145.1
-6.5	400
-5.8	550
0	1105

13 Heracleea	
13500	
-16	0
-15.8	0
-9	294.5
-7.3	294.5
-6.5	400
-5.8	850
0	1476.2
40 Albatros	
28700	
-16	0
-15.8	0
-7.3	0
-6.5	450
-5.8	2100
0	2910
1 Ovidiu	
71000	
-16	0
-15.8	0
-9	223.1
-7.3	223.1
-6.5	2200
-5.8	2450
0	3670

Table 5.3 The *blacksea.sub* file used in the model. For each well, the name and the position (m) along the modeled profile are given. The first column is simulated time (myr) and the the second column the corrected thickness obtained from subsidence analysis.

5.3.2. Results

The best-fit models of the simulation are shown in Figures 5.7 (no isostatic compensation) and 5.8 (isostatically compensated). For comparison, a seismic profile that crosses the shelf in a NW-SE direction close to the modeled line is shown in Figure 5.9.

The first step in our simulation was to adjust some of the input parameters in order to obtain a sedimentary body that has a realistic size compared to the seismic data. Thus, the non-marine and the marine diffusion constants were set to 75,000 m^2/yr and 300 m^2/yr respectively, to obtain clinoforms similar to those in the seismic data. Based on information from the literature, the non-marine constant is on the order of 10,000 – 100,000 m^2/yr, while the marine constant is on the order of 100 – 1,000 m^2/yr (Jordan and Flemings, 1991). The set of parameters that yielded an adequate model is given in the clastic sediment file (blacksea.clas in Table 5.2). This file was modified until a sedimentary body with a vertical extent similar to that in the seismic data was obtained.

Figure 5.7 shows the simulation without isostatic compensation. The simulated model is shown in the upper panel, while the main erosional unconformities mapped on the seismic data are highlighted in the lower panel. Simulation began with the erosional unconformity that marks the base of the Badenian-Sarmatian unit. The final model shows that the Badenian-Sarmatian formation extends to the SE on the outer shelf, while this extension is not obvious in the seismic data because of their low vertical resolution. The second unconformity (BPU) could also be simulated over the entire profile. However, only two of the intra-Pontian unconformities, namely IPU 2 and IPU 3, could be simulated. IPU 1 occurs only locally in the seismic data and did not appear in the simulation. The Pontian deposits could be simulated satisfactorily, but this is not true for the position of IPU 2 and IPU 3 because of insufficient data. While the shapes of these unconformities are well-modeled on the inner shelf (left part of Fig. 5.7), basinward the dip of IPU 2 is too large and position of IPU 3 is too high. We attribute this to a lack of lithologic information between the wells *13 Heracleea* and *40 Albatros* as well as between *40 Albatros* and *1 Ovidiu*. A second problem is uncertainties in the age of the formations bounding these unconformities since these intra-Pontian unconformities are not seen in the borehole data. In addition, the strong influence of tectonisc on Pontian sedimentation in this area could not be taken into account during the simulation. The internal seismic characteristics of the intra-Pontian units P2 and P3 could be well-modeled. The Lower Pontian comprises two different seismic facies: thin divergent reflectors on the inner shelf and parallel reflecting packages that thicken basinward on the middle and outer shelves. P3 (the intra-Pontian unit between IPU 2 and IPU 3) has a modeled thickness larger than that deduced seismically but has the required internal pattern, namely wedge-shaped reflectors that downlap at the lower boundary but are erosionally truncated at the top. They dip steeply in the west but are almost horizontal in the east. Above IPU 3, parallel reflectors characteristic for the Upper Pontian-to-Quaternary are modeled.

The Wheeler diagram in the lower part of Figure 5.7 shows the chronostratigraphic development during the simulation period. The water depth at the time of deposition is color-coded. Light and dark grey fields mark areas of zero accumulation (see figure legend for details). During the first 7 myr of simulation, the Badenian-Sarmatian unit, which has a non-depositional hiatus in the middle part of the profile, was deposited. Two periods of non-deposition (3-3.4 myr and 4-5 myr) occurred in the proximal part of the profile. Although sedimentation dominated during the Badenian-Sarmatian, the deposits are extremely thin, reaching only a maximum of 250 m on the inner shelf. This low sedimentation rate was controlled by low sediment input and slow subsidence; sea level fluctuations were less important. Since subsidence of the Badenian-Sarmatian deposits was insignificant during this time period, their reduced thickness must be the result of low sediment input from land (see Table 5.2). This is consistent with our hypothesis that during the Badenian-Sarmatian, when major uplift of the Carpathians occurred, most of the sediments eroded from the Carpathians were deposited in the Romanian foreland basin and only a very small amount reached the Romanian shelf (see Chapter 4). The Wheeler diagram shows another hiatus on the inner shelf (the left side of the diagram) at the end of the Badenian-Sarmatian (~8.5 myr), which corresponds to the sequence boundary (SB) that formed in response to sea level fall. This SB is marked by the BPU in our seismic data. The hiatus cannot be followed basinward, instead there is an abrupt increase in water depth in the distal part from about 200 m to 800 m. Thus, the Badenian-Sarmatian sediments were deposited on the shelf and in part on the continental slope, while Lower Pontian deposits are found in deeper waters in the central basin. Above the unconformity BPU, the reflectors are divergent (on the inner shelf) to parallel (on the middle and outer shelves), with palaeo-water depths varying from approximately 50 m at the beginning of the profile to over 1,000 m on the present-day outer shelf. The next unconformity (~10-10.5 myr) corresponds to the seismically mapped IPU 2. It could not be simulated over the entire shelf, but only in three areas, outside which the unconformity is marked by an abrupt increase in water depth. IPU 2 corresponds to a transgression and the subsequent highstand, as indicated by the sea level curve, and ends at the beginning of the subsequent lowstand. It is at the same time a sequence boundary. Above the SB, P3 (the unit between IPU 2 and IPU 3) developed at water depths of around 50 m on the present-day inner shelf to 1,700 m on the present-day outer shelf, i.e., the depositional environment underwent a transition from shelf (left side) to basin (in the central and proximal areas). IPU 3 is also represented on the diagram (~11.5-11.75 myr), but only in areas where borehole data are available. The Pontian sediments were deposited over a very short time interval of ~2 myr; nevertheless, they are very thick. This implies that there was a large input of sediments from the Carpathians, which filled the foreland basin and were then laid down on the continental shelf (Table 5.2). The oldest unconformity appears at about 13 myr in the Romanian on the Wheeler diagram, but it could not be identified in the seismic data. Our simulation shows that Romanian-Quaternary sedimentation after the formation of this unconformity was quiet.

Figure 5.8 shows the stratigraphic model with isostatic compensation. Hereby the lithosphere was assumed to behave as an elastic beam with a flexural rigidity of 10^{23}. The best-fit model requires a much larger sediment influx to the basin during the Pontian to Quaternary (Table 5.2 and Fig. 5.9). All other parameters have been kept at the same values as in the previous model.

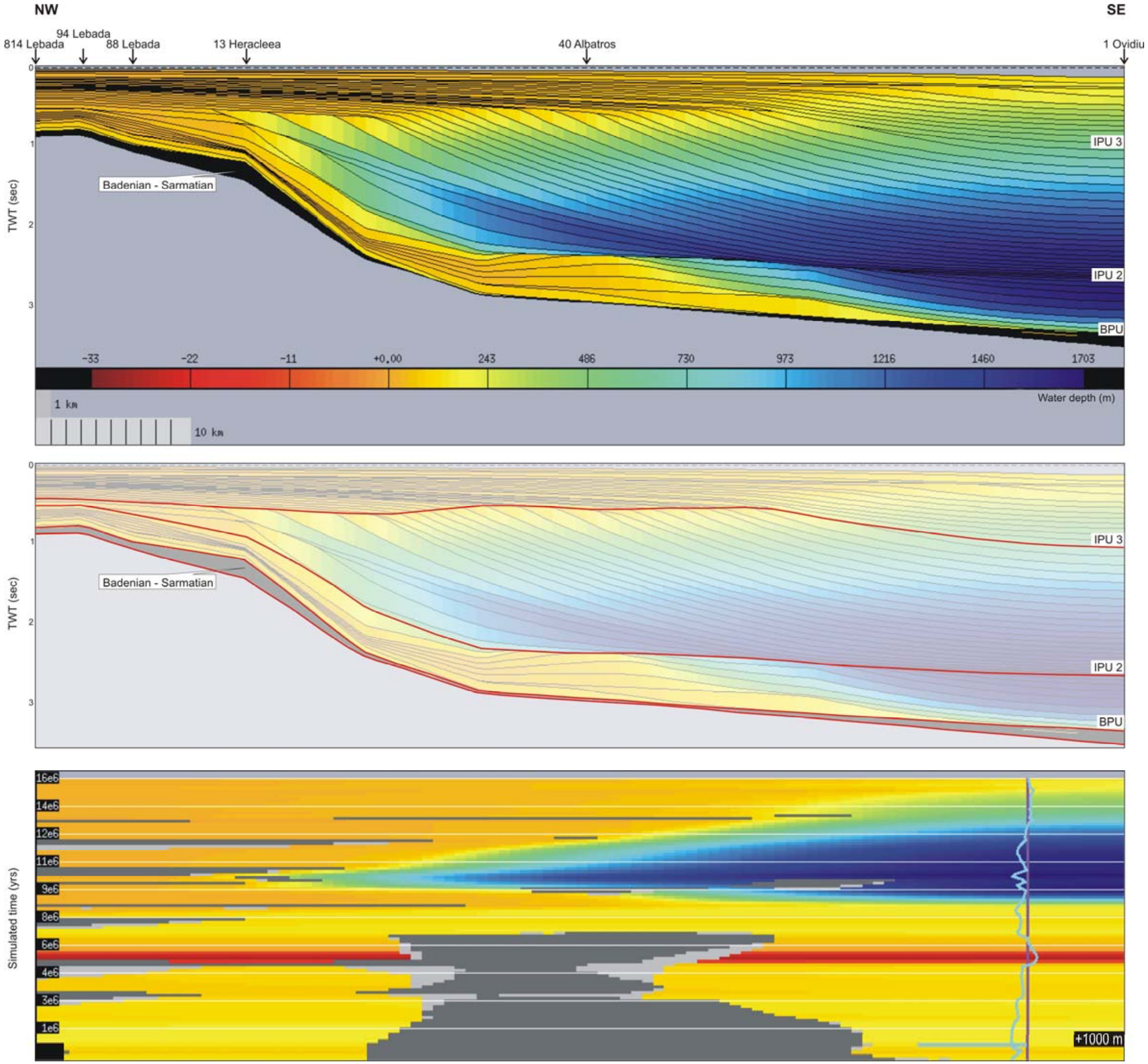

Figure 5.7 Modeled profile for the simulation without isostatic compensation.
Upper panel: the simulated model with color-coded water depths at the time of deposition of the different units. Middle panel: major interpreted erosional unconformities that were mapped seismically. Lower panel: the corresponding Wheeler diagram. For this panel, the vertical scale is simulation time in yrs, 0 marks the start of simulation. The sea level curve is plotted in light blue on the right, the vertical violet line represents present-day sea level. The light blue line to the left of the violet line gives the sea-level scale. The water depth at the time of deposition is color-coded. Light and dark grey fields mark the areas of zero accumulation: the former corresponds to locations where sediment was deposited but was subsequently eroded, and the latter locations where deposition never occurred (hiatuses).

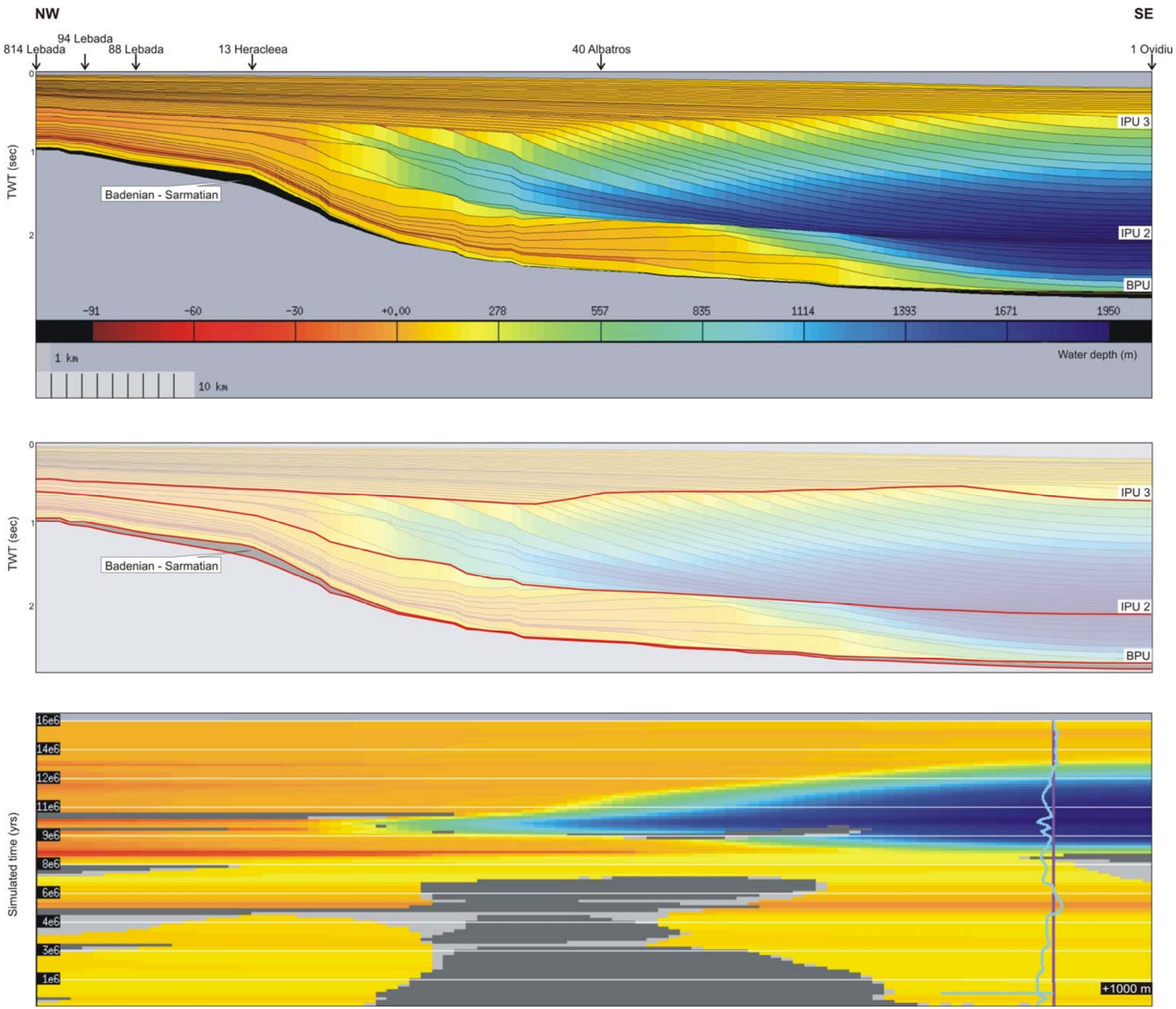

Figure 5.8 Modeled profile for which isostatic compensation was taken into account; the flexural rigidity was chosen to be 10^{23}. See Fig. 5.7 for the legend of the figure.

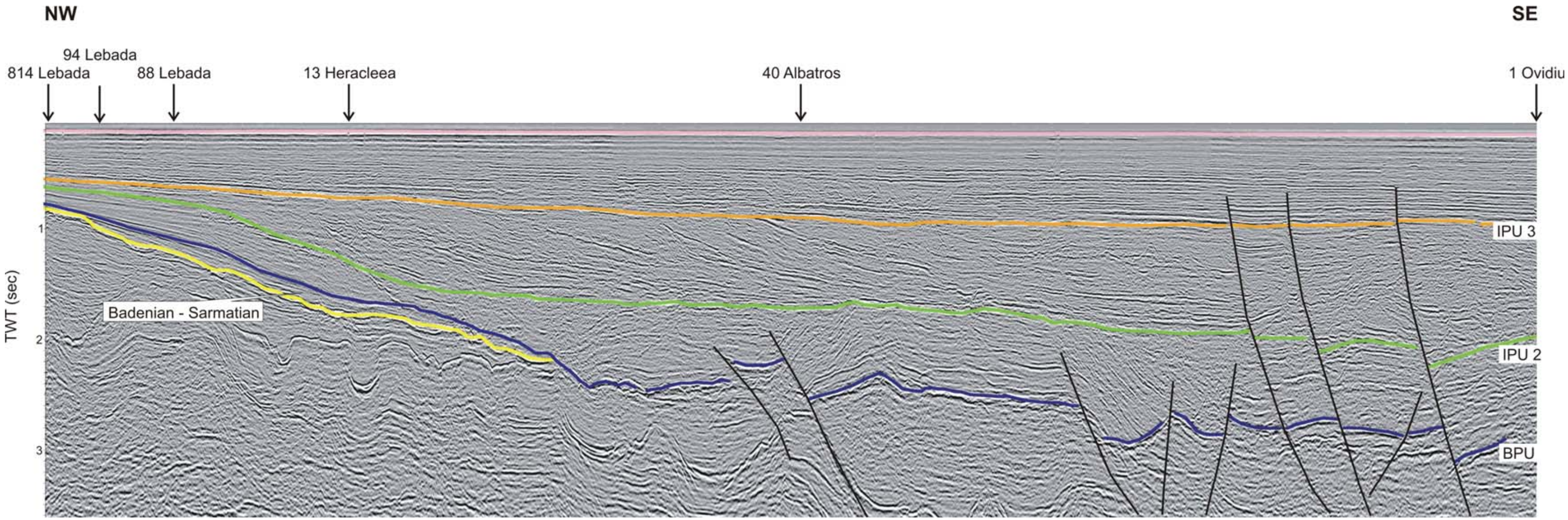

Figure 5.9 Seismic profile crossing the shelf in a NW-SE direction (See Fig. 5.5 for profile location).

5.4. Factors controlling sedimentation

5.4.1. Introduction

The dominant factors that control sedimentation and facies characteristics on a passive continental margin are sediment supply, subsidence, and relative sea level change. An analysis of these factors led to the conclusion that the most important factors controlling sedimentation in our study area are sediment input and subsidence (see chapters 4 and 5). Our simulation of stratigraphic models with and without accounting for relative sea level changes resulted in almost identical models, suggesting that relative sea level played only a minor role in Mio-Pleistocene sedimentation.

5.4.2. Sediment input

Sediment input was an important factor controlling Mio-Pleistocene sedimentation. Its effect was analyzed for two different scenarios: the first did not account for the influence of isostasy on sedimentation, and in the second, isostatic compensation was taken into account. Obviously, the second scenario is more realistic. For these two scenarios, terrestrial sediment input (via the Danube) to the basin is a function of the source area and sediment transport, which are, in this case, the Carpathians and the Romanian foreland basin respectively (Table 5.2). Sedimentation in the Romanian foreland basin (the Focşani Depression) has been studied by Tărăpoancă (2004).

We note that during the Badenian-Sarmatian (0-8 myr BP, Table 5.2), little sediments were delivered to the Romanian shelf. This coincides with the beginning of the uplift of the Carpathian Mountains. During this long time interval, most of the sediments eroded from the Carpathians were transported to and deposited in the Romanian foreland and only a small remainder reached the shelf. Thus, over a period of ~ 8 myr, only a thin sediment veneer (maximum 250 m) was deposited on the shelf. In contrast, sediment influx to the shelf was much higher during the Pontian (~ 8.7-11 myr, Table 5.2). This large influx is a result of the fact that the foreland basin was filled up during the Badenian-Sarmatian, so that bypass of this basin was possible. During the Dacian-to-Quaternary (~ 11-14 myr, Table 5.2), the sediment input rate was lower than during the Pontian, but was still very high compared to the beginning of the Miocene.

5.4.3. Subsidence

The influence of subsidence on sedimentation is similar to that of sediment input; in fact, the two factors are coupled. We observe that the tectonic subsidence played an important role in Pontian sedimentation; it increased the accommodation space in the Histria Depression and enabled the deposition of thick sedimentary packages. This tectonic phase was also responsible for the high sediment supply during the Pontian and for the pre-Pontian formation of the Histria Depression. The Badenian-Sarmatian and the Dacian-to-Quaternary were tectonically less active and the accommodation space was considerably smaller. Hence, the corresponding sections were much thinner and the sedimentation more quiescent than during the Pontian.

5.4.4. Sea level change

Since in the stratigraphic model reported in this chapter, the influence of sea level is less important, we consider this factor as a part of the influence that subsidence played on sedimentation. Sea level fluctuations control sedimentation by creating more or less accommodation space. During transgressions when the sea level rises and reaches a maximum, accommodation space is created, while during regressions, less accommodation space is available for sedimentation.

6. Conclusions

Structural and sedimentological analyses of the Mio-Pleistocene deposits on the Romanian Black Sea shelf using seismic and borehole data show a changing evolution during a relatively short period of time. This evolution is directly related to the pre-Miocene evolution of the Romanian shelf as well as to the evolution of the adjacent land (uplift of the Carpathians and sedimentation in the foreland basin). The available seismic data, which is relatively uniform distributed over the study area, yield important information on the stratigraphic and tectonic evolution of these deposits. The boreholes, most of which are distributed on the inner shelf with only a few covering the remainder of the shelf, give depth and litho-stratigraphic information for a reconstruction of the subsidence history. They also play an important role in ground-truthing the interpretation of the seismic data.

Our structural analysis of the seismic data show that the Mio-Pleistocene comprises five regional stages on the Romanian shelf: Badenian-Sarmatian, Pontian, Dacian, Romanian, and Quaternary. The Pontian was subdivided into four subunits: P1, P2, P3, and P4 respectively. From the base of the Miocene to the present, the following erosional unconformities have been distinguished:

- the BBU, which represents the unconformity at the base of the Badenian-Sarmatian deposits,
- the BPU, the unconformity at the base of the Pontian,
- IPU 1, the unconformity that separates the P1 and P2 subunits, occurs only locally on the inner shelf,
- IPU 2, separating the P2 and P3 subunits,
- IPU 3, separating the P3 and P4 subunits, and
- PDU, the unconformity at the base of the Dacian.

In contrast, the boundary between the Romanian and Quaternary sequences is conformal in character.

The Mio-Pleistocene sedimentary evolution of the Romanian shelf is highly variable. This is a consequence of the variability of factors that controlled sedimentation. These include: (1) variable sediment input from land which is directly related to uplift of the Carpathians and to the evolution of the Romanian foreland, (2) important tectonic activity in the Histria Depression during the Pontian, almost a complete lack in and highly reduced tectonic influence during the Badenian-Sarmatian and the Dacian-to-Quaternary respectively, and (3) sea level fluctuations. Thus, the Badenian-Sarmatian section, which was deposited over a long time period (~ 8 myr), occurs only locally on the shelf and reaches a thickness of no more than 250 m. This is attributed to the low sediment input from land during this time, since the Romanian foreland basin functioned as an effective buffer. In contrast, during the Pontian (~ 2 myr), when the foreland basin was filled up and most of the sediments could be transported to and deposited on the shelf, resulting in correspondingly thick sections, reaching some 4000 m at the center of the Histria Depression. This large sediment loading disturbed the equilibrium reached after the formation of the Oligocene Histria Depression and contributed to a reactivation of tectonic activities in the basin. During the Dacian-to-Quaternary period, sediment input decreased and tectonic activity slowed down or came to a halt. The Dacian and the Romanian-Quaternary sediments have a parallel reflection pattern and reach thicknesses of up to 1200 m and 600 m respectively on the continental slope.

A sea level curve for the Black Sea shelf during the Mio-Pleistocene time span using the global sea level curve of Haq et al. (1987), an unpublished sea level curve based on seismic data from the northeastern Black Sea shelf, and salinity information (Jones et al., 1997) was estimated. This sea level curve was used to reconstruct the subsidence history of the shelf and for a sequence-stratigraphic characterization of the Mio-Pleistocene units.

Mio-Pleistocene subsidence of the Romanian Black Sea shelf is directly dependent on sediment input, tectonic activity and sea level fluctuations and is highly variable. Subsidence during the Badenian-Sarmatian and the Dacian-to-Quaternary was limited. The subsidence history calculated along the WNW-ESE profile increases slowly from the inner to the outer shelf while in the NW-SE direction low subsidence values showing almost no variation along the profile are observed. In contrast, during the Pontian, there was strong subsidence from the inner to the outer shelf as well as from NW to SE. On the outer shelf, much higher subsidence values compared to the rest of the shelf can be observed. This was the result of a large sediment input to the basin and of significant tectonic activity in the Histria Depressions as discussed above.

Based on the available seismic data, the reconstructed subsidence history and the sea level curve, the Mio-Pleistocene sedimentary section was divided into 8 systems tracts. The Badenian-Sarmatian unit was attributed to a HST (highstand systems tract), being deposited in a late highstand when the sea level began to fall slowly after reaching a maximum. The next cycle cannot be observed in the seismic data, because it corresponds to sedimentation on the Romanian shelf during Meotian time, and was subsequently completely eroded. The unit P1, which was laid down on the slope at the time of deposition, is progradational and attributable to the lowstand wedge of a LST (lowstand systems tract). Unit P2 is likewise also attributed to a LST, having the continental slope and the deep basin as palaeo-depositional environments. Because the boundary between units P1 and P2 occurs only locally and could not be correlated with our estimated sea level curve, it was presumed to have formed during a higher order sea-level cycle. Unit P2 is followed by a non-depositional hiatus that separates unit P2 from P3. On the sea level curve, it corresponds to the HST and TST (transgressive systems tract) that followed the LST of P2 and ends with a sequence boundary. The reflection terminations and the wedge-shape of P3 suggest that it was deposited in the deep basin during a sea level lowstand. The succeeding TS (transgressive surface) corresponds on the seismic data to the erosional unconformity between the units P3 and P4. This TS is followed by the next TST and HST that developed during the deposition of P4, but a MFS (maximum flooding surface) is missing in the seismic data because of insufficient vertical resolution.

Unit P4 was deposited on the inner and middle shelves, as deduced from its reflection terminations and seismic facies characteristics. The boundary between P4 and the Dacian is represented by another erosional hiatus, which comprises the LST that follows the formation of the sequence boundary at the end of the Pontian. During the Dacian-to-Quaternary, the subsequent TST and HST were deposited on the inner and middle shelves. The MFS that separates the TST and the HST could not be observed in the available data.

Tectonically, the most active period of the Mio-Pleistocene was the Pontian. The Badenian-Sarmatian was largely tectonically quiescent and the Dacian-to-Quaternary saw a decrease in the Pontian tectonic activity, possibly even to a halt. We classified the faulting that affected the Pontian deposits both temporally and spatially. From the temporal point of view, we separated (1) faults that began their activity in the Pre-Oligocene and remained active up to the Pontian, (2) faults that developed during the Oligocene-Pontian, and (3) faults that were active only during the Pontian. The first are supposedly reactivated faults that developed during the formation of the Histria Depression, the second are gravitational faults that developed in sediments of a similar facies, and the last are gravitational faults related to the extensional phase in the Pontian. Spatially, we separated (1) extensional faults that accompanied the development of the NE-SW depression, which has its depocenter along a line joining the wells *1 Ovidiu* and *75 Cobălcescu*, and (2) gravitational faults at the shelf-break.

Sedimentation along the Romanian Black Sea shelf during the Mio-Pleistocene was controlled by three important factors: sediment supply, subsidence, which is in turn strongly affected by tectonics, and sea level fluctuations. The stratigraphic model obtained by simulation of the seismic section, in which the subsidence history and the sea level curve estimated in Chapter 4 were taken into account, shows a strong influence of sediment input and subsidence on sedimentation, while sea level fluctuations played a lesser role. The sediment input is related to the evolution of the adjacent land, while subsidence is dependent on sediment supply, tectonic activity and sea level fluctuations. Thus, these two factors are not totally independent.

Acknowledgements

Since I began this PhD Thesis at the University of Hamburg, many people have helped me in different ways. To all these people, who helped me scientifically or gave me a personal support, I want to thank in the following.

I begin by thanking Prof. Dr. How Kin Wong firstly for accepting to promote my PhD and afterwards for his permanent suggestions and discussions as well as for his personal support. I also thank Prof. Wong for the opportunity he gave me to participate to the research cruise in the Sea of Okhotsk; this was a very nice scientific and personal experience for me. Prof. Dr. Corneliu Dinu I thank for co-promoting my PhD and for providing me with the data I needed to begin this study. I also thank him for all his suggestions and comments that have improved the quality of this Thesis.

Dr. Thomas Lüdmann, Kai Berglar, and Niko Baristeas I want to thank for the nice period spent in the AG-Wong. I am happy for meeting Niko and creating a very nice greek-romanian atmosphere in our group. The people from the 9th floor I thank for the pleasant time spent since I came to Hamburg. I have enjoyed the company of Ariane, Helge, Hjalmar, Katja, Nils, Stefan, Merle and all the others.

My parents gave me a lot of support, even if they were quite far from me during all this time. I thank them for this and I suppose my father is now eased that I am “finally” ready with my PhD. My parents-in-law, Franziska and Volker, I want to thank firstly for their financial support to begin my PhD, and, afterwards for all their personal support during these years since I am in Hamburg. I thank them for treating me from my first day in Hamburg like their daughter.

Leni and Auraş I thank for writing me almost every day, for listening and supporting me during all this time. Raveca also gave me a lot of personal support during this period (and not only) and for this I want to thank her. Many thanks also to my Romanian friends who helped me to forget that I am far from home: Adi, George, Gina, Ingrid, Felicia, Daciana, Carmen, Maria, and Victor. Raveca, Ingrid, and George I thank for reading the Romanian version of the abstract and for their suggestions. Maria, George, and Victor I also thank for the very nice time we spent together during their stay in Hamburg.

The most I thank Philipp for his support, patience, encouragement and love he gave me during all this time. Not to forget about the scientific help, from initiating me in all the computer programms, for the discussions and his suggestions, and for reading the manuscript.

References

ALLEN, P.A., and J.R. ALLEN, 1990, Basin Analysis: Principles and Applications: Blackwell Science Ltd, Oxford, UK, p. 263-277.

ANDRUSOV, N.L., 1890, Need for deep-water investigations in the Black Sea: Izv. Russk. Geogr. Obshch., vol. 26, p. 171-185.

ATHY, L.F., 1930, Density, porosity and compaction of sedimentary rocks: Bull. Am. Assoc. petrol. Geol., vol. 14, p. 1-24.

BANKS, C.J., 1997, Basins and thrust belts of the Balkan coast and the Black Sea. In: A.G. ROBINSON (Ed.), Regional and Petroleum Geology of the Black Sea and Surrounding Region: AAPG Memoir 68, p. 115-128, Tulsa, OK.

BANKS, C.J., and A.G. ROBINSON, 1997, Mesozoic strike-slip back-arc basin of the Western Black Sea region. In: A.G. Robinson (Ed.), Regional and Petroleum Geology of the Black Sea and Surrounding Region: AAPG Memoir 68, p. 53-62, Tulsa, OK.

BARBU, C., N. ALI MEHMED, and C. PARASCHIV, 1969, The Paleozoic in the East Carpathian foreland between Buzău Valley and the northern border of Romania: Petrol şi Gaze XX, vol. 12, p. 863-868 (in Romanian).

BĂNCILĂ, I., Th. NEAGU, R. MUȚIU, and O. DRAGASTAN, 1997, Jurassic-Cretaceous stratigraphy and tectonic framework of the Romanian Black Sea offshore: Rev. Roum. Geol., vol. 41, p. 65-76.

BOND, G.C., and M.A. KOMINZ, 1984, Construction of tectonic subsidence curves for the early Paleozoic miogeocline, southern Canadian Rocky Mountains: implication for subsidence mechanisms, age of breakup, and crustal thinning: Geological Society of American Bulletin, vol. 95, p. 155-173.

BROWN, L.F., and W.L. FISHER, 1977, Seismic-stratigraphic interpretation of depositional systems: exemples from Brazil rift and pull-apart basins. In: C.E. PYATON (Ed.), Seismic stratigraphy-applications to hydrocarbon exploration: AAPG Memoir 26, p. 213-248.

BURG, J.-P., L.-E. RICOU, I. GODFRAUX, D. DIMOV, and L. KLAIN, 1996, Syn-metamorphic nape complex in the Rhodope Massif. Structure and kinematics: Terra Nova 8, p. 6-15.

CHATALOV, G., 1990, Geology of Strandzha Zone in Bulgaria: Geologica Balcanica, Series Operum Singulorum No. 4, Bulgarian Academy of Science.

CHEN, F., W. SIBEL, M. SATIR, M.N. TERZIOGLU, and K. SAKA, 2002, Geochronology of the Karadere basement (NW Turkey) and implications for the geological evolution of the Istanbul Zone: Int. Journal of Earth Science 91, p. 469-481.

DABOVSKI, C., I. ZAGORCHEV, and G. GEORGIEV, 2004, East European Craton-Scythian Platform-Dobrogea-Balkanides-Rhodope Massif-Hellenides-East Mediterranean-Cyrenaica, From the Moesian Platform to the Balkanides and East Rhodope Massif: TRANSMED Transect VII.

DACHEV, C., V. STANEV, and P. BOKOV, 1988, Structure of the Bulgarian Black Sea area: Bolletino di Geofisica Teorica e Applicata No. 117-118, vol. 30, p. 79-107.

DEAN, W.T., O. MONOD, R.B. RICKARDS, O. DEMIR, and P. BULTYNCK, 2000, Lower Palaeozoic stratigraphy and palaeontology, Karadere-Zirze area, Pontus Mountains, northern Turkey: Geol. Mag. 137, p. 555-582.

DERCOURT, J., L.E. RICOU, and B. VRIELYNCK (Eds.), 1993, Atlas Tethys, Paleoenvironmental Maps: Gauthier-Villars, Paris, p. 307, maps 14, pl. 1.

DINU, C., H.K. WONG, and D. ȚAMBREA, 2002, Stratigraphic and tectonic syntheses of the Romanian Black Sea shelf and correlation with major land structures: Bucharest Geoscience Forum, Special Volume No. 2, p. 101-117.

DRAGASTAN, O., Th. NEAGU, I. BĂCILĂ, and R. MUȚIU, 1993, Jurassic-Cretaceous stratigraphy and tectonic framework of the Romanian Black Sea offshore: The AAPG Annual Meeting, New Orleans, April 25-28.

ERSHOV, A.V., M.-F. BRUNET, A.M. NIKISHIN, S.N. BOLOTOV, M.V. KOROTAEV, and S.S. KOSOVA, 1998, Evolution of the eastern Fore-Caucasus basin during the Cenozoic collision: burial history and dynamic modeling. In: CRASQUIN-SOLEAU, S., and E., BARRIER (Eds.), Peri-Tethys Memoir 4: Epicratonic Basins of Peri-Tethyan Platforms: Mémoires du Muséum national d'Histoire naturelle, Paris, vol. 179, p. 111-130.

ERSHOV, A.V., M.-F. BRUNET, M.V. KOROTAEV, A.M. NIKISHIN, and S.N. BOLOTOV, 1999, Late Cenozoic burial history and dynamics of the Northern Caucasus molasse basin: implications for foreland basin modeling. In: STEPHENSON, R.A., M. WILSON, and V.I. STAROSTENKO (Eds.), EUROPROBE Georift. Vol. 2: Intraplate Tectonics and Basin Dynamics of the Eastern European Craton and its Margins: Tectonophysics 313, p. 219-241.

ERSHOV, A.V., M.-F. BRUNET, A.M. NIKISHIN, S.N. BOLOTOV, B.P. NAZAREVICH, and M.V. KOROTAEV, 2003, Northern Caucasus basin: thermal history and synthesis of subsidence models: Sedimentary Geology 156.

GEORGESCU, M., 1994, Studiul micropaleontologic al foraminiferelor planctonice din Jurasicul superior şi Cretacicul platformei continentale româneşti a Mării Negre: Teză de doctorat, Universitatea Bucureşti, Facultatea de Geologie si Geofizică.

GILDNER, R.F., and J.L. CISNE (Eds.), 1990, Quantitative Modeling of Carbonate Stratigraphy and Water-Depth History Using Depth-Dependent Sedimentation Function in Cross, T.A.: Quantitative Dynamic Stratigraphy, Prentice Hall, New Jersey.

GILLET, H., G. LERICOLAIS, J.-P. REHAULT, and C. DINU, 2003, La stratigraphie oligo-miocène et la surface d'érosion messinienne en mer Noire, stratigraphie sismique haute résolution : C. R. Geoscience 335, p. 907-916.

GILLET, H., 2004, La stratigraphie tertiaire et la surface d'erosion messinienne sur les marges occidentales de la Mer Noire: stratigraphie sismique haute resolution, L'universite de Bretagne Occidentale.

GOLMSHTOK, A.Y., L.P. ZONENSHAIN, A.A. TEREKHOV, and R.V. SHAINUROV, 1992, Age, thermal evolution and history of the Black Sea Basin based on heat flow and multichannel reflection data: Tectonophysics, vol. 210, p. 273-293.

GÖRÜR, N., 1988, Timing of opening of the Black Sea basin: Tectonophysics, vol. 147, p. 247-262.

GÖRÜR, N., O. MONOD, A.I. OKAY, A.M.C. SENGÖR, O. TÜYSÜZ, E. YIGITBAS, M. SAKINC, and R. AKKÖK, 1997, Palaeogeographic and tectonic position of the Carboniferous rocks of the western Pontides (Turkey) in the frame of the Variscan belt: Bull. Soc. Géol. France 168, p. 197-205.

GRĂDINARU, E., C. DINU, and O. DRAGASTAN, 1989, Stratigrafia platformei continentale dobrogene a Mării Negre in analiza condițiilor de formare, migrație şi acumulare a hidrocarburilor pe platoul continental al Mării Negre, în vederea orientării lucrărilor de cercetare geologică: Raport Intern, vol. 1, Universitatea Bucureşti, p. III.39-III.85.

HAYDOUTOV, I., and S. YANEV, 1997, The Protomoesian microcontinent of the Balkan Peninsula - a peri-Gondwanaland piece: Tectonophysics, vol. 272, p. 303-313.

HAQ, B.U., J. HARDENBOL, and P.R. VAIL, 1987, Chronology of fluctuating sea levels since the Triassic: Science, vol. 235, p. 1156-1167.

HEDBERG, H.D., 1936, Gravitational compaction of clays and shales: Am. J. Sci., vol. 31, p. 241-287.

HSÜ, K.J., and F. GIOVANOLI, 1979, Messinian event in the Black Sea: Palaeogeography, Palaeoclimatology, Palaeoecology, vol. 29, p. 75-93.

ILIESCU, V., 1974, Preliminary results of the palyno-protistological study of the pre-Silurian deposits from the basement of the Moldavian Highland: D. S. Inst. Geol. LX/3, p. 225-234 (in Romanian).

IONESCU, G., 2000, Modele faciale ale formațiunilor Paleogene pe şelful nord-vestic al Mării Negre: Teză de doctorat, Universitatea Bucureşti, Facultatea de Geologie si Geofizică.

JONES, R.W., and M.D. SIMMONS, 1997, A review of the stratigraphy of Eastern Paratethys (Oligocene-Holocene), with particular emphasis on the Black Sea. In: A.G. Robinson (Ed.), Regional and Petroleum Geology of the Black Sea and Surrounding Region: AAPG Memoir 68, p. 39-52, Tulsa, OK.

JORDAN, T.E., and P.B. FLEMINGS, 1991, Large-Scale Stratigraphic Architecture, Eustatic Variation, and Unsteady Tectonism: A Theoretical Evaluation: Journal of Geophysical Research, No. B4, vol. 96, p. 6681-6699.

KARANTSEV, Y.V., 1982, Tectonics of the Crimea: Nauka, Moskow.

KARYAKIN, Yu.V., 1989, Geodynamics of Volcanic Complex Formation in the Lesser Caucasus: Nauka, Moskow, p. 150.

KHAIN, V.Ye., 1984, Regional Geotectonics. The Alpine-Mediterranean Belt: Nedra, Moscow.

KORONOVSKY, N.V., and V.S. MILEYEV, 1974, About the relationships of Tauric series and Eskiorda suite in the Bodrak river valley (Mountain Crimea): Vestnik Mosk. Univ., Geologiya, vol. 1, p. 80-87.

LORDKIPANIDZE, M.B., 1980, Alpine Volcanism and Geodynamics of the Central Segment of the Mediterranean Fold Belt: Metsniereba, Tbilisi, p. 162.

LUȚAC, D., 2000, Procese sedimentare şi tectonice la baza paleopantei Bazinului Histria: Teză de doctorat, Universitatea Bucureşti, Facultatea de Geologie si Geofizică.

MACAROVICI, N., 1971, La faune silurienne du fondament du Plateau Moldave (les forages de Jassy et de Todireni-Botosani) : Anal. St. Univ. "Al. I. Cuza" s.n. (s. II, b. Geol.) XVII, p. 99-115.

MILANOVSKY, E.E., 1991, Geology of the URSS, Part 3: Moskow Univ. Press, Moskow, p. 272.

MILEYEV, V.S., E.Yu. BARABOSHKIN, M.Yu. NIKITIN, S.B. ROZANOV, and I.V. SHALIMOV, 1996, Evidence that the Upper Jurassic deposits of the Crimean Mountains are allochthons: Transactions (Doklady) of the Russian Academy of Sciences, Earth Science Sections 342 (4), p. 121-124.

MILEYEV, V.S., S.B. ROZANOV, E.Yu. BARABOSHKIN, and I.V. SHALIMOV, 1997, The tectonic structure and evolution of the Mountain Crimea. In: MILANOVSKY, E.E., V.S. MILEYEV, A.M. NIKISHIN, and B.A. SOKOLOV (Eds.), Geological Study of Crimea: Geological Faculty MSU Publishers, Moscow, p. 187-206.

MITCHUM, R.M., 1977, Seismic stratigraphy and global changes of sea level, Part 1: Glossary of terms used in seismic stratigraphy. In: C.E. PAYTON (Ed.), Seismic Stratigraphy - applications to hydrocarbon exploration: AAPG Memoir 26, p. 205-212.

MOROŞANU, I., 2002, Inverted Structural Types of the Romanian Offshore -Black Sea-. In: DINU, C., and V. MOCANU (Eds.), Geology and Tectonics of the Romanian Black Sea Shelf and its Hydrocarbon Potential: BGF Special Volume No. 2, p. 21-28.

MURATOV, M.V, 1969, Geology of the URSS, Crimea, Part 1: Geology, vol. VIII, Nedra, Moscow, p. 576.

MUREŞAN, M., 1975, Privire de ansamblu asupra succesiunii de formare a rocilor magmatice paleozoice sin-orogene şi subsecvenţa din Dobrogea de Nord: D.S. Instit. Geol. Geof., 61-5, Bucureşti.

NEPROCHNOV, Y.P., and D.A. ROSS, 1978, Black Sea geophysical framework: Initial reports of the Deep Sea Drilling Project, 42 (2), U.S. Govt. Printing Office, Washington, D.C., 1043-1055.

NIKISHIN, A.M., S. CLOETINGH, M.-F. BRUNET, R. STEPHENSON, S.N. BOLOTOV, and A.V. ERSHOV, 1998, Scythian Platform and Black Sea region: Mesozoic-Cenozoic tectonic and dynamics. In: CRASQUIN-SOLEAU, S., and E. BARRIER (Eds.), Peri-Tethys Memoir 3: Stratigraphy and Evolution of Peri-Tethyan Platforms, Mémoires du Muséum national d'Histoire naturelle, Paris, vol. 177, p. 163-176.

NIKISHIN, A., P.A. ZIEGLER, D.I. PANOV, B.P. NAZAREVICH, M.-F. BRUNET, R.A. STEPHENSON, S.N. BOLOTOV, M.V. KOROTAEV, and P.L. TIKHOMIROV, 2001, Mesozoic and Cenozoic evolution of the Scythian Platform-Black Sea-Caucasus domain. In: P.A., ZIEGLER, W. CAVAZZA, A.H.F. ROBERTSON, and S. CRASQUIN-SOLEAU

(Eds.), Peri-Tethys Memoir 6: Peri-Tethyan Rift/Wrench Basins and Passive Margins, Mémoires du Muséum national d'Histoire naturelle, Paris, vol. 186, p. 295-346.

NIKISHIN, A.M., M.V. KOROTAEV, A.V. ERSHOV, and M.-F. BRUNET, 2003, The Black Sea basin: tectonic history and Neogene-Quaternary rapid subsidence modeling: Sedimentary Geology, vol. 156, p. 149-168.

OKAY, A.I., A.M.C. SENGÖR, and N. GÖRÜR, 1994, Kinematic history of the opening of the Black Sea and its effect on the surrounding regions: Geology, vol. 22, p. 267-270.

OKAY, A.I., and O. TÜYSÜZ, 1999, Tethyan sutures of northern Turkey. In: DURAND, B., L. JOLIVET, F. HORVÁTH, and M. SÉRANNE (Eds.), The Mediterranean Basins, Tertiary Extension within the Alpine Orogen: Geol. Soc. London Spec. Publ., vol. 156, p. 475-515.

PARASCHIV, D., 1985, The present state of knowledge of Precambrian and Paleozoic formations from the Moldavian Platform: Mine, Petrol şi Gaze, vol. 11 (in Romanian).

PĂTRULIUŞ, D., and M. IORDAN, 1974, On the presence of the Pogonophore Sabellidites cambriensis Ian. and the algae Vendotaenia antiqua Gnil. in the pre-Silurian deposits from the Moldavian Highlands: D.S. LX/4 (in Romanian).

PĂTRUȚ, I., 1975, Cercetări asupra structurii geologice a platformei continentale a Mării Negre şi poziția primelor foraje: Ministerul Petrolului, Raport Intern, Bucureşti.

ROBINSON, A.G., J.H. RUDAT, C.J. BANKS, and R.L.F. WILES, 1996, Petroleum geology of the Black Sea: Marine and Petroleum Geology No. 2, vol. 13, p.195-223.

ROSS, D.A., P. STOFFERS, and E.S. TRIMONIS, 1978, Black Sea sedimentary framework: Initial reports of the Deep Sea Drilling Project, 42 (2), U.S. Govt. Printing Office, Washington, D.C., p. 359-372.

RUBEY, W.W., and M.K. HUBBERT, 1960, Role of fluid pressure in mechanics of overthrust faulting, II, Overthrust belt in geosynclinal area of western Wyoming in light of fluid-pressure hypothesis: Bull. geol. Soc. Am., vol. 60, p. 167-205.

SĂNDULESCU, M., 1978, The Moesic Platform and the North Dobrogea orogen. In: M. LEMOINE (Ed.), Geological atlas of Alpine Europe and adjoining areas: Elsevier, Amsterdam, p. 427-460.

SĂNDULESCU, M., 1984, Geotectonica României: Editura tehnică, Bucureşti.

SCLATER, J.G., and P.A.F. CHRISTIE, 1980, Continental stretching: an explanation of the Post-Mid-Cretaceous subsidence of the central North Sea basin: Journal of Geophysical Research 87, vol. 85, p. 3711-3739.

SEGHEDI, A., 2001, The North Dobrogea orogenic belt (Romania): a review. In: ZIEGLER, P.A., W. CAVAZZA, A.H.F. ROBERTSON, and S. CRASQUIN-SOLEAU (Eds.), Peri-Tethys Memoir 6: Peri-Tethyan Rift/Wrench Basins and Passive Margins, Mémoires du Muséum national d'Histoire naturelle, Paris, vol. 186, p. 237-257.

SEGHEDI, A., G. OAIE, D. IOANE, and R. DIMITRIU, 2004, East European Craton-Scythian Platform-Dobrogea-Balkanides-Rhodope Massif-Hellenides-East Mediterranean-Cyrenaica; Eastern European Craton, Scythian Platform, N. Dobrogea Orogen and Moesian Platform: TRANSMED Transect VII.

STEPHENSON, R., Y. MART, A. OKAY, H.F. ROBERTSON, A. SAINTOT, S. STOVBA, and O. KHRIACHTCHEVSKAIA, 2004, Eastern European Craton-Crimea-Black Sea-Anatolia-Cyprus-Levant Sea-Sinai-Red Sea: TRANSMED Transect VIII.

SUNAL, G., and O. TÜYSÜZ, 2002, Palaeostress analysis of tertiary post-collisional structures in the Western Pontides, northern Turkey: Geological Magazine, vol. 139, p. 343-359.

TEKELI, O., 1981, Subduction complex of pre-Jurassic age, northern Anatolia, Turkey: Geology, vol. 9, p. 68-72.

TÜYSÜZ, O., 1999, Geology of the Cretaceous sedimentary basins of the Western Pontides: Geological Journal, vol. 34, p. 75-93.

TĂRĂPOANCĂ, M., 2004, Architecture, 3D geometry and tectonic evolution of the Carpathians foreland basin: Netherlands Research School of Sedimentary Geology (NSG), publication no. 2004.01.03.

ȚAMBREA, D., V. ŞINDILAR, and R. OLARU, 2000, The Pontian from the Romanian continental shelf of the Black Sea: Romanian Oil Journal, vol. 7 (1), p. 9-20.

VAN WAGONER, J.C., H.W. POSAMENTIER, R.M. MITCHUM, P.R. VAIL, J.F. SARG, T.S. LOUTIT, and J. HARDENBOL, 1988, An overview of sequence stratigraphy and key definitions. In: C.W. WILGUS et al. (Eds.), Sea level changes: an integrated approach: Society of Economic Paleontologists and Mineralogists Special Publication No. 42, p. 39-45.

VAN WAGONER, J.C., R.M. MITCHUM, K.M. CAMPION, and V.D. RAHMANIAN, 1990, Siliciclastic sequence stratigraphy in well logs, cores, and outcrops: concepts for high-resolution correlation of time and facies: AAPG Methods in Exploration Series, No. 7.

VISARION, M., M. SĂNDULESCU, V. ROŞCA, D. STĂNICA, and L. ATANASIU, 1990, La Dobrogea dans le cadre de l'avantpays Carpatique: Rev. Roum. Géophys. 34, p. 55-65.

USTAÖMER, T., and A.H.F. ROBERTSON, 1994, Late Palaeozoic marginal basin and subduction-accretion, the Paleotethyan Küre Complex, Central Pontides, northern Turkey: Journal of Geol. Soc. London, vol. 151, p. 291-305.

USTAÖMER, T., and A.H.F. ROBERTSON, 1997, Tectonic-sedimentary evolution of the north Tethyan margin in the Central Pontides of northern Turkey. In: A.G. ROBINSON (Ed.), Regional and Petroleum Geology of the Black Sea and Surrounding Regions: AAPG Memoir 68, p. 255-269, Tulsa, OK.

USTAÖMER, P.A., and G. ROGERS, 1999, The Bolu Massif: remnant of a pre-Early Ordovician active margin in the west Pontides, northern Turkey: Geological Magazine, vol. 126, p. 579-592.

WINGUTH, C., 1998, Pleistozäne Meeresspiegelschwankungen und Sedimentation im nordwestlichen Schwarzen Meer: Zentrum für Meeres- und Klimaforschung der Universität Hamburg, Institut für Biogeochemie und Meereschemie.

YIGITBAS, E., A. ELMAS, and Y. YILMAZ, 1999, Pre-Cenozoic tectono-stratigraphic components of the western Pontides and their geological evolution: Geological Journal, vol. 34, p. 55-74.

YILMAZ, Y., O. TÜYSÜZ, E. YIGITBAS, S. CAN GENC, and A.M.C. SENGÖR, 1997, Geology and Tectonic evolution of the Pontides. In: A.G. ROBINSON (Ed.), Regional and Petroleum Geology of the Black Sea and Surrounding Regions: AAPG Memoir 68, p. 183-226, Tulsa, OK.